The University Of Sheffield.

Innovative heat transfer enhancements for thermal energy storage systems based on phase change materials

By:

Ahmed Hussein Nasser Al-mudhafar

Thesis submitted in partial fulfilment of the requirements for the degree of Doctor of Philosophy

The University of Sheffield

Department of Mechanical Engineering

June 14, 2019

Abstract

Rapid economic growth has led to increased use of fossil fuels as an energy source. This has a major impact on greenhouse gas emissions. Scientists around the world are investigating new, more economic and renewable sources of energy. A complementary approach is to improve existing energy storage systems, which are as important as the development of new energy sources. Thermal energy is widely available in nature as a by-product of numerous energy conversion plants. Thermal energy could be accumulated using latent, sensible and thermo-chemical storage methods.

The latent heat thermal energy storage method that utilizes phase change materials (PCMs) is the most promising energy storage technique. The method has a high energy storage density and is characterized by a slight variation in temperature during the process of energy storage. The low thermal conductivity is a major drawback of the PCMs and limits their application as latent heat thermal energy storage materials. That low thermal conductivity of PCMs increases their thermal energy storage and release times. The present study investigates various PCMs-based solutions to enhance the overall storage system thermal performance.

The solutions proposed in this thesis comprise an innovative design of metallic fins and the introduction of innovative heat exchanger geometries. Numerical simulations that monitor melting (charging) and solidification (discharging) processes, are conducted to evaluate the proposed solutions.
This manuscript is divided into four main parts that report the results of the investigations

seeking to improve the latent heat energy storage systems utilising PCMs.

In the first part of this study, innovative fin shapes were introduced to enhance the thermal performance of PCM in a triple tube heat exchanger. These fins included: tee fins and plus fins. To evaluate the thermal performance of these fins, a comparison was made with the traditional longitudinal fins. The results showed significant improvement in the PCM thermal performance when using the plus fins shape as compared to the longitudinal fins and tee fins configurations. When utilizing the plus fins, the PCM melting time reduced by 22% and the solidification time decreased by 25% compared with using the longitudinal fins.

In the second part of this study, novel fin shapes were introduced to improve the thermal performance of PCM in a shell and tube heat exchanger. These fins included: tee fins, and tree fins. To evaluate the thermal performance of these fins a comparison was made with the traditional longitudinal fins. Similar to the triple tube heat exchanger, the results showed significant enhancement in the PCM thermal performance when utilizing the tee fins as compared to the longitudinal fins. For the tee fins, the PCM melting time reduced by 33% and the solidification time decreased by 33% when compared with using the longitudinal fins.

In the third part of this study, an innovative heat exchanger geometry (webbed tube heat exchanger) was introduced to improve the thermal performance of PCM. To demonstrate the value of the webbed tube heat exchanger design, its thermal performance was compared against conventional heat exchangers, which included: triple tube heat exchanger, shell and tube heat exchanger, and multitube heat exchanger. When utilizing the webbed tube heat exchanger, the PCM melting time reduced by 50% and the solidification time decreased by 45% as compared to using the triple tube heat exchanger. Moreover, by utilizing the webbed tube heat exchanger, the PCM melting time reduced by 72% and the solidification time decreased by 66% when compared with using the multitube heat exchanger.

Finally, the webbed tube heat exchanger, introduced in the third part of this thesis, was employed instead of the inner and middle tubes of the triple tube heat exchanger

to produce the modified webbed tube heat exchanger. The modified webbed tube heat exchanger was proposed as a novel heat exchanger design to improve the thermal performance of the latent heat thermal energy storage systems that are based on PCMs. The study proved that by utilizing the modified webbed tube heat exchanger, the PCM melting time was reduced by 38% and the solidification time was decreased by 41% when compared to using the webbed tube heat exchanger.

Comparisons were made with previous related experimental studies. The numerical results showed good agreement with the available experimental results and justify the investigations of cases that have not previously been studied. This systematic approach could constitute guidance for any practitioner looking to improve PCMs-based solutions.

Acknowledgements

This study has been conducted at the Department of Mechanical Engineering, The University of Sheffield, under the supervision of Dr. Andrew Nowakowski.

I want to thank the Iraqi Ministry of Higher Education and Scientific Research (MOHESR), and Iraqi Cultural Attaché in London, UK for their financial support and sponsorship.

I would like to express my deep gratitude to my supervisor Dr. Andrew Nowakowski for his inspiration, wisdom, patience, guidance, and support during my study. I am also very grateful to my second supervisor Dr.Franck Nicolleau for his help and support during my study.

Many thanks to all my family members for their support and patient along my study.

I would also like to thank all of my colleagues and friends for their support along this time.

Contents

List of Figures

List of Tables

Nomenclature

ΔH	Latent enthalpy that could be change between (L) for liquid and zero for (solid) (J/kg)
C	Constant represent the mushy zone morphology (kg/m^3 s)
C_P	Specific heat (J/kg K)
g	Gravity acceleration (m/s^2)
H	Total enthalpy (J/kg)
h	Sensible enthalpy (J/kg)
k	Thermal conductivity (W/m K)
L	Latent heat of PCM (J/kg)
p	Pressure (Pa)
S_i	Source term (porosity function) in the momentum equation (Pa/m)
T	Temperature (°C)
T_l	PCM melting temperature (°C)
T_s	PCM solidification temperature (°C)
u_i	Fluid velocity (m/s)

Abbreviations

HTF Heat transfer fluid

LHTES Latent heat thermal energy storage

MTHX Multi tube heat exchanger

MWTHX Modified webbed tube heat exchanger

PCM Phase change material

SHTES Sensible heat thermal energy storage

STHX Shell and tube heat exchanger

TES Thermal energy storage

TTHX Triple tube heat exchanger

WTHX Webbed tube heat exchanger

Greek symbols

β PCM thermal expansion coefficient (1/K)

γ Liquid fraction

μ Dynamic viscosity of fluid (kg/ms)

ρ Density of materials (kg/m^3)

ε Very small value number

Scripts

l liquid

o reference

s solid

Publications

Published papers

- A. H. Al-Mudhafar, A. F. Nowakowski, and F. C. Nicolleau, "Thermal performance enhancement of energy storage systems via phase change materials utilising an innovative webbed tube heat exchanger," *Energy Procedia*, vol. 151, pp. 57–61, 2018.

Submitted manuscripts

- Performance enhancement of PCM latent heat thermal energy storage system utilizing a modified webbed tube heat exchanger.
- Numerical study of PCM melting enhancement in a triplex tube heat exchanger using innovative fins configurations.

Chapter 1

Introduction

The continued demand for energy has generated widespread concerns over climate change, due to the increased use of fossil fuels. It is therefore necessary to reduce the utilization of fossil fuels and focus more on renewable resources to generate energy. Solar energy is one of the promising renewable energy sources, being free and abundantly available. According to the estimation of Paris-based International Energy Agency of the Organisation for Economic Co-operation and Development (OECD) [1], by 2050, 27% of the world's electricity should be produced from solar power. The main challenge associated with utilizing solar energy is that it depends on time, weather and location. Hence, energy storage systems are needed to store solar energy in the form of electrochemical or thermal energy [2, 3]. Although utilizing solar energy to drive cooling systems is an attractive option, the periodic nature of solar energy limits its widespread use [4]. Therefore, a thermal energy storage (cold or hot) system should be integrated with the solar cooling system [5, 6]. Latent heat thermal energy storage (LHTES) has an advantage over sensible heat thermal energy storage (SHTES) because of its large energy storage density [7]. The materials utilized to store thermal energy in the LHTES systems are called phase change materials (PCMs). PCMs are capable of storing large amounts of thermal energy during the phase change process, which takes place with a small variation in the temperature of storage the material [8]. In recent years PCMs have had various applications in the

air conditioning of buildings, solar cooling systems, greenhouses, electronic cooling, food cooling, solar water heating, solar power plants, medical applications such as transport of blood and in textiles for human comfort [9, 10].

1.1 Energy Storage

Energy storage systems have become an essential part of renewable energy technology. Storage systems are needed to correct the mismatch between energy generation and energy demand, in addition to storing excess energy or free energy that would otherwise be wasted. There are many types of energy storage methods which include: mechanical, electric and thermal energy storage solutions [11]. An overview of various energy storage techniques is shown in Fig. 1.1.

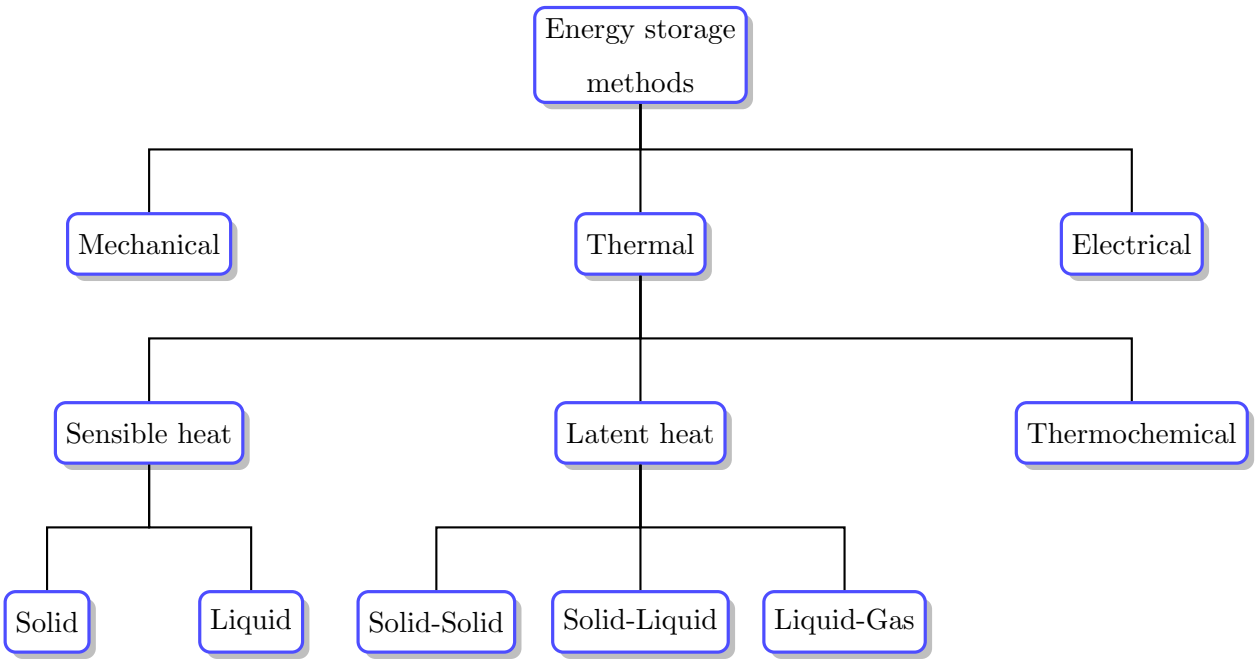

Figure 1.1: Energy storage methods

1.1.1 Thermal energy storage

Thermal energy storage (TES) systems store thermal energy by cooling/heating, or melting/solidifying, or condensing/evaporating the storage medium, or through thermo-chemical reactions. Then the stored energy can be utilized later for cooling or heating applications or for electricity generation [12]. TES is a promising option for solar energy applications, because of its high storage density and relatively low cost. The TES heat storage capacity is usually 1000 times greater than hydraulic energy storage and two times higher than electric energy storage capacity [13]. TES can be classified into three types: latent heat thermal energy storage (LHTES), sensible heat thermal energy storage (SHTES), and thermochemical energy storage. Various thermal energy storage methods are illustrated in Fig. 1.2. In SHTES, energy is stored or released by raising or decreasing the temperature of the storage medium, which can be rock, water, brine, soil, oil, etc. The amount of TES stored in SHTES system depends on the mass of the storage substance and its heat capacity as well as the temperature difference before and after the storage operation. The sensible heat storage ($Q_{sensible}$) can be represented by

$$Q_{sensible} = m \times C_p \times \Delta T. \tag{1.1}$$

In LHTES, energy is stored during phase change [14]. The materials used for LHTES are called phase change materials (PCMs). Examples of PCMs are water/ice, paraffin, and eutectic salts. The latent heat storage (Q_{latent}) can be represented by

$$Q_{latent} = m \times L, \tag{1.2}$$

where C_p is the specific heat, m is the mass of the storage substance, ΔT is the temperature difference and L is the latent heat of melting.

LHTES has a higher energy storage capacity when compared to SHTES, hence, LHTES units are generally smaller than SHTES units.

In thermochemical storage systems, energy is stored by utilizing exothermic/endothermic chemical reactions [15]. TES systems based on chemical reactions are appropriate for long-term storage applications because the process not involve energy losses during the

storage period. Thermochemical energy storage systems store thermal energy usually at ambient temperature. The principle of thermochemical TES is based on the chemical reaction that can be reversed:-

$$C + \text{heat} \rightleftharpoons A + B$$

In this thermochemical reaction, thermochemical material (C) absorb thermal energy and is converted chemically into two materials (A and B). The reverse chemical reaction occurs when components A and B combined together to form C. Thermal energy is released during this reaction. The storage capacity of the thermochemical TES system is the heat of reaction when the material C is formed. The thermochemical TES cycle includes three main process:- charging, storage and discharging see Fig. 1.2 (a). The thermochemical energy storage has high energy storage capacity, but it is expensive and still at an early research stage [16].

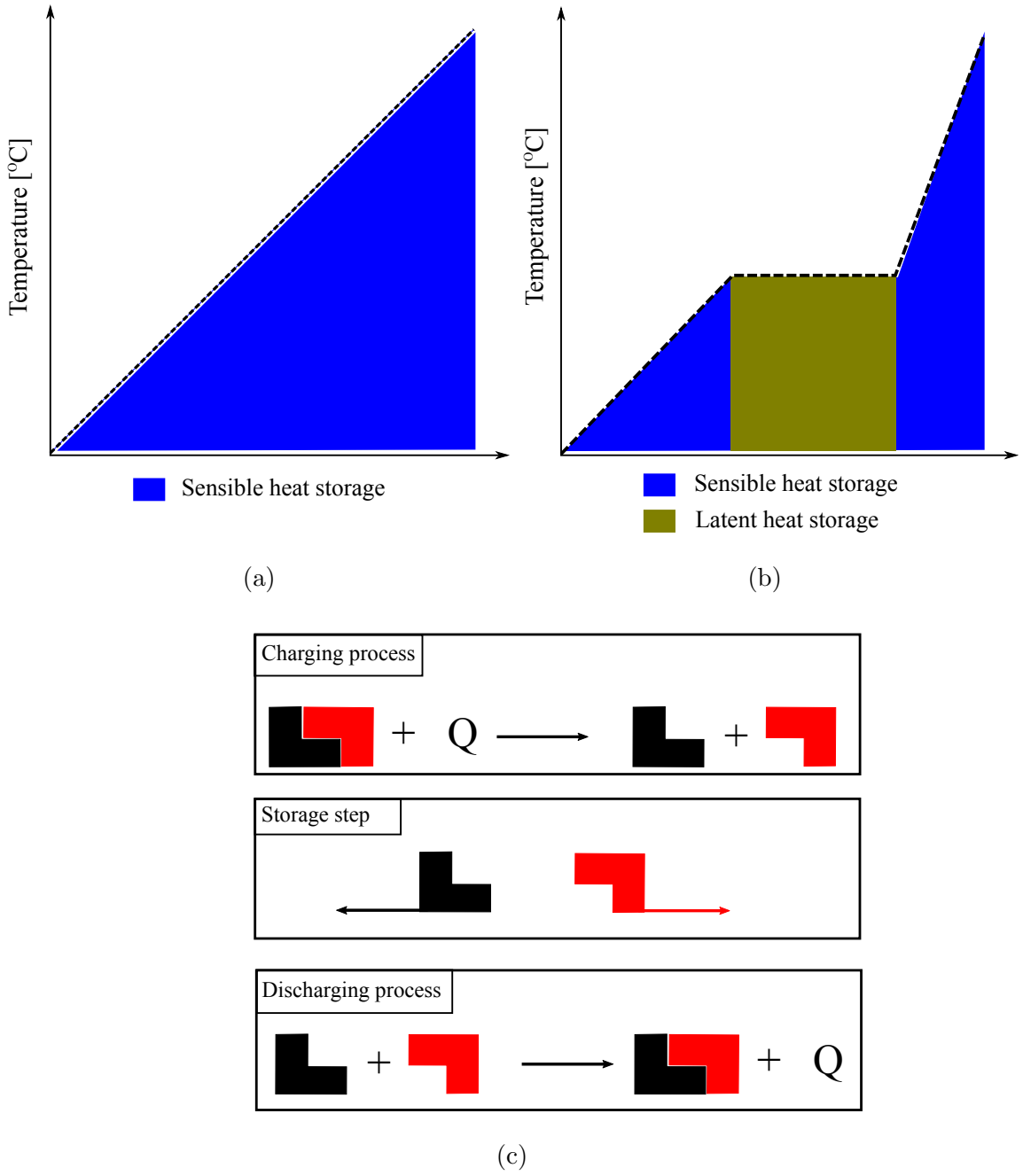

Figure 1.2: Methods of thermal energy storage: (a) sensible heat storage; (b) latent heat storage; and (c) thermochemical reactions.

1.2 Latent Heat Thermal Energy Storage

LHTES is a promising energy storage technique because of its high energy storage capacity. Furthermore, LHTES enables the storage or release of energy at a nearly constant temperature when compared to SHTES. LHTES depends on heat absorbed or released when substances undergo a phase change, such as from solid to liquid, solid to solid or liquid to gas and vice-versa. The liquid to gas phase change requires a large volume vessel, while the solid to solid phase change has a low energy storage capacity per unit volume of substance. Therefore, the solid to liquid phase change is preferred, compared to other types, owing to its high energy storage capacity and only slight volume change during the phase change process [17]. The materials used to store energy in LHTES are called phase change materials (PCMs). The main disadvantage of PCMs' application in TES is their poor thermal conductivity, which leads to increased energy storage and release time.

1.3 Definition of the Problem

The poor thermal conductivity of PCMs results in low heat transfer and low heat storage/release rates, which is the main obstacle to the widespread utilization of PCMs in TES systems requiring rapid energy storage/release [18]. As such, the utilization of heat transfer enhancement techniques is essential for any TES systems based on PCMs.

1.4 Aims and Objectives

The low thermal conductivity is the main problem that limits utilizing PCMs in thermal energy storage (TES) applications. The ultimate aim of this thesis is to enhance the thermal performance of TES systems based on PCMs by investigating various heat transfer enhancement techniques. It is hoped that the innovative solution will accelerate energy storage/release for TES systems based on PCMs.
The major aim of this work will be achieved by successfully completing the following objectives:

1. Introduce novel fin shapes to enhance the thermal performance of PCMs used to store thermal energy in a triple tube heat exchanger and shell and tube heat exchanger.
2. Compare the suggested fins with traditional fins to evaluate their thermal performance.
3. Introduce innovative heat exchanger geometries that can be utilized to improve the thermal performance of the TES systems based on PCMs.
4. Compare the suggested heat exchangers with traditional heat exchangers to evaluate their thermal performance.

1.5 Thesis Outline

The thesis is divided into eight chapters. **Chapter 2** reviews the literature and research studies on utilizing PCMs in thermal energy storage, focusing on heat transfer enhancement techniques. These techniques include the dispersion of high thermal conductivity nanoparticles into PCM, using porous materials, using multiple PCMs and utilizing metal fins. The review has found that the majority of heat transfer enhancement techniques for PCMs have been based on the application of fins because of their easy design, low cost,

and easy fabrication.
The geometric design of fins has strongly influenced the energy storage and release times of LHTES systems based on PCMs. Therefore, exploring the possible innovative geometric designs of the fins to improve the thermal performance of PCMs LHTES systems is of paramount importance.
The literature review also shows that changing the heat exchanger geometry could enhance the thermal performance of PCMs LHTES systems.

Chapter 3 covers the governing equations that are used to solve the problem of phase change materials.

Novel fin configurations, introduced to improve the thermal performance of PCM in a triple tube heat exchanger, are addressed in **Chapter 4**. Then a comparison is made between the novel fins and the traditional longitudinal fins to evaluate their thermal performance.

Chapter 5 introduces novel fin configurations to improve the thermal performance of PCM in a shell and tube heat exchanger. This is followed by a comparison between the novel fins and the traditional longitudinal fins to evaluate their thermal performance.

The idea of utilizing a webbed tube heat exchanger (WTHX), as a novel heat exchanger design to improve the thermal performance of PCM in LHTES system, is investigated in **Chapter 6**. As in previous cases, the WTHX is compared with the conventional heat exchangers to evaluate its thermal performance.

There is no study that has combined a triple tube heat exchanger with a webbed tube heat exchanger in the existing literature. **Chapter 7** attempts to couple these two heat exchangers, to produce a new heat exchanger. As a result, the new heat exchanger (a modified webbed tube heat exchanger) is proposed. It consists of the webbed tube heat exchanger that replaces the inner and middle tubes of the triple tube heat exchanger. Then

a comparison is made between the modified webbed tube heat exchanger (MWTHX) and the WTHX to evaluate its thermal performance.

The conclusions from the current work and recommendations for future work are presented in **Chapter 8**.

Chapter 2

Literature Review

2.1 Phase change materials

PCMs are the heart of any LHTES system. Compared to SHTES, the LHTES is favoured because of its high energy storage capacity and nearly isothermal energy store process. PCMs could store 5 to 14 times more heat per unit volume when compared to traditional SHTES substances, such as rock or water [4].

PCMs can be categorized based on the change of state during the phase change process: liquid-gas, solid-liquid, solid-solid, and vice versa [19, 13]. The liquid-gas PCMs have large latent heat during the phase change but involve high volume change during phase transition, which creates substantial containment vessel problems and significantly limits their use in LHTES applications. The solid-solid PCMs change their crystalline structure with almost negligible volume change when absorbing or releasing heat at a fixed temperature. The solid-solid PCMs have low latent heat, which restricts their use in LHTES applications. The solid-liquid PCMs are considered the most practical choice for LHTES applications due to their high latent heat and limited volume variation during the phase change process [2]. The solid-liquid PCMs are substances with a high latent heat of fusion, which undergo melting or solidification at a certain temperature. They absorb or release a large amount

of heat during the melting or freezing process, which takes place at a nearly constant temperature [20].

The solid-liquid PCMs could be classified, depending on their chemical composition, into: organic, inorganic, and eutectic see Fig. 2.1. The eutectic PCM is a homogeneous mixture of two or more types of PCM compounds that can melt or freeze without segregation [19].

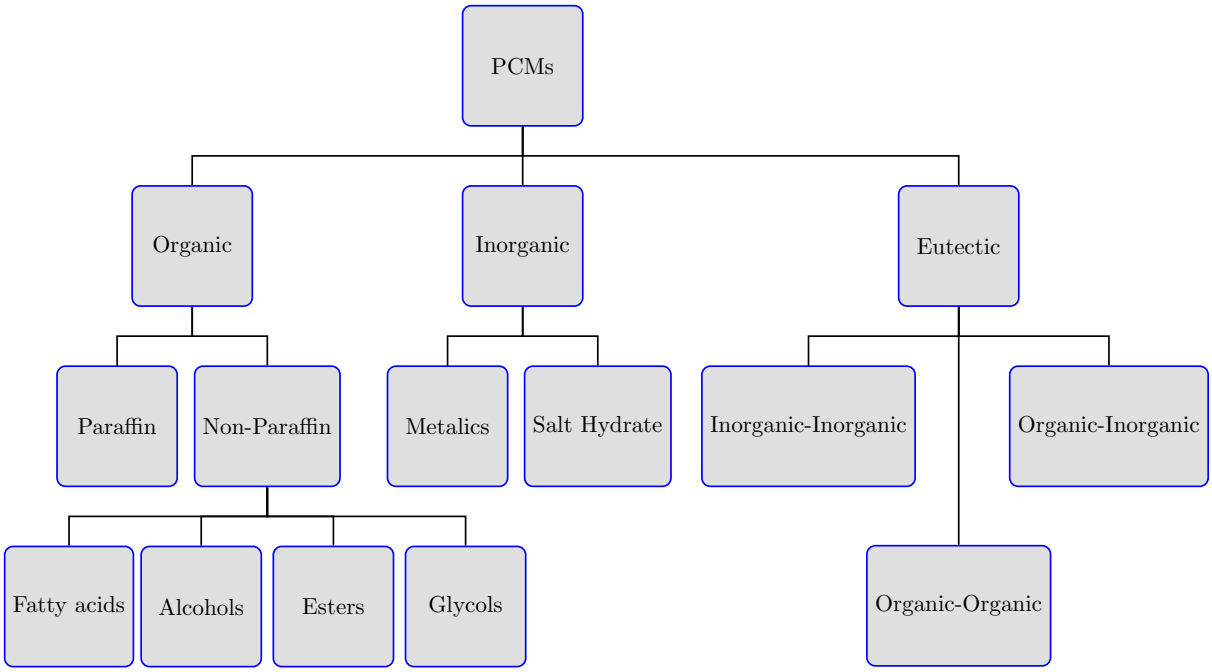

Figure 2.1: Types of solid-liquid PCMs

The selection of PCM for any application depends on its latent heat of fusion, melting temperature and thermo-physical characteristics [12]. The main desirable properties for PCMs are shown in Table 2.1 [16, 21, 22].

PCMs have been used for numerous applications over recent decades. These applications included solar cooling and heating systems, air conditioning systems, solar power plants, electronic cooling, solar water heating, greenhouses and preservation of food [23].

The main drawback associated with PCMs is their poor thermal conductivity, which is the main obstacle to their widespread utilization in LHTES applications [24]. The

thermal conductivity of PCMs generally ranges between 0.2 and 0.7 W/m K [25]. The low thermal conductivity delays the energy storage/release processes for LHTES systems. Thus, efficient heat transfer enhancement techniques should be adopted to enhance their thermal performance.

Table 2.1: The main desired properties for PCMs.

Thermal properties	High thermal conductivity.
	A melting temperature should be within the required application temperature scope.
	High density.
	High specific heat.
	High latent heat of melting.
Physical properties	High energy storage per unit volume.
	Low volume variation during phase change.
	No or little sub-cooling during solidification.
Chemical properties	No segregation.
	Corrosion resistance to container materials.
	Chemically stable.
	Non-explosive, non-flammable, non-toxic.
Economic aspects	Availability in large amounts.
	Low price.
	Good recyclability.

2.2 Applications of PCMs in thermal energy storage

2.2.1 Free cooling and heating for buildings

TES systems based on PCMs are used to store outside cold and release it to the interior of the building, during daytime in the summer season. The PCMs are solidified during the cold storage process and melted during the cold release process. They are also used to store thermal energy in daytime, then release it to the interior of the building, during the night, in winter. These systems can reduce the electric energy consumption that is needed for heating or cooling buildings. They also enable shifting the peak cooling and heating load to off-peak electricity periods [26].

Xiang and Zhou [27] numerically and experimentally tested the thermal performance of a PCM-cooling storage unit attached to the window in an office building. This unit consisted of three major parts: fans, PCM and air filter. The cooling unit stores the free outside cold at night by natural ventilation and releases it to the interior during the daytime. A south facing office room located in Beijing (China) was used to investigate the operation of this unit. The numerical analyses were performed by applying a transient 3D model, simulating heat transfer within the unit. Results showed that if the night ventilation is employed with this unit, the inside room temperature could be decreased by 3.3°C and could save 1.9 kW of electricity per hour. The energy efficiency ratio of the unit can reach 8.7. The study also revealed that this cooling storage unit has the advantage of easy installation in existing buildings.

Osterman *et al.* [28] numerically and experimentally studied the thermal performance of a LHTES unit for cooling or heating office buildings. The thermal storage unit contained 30 plates filled with PCM (paraffin). The system was used to store coldness during the night, in order to release it to the interior of the building during the daytime. It can also store heat from solar air collector during daylight hours, then discharge it at night or in the morning. ANSYS Fluent software was utilized in the simulation. The results indicated that the best performance of this unit was in summer when there was a high fluctuation

between day and night temperatures. The largest amount of energy saving in the winter season was in March because of the large quantity of solar heat available. It was found that 142 kWh of annual energy consumption was saved by using this unit.

Mosaffa *et al.* [29] numerically and experimentally investigated thermal performance of a free cooling unit designed to store cold. The unit consisted of many parallel layers of PCM sheets. Two PCMs with different melting temperatures were contained in each sheet, and air was allowed to flow through channels between sheets. COMSOL software was utilized to perform simulations. The results indicated that the exergy efficiency for the cold charging process was enhanced by decreasing the inlet air temperature.

Raj and Velraj [30] experimentally and numerically tested a shell and tube heat exchanger as a cold store system for a free cooling application. This system consisted of many modular units with air spaces between each module. In each module the PCM (paraffin) was encapsulated in the shell section and air flowed through tubes. The PCM annular section was cooled by cold air passing through inner pipes produced by a climate simulator. ANSYS Fluent software was employed in the numerical simulation. The influence of the inlet air temperature and its velocity on the PCM solidification process were studied. The results indicated that the air spacer between the modules enhances heat transfer for frontal velocities lower than 1 m/s. Moreover, the PCM solidification process accelerated by increasing the inlet air velocity by up to 2 m/s.

Navarro *et al.* [31] experimentally investigated incorporating PCM in a hollow concrete slab (active slab). The concrete slab was used as an internal partition for a cubicle located in Spain. The PCM was contained inside the hollows of the slab. The slab was used to store free coldness by flowing the outside cold air through it at night. During daytime, the coldness was released to the interior ambient air by heat exchange with the PCM. Two identical house-like cubicles were used in this experiment, with the only difference between them being that one contained the active slab while the other contained the conventional slab without PCM. The results showed that between 15-55% of cooling energy could be saved by using the active slab as compared to the slab without PCM.

Stritih and Butala [26] experimentally studied utilizing a PCM cold storage unit to store free cooling to cool a building. The PCM-cold store unit consisted of a metal container

containing PCM (paraffin), located inside air duct. The storage unit was integrated with industrial fins to enhance the poor thermal conductivity of PCM. During the night, the outside cold air was passed through the unit to store coldness by solidifying the PCM. In daytime, the inside warm air was passed over the unit, which cools due to the PCM melting process. The investigation highlighted that the PCM should be carefully chosen depending on the local weather conditions. The wrong choice of PCM could lead to inadequate cold storage. The study recommended simplification via utilizing PCMs in free cooling applications by producing prefabricated cold storage units.

To summarize, the free cooling concept is only practical in weather conditions with high fluctuations in temperature between day and night in summer. A 15 °C temperature variation between the night and daytime is preferred [32]. The night ventilation enhances the effectiveness of free cooling systems based on PCMs.

2.2.2 Thermal energy storage in buildings' structures

PCMs have high thermal energy storage density compared to other conventional building materials. Given this, integrating PCMs in buildings' structures could improve the thermal comfort for buildings' residents and users.

Gracia *et al.* [33] experimentally tested a new type of ventilated facade incorporated with PCMs (salt hydrate) in its air gap, used as a cold storage unit. Two identical residential buildings located in Spain were used in this experiment. The only difference between the buildings was that one has the ventilated facade in its south wall and the other did not. The facade was utilized to prevent overheating of the building or used to store the free coldness at night. Six automatically opening gates were utilized in the facade to change its operating mode. The study highlighted that the free cooling could reduce building cooling load and enhance thermal comfort. Furthermore, to enhance the efficiency of the cold storage facade, the outer side of the facade should be insulated to reduce the

heat gain. The use of a programmable thermal control is necessary to prevent outside hot air from entering the facade during charging, which may increase the cooling load and reduce the system's efficiency.

Principi and Fioretti [34] experimentally and numerically studied PCM insertion in a hollow block to improve its thermal performance. COMSOL software was used in the simulation to test the thermal behaviour of the block, before and after the PCM insertion. A test apparatus box was built to test experimentally the thermal behaviour of the block by measuring the heat flux and temperature. The results showed that by utilizing the PCM, the peak load can be shifted by about 6 h and its value reduced by 25%.

Barzin *et al.* [35] experimentally tested utilizing PCM-impregnated gypsum boards in lightweight buildings for cooling purposes in New Zealand. Two identical test huts were employed in this study. The only difference between these huts was that the first contained PCM-impregnated gypsum boards and the second contained ordinary gypsum board. The results showed that by utilizing night ventilation and free cooling to store coldness in the PCM-boards, 73% of the electricity could be saved during a one week period. The study recommended using the PCM-boards to store free coldness in office buildings by using night ventilation. The study also highlighted the necessity of using a proper control system with the PCM storage system, otherwise the electricity used for the cooling may be increased.

Sayyar *et al.* [36] developed a composite nano-PCM and incorporated it into gypsum wall boards. Capric acid (CA) 75.2wt% and palmitic acid (PA) 24.8wt% were mixed to form CA-PA eutectic PCM. To form nano-PCM, 92wt% of CA-PA PCM was added to 8wt% of graphite interconnected nanosheets (GNP). The thermal performance of the wall boards integrated with PCM was compared with the commercial drywall panels by constructing two test rooms containing many thermocouples to measure temperature. The experimental results showed that by using the wall boards integrated with PCM, the temperature fluctuations inside the room reduced to 18.5-26.5 °C compared to 13-32 °C for the room which contained the commercial drywall panels. Moreover, numerical simulation was used to test the thermal performance of the room that contained the PCM wall boards and compared it to the room without PCM. The numerical results indicated that by employing

PCM wall boards, the cooling and heating energy consumption was reduced by 75% and 83% respectively.

Kośny *et al.* [37] experimentally tested the thermal performance of a photovoltaic roof integrated with PCM and compared it with a control asphalt shingle roof. The photovoltaic-PCM roof consisted of PCM, fiberglass insulation with reflective foil facing, a ventilated air gap and PV plates. In winter, the roof stores solar heat in daytime and releases it to the interior of the building at night. In summer, the roof absorbs the heat from the interior of the building during the day and releases it to the outside at night. Experiments carried out in Tennessee, USA showed that by using the photovoltaic-PCM roof, the cooling load during summer reduced by about 55% compared to the shingle roof. Furthermore, the heating load during winter reduced by about 30% compared to the shingle roof.

Novais *et al.* [38] manufactured ceramic tiles incorporated with PCM to improve buildings' thermal performance. The PCM ceramic tile consisted of two layers where the PCM was impregnated, under vacuum, into the bottom layer. Experimental results showed that the PCM tiles reduce indoor temperature fluctuations by 22% and improve indoor thermal comfort. The optimum content of the PCM in the ceramic tile was found to be 5.4 wt%, which is a small amount compared to other alternatives of the building parts containing PCMs. The PCM-incorporated tiles reduce building cooling and heating energy consumption compared to conventional tiles without PCM. Additionally, the PCM tiles increase building thermal inertia. Hence, the tiles could be integrated with the under-floor cooling/heating system to store cooling or heating energy in the off-peak periods for use during peak periods to reduce power consumption costs.

To summarize, the applications of PCM in buildings structures for cooling and heating depend on many factors. These factors include melting temperature of PCM, the location of PCM, and the fluctuations in temperature between the daytime and night. The use of PCM could reduce and shift the peak cooling load which leads to reducing the cost of air conditioning device by reducing its capacity.

The integration of PCMs in building envelop is recommended for office buildings because they only occupy on daytime. So the night ventilation used to store free coldness does not

disturb the people. Several studies also showed the capabilities of PCM in reducing the urban heat island effect by reducing the surface temperature.
PCMs should be carefully chosen depending on the application temperature range. The wrong choice of the PCM could increase energy consumption used to cool or heat the building.

2.2.3 Storing off peak cooling from cooling systems

Utilizing the PCM to store cooling and heating energy could reduce the cooling/heating energy consumption by shifting the peak load to off-peak hours. Using PCM to store coldness during a cold night could minimize energy consumption for the cooling system used for charging it, because it works more efficiently at night.
Bruno *et al.* [39] numerically investigated using a PCM-thermal storage unit to store coldness from a domestic chiller to employ it at a peak period. The storage unit is a tube in a tank heat exchanger where the HTF passes through tubes and the PCM was placed in the tank. The results showed that about 13.5% of cooling energy could be saved by utilizing the PCM with a 10°C melting temperature. Additionally, the charging, during the cold part of the night, is an effective strategy to increase energy saving because a cooling device can work with higher efficiency. Moreover, accelerating cold discharge during the day time is important for load shifting which could be achieved by increasing the thermal conductivity of PCM.
Moreno *et al.* [40] experimentally investigated using a cold thermal energy storage (TES) tank to store coldness from a heat pump. The TES was used to store coldness at off-peak periods, then used to cool the building during peak-periods. For this experiment two types of storage tanks of the same size were compared. The first storage tank contained 67 kg of PCM, and the second was filled with water. The experiment was performed by cooling a small house, under summer weather conditions. The results showed that the PCM storage tank could provide 15% additional cold and keep the inside thermal comfort 20% longer, compared to the water storage tank. Due to the poor thermal conductivity of PCM, its

charging process was slower when compared to the water charging process. Hence, the charging time of the PCM tank was about 4.5 times that of the water tank.

Zhai *et al.* [41] experimentally and numerically studied enhancing the thermal performance of PCM in a cold storage unit by using fins and compared it to a unit without fins. The finned PCM-storage unit consisted of a central axis copper finned pipe surrounded by a cylindrical container. The HTF flowed through the pipe while the PCM was contained inside the cylinder. The interior space was divided to 20 sections using 4 rectangular and 4 annular fins. The external surface of the unit was insulated using polyurethane foaming plastic. Melting and solidification for the PCM inside the storage unit were numerically simulated using ANSYS Fluent program. The results showed that by using fins, the phase change time reduced by 70%, compared to the unit without fins.

2.2.4 Storing cold in freezers and refrigerated vehicles

TES systems based on PCMs could be utilized to store coldness from air conditioning or refrigeration systems during off-peak hours to utilize it during peak load hours [42]. This could reduce the electric energy consumption because the cooling systems work more efficiently during off-peak hours, which are normally at night. Utilizing the thermal cold storage could decrease the peak cooling load and this could minimize the capacity of the cooling system and reduce its cost [43]. Moreover, the cold storage systems could also be used to store coldness from solar air conditioning systems for use at night.

Oro *et al.* [44] experimentally studied adding PCMs to a low temperature food storage chamber to evaluate its thermal response under refrigeration system failure. Two PCMs were used in this study (Climsel C-18 and Cristopia E-21), and their responses were compared under the same environment. A 270 L vertical freezer was used as a low temperature storage system in this experiment, where the PCM was encapsulated in a container placed inside the freezer. The volume of the PCM represented 3.36% of the freezer volume. The results indicated that by utilizing the PCM, the temperature of food and air remained at a lower temperature for a longer period when refrigeration system

failure or not worked as compared to the case not utilizing the PCM. Moreover, the use of E-21 as a PCM in the storage system was more effective than C-18 because it maintained the stored food at a lower temperature for a longer period.

Liu *et al.* [45, 46] numerically and experimentally studied developing a new refrigeration system for a refrigerated vehicle by using a PCM thermal storage unit (PCMTSU). The TRANSYS program was used first for numerical simulation. Simulation results indicated that the PCM melting process accelerated and the heat transfer rate improved by increasing the temperature or the mass flow rate of the HTF. Following this, the PCMTSU was experimentally studied. The PCMTSU can be charged with refrigeration using an external stationary electrical refrigeration system, located outside the vehicle when the vehicle is stationary. When the vehicle moves in the road, it uses the stored coolness energy in the PCMTSU to cool the refrigerated products inside it. The PCMTSU consisted of 360 kg of PCM encapsulated inside 27 parallel flat containers, and the gap between the containers was 4 mm. An experimental stationary refrigeration system was used to cool a room with dimensions (3.4 *2.2 *2.2 m). The room was constructed to simulate the thermal performance of the refrigerated space of the refrigerated vehicle. The room walls' material was similar to the refrigerated vehicle, and this room was refrigerated using the PCMTSU. Moreover, the cost of the refrigeration system energy reduced by 86.4% compared to a conventional refrigeration system powered by diesel. Additionally, this system operated with lower noise and fewer greenhouse gases' emissions, compared to the conventional system.

2.2.5 Solar cooling and heating systems

The fluctuating nature of the solar energy used to power solar cooling systems is one of the major disadvantages of these systems. To eliminate this problem, energy storage systems are used to store excess solar energy or the coldness produced by the solar cooling systems for use at night.

Agyenim *et al.* [47, 48] experimentally investigated employing a shell and tube PCM-TES

system to store excess solar thermal energy to operate a solar $LiBr/H_2O$ absorption cooling unit. Three thermal conductivity improvement methods were employed to enhance the poor thermal conductivity of the PCM (Erythritol), which included using: longitudinal fins, circular fins, and a multitube system. The results indicated that the lowest complete melting time was achieved by using the multitube system, followed by the longitudinal finned system, and the circular finned system.

Fan *et al.* [49] numerically and experimentally studied connecting a PCM-TES unit to a solar absorption cooling system for an office building located in the Netherlands. Hydroquinone was used in the proposed application as the PCM because of its lower degree of sub-cooling compared to other PCMs. The results showed that to achieve the peak cooling load demand (100 kW) for a 2400 m^2 building without any other energy source, a 12.55 m^3 PCM-storage system is needed. Numerical results were compared with the experimental results and deviation was observed due to neglecting the convection heat transfer for the liquid PCM in the modelling. Given this, the natural convection heat transfer mechanism cannot be neglected during PCM modelling.

Gil *et al.* [50] experimentally studied the thermal performance of a PCM-TES tank utilized for a solar cooling unit. The PCM-storage tank was used to store and release heat. To simulate the real energy consumption of an absorption chiller, a 20 kW electric boiler was used to heat the HTF during the charging process and a 20 kW air heat exchanger was used to cool the HTF during the discharging process. Two identical shell and tube storage tanks were tested. The only difference between them was that one contained fins in the tube bundle and the other was without fins. The HTF flowed through the tube bundle and the PCM was placed in the shell side. The results showed that in to accelerate the energy discharge process, it is necessary to avoid the possible dead PCM volume in the storage tank. Moreover, using fins is more beneficial for the laminar HTF flow, compared to the turbulent flow.

Godarzi *et al.* [51] used exergoeconomic and genetic algorithms to optimize a $LiBr/H_2O$ absorption solar cooling chiller for an apartment. The exergoeconomic investigation was based on improving the system' thermal performance but taking into account the economic side. After optimizing, a rectangular PCM-thermal storage unit was added to the chiller

to store the thermal energy and use it to operate the chiller when solar radiation was unavailable.

Cheng *et al.* [4] numerically and experimentally studied utilizing a packed bed cold storage system to store coldness for a solar air conditioning system. The cold storage system consists of 450 spherical capsules filled with a PCM, placed in a cylindrical container. The numerical results indicated that the charging capacity of the storage system was highly affected by changing the HTF temperature and less influenced by changing the HTF flow rate. If the HTF temperature increased from 7 °C to 12 °C at a constant HTF flow rate, the charging capacity decreased by more than 40%. Additionally, the exergetic efficiency was highly affected by changing the HTF flow rate. If the HTF flow rate was reduced from 250 L/h to 50 L/h at a constant HTF temperature, the exergetic efficiency increased by more than 38%. Moreover, the solar cooling unit was more stable when integrated with the cold storage system.

Qv *et al.* [52] developed a PCM TES system and connected it to a solar air source heat pump (SAHP) used to cool or heat a building located in Shanghai (China). The TES unit could be utilized to store coldness during the night in summer and employ it during peak load hours. Alternatively, it could be used to store the solar thermal energy during daytime in winter to use it at night. Experimental results showed that the operating performance of the SAHP was enhanced by using the TES system. The cooling COP of the SAHP increased by about 17% when using the TES system.

Hu *et al.* [53] experimentally tested the application of a gravity-assisted heat pipe (GAHP) as a TES in solar cooling applications. The GAHP-TES contained a composite granular PCM. The granular PCM consisted of polyethylene and PCM (RT100), constructed as small balls with 8 mm diameter used as porous PCM, with the HTF (water) flowing between them. The results showed that the GAHP-TES system has a good thermal performance during charging and discharging thermal energy. The study highlighted that the GAHP-TES, by utilizing the PCM, has potential in TES for industrial applications.

Fiorentin *et al.* [54] developed a new PCM TES system. This system was used to store coldness or heat from an air-based photovoltaic-thermal (PVT) collector. This PCM storage system was used to assist an HVAC system, being integrated with it by ducts.

During summer, the system stored coldness by using night-time sky radiation, while during winter the system stored heat by using day time solar radiation. The PVT collector cools or heats the outside air and uses it directly to cool or heat the building or store it in the PCM TES system, to be used later. The efficiency of the PVT collector increased in the winter season because the heat released from it was stored in the TES system and used later to heat the building.

Dheep and Sreekumar [55] experimentally checked the compatibility of utilizing two new PCMs (sebacic acid and benzamide) for TES in solar cooling applications. These materials were exposed to one thousand quick melting and solidification cycles to examine the percentage variation of the melting temperature and the latent heat of melting. The study showed that sebacic acid and benzamide have promising potential for utilization in solar TES, especially in solar absorption cooling.

2.3 Types of heat exchangers utilized for PCMs-TES

Heat exchangers are used to transfer heat from the heat source to the heat storage medium. PCMs used for the LHTES have a low thermal conductivity, which increases their charging and discharging times. Given this, the heat exchangers utilized to store thermal energy in PCMs should be carefully designed by providing a higher effective heat exchange surface area. The main heat exchangers utilized in the LHTES could be divided into three categories: shell and tube heat exchanger (STHX) Fig. 2.2 (a), multi-tube heat exchanger (MTHX) Fig. 2.2 (b), and triple tube heat exchanger (TTHX) Fig. 2.2 (c). In the STHX, the PCM is placed in the shell side and the HTF flows through the tube. In the MTHX the PCM is placed in the shell side and the HTF flows through the inner tubes. In the TTHX the PCM is placed in the middle tube and the HTF flows through the inner and outer tubes.

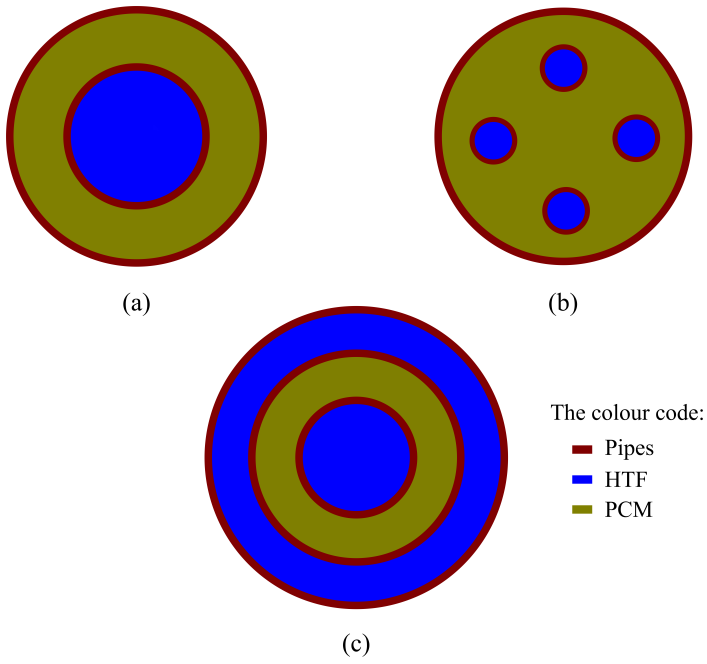

Figure 2.2: Cross sectional area of various types of heat exchangers (a) shell and tube heat exchanger; (b) multi-tube heat exchanger; and (c) triple tube heat exchanger.

2.4 Heat transfer enhancement techniques

The poor thermal conductivity of PCMs weakens their thermal response and increases the time needed to store/release the thermal energy in the PCMs, thereby, limiting their widespread utilization. Therefore, heat transfer enhancement techniques should be employed to improve the thermal response of PCMs to make them suitable for usage in LHTES systems.

Numerous heat transfer enhancement methods have been used to improve the poor thermal performance of PCMs. These methods included utilizing extended metal surfaces (fins), using multiple PCMs (cascaded storage), dispersion of high thermal conductivity nanoparticles into PCM, and utilizing porous materials. Fig. 2.3 illustrates most of heat enhancement techniques utilized with TES systems based on PCMs.

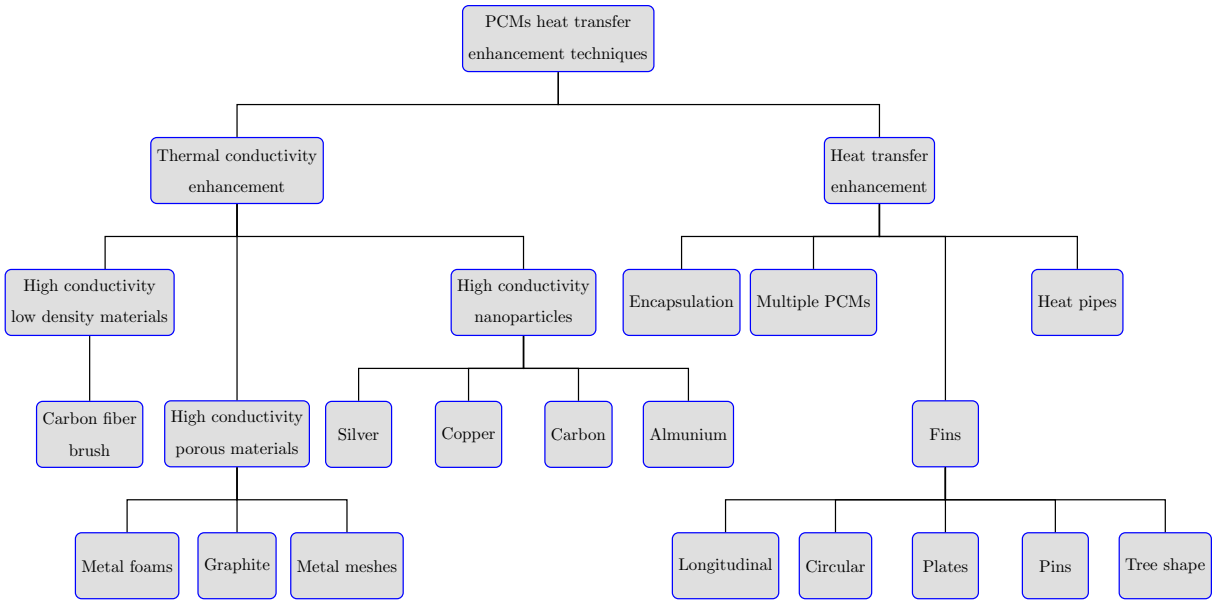

Figure 2.3: PCMs heat transfer enhancement techniques.

2.4.1 Enhancement by utilizing fins

Using fins to enhance the thermal performance of PCMs is a particularly desirable method because of the effectiveness in performance, low construction cost, and easy fabrication [18]. It is also relatively easy to optimize the design of the fins by using computer simulation programs, and this reduces the research cost. Fins improve heat transfer between PCM and HTF due to increasing the heat transfer area. Various fin types have been utilized to enhance the thermal performance of LHTES systems, including longitudinal fins and circular fins. Many studies have been published about the usage of fins to enhance the thermal performance of PCMs.

An early study on using fins to enhance the thermal performance of PCM was undertaken by Lacroix [56]. The author developed a mathematical model to study utilizing annular fins to improve the thermal performance of PCM in a shell and tube heat exchanger (STHX). The theoretical model was then validated with the experimental data. The theoretical results showed that the fins are more effective for low HTF temperatures and moderate HTF flow rates.

Agyenim [48] experimentally investigated enhancing the thermal performance of PCM in a STHX by utilizing different fin shapes, and multitubes. The fins' shapes tested included longitudinal fins and circular fins. The PCM was placed in the shell side, with the HTF circulating through the tube/tubes. The experiments were performed by comparing the complete charging (melting) and discharging (solidification) times by utilizing these techniques. The results indicated that the shortest melting time was achieved by utilizing multitubes. During the discharging process, the best thermal performance was achieved when using the longitudinal fins. The researcher recommended studying the integration of multitubes together with longitudinal fins to improve the charging/discharging process.
Sciacovelli *et al.* [57] conducted a numerical study to enhance the thermal performance of PCM in a STHX by introducing Y-shaped fins (Fig. 2.4). The optimum design of the Y-fin shape by using single and double Y-fin bifurcations and the effect of the fin's bifurcation angle were studied. The results indicated that the optimum fin shape was the Y-fins shape with two bifurcations; by utilizing them, the thermal storage system efficiency increased by 24%. The results indicated that using fins with a small bifurcation angle is preferred for a long operation time, while using fins with a large bifurcation angle is better for a short operating time.

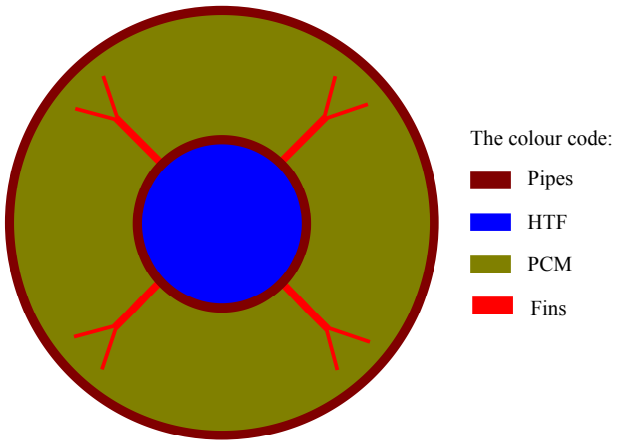

Figure 2.4: Shell and tube TES system with Y fins shape.

Ji *et al.* [58] numerically studied the influence of the direction of plate fins on heat distribution in a PCM contained in a rectangular enclosure, vertically heated from

the left side (Fig. 2.5). The melting process was investigated. The rectangular PCM container contained two parallel plate fins. Fins with different inclination angles were tested which were: 0°, 15°, 30°, -15° and -30° from the horizontal. The results showed that by using inclined fins towards the top, the non-uniform heat distribution increased, whereas using downward inclined fins decreased the non-uniform heat distribution. The total PCM charging time increased by using the fins inclined upward as compared to the case with horizontal fins, while it decreased by using the downward inclined fins. The results also indicated that the melting time increased by 71% when utilizing fins inclined by +30°, in comparison to using horizontal fins. The melting time decreased by about 23% when using fins inclined by -15°. Moreover, the length of the fins has a significant impact on the charging process; by increasing the fins' length the total PCM melting rate increased.

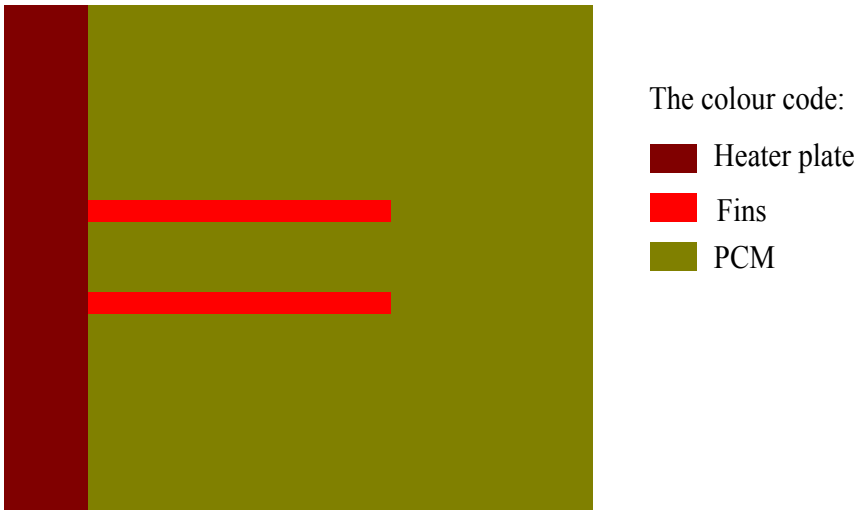

Figure 2.5: PCM rectangular container with two parallel plate fins.

Rozenfeld *et al.* [59] numerically and experimentally studied the thermal performance enhancement for PCM in shell and tube LHTES by utilizing novel helical fins. These fins were welded to the HTF tube to increase the heat transfer area. The HTF flows through the tube and the PCM was placed in the shell side. Two experimental tests were performed to compare the PCM melting time. In the first test, the PCM shell was exposed to the ambient air, while, in the second, the PCM shell was exposed to slight heating to

obtain close contact melting to accelerate the melting process. Results showed that the melting time reduced by a third by utilizing the helical fins and close contact melting.

Agyenim *et al.* [47] experimentally studied enhancing the PCM thermal performance in a STHX by utilizing longitudinal fins. The system was connected to a solar absorption cooling unit. The HTF passes through the tube and the PCM (Erythritol) was contained in the shell side. Eight longitudinal fins were welded to the external surface of the HTF tube. The experiments were done by performing the charging/discharging process to determine the optimum HTF temperature and mass flow rate to operate the absorption cooling unit. The results indicated that the optimum mass flow rate of HTF and HTF temperature to charge the PCM to operate the solar absorption cooling unit were 30 kg and 140 °C respectively.

Khan *et al.* [60] numerically studied enhancing the PCM melting process in the shell and tubes LHTES system. The PCM (paraffin) was placed in the shell side with the HTF passing through the tubes. To increase the heat transfer area, longitudinal fins were connected to the outside surfaces of the HTF tubes. The results indicated that the PCM melting process accelerated if the number of HTF tubes increased. The melting time was minimized by more than 40% if the HTF tubes increased from 12 to 21. Furthermore, increasing fins' length has a strong influence on the charging process compared to the increasing thickness of fins, which has a weak influence. If the fins' length changed from 12.7 mm to 38.1 mm the charging time decreased to half. Moreover, if the HTF temperature was raised from 50 °C to 70 °C the melting time reduced by 60%.

Ismail *et al.* [61] experimentally and numerically investigated utilizing fins to accelerate the PCM solidification process in a STHX. The PCM was contained in the shell side with the HTF passing through the inner tube. Many factors were studied to show their effect on the PCM solidification process. These factors included the dimensions of fins, the number of fins, and the difference in temperature between the PCM and the HTF. The results indicated that fins' length and the number of fins have a strong effect on the solidification process. However, the fins' thickness has a weak effect on the solidification process. Moreover, the solidification process accelerated by increasing the difference in temperature between the PCM and the HTF.

Rathod and Banerjee [62] experimentally compared the solidification and melting time for PCM in a STHX, with and without fins. The HTF flows through the tube while the PCM was contained in the shell. The effect of changing the HTF flow rate and the HTF temperature were investigated. Three longitudinal fins were welded to the HTF tube to improve the thermal performance of the PCM. Results indicated that the solidification time reduced by 40% when using fins, compared to not using them. Moreover, increasing the difference in temperature between the PCM and the HTF was a more significant influence on the melting/solidification process, compared to increasing the HTF flow rate.

Yuan *et al.* [63] numerically studied the influence of fin direction on the PCM melting process in a STHX. Two centrally symmetric longitudinal fins with different installation angles were used. The fins' installation angles investigated were: 0° (vertical), 30°, 45°, 60°, and 90° (horizontal). The results showed that the best position for the fin is the vertical position. Moreover, to minimize the PCM melting time, fins should be installed in the lower part of the PCM shell. Additionally, if the HTF temperature was raised from 60 °C to 80 °C, the PCM melting time decreased by 50%.

Al-Abidi *et al.* [64] numerically investigated accelerating the PCM melting process in a triple tube heat exchanger (TTHX) for a LHTES system, by using longitudinal fins. This system was used to store thermal energy to power a liquid desiccant cooling system. A 2D numerical model was used in the simulation by considering the natural convection heat transfer mechanism. The HTF flows through the internal and external tubes and the PCM (RT82) was placed in the middle tube. Many factors were investigated, including the HTF temperature, fins' dimensions, and the number of fins. The results indicated that the length of fins has a strong influence on the melting process compared to fin thickness' which has a weak influence. Additionally, the PCM melting time reduced by more than 60% when using eight fins, compared to the case without fins.

Mat *et al.* [65] numerically studied the PCM melting process in a TTHX. The PCM (RT82) was contained in the middle tube, with the HTF (hot water) flowing through the inner and outer tubes. Three methods of PCM heating were tested: heating by using the inner tube only, heating by using the outer tube only and heating by using both inner and outer tube. The results indicated that heating by using both the outer and inner tube required a

lower total melting time, followed by heating using the outer tube only. However, heating using only the inner tube needed a longer melting time. Additionally, the influence of welding longitudinal fins to the external surface of the inner tube (internal fins) only, or these being welded to the internal surface of the middle tube (external fins) only, or welded to both the inner and the middle tubes, were investigated. The results indicated that the PCM melting time decreased to 43.3% when utilizing the TTHX with eight internal and external fins, as compared to the TTHX without fins. Furthermore, there was no significant difference between different fins' positions (inner or outer or both inner and outer) on the total PCM melting time.

Al-Abidi *et al.* [18] numerically studied enhancing the PCM solidification process in a TTHX LHTES system by utilizing internal and external longitudinal fins. Three methods were used to pass the HTF to release the thermal energy from the PCM which:- passing the HTF through the inner tube only, passing the HTF through the outer tube only, and passing the HTF in both the outer and inner tube. Results indicated that the solidification process was completed in less time when passing the HTF in both the outer and inner tube, compared to the inner tube only or the outer tube only. Many factors were studied to show their effect on the solidification process. These included fins' dimensions and the number of fins. The results indicated that the solidification rate increased significantly by increasing the fins' length, due to the increase in the heat transfer area. However, increasing the fin' thickness had a weak effect on the PCM solidification process. Moreover, the solidification process accelerated by increasing the number of fins. Additionally, utilizing the TTHX with eight fins, with the HTF passing through the inner and outer tubes, meant the complete solidification time reduced to 39% compared to the TTHX with the same number of fins where the HTF passed through the inner tube only.

Al-Abidi *et al.* [66] experimentally investigated enhancing the PCM solidification and melting process in a TTHX by utilizing internal and external fins. The influence of changing the HTF flow rate and HTF temperature were investigated. Results indicated that the HTF temperature has a strong effect on the PCM solidification/melting process compared to the HTF flow rate, which has a weak effect.

Many researchers have recommended using longitudinal fins in a STHX because they

greatly enhance conduction and convection heat transfer rates in comparison to circular fins [67].

2.4.2 Enhancement by utilizing multiple PCMs

Utilization of multiple PCMs means that the LHTES system contains more than one kind of PCM, with different melting temperatures, placed layer by layer either in the radial orientation or in the HTF flow orientation [68]. Compared to the conventional single PCM storage systems, the multiple PCMs storage systems could improve the efficiency of energy storage systems [69]. The heat transfer to the PCM during energy storage/release depends on the difference in temperature between the PCM melting temperature and the HTF temperature. When utilizing a single PCM, the difference in temperature between the PCM and the HTF decreased in the flow direction, thereby reducing the heat transfer rate. Utilizing multiple PCMs with various melting temperatures, and arranging them in series in the HTF flow direction in decreasing order of their melting temperature, leads to a nearly constant heat flow rate in the flow direction. However, the HTF temperature decreased in the direction of flow during the melting (charging) process. During the solidification (discharging) process, if the HTF flow direction is inverted the PCMs stay in an increasing arrangement of their melting temperature, meaning a roughly constant temperature difference between the HTF and the PCMs could be achieved. The working principle of multiple PCMS LHTES system is illustrated in Fig. 2.6.

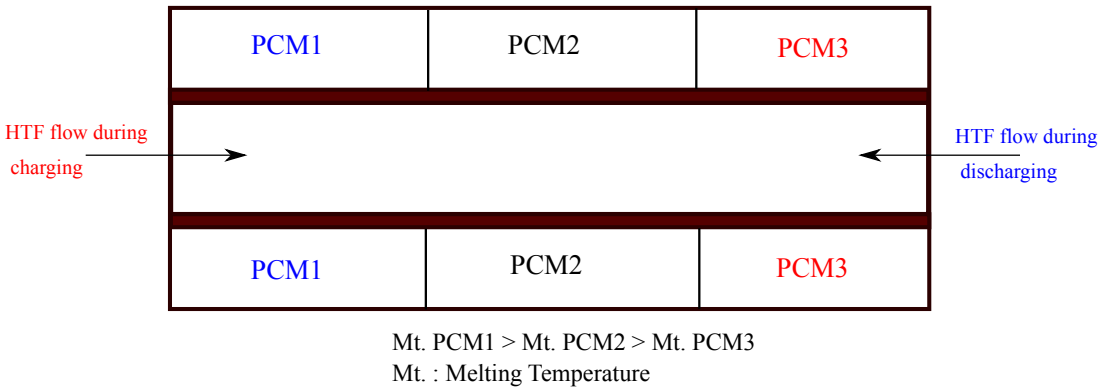

Figure 2.6: Multiple PCMs on a shell and tube LHTES system.

Seeniraj and Narasimhan [70] numerically studied enhancing the thermal performance of the LHTES system by using a multiple PCMs system and compared it to the single PCM system. In results, the multiple PCMs system showed better thermal performance compared to the single PCM system. In another study, Tian [13] also numerically and experimentally investigated using multiple PCMs in a TES system and compared it with the single PCM system. The results showed that utilizing the multiple PCMs can increase the heat transfer rate as compared to the single PCM system.

Sefidan *et al.* [71] investigated numerically the solidification process for a double layer of different PCMs with different melting temperatures in a TTHX, to compare it with a double layer of the same PCM. The TTHX consisted of three concentric tubes where the PCMs were contained in the outer and middle tubes, with the HTF flowing through the inner tube see Fig. 2.7 (a). Two PCMs with different melting temperatures were used in this study, which included RT35 and RT50. A 2D numerical model was utilized in the simulation see Fig. 2.7 (b). The boundary conditions used were a constant HTF temperature applied to the inner tube wall, while the outer tube was thermally insulated. Several factors were investigated to show their effect on the total PCMs solidification time. These factors included: various PCMs arrangements, PCMs layer thickness, changing the HTF temperature, and fins' dimensions. The results showed that when the PCM (RT35) was placed in the middle annulus and the PCM (RT50) was placed in the outer annulus the solidification time reduced compared to when the PCM (RT50) was placed in the middle annulus and the PCM (RT35) was placed in the outer annulus. Moreover, the solidification process in both PCMs sections accelerated by reducing the HTF temperature.

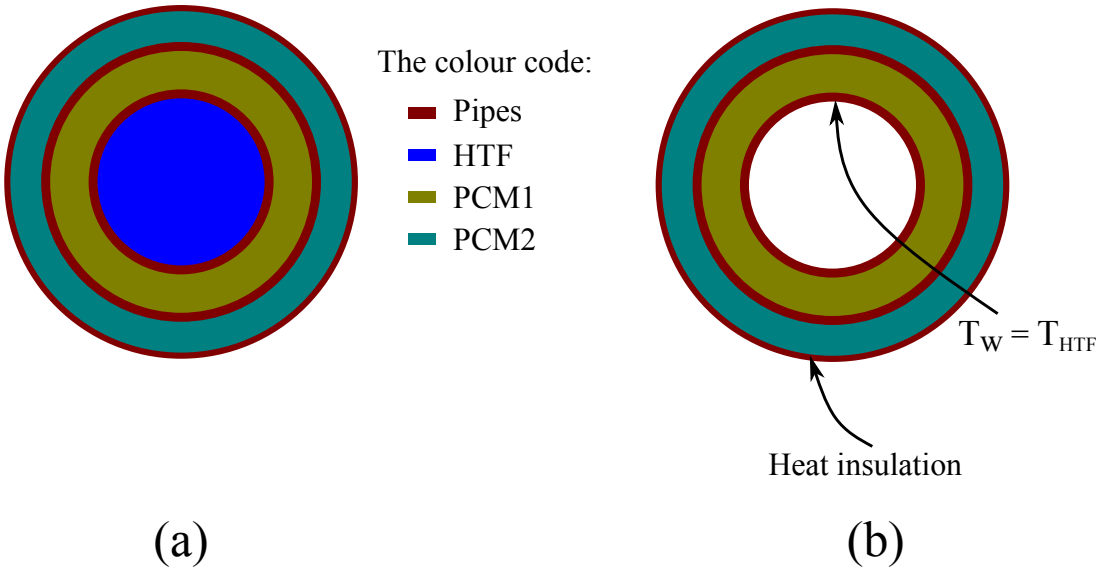

Figure 2.7: Multiple PCMs in a triple tube heat exchanger (a) the cross-sectional area of the physical model; (b) computational domain with the indicated boundary conditions.

2.4.3 Enhancement by using nanoparticles

The poor thermal conductivity of PCMs delays the thermal response and increases thermal energy storage/release times. Hence, nanoparticles with high thermal conductivity could be inserted into the PCMs to enhance their thermal performance. Nanoparticles can be divided into metallic nanoparticles and carbon-based nanoparticles. The commonly used carbon-based nanoparticles include: graphite, carbon nano-tubes, and carbon fibre [9]. Mahdi and Nsofor [15] conducted a numerical study to accelerate the PCM solidification process in a TTHX by utilizing nanoparticles and longitudinal fins. Alumina was used as nanoparticles and RT82 was used as PCM. Several factors were investigated to show their effect on the PCM solidification process. These factors included volume concentration of nanoparticles and the dimensions of fins. Various fins and nanoparticles arrangements were tested, which included utilizing fins alone, utilizing nanoparticles alone, and utilizing a combination of both nanoparticles and fins. In results, for the same volume usage, utilizing fins alone showed better thermal enhancement and reduced the PCM solidification time when compared to using a combination of nanoparticles and fins or nanoparticles alone.

Abdulateef *et al.* [72] numerically studied enhancing PCM thermal performance in a TTHX by utilizing nanoparticles and longitudinal fins. Three fins' positions were tested. Fins were welded to the internal surface of the middle tube only, fins were welded to the external surface of the inner tube only, and fins were welded to both the inner and middle tubes. Results indicated that the PCM completely melted in a shorter time when fins were welded to the middle tube only, compared to the other cases. Additionally, the PCM total melting time for fins welded to the middle tube reduced by 17% if 10% of the nanoparticles (alumina) were added to the PCM.

Al-Maghalseh [73] numerically studied enhancing thermal performance for PCM in a STHX by utilizing metal nanoparticles. The HTF passes through the tube and PCM was placed in the shell side. Three nanoparticles types were tested: Al_2O_3, ZnO and CuO. The results indicated that the PCM melting time reduced by 31.7%, 28.6% and 27.2% when using 6% volume concentration of CuO, Al_2O_3 and ZnO respectively.

Seki *et al.* [74] prepared binary mixtures of sebacic acid (SA) and adipic acid (AA) to test their potential when utilized as a PCM for a solar TES application. The binary mixture of the SA and the AA with a ratio of 52:48% by weight has a latent heat of melting of 206 kJ/kg and a melting temperature of 116 °C. Multilayer graphite nanoplates (GNP) were loaded into the SA-AA mixture to improve its thermal conductivity. The results showed that adding 0.5% by weight of the GNP into the SA-AA mixture improved thermal conductivity. The study highlighted the potential use of the SA-AA eutectic mixture loaded with GNP as a new PCM for high-temperature applications, especially for solar absorption cooling systems.

Hosseinzadeh *et al.* [75] numerically investigated accelerating the PCM solidification process in a STHX by employing nanoparticles and tree-like branching fins. TiO_2-Cu was utilized as nanoparticles and water was used as the PCM. The effects of different parameters were investigated which included: the fins' bifurcation angle and the nanoparticles shape factor. The results indicated that the PCM solidification process accelerated by increasing the nanoparticles' shape factor. Moreover, increasing the fins' bifurcation angles enhanced the thermal penetration depth, hence accelerating the solidification process.

It should be noted that the employment of high conductivity nanoparticles to enhance PCM

thermal conductivity suffers from a problem associated with particle sedimentation [76].

2.4.4 Enhancement by using metal foams

Metal foams, like aluminium and copper, have high porosity and thermal conductivity, so they are utilized to improve the thermal performance of PCMs.
Liu *et al.* [77] numerically studied enhancing the thermal conductivity of PCM in a STHX by incorporating it into metal foam (Fig. 2.8). Many factors were investigated to show their influence on PCM melting which included: the structural parameter of the metal foam and the effect of changing HTF temperature. The results indicated that the heat transfer rate when utilizing metal foam increased by seven times, as compared to using pure PCM. Moreover, the metal foam structural parameters have significant influences on the PCM melting process.

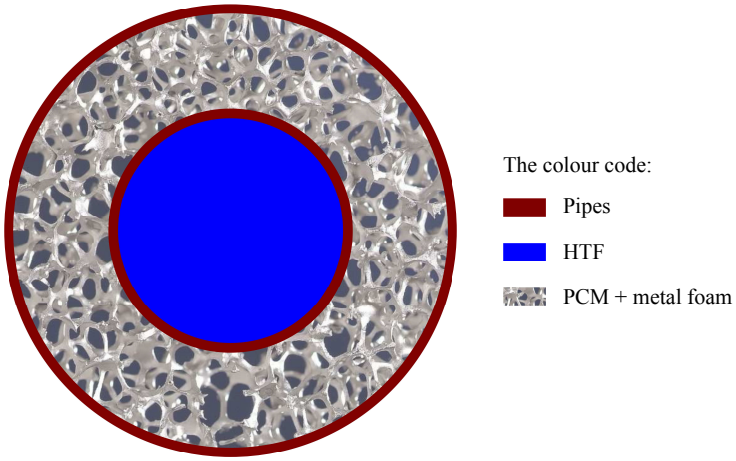

Figure 2.8: PCMs thermal conductivity enhancement on a STHX by using metal foam.

Mahdi and Nsofor [78] numerically investigated enhancing the PCM solidification rate in a TTHX by utilizing a combination of metal foam and nanoparticles. Many factors were studied to show their effect on the PCM solidification process, which included: metal foam porosity and nanoparticles volume fraction. The results indicated that the PCM solidification process accelerated significantly by using the copper foam. Moreover, the solidification process could be accelerated further by dispersion of alumina nanoparticles.

When using a combination of metal foam and nanoparticles, the PCM had complete solidification in a shorter time, compared to cases using the metal foam alone or the nanoparticles alone.

Tian *et al.* [79] numerically investigated enhancing the thermal performance of PCM by utilizing metal foams. The results showed that the heat transfer of PCMs enhanced by more than ten times when utilizing the metal foam, compared to pure PCM. Moreover, the metal foams with smaller porosity and small pore size achieved better thermal performance when compared to those with higher porosity and larger pore size.

Mahdi and Nsofor [80] numerically investigated enhancing the thermal performance of PCM in a STHX by utilizing cascaded or multiple-segment metal foams with different porosities. The metal foam segments were arranged by increasing porosity in the heat flow direction. Four cascading configurations of metal foams, with an average porosity of 0.95, were tested and compared (Fig. 2.9). The results indicated that the PCM charging and discharging times reduced when using multiple-segment metal foam as compared to single segment metal foam.

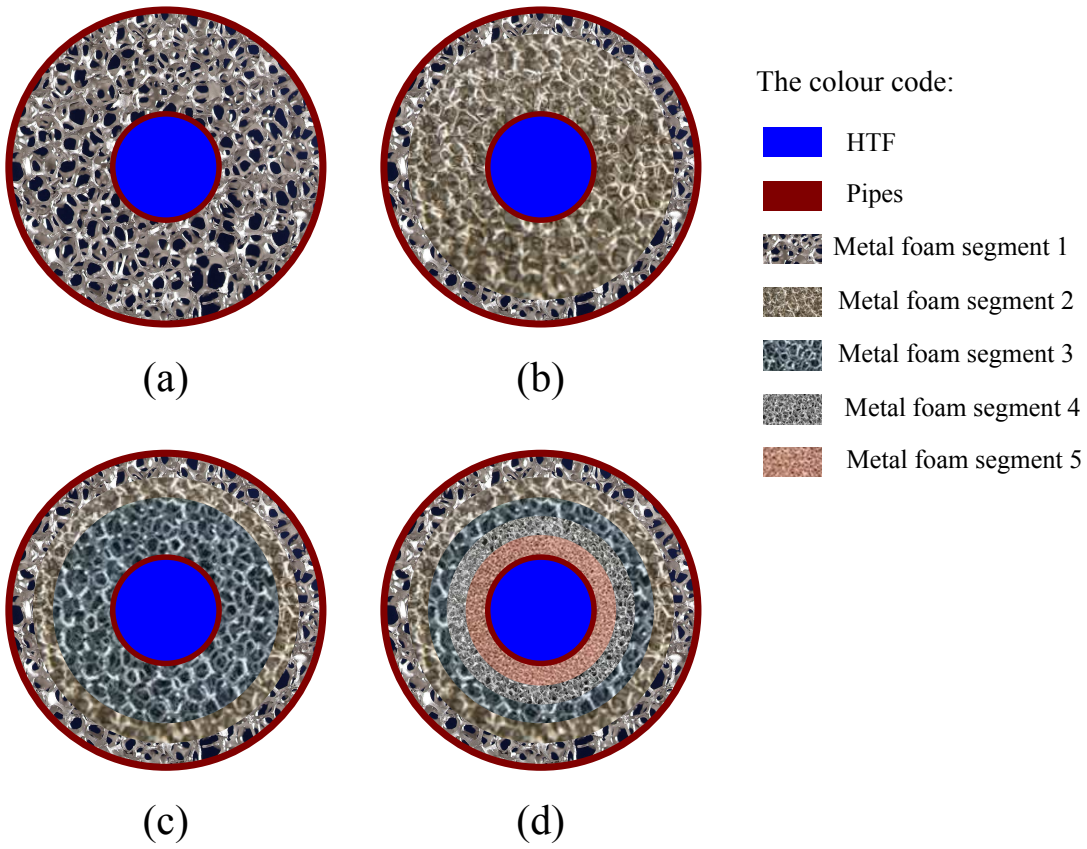

Figure 2.9: PCM embedded in multiple-segment of metal foams in STHX: (a) 1-segment, (b) 2-segment, (c) 3-segment, and (d) 5-segment.

2.4.5 Enhancement by using expanded graphite

Mixing liquid PCMs with expanded graphite, which has a high absorbability and high thermal conductivity, can boost their thermal conductivity and increase the heat transfer rates of LHTES systems.

Wang *et al.* [81] experimentally prepared a composite sebacic acid/expanded graphite (SA/EG) to use it as a PCM for TES in the solar application. The composite of the SA/EG PCM consisted of 85% SA and 15% EG by mass. Liquid leakage was prevented because the SA uniformly distributed in the EG pores. The SA/EG latent heat and melting temperature were experimentally determined and were equal to 187 kJ/kg and 128 °C respectively. The SA/EG composite has better thermal conductivity and lower extent of

sub-cooling compared to the SA alone. These properties make the composite SA/EG a promising PCM for solar TES applications.

2.4.6 Enhancement by modifying the geometry of the heat exchanger

Agyenim *et al.* [82] experimentally compared the thermal performance of a STHX with a single HTF tube with a STHX with a multi-tube HTF. The PCM (Erythritol) was placed in the shell side, with the HTF passing through the HTF tube/tubes. The same amount of PCM was used during both tests. Melting and solidification processes were investigated. Hot oil was used as a HTF for the melting process while water was utilized as a HTF for the solidification process. The results indicated that the solidification/melting processes accelerated when utilizing the multi-tube HTF system, compared to utilizing the single tube HTF system.

Esapour *et al.* [83] numerically investigated the use of a multi-tube instead of the inner tube in the triple tube heat exchanger to accelerate the PCM melting process. To evaluate the proposed design, it was compared with the triple tube heat exchanger (TTHX). The HTF passes through the inner tube/tubes and outer tube, and the PCM (RT35) was placed in the middle tube (Fig. 2.10). The effect of changing the number of inner HTF tubes on the PCM melting process was studied. To utilize the same amount of PCM in all cases, the diameters of the tubes were carefully chosen. The results indicated that if the number of the inner HTF tubes increased from one (TTHX) to four, the heat transfer rate increased and the melting time reduced by 29%. In another study Esapour *et al.* [84] also numerically studied the influence of inner tubes' position on the PCM melting process. It was concluded that for the same inner tubes numbers, the PCM melting process accelerated by increasing the number of the HTF tubes in the lower half of the PCM shell.

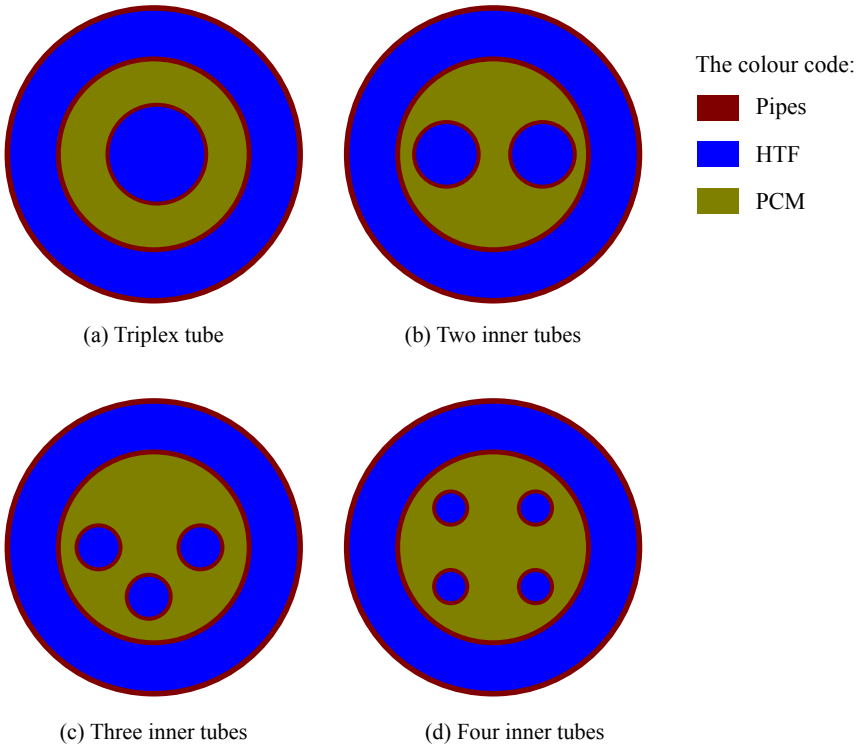

Figure 2.10: Physical configurations of multi-tube heat exchanger in comparison with the triplex tube heat exchanger.

Dandotiya and Banker [85] numerically investigated utilizing a multi-tube heat exchanger (MTHX) integrated with various fins' configurations to improve the thermal performance of PCM. The MTHX consisted of four inner tubes contained in the shell. The HTF passes through the inner tubes and the PCM was placed in the shell side. Two modifications were suggested to enhance the thermal performance of the heat exchanger. In the first modification, two fins were utilized to connect the four inner tubes diagonally, while in the second, two perpendicular fins were arranged between the four inner tubes. The same amount of PCM was used in all cases; this was achieved by carefully changing the diameters of the HTF tubes. The results showed that the total PCM melting reduced by 26.3% when connecting the inner tubes diagonally by using fins, in comparison to the case without fins. Moreover, the total PCM melting time decreased by about 42% when using two perpendicular fins between the inner tubes, as compared to the base case without fins.

Pahamli *et al.* [86] numerically studied enhancing PCM thermal performance in a double pipe TES system. A three-dimensional numerical model was used in the simulation. Natural convection was considered during the simulation. The HTF (water) flows through the inner pipe, while the PCM (RT50) was placed between the inner and outer pipe. The downward movement of the inner pipe (HTF-pipe) from the centre was studied to investigate the influence of the natural convection on the PCM melting. The inner pipe was moved downward from the centre by 7.5, 15 and 22.5 mm. The influences of changing the HTF mass flow rate and the HTF temperature were also studied. The results showed that the conduction was the predominant heat transfer mechanism at the start of the charging process. Then, after part of PCM had melted, the natural convection became the predominant heat transfer mechanism. The melted PCM in the upper part of the shell was more, compared to the lower part, due to the buoyancy effect. The total PCM melting time reduced by 64% if the HTF-pipe was moved downward from the centre by 22.5 mm. Moreover, the melting process accelerated by increasing the HTF temperature. However, changing the HTF mass flow rate has a weak influence on the PCM melting process.

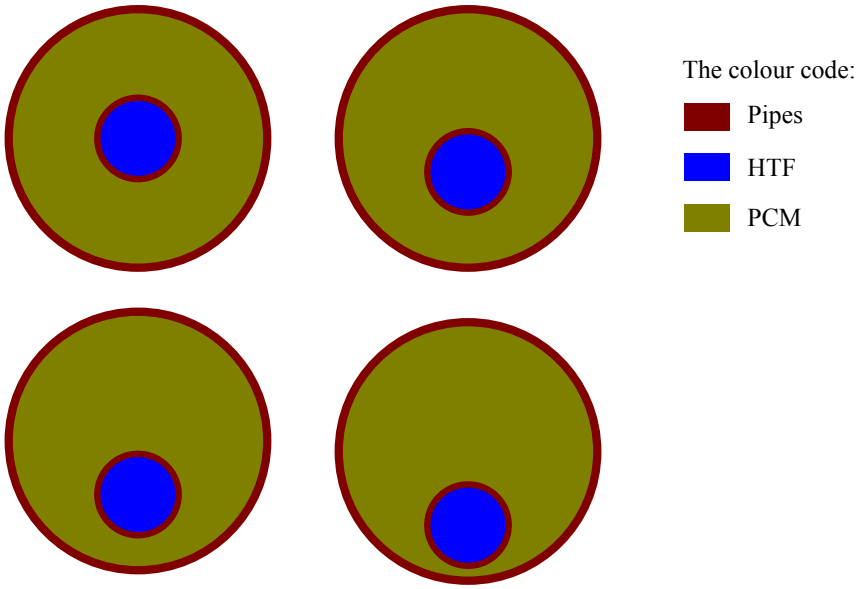

Figure 2.11: Various downward movements for inner HTF pipe.

Alizadeh *et al.* [87] numerically investigated enhancing the PCM thermal performance in a STHX by using the Koch snowflake fractal pattern for the inner tube. The HTF

flows through the tube, which has the Koch snowflake fractal pattern cross-section and the PCM was placed in the shell side. The Galerkin Finite Element Method was used to simulate the PCM (water) solidification process. A two-dimensional numerical model was used in the simulation. The zero and first three fractal pattern iterations (n) were tested to show their effect on the PCM solidification process (Fig. 2.12). The results showed that utilizing the Koch snowflake fractal pattern cross-section with higher iterations accelerated solidification process. This is due to the increase in heat transfer area and the enhancement of thermal penetration depth.

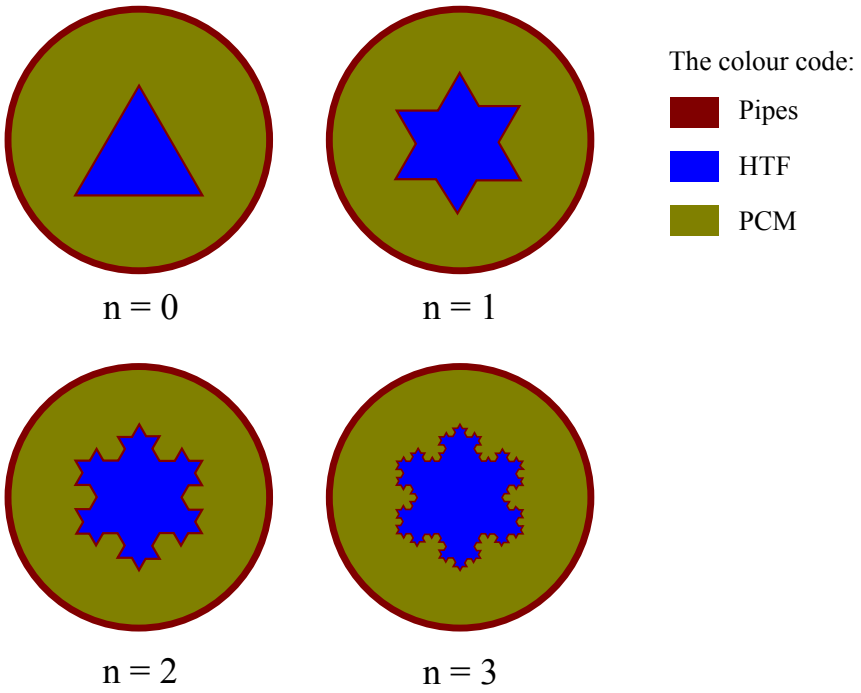

Figure 2.12: LHTES system with the Koch snowflake fractal pattern for inner HTF tube.

Pourakabar and Darzi [88] numerically studied the PCM melting and solidification processes in a STHX, using various shell shapes and a different number of inner tubes to find the best configuration (Fig. 2.13). an elliptical shell shape was introduced and compared with the conventional circular shape. The PCM was placed in the shell side with the HTF passing through the inner tube/tubes. The results showed that the shortest complete melting and solidification time was achieved when using the circular shell shape with four inner tubes in a diamond array.

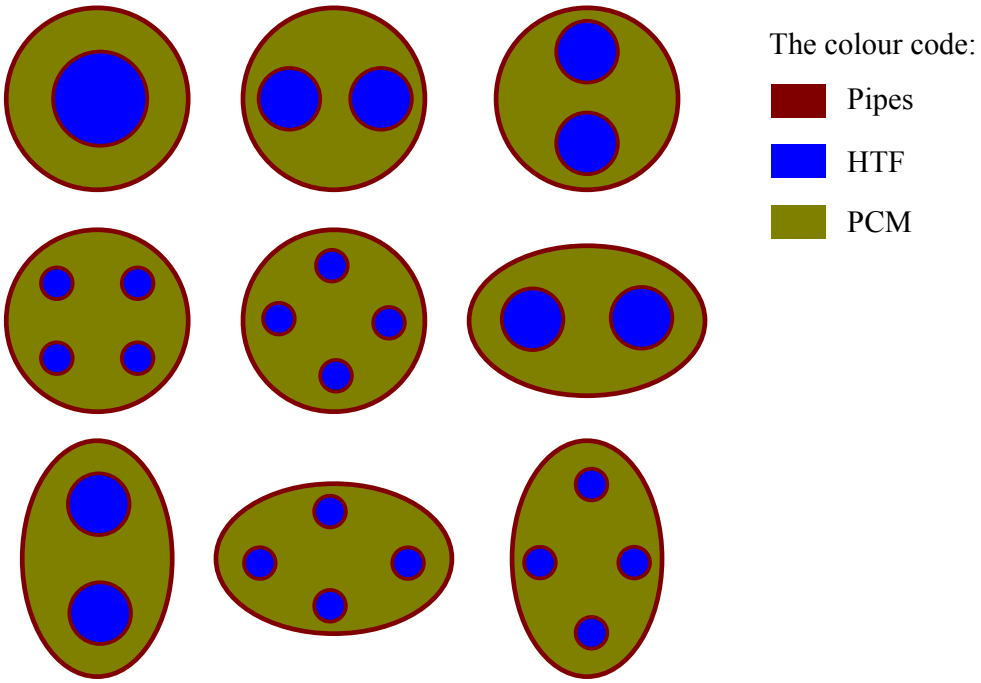

Figure 2.13: Physical configurations of a STHX with different shell shapes and different numbers of inner tubes.

2.5 Conclusions and scope of the present work

Energy storage systems are needed to correct the mismatch between energy generation and energy demand, as well as to store excess energy or free energy that could otherwise, be wasted. There are many types of energy storage methods which include, mechanical, electric and thermal.

The thermal energy storage system has a higher energy storage density and low cost when compared to other energy storage techniques. There are three methods to store thermal energy: sensible, latent and thermochemical. The latent heat storage method is preferred because of its high energy storage capacity and little variation in temperature during the energy storage process, compared to the sensible heat storage method. The latent heat storage materials could store 5-14 times higher energy compared to sensible heat storage materials with the same volume. The materials used for latent heat storage are called

PCMs. One of the major disadvantages of PCMs is the poor thermal conductivity. To improve the thermal performance of PCMs, various heat transfer enhancement techniques have been considered. The heat transfer enhancement techniques included the utilization of fins, utilizing porous materials, dispersion of high thermal conductivity nanoparticles into the PCM and utilizing multiple PCMs.

Most heat transfer enhancement techniques of PCMs have been based on the application of fins because of their easy design, low cost, and they require less maintenance during the operation, compared to the dispersion of nanoparticles and the usage of porous materials [57]. The thermal performance of PCMs showed better improvement by utilizing fins, compared to using nanoparticles [15, 89]. The types of fins that were considered to improve the thermal performance of energy storage systems include longitudinal, annular, plates and pins fins. Better thermal performance was achieved by utilizing longitudinal fins, especially with cylindrical PCM containers.

The fins inserted into the PCM side of the LHTES systems, do not affect the HTF flow and they do not cause a pressure drop in it. This feature is their advantage compared with other non-PCMs systems. Although considerable research has been devoted to utilizing fins to improve the thermal performance of PCMs TES systems, rather less attention has been paid to the geometric design of fins. The geometric design of fins has a strong influence on the energy storage/release for TES systems based on PCMs [2]. More research is still required to explore possible innovative geometric designs of the fins to improve the thermal performance of PCMs-LHTES systems and to reduce charging/discharging time.

In this thesis, innovative fin shapes are suggested to improve heat transfer thermal performance for thermal energy storage systems based on PCMs and compared with traditional fins shapes to evaluate their performance.

Moreover, this literature review has shown that, changing the heat exchanger geometry could enhance the thermal performance of PCMs TES systems. Heat exchangers must be designed to permit rapid thermal energy storage/release rate by increasing the heat transfer surface area. Consequently, an innovative heat exchanger geometry (webbed

tube heat exchanger) is introduced in this thesis to improve thermal performance of TES systems based on PCMs. In order to evaluate the thermal performance of the webbed tube heat exchanger, a comparison has been done with traditional heat exchangers.

The numerical approaches offer a good platform to solve the phase change problem. Most numerical and analytical solutions for PCMs problems presented in the literature are based on one or two-dimensional space, due to the complexity of the phase change problem. Utilizing numerical simulation to optimize the design of PCM TES systems is an effective way to save time and money. Many CFD packages have been utilized to simulate PCM thermal performance such as Comsol Multiphysics, ANSYS Fluent, and Star-CCM+. The most frequently used software in the literature reviewed was ANSYS Fluent.

Chapter 3

Numerical Methodology

This chapter describes the equations involved in the heat transfer process for the materials undertaking phase change process. The key feature for solidification/melting (phase change) process which known as Stefan problem is the presence of a moving boundary between solid and liquid phase. This made complexity in the computation of heat transfer due to the difficulty of modelling the velocity field.

In this work, ANSYS Fluent is used in the numerical simulations. The mathematical equations employed to solve the melting and solidification process in Fluent depend on the finite volume method and enthalpy-porosity technique.

3.1 Governing equations

The governing equations for PCM which include continuity, momentum and energy equations could be written as follows [64]:-

Continuity equation:-

$$\partial_t(\rho) + \partial_i(\rho u_i) = 0 \tag{3.1}$$

Momentum equation:-

$$\partial_t(\rho u_i) + \partial_i(\rho u_i u_j) = \mu \partial_{jj} u_i - \partial_i p + \rho g_i + S_i \tag{3.2}$$

Energy equation:-

$$\partial_t(\rho h) + \partial_t(\rho \Delta H) + \partial_i(\rho u_i h) = \partial_i(k \partial_i T) \tag{3.3}$$

Where ρ is the PCM density, μ is the dynamic viscosity of fluid, u_i is the fluid velocity, g_i is the gravity acceleration, p is the pressure, S_i is the Darcy source term, h is the sensible enthalpy, k is the thermal conductivity, T is the temperature and ΔH is the latent heat.

3.2 Simplifications and assumptions

In order to simplify the solution of fluid equations, the following assumptions were made which include [90, 71]:-

1. The flow was unsteady, laminar and incompressible.
2. Constant thermo-physical properties of the PCM and independent on temperature.
3. The influence of natural convection during PCM solidification/melting process is considered by using the Boussinesq approximation, which takes into account the PCM density change due to buoyancy force.

3.3 The enthalpy-porosity technique

The enthalpy-porosity technique presented by Voller *et al.* [91] is utilized for the numerical solution of the phase change problems with the mushy zone (solid plus liquid). In this technique, the solid-liquid mushy region is treated as a porous region with porosity equal to the liquid fraction which lies between zero (solid) and 1 (liquid) [92]. When the material solidifies the porosity decreases from 1 to 0. As the material completely solidified, the porosity becomes zero, thereby the velocity drop to zero. The main feature of this method is the representation of latent heat and flow in the mushy zone with suitable source terms.

The simplicity of tracking the solid-liquid interface of this approach led to simplification numerical modelling requirement.

3.3.1 The latent heat source term

The key feature of the enthalpy-porosity technique for the phase change problems is the usage of the latent heat source term in the energy equation. The total enthalpy, for a system undergoing a change of phase under heat transfer, is expressed
as [93]:-

$$H = h + \Delta H \tag{3.4}$$

Where h is the sensible enthalpy, $\Delta H = \gamma$ L is the latent heat content which depends on temperature and could change between (L) for liquid and (zero) for solid, γ is the liquid fraction and L is the PCM latent heat of melting.
The sensible enthalpy h can be defined as [92]:-

$$h = h_o + \int_{T_o}^{T} C_p dT \tag{3.5}$$

Where h_o is the reference enthalpy at reference temperature T_o and C_p is the specific heat capacity.
The value of the liquid fraction (γ) lies between 0 and 1 based on the PCM temperature. γ can be mathematically formulated as [91]:-

$$\gamma = \begin{cases} 0 & if\ T < T_s\ (solid\, phase). \\ (T - T_s)/(T_l - T_s) & if\ T_s < T < T_l\ (phase\, change). \\ 1 & if\ T > T_l\ (liquid\, phase). \end{cases} \tag{3.6}$$

Where T_s is the PCM solidification temperature and T_l is PCM melting temperature.
Equation 3.6, differentiates three phases developed during the melting/solidification process, which are, the liquid phase ($\Delta H = L$), the solid phase ($\Delta H = 0$) and the mushy phase ($0 < \Delta H < L$). The mushy phase is the transition zone between the liquid and solid phase.

The latent heat source term (S_L) in the energy equation, Equation 3.3 can be defined as [91]:-

$$S_L = \partial_t(\rho \Delta H) \tag{3.7}$$

3.3.2 The Boussinesq approximation

The Boussinesq approximation is used to consider the change of density in the fluid resulting from the temperature variation in the buoyancy term in the momentum equation, without considering this variation of density into account in the other terms of the Navier-Stokes equations [94]. This means that the change of density of fluid due to temperature gradients is taken into account in the gravity terms and neglected in the inertia terms. For liquid PCM, incompressibility could be assumed. The coefficient of thermal expansion (β) could be written as:-

$$\beta = -\frac{1}{\rho}\frac{\partial \rho}{\partial T} = constant \tag{3.8}$$

Then,

$$\Delta\rho = -\beta\rho\Delta T \tag{3.9}$$

or

$$\rho - \rho_o = -\beta\rho(T - T_o) \tag{3.10}$$

The density (ρ) can be written as:

$$\rho = \frac{\rho_o}{\beta(T - T_o) + 1} \tag{3.11}$$

This can be written in a series as:

$$\rho = \rho_o[1 - \beta(T - T_o) + [\beta(T - T_o)]^2 - [\beta(T - T_o)]^3 + ...] \tag{3.12}$$

The Boussinesq approximation usually utilizes only the first-order term in the series and neglect the remaining terms because they are very small $<<<$ 1. The density (ρ) can be written as [95]:-

$$\rho = \rho_o[1 - \beta(T - T_o)] \tag{3.13}$$

Where ρ_o is the reference density of PCM at reference temperature (T_o).
The value of the PCM density employed in the simulations is the solid density and it is value (950 kg/m^3).
Then the gravitational term in the momentum equation, Equation 3.2 modified by adding the Boussinesq source term (S_b):

$$S_b = -\rho_o g_i \beta (T - T_o) \tag{3.14}$$

This source term will be considered during the natural convection.

3.3.3 Darcy law source term

The mushy regions (partially solidified regions) treated in the enthalpy-porosity technique as a porous medium. The source term S_i added to the momentum equation, Equation 3.2 which represents the influence of the mushy region is called Darcy source term. This source term is utilized to simulate the motion in the mushy zone. This source term is a function of liquid fraction or porosity. It is useful for modelling the mushy region for non-isothermal phase change process (melting/solidification processes does not take place at a constant temperature, where the mushy region occurs). The Darcy source term can be written as [96]:

$$S_i = C(1-\gamma)^2 \frac{u_i}{(\gamma^3 + \varepsilon)} \tag{3.15}$$

Where C is constant represent the mushy zone morphology which value varies from 10^4 to 10^7 for current calculation the value is taken to be 10^5 [64] and ε is a very small value number (0.001) to prevent division by zero when the liquid fraction is zero.

3.4 Response surface method optimization

Optimization refers to improving the performance of a process, a system or a product in order to obtain the maximum benefit from it. Response surface method (RSM) is a group of statistical and mathematical techniques is utilized for optimization. The RSM can be used for the applications in which several variables control the response of the system during a process. This method has several advantages including reduced computational cost, prediction of non-linear process optimization and simplicity [89].

The first stage in the application RSM in optimization is to find a relationship to estimate the influence of optimization factors on the response. It is common to utilize second-order polynomial according to the equation below [89]:

$$y(x) = a_0 + \sum_{i=1}^{n} a_i x_i + \sum_{i=1}^{n} a_{ii} x_i^2 + \sum_{1 \leq i \leq j}^{n} a_{ij} x_i x_j \tag{3.16}$$

where a_0 is the constant term, a_i, a_{ii} and a_{ij} represents the coefficients for liner, quadratic and interaction parameters respectively and x_i represents design parameters.

The values of the coefficients in Equation 3.16 can be determined via singular value decomposition using a set of sample points from the true limit state function, $y(x)$. The central composite design is a common sampling approach for this case. In the central composite design the number of sample points were estimated according to $N = n^2 + 2n + c_p$, where n is the factor number and (c_p) is the replicate number of the central point.

In RSM, the optimum value is determined using a parameter called desirability. The value of the desirability is between zero and one, and in the optimization procedure, it is tried to reach its values close to one. The desirability is obtained based on whether the goal is maximization or minimization of the response.

3.5 Average temperature

Average temperature value on the face of a body which calculated by using ANSYS FLUENT is not only finding a simple average over a number of nodes-the nodes temperature values need to be weighted by the amount of element face area associated with each node. ANSYS Fluent can find the area of element faces associated with each node, and a weighted average can be formed.

3.6 Total melting time and total solidification time

The total melting time means the time needed to melt 100% of the PCM. The total solidification time means the time needed to solidify 100% of the PCM.
The total melting time reduction (T_{mtr}) can be written as:

$$T_{mtr} = (\frac{T_{mtb} - T_{mtc}}{T_{mtb}}) * 100\% \tag{3.17}$$

Where T_{mtb} is the total melting time for the base case and T_{mtc} is the total melting time for the case.
The total solidification time reduction (T_{str}) can be written as:

$$T_{str} = (\frac{T_{stb} - T_{stc}}{T_{stb}}) * 100\% \tag{3.18}$$

Where T_{stb} is the total solidification time for the base case and T_{stc} is the total solidification time for the case.
The dimensionless melting time (τ_m) can be written as [61]:

$$\tau_m = (\frac{kT_{mtc}}{\rho C_p r_i^2}) \tag{3.19}$$

The dimensionless solidification time (τ_s) can be written as:

$$\tau_s = (\frac{kT_{stc}}{\rho C_p r_i^2}) \tag{3.20}$$

Where r_i is the internal radius of the inner HTF tube.

Chapter 4

Using Fins to Enhance the Thermal Performance of PCM in a Triple Tube Heat Exchanger

Utilizing a triple tube heat exchanger in PCM thermal energy storage (TES) systems is an effective strategy compared to the shell and tube heat exchanger. This is because the heat transfer fluid (HTF) flows on both sides of the PCM. Hence, the heat transfer area increases and the PCM melting/solidification rate increases [66]. Using fins to enhance the poor thermal performance of PCMs is a particularly desirable method because of the effectiveness in performance, low construction cost, and easy fabrication. In this chapter, novel fin shapes are proposed to enhance the thermal performance of PCM in the TTHX. To evaluate the thermal performance of these fins, a comparison was made with the traditional longitudinal fins.

4.1 Triple tube heat exchanger with fins

4.1.1 Model description and dimensions

The triple tube heat exchanger (TTHX) consisted of three horizontal concentric tubes where the PCM is placed in the middle tube and the HTF passes through the inner and outer tubes. This TTHX was utilized as a thermal energy storage container for a solar-powered liquid desiccant air-conditioning system. The TTHX physical model is shown in Fig. 4.1. This model has an inner tube diameter of 50.8 mm (d_i) and 1.2 mm thickness. The middle tube has an inner diameter (d_m) of 150 mm and thickness of 2 mm. The outer tube has an inner diameter (d_o) of 200 mm and thickness of 2 mm. The PCM used in this case is (RT82) paraffin manufactured by (RUBITHERM GmbH-Germany). RT82 was used because it has an unlimited lifetime and provides stable performance in repeated phase-change cycles [76]. It also can achieve the phase-change process with no super cooling effect. Thermophysical properties of the PCM (RT82), as reported by the manufacturer, are shown in Table 4.1.

In this test, the novel plus fins shape was introduced to enhance the poor thermal performance of the PCM. These fins were connected to the external surface of the inner HTF tube. The plus fin dimensions are 42 mm length (L), 42 mm width (W) and 1 mm thickness (t). Copper was utilized for pipes and fins.

Fig. 4.2 shows the computational domain with the indicated boundary conditions.

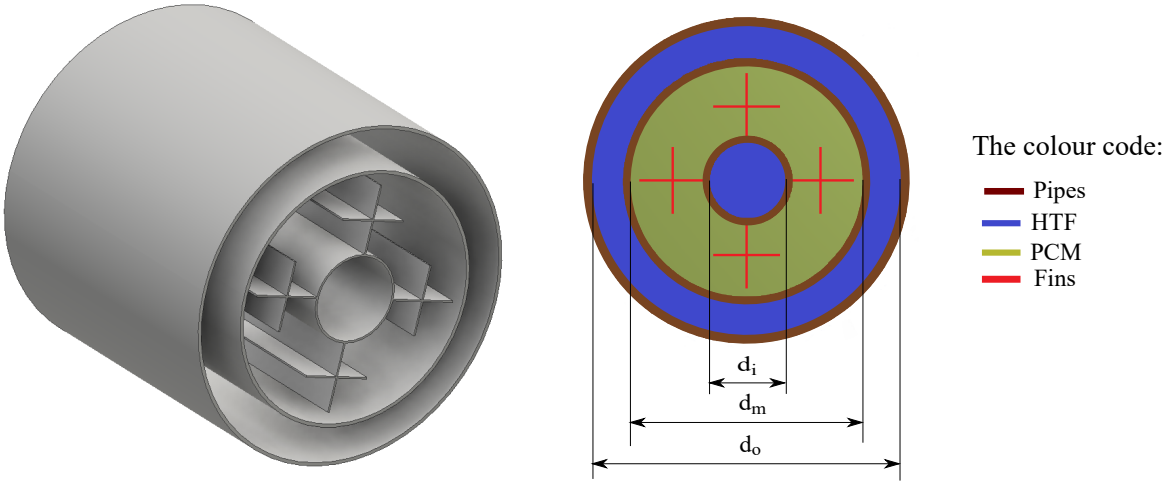

Figure 4.1: Triple tube heat exchanger physical model with the major dimensions, left 3D, right cross-sectional area.

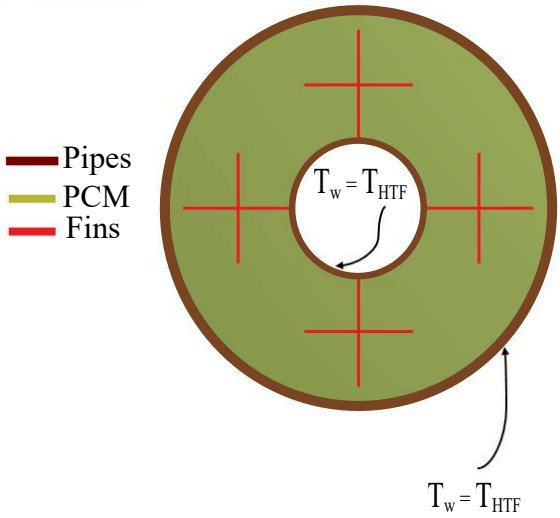

Figure 4.2: The computational domain with the indicated boundary conditions for TTHX with four plus fins.

Table 4.1: Thermal and physical properties of PCM (RT82) [97]

Material Property	**Range**
Melting temperature (^{o}C)	85
Solidification temperature (^{o}C)	77
Thermal conductivity (W/m K)	0.2
Latent heat of melting (kJ/kg)	176
Specific heat (kJ/kg K)	2
Solid / liquid Density (kg/m^3)	950 / 770
Dynamic viscosity (kg/ms)	0.03499
Coefficient of thermal expansion (1/K)	0.0001

4.1.2 Validation of Numerical Model

The model used for validation is a triple tube heat exchanger (TTHX), which has been taken from the experimental work of Al-Abidi *et al.* [64]. The TTHX consisted of three horizontal concentric tubes with eight longitudinal fins. Four fins were welded to the external surface of the inner tube and four fins were welded to the internal surface of the middle tube. The PCM (RT82) was contained in the middle tube and the HTF (water) passes through the inner and outer tubes. The cross-sectional area of the TTHX used is shown in Fig. 4.3. This model has an inner tube diameter of 50.8 mm (d_i) and 1.2 mm thickness. The middle tube has an inner diameter (d_m) of 150 mm and thickness of 2 mm. The outer tube has an inner diameter (d_o) of 200 mm and thickness of 2 mm. The fins' dimensions were 42 mm length and 1 mm thickness. Copper was used for tubes and fins.

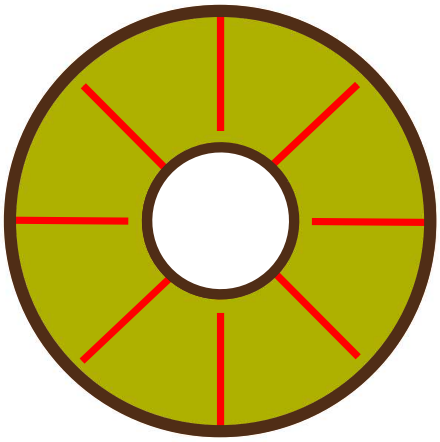

Figure 4.3: The computational domain of the TTHX used for validation with Al-Abidi *et al.* [64].

The melting process was considered for validation purpose. The initial solid PCM temperature used was 27 °C. The boundary condition used for the HTF temperature of 90 °C was imposed along the HTF inner and outer tubes walls.

Fig. 4.4 shows the comparison of the present numerical results with experimental and numerical data reported by Al-Abidi *et al.* [64] for average PCM temperatures. The comparison shows that the current numerical results are in good agreement with the experimental and numerical results of Al-Abidi *et al.* [64].

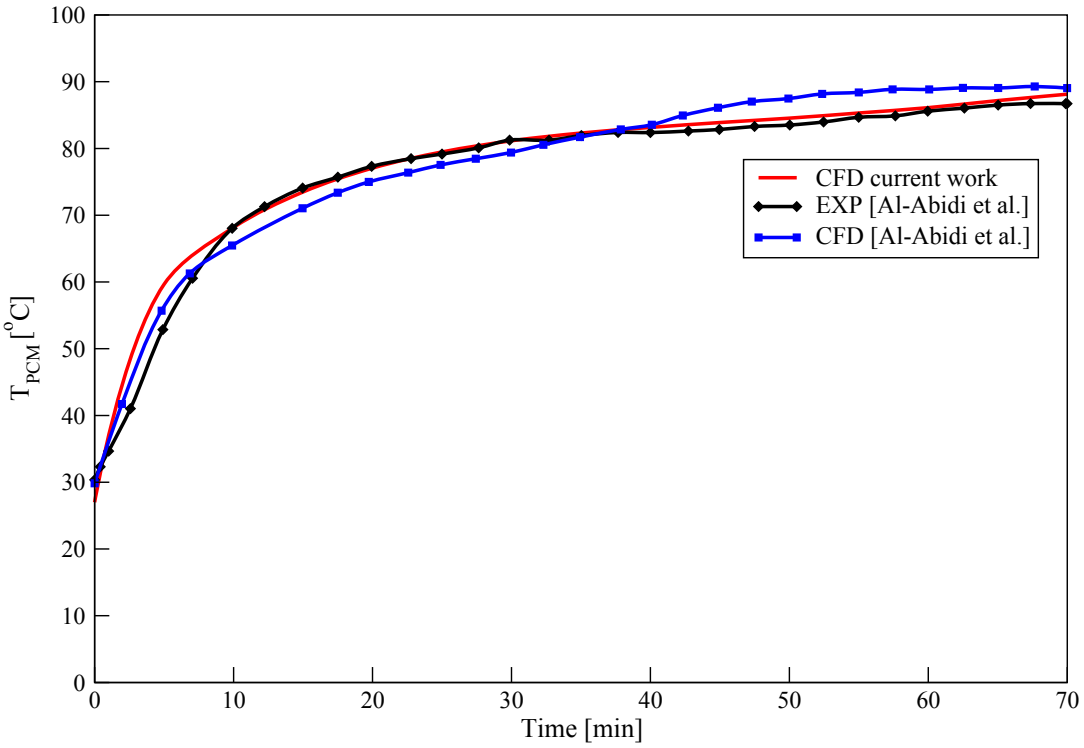

Figure 4.4: Validation of the current work vs. experimental and numerical work of Al-Abidi *et al.* [64] average PCM temperature.

4.1.3 Numerical procedure

ANSYS Fluent 15 software was used in the simulations. Fluent utilizes the finite volume method and the enthalpy-porosity technique to solve the continuity, momentum and energy equations. The solidification and melting model was used to model the PCM melting/solidification process. Two-dimensional computational domains were used in the simulations. A Transient Pressure-Based solver was employed to solve the governing equations for incompressible flow. The SIMPLE scheme was utilized for pressure-velocity coupling. The PRESTO scheme was employed for pressure discretization, which is recommended for solving natural convection flow [15, 98]. The second order upwind scheme was employed for solving the energy and momentum equations. The under-relaxation factors for momentum, pressure, liquid fraction and energy were 0.7, 0.3, 0.9 and 1 respectively. The convergence criterion for energy equation was set to 10^{-6} and 10^{-4} for continuity and

momentum equations.

4.1.4 Mesh and time step independent test

For this test, the TTHX with four tee fins was used. The melting process was considered for this test. The result of the mesh independent test is shown in Fig. 4.5. A 5 s time step was used in this test. It is clear from this figure that the results were identical between 45505 cells and 59973 cells. As such mesh consisting of 45505 cells will be used in the following simulations, as shown in Fig 4.6. The result of the time step independent test is shown in Fig. 4.7. The mesh used for this test was 45505 cells. It is clear from this figure that there are identical results for time steps 1 s, 5 s, and 10 s. Given this, a 10 s time step will be used in the following simulations.

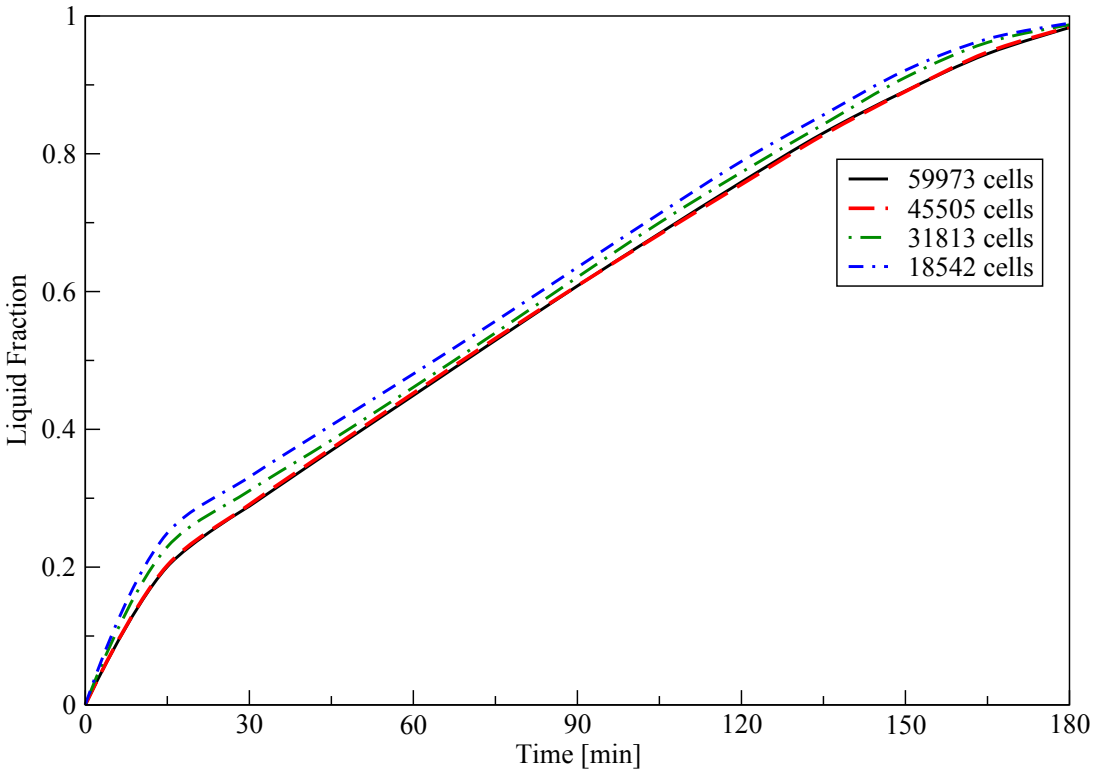

Figure 4.5: TTHX mesh independent test, liquid fraction.

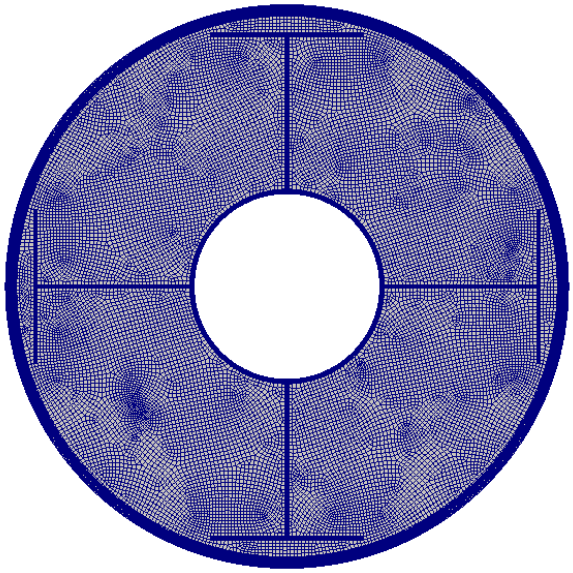

Figure 4.6: TTHX mesh 45505 cells.

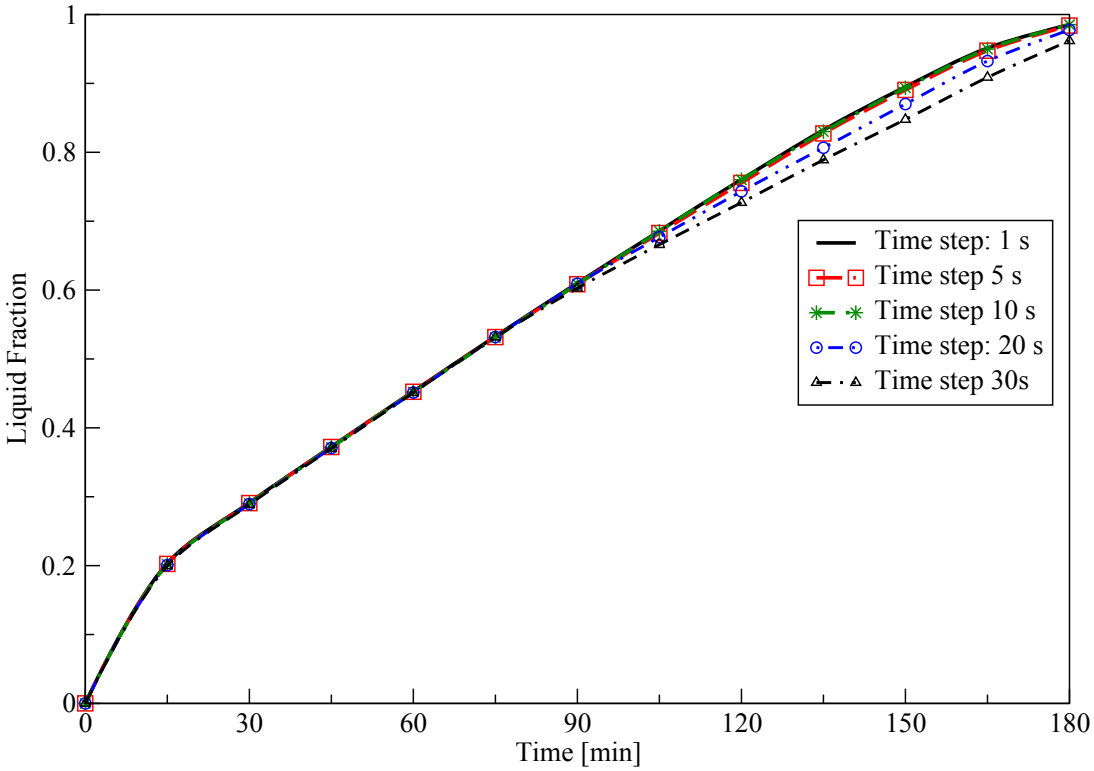

Figure 4.7: TTHX time step independent test, liquid fraction.

4.2 Initial and boundary conditions

4.2.1 Melting process

At the initial time (t = 0), the PCM was in the solid state, with its temperature at 27 °C, which is below the PCM melting temperature. The HTF had a constant temperature ($T_w = T_{HTF} = 90$ °C), which is higher than the PCM melting temperature. This temperature was imposed along the HTF inner and outer tubes walls as shown in Fig. 4.2. Therefore, the initial and boundary conditions can be listed as

$T = T_{initial} = 27$ °C at (t = 0).

At $d = d_i$, $T = T_{HTF} = 90$ °C.

At $d = d_m$, $T = T_{HTF} = 90$ °C.

4.2.2 Solidification process

At the initial time (t = 0), the PCM was in the liquid state, hence its temperature was 93 °C, which is above the PCM solidification temperature. The HTF had a constant temperature ($T_w = T_{HTF} = 68$ °C), which is lower than the PCM solidification temperature. This temperature was imposed along the HTF inner and outer tubes walls as shown in Fig. 4.2. Therefore, the initial and boundary conditions can be listed as

$T = T_{initial} = 93$ °C at (t = 0).

At $d = d_i$, $T = T_{HTF} = 68$ °C.

At $d = d_m$, $T = T_{HTF} = 68$ °C.

4.3 Comparison between plus fin, longitudinal fin and tee fin

To evaluate the thermal performance of the suggested novel fins shapes, its thermal performance was compared with the traditional longitudinal fin shape. Three fins' configuration were tested, which included longitudinal fins Fig. 4.8a, tee fins Fig. 4.8b and plus fins Fig. 4.8c. For this test, the TTHX with four longitudinal fins is compared with the TTHX with four tee fins and the TTHX with four plus fins. The computational domains of various TTHX with various fins shapes are shown in Fig. 4.9. The total cross-section area of all fins types was kept constant to compare different fins' thermal performance. To achieve this, the fins' dimensions were carefully chosen. For various fins' systems, the same amount of PCM was used in all cases, therefore the same amount of energy could be stored in all systems. The dimensions of the fins are shown in Fig. 4.8 and Table 4.2.

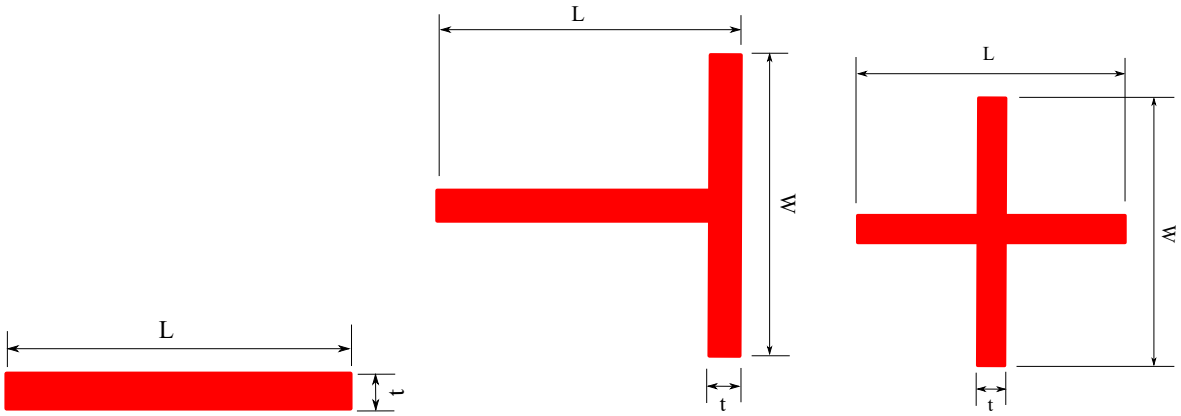

(a) Longitudinal fin (b) tee fin (c) plus fin

Figure 4.8: Various fins' configurations and dimensions.

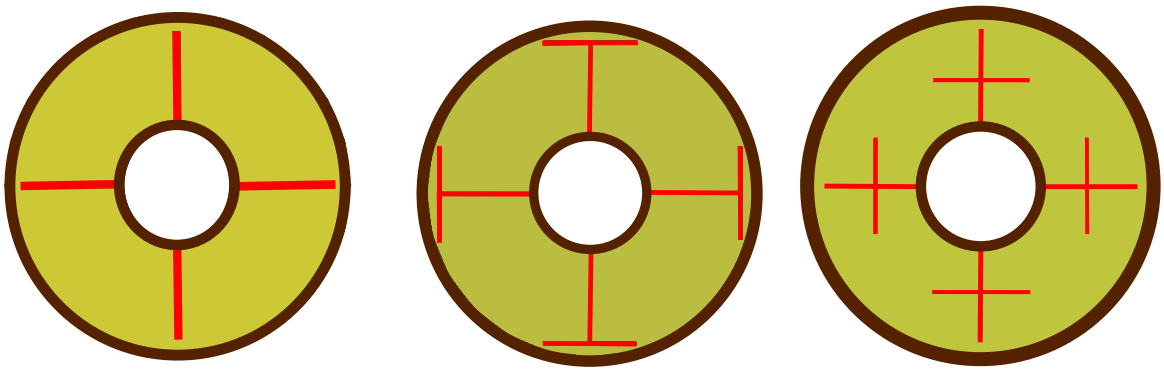

(a) Longitudinal fins (b) tee fins (c) plus fins

Figure 4.9: Computational domains for the TTHX with various fins' configurations.

Table 4.2: Dimensions of various fins' shapes

Fin shape	**Length (L) (mm)**	**Width (W) (mm)**	**Thickness (t) (mm)**
Longitudinal fin	42	0	2
Tee fin	42	42	1
Plus fin	42	42	1

4.3.1 Melting process

The liquid fraction for various fins' configuration cases is illustrated in Fig. 4.10. It is clear from this figure, that for all time intervals the liquid fraction when employing the plus fins is more than when using the longitudinal fins or the tee fins. This figure also shows that the case with plus fins has about 90% liquid fraction after 2.5 hours, while, the one with longitudinal fins has around 70% liquid fraction at the same time. When using the plus fins, the total PCM melting time is about 3.5 hours, while the time needed to complete melting when using the longitudinal fins about 4.5 hours. As such, the total PCM melting time reduced by about 22% when using the plus fins, as compared to using longitudinal fins. The melting rate improved by employing the plus fins as compared

to utilizing the longitudinal fins due to the enhancement of thermal penetration depth and the increase of the heat exchange area. The melting process accelerated by utilizing the plus fins shapes compared to the longitudinal fins and tee fins, this is because when utilizing the plus fins the fins reached the isolated middle part of the PCM which located between the inner and middle tube which relatively far away from the inner and outer HTF tubes. This demonstrated that the fins should not be considered just as extended heat transfer surfaces, when fins properly designed and oriented, they accelerate the PCM melting process. The total melting time and melting time reductions for the various fins' configurations are shown in Table 4.3. The average PCM temperature for various fins' configurations is shown in Fig. 4.11. It can be seen from this figure that the plus fins case shows better thermal performance compared to the cases utilizing the longitudinal fins or the tee fins. The heat transfer rate increased by utilizing the plus fins, as compared to the cases with the longitudinal fins or the tee fins. Hence, the PCM melting process accelerated. Liquid fraction contours for various fins' configurations at different moments are shown in Fig. 4.12. It can be seen that utilize the plus fins achieves a higher melting rate compared to cases utilizing the longitudinal fins or the tee fins. At early stages, the melting process is dominated by conduction so the melted part is located symmetrically between the lower and upper parts of the PCM containers, whereas at the later stages convection plays the decisive role. The role of convection increase with time especially in the upper part of the PCM, thus the PCM melting in the upper parts of the PCM containers is more rapid compared to lower parts. Hence, the solid phase is not located symmetrically between the lower and upper parts of the PCM containers.

It can be seen from Fig. 4.12 in case of using plus fins the melting rate is high in the middle part of the PCM-annular around these fins. This because the high conductivity fins increase the zone effect of the HTF in this region of PCM which has low thermal conductivity. Hence the amount of solid PCM decreases in this region and this significantly accelerates the melting rate.

Surface heat flux contours for various fins' configurations at different moments are shown in Fig. 4.13. It can be seen that utilize the plus fins achieves uniform heat flux distribution compared to cases utilizing the longitudinal fins or the tee fins.

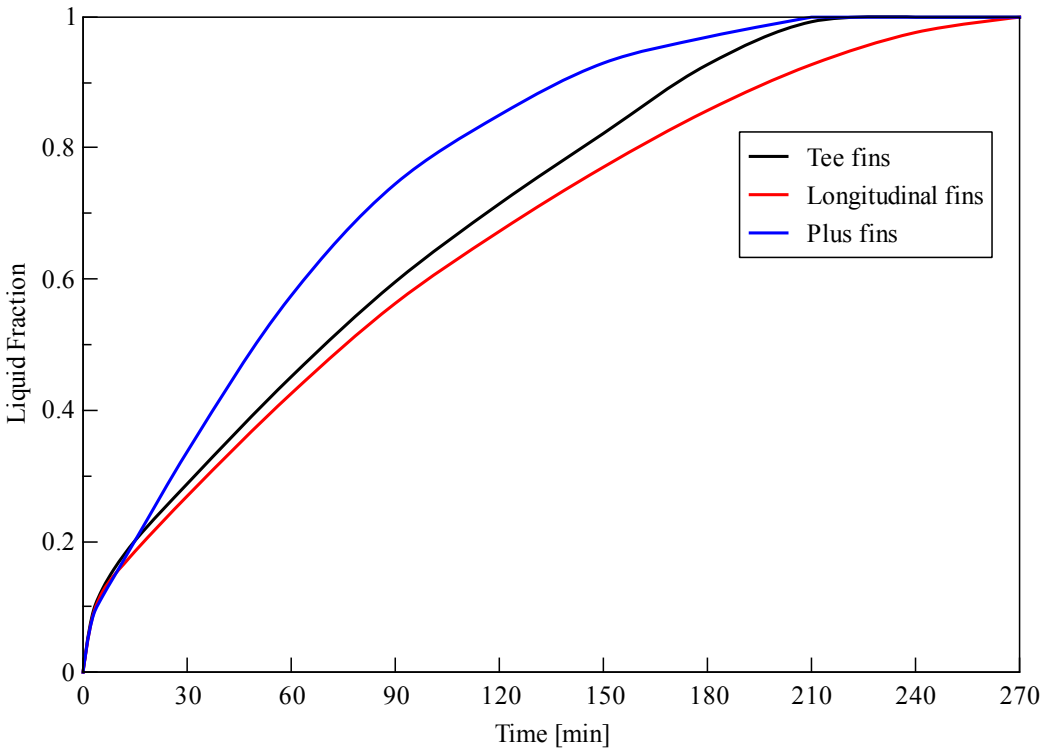

Figure 4.10: Liquid fraction comparison for melting process for TTHX with four tee, longitudinal and plus fins.

Table 4.3: Melting time and melting time reduction for various fins' shapes

Fin shape	**Melting time (min)**	**Reduction (%)**
Longitudinal (base case)	270	—
Tee	216	20
Plus	210	22

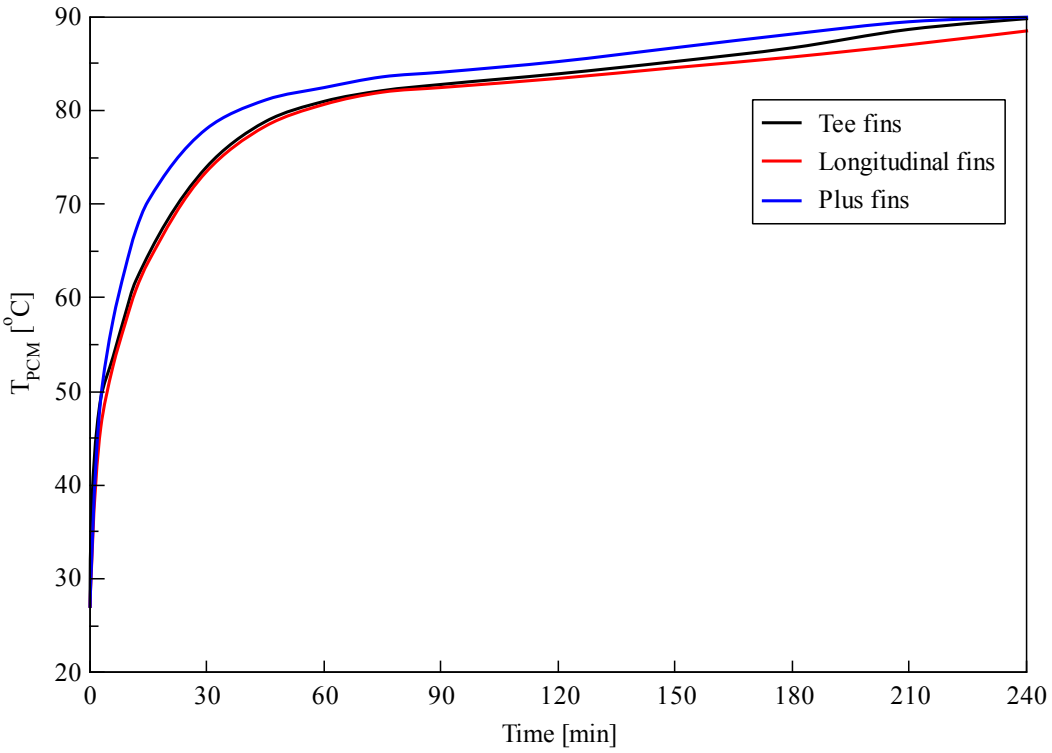

Figure 4.11: Average PCM temperature comparison for melting process for TTHX with four tee, longitudinal and plus fins.

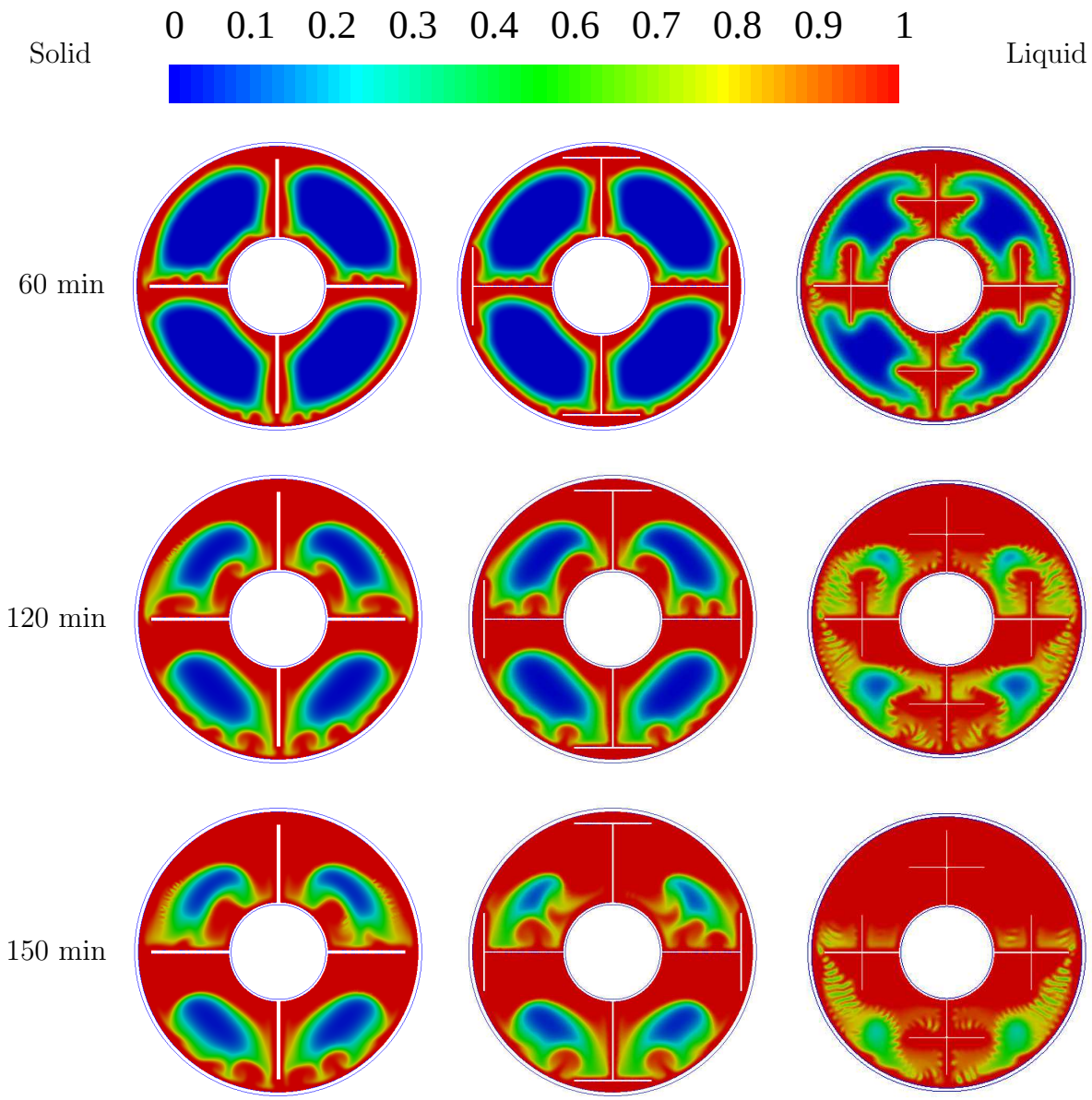

Figure 4.12: Liquid fraction contours at different times for melting process for different fins' configurations: longitudinal fins left, tee fins centre and plus fins right.

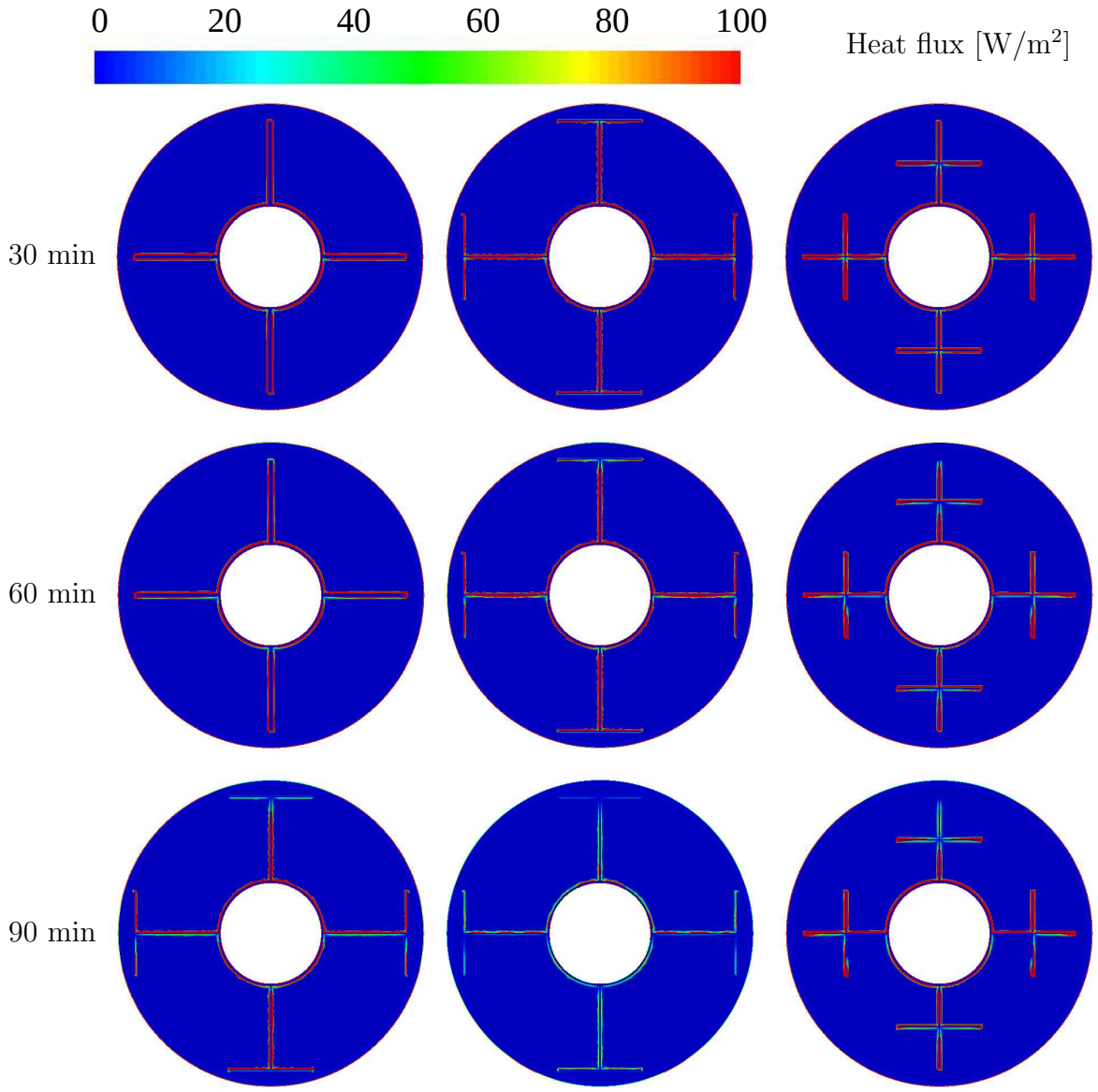

Figure 4.13: Surface heat flux contours at different times for melting process for different fins' configurations: longitudinal fins left, tee fins centre and plus fins right.

4.3.2 Solidification process

Fig. 4.14 shows the liquid fraction versus time for various fins' shapes. It is clear from this figure that at all time intervals the liquid fraction for plus fins is less than the longitudinal fins or the tee fins. The total PCM melting time for the plus fins case was 3 hours, while for

the cases using longitudinal or tee fins the total solidification time was 4 hours. Given this, the total solidification time reduced by about 25% when using the plus fins, compared to the longitudinal or tee fins. The total solidification time and solidification time reductions for the various fins' configurations are shown in Table 4.4. The average PCM temperature for various fins' shapes is shown in Fig. 4.15. It is clear from this figure that the plus fins' case shows better thermal performance compared to those of longitudinal or tee fins. The heat transfer rate increased for the plus fins' case, so the average PCM temperature reduced compared to cases of longitudinal or tee fins. Contours of liquid fraction for various fins' configuration at different times are shown in Fig. 4.16. It is clear that the solidification rate increases by utilizing the plus fins as compared to using the longitudinal or the tee fins. At the beginning of the solidification process convection is the dominant heat transfer mechanism, but as time passes more PCM solidifies, hence conduction becomes the main mode of heat transfer. It can be seen from Fig. 4.16 that the PCM completed solidification at a shorter time in case of utilizing the plus fins because these fins reached the isolated parts of PCM (located in the middle of the PCM shell). Surface heat flux contours for various fins' configurations at different moments are shown in Fig. 4.17. It can be seen that utilize the plus fins achieves uniform heat flux distribution compared to cases utilizing the longitudinal fins or the tee fins.

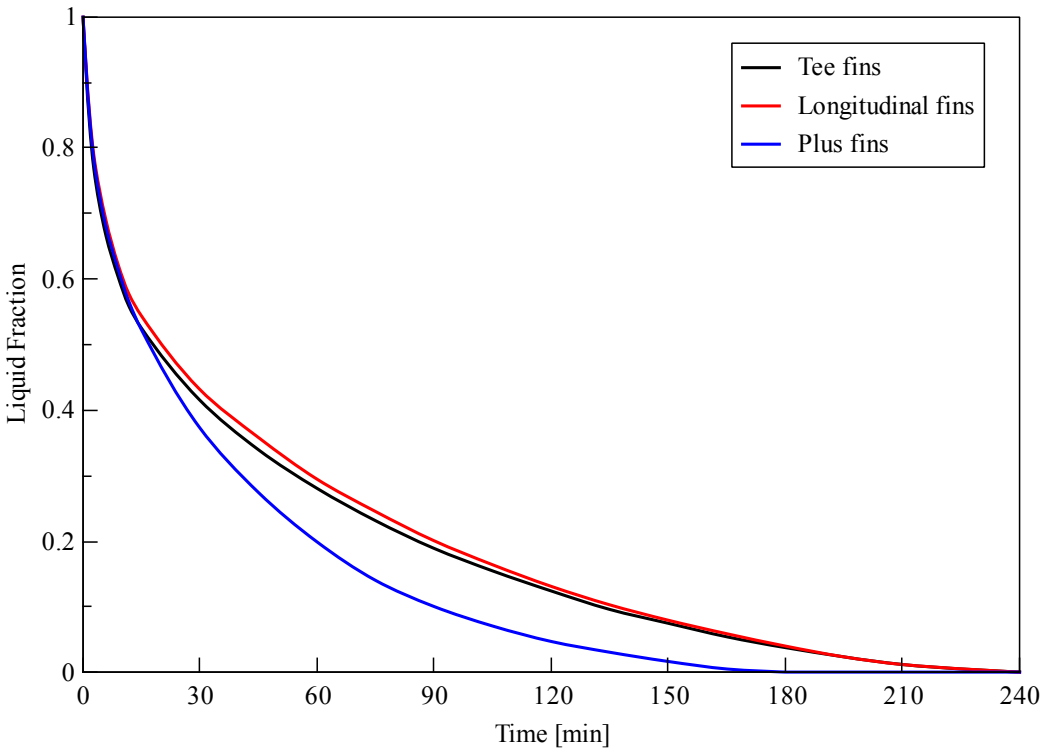

Figure 4.14: Liquid fraction comparison for solidification process for the TTHX with four tee, longitudinal and plus fins.

Table 4.4: Solidification time and solidification time reduction for various fins' shapes

Fin shape	**Solidification time (min)**	**Reduction (%)**
Longitudinal (base case)	240	—
Tee	240	0
Plus	180	25

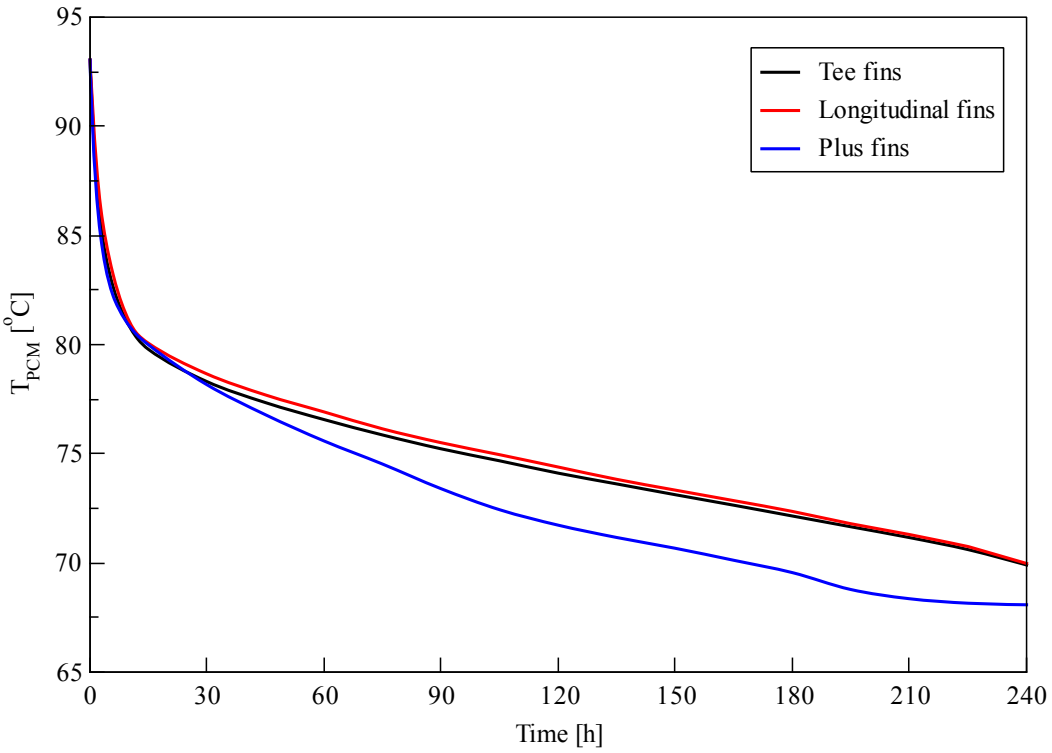

Figure 4.15: Average PCM temperature comparison for solidification process for TTHX with four tee, longitudinal and plus fins.

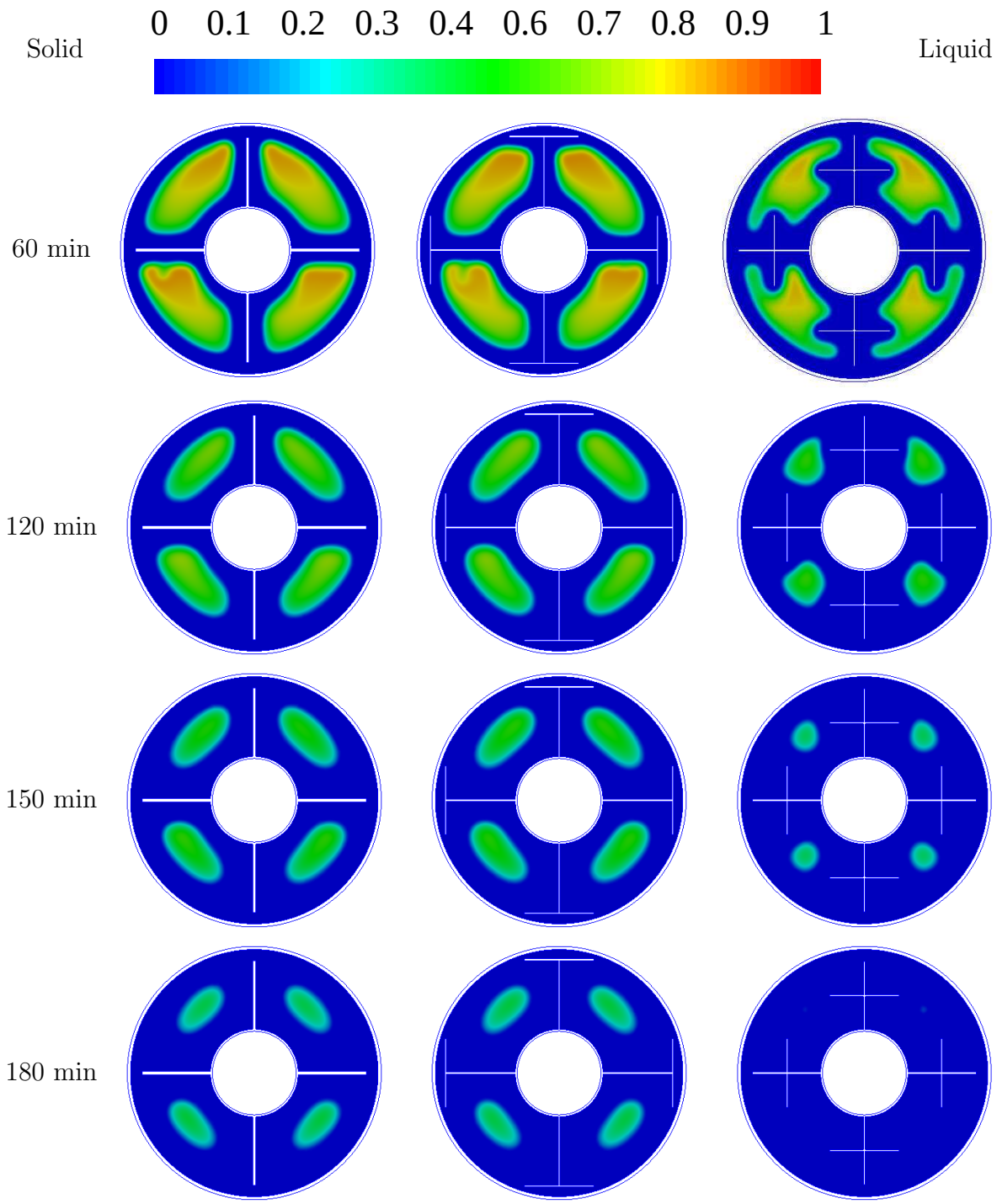

Figure 4.16: Liquid fraction contours at various times for solidification process for various fins configurations: longitudinal fins left, tee fins centre and plus fins right.

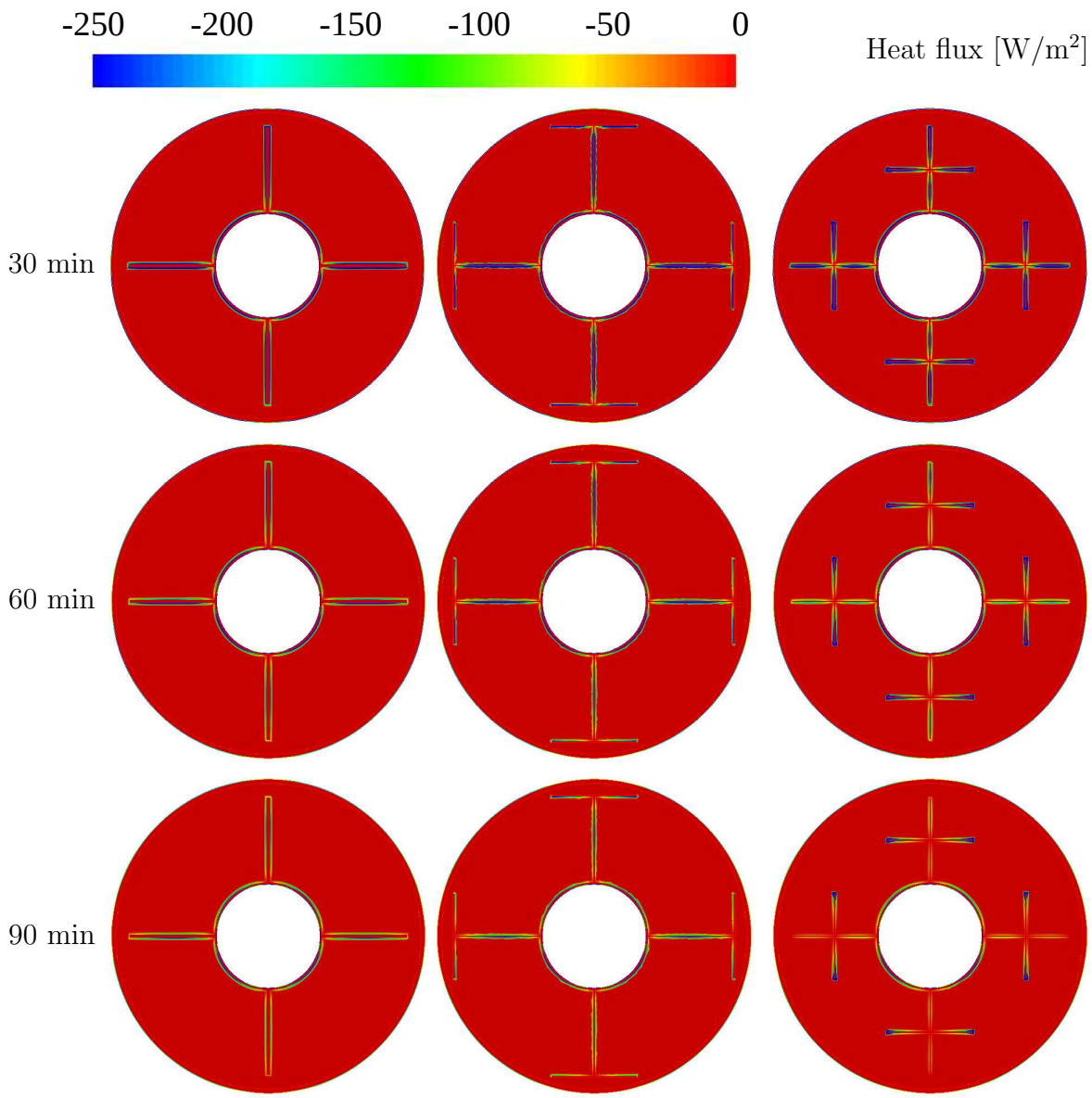

Figure 4.17: Surface heat flux contours at different times for solidification process for different fins' configurations: longitudinal fins left, tee fins centre and plus fins right.

4.4 Effect of the number of plus fins on the TTHX thermal performance

For this test, the influence of using a different number of plus fins for the TTHX was investigated and compared with the TTHX without fins. The computational domains for various numbers of plus fins' configurations are shown in Fig. 4.18. Four TTHX configurations were tested and compared which as follows: TTHX without fins Fig. 4.18a, TTHX with four fins Fig. 4.18b, TTHX with six fins Fig. 4.18c, and TTHX with seven fins Fig. 4.18d. The fins' dimensions used in this test were 42 mm length (L), 42 mm width (W) and 1 mm thickness. The angular distance between fins was equally distributed in all cases.

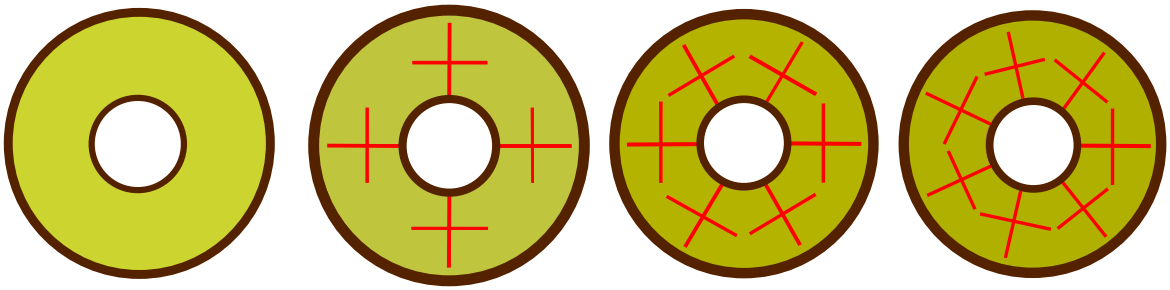

(a) without fins (b) four fins (c) six fins (d) seven fins

Figure 4.18: Computational domains for various numbers of plus fins configurations.

4.4.1 Melting process

Fig. 4.19 illustrates the PCM liquid fraction for, different numbers of fin cases. It can be concluded from Fig. 4.19 that increasing the number of fins accelerates the PCM melting significantly. In the case without fins, after 4 hours only around 77% of PCM had melted. When using four fins, the PCM had completely melted after 3 hours. The total melting time reduced to about 2 hours when using six fins. The total PCM melting time increased if the fin numbers increased from six to seven, thereby demonstrating the strong effect of

fins' positions in the PCM container on the PCM melting process. This indicates, that adopting an appropriate fins' arrangement between the bottom and top halves of the PCM container can accelerate the PCM melting. The heat conduction was enhanced by increasing the number of fins and this enhances the melting process; on the other hand, increasing the number of fins restricted the development of natural convection. The total PCM melting time reduced by 33% when using six fins compared to when four fins were utilized. The total melting time and melting time reductions for different numbers of plus fins are shown in Table 4.5.

Fig. 4.20 presents the average PCM temperature for various numbers of fins cases. It is obvious from this figure that utilizing more fins increases the PCM temperature due to the increase of the heat exchange area between the PCM and the HTF, which assists in ameliorating the conduction heat transfer. Hence, the melting rate increases and the total PCM charging time decreases. It is also clear from this figure that there is no clear difference in temperature between the case with six fins and the one with seven fins. Given this, the optimum fins number are six.

Contours of liquid fraction for different fins numbers' configuration at different times are shown in Fig. 4.21. From this figure, it can be seen that increasing fin numbers improves the PCM melting rate, due to the increase of the heat exchange area. Moreover, increasing the fins number increases thermal penetration depth, hence, accelerating the PCM melting process. The upper half of the domain is dominated by natural convection while the lower half of the domain dominated by conduction. Hence the upper half of the domain completes melting at a shorter time compared to the lower domain.

Contours of surface heat flux for different fins numbers' configuration at different times are shown in Fig. 4.22. From this figure, it can be seen that increasing fin numbers increases the thermal penetration depth. Contours of temperature for different fin numbers' configuration at different times are shown in Fig. 4.23. It is clear from this figure that increased fin numbers enhance the heat transfer rate, hence accelerating the melting process. At the beginning of the melting process, conduction is the dominant heat transfer mechanism. As time progress, more PCM melted hence convection heat transfer enhanced. This results in the upper half higher temperature compared to the lower part of the PCM

container.

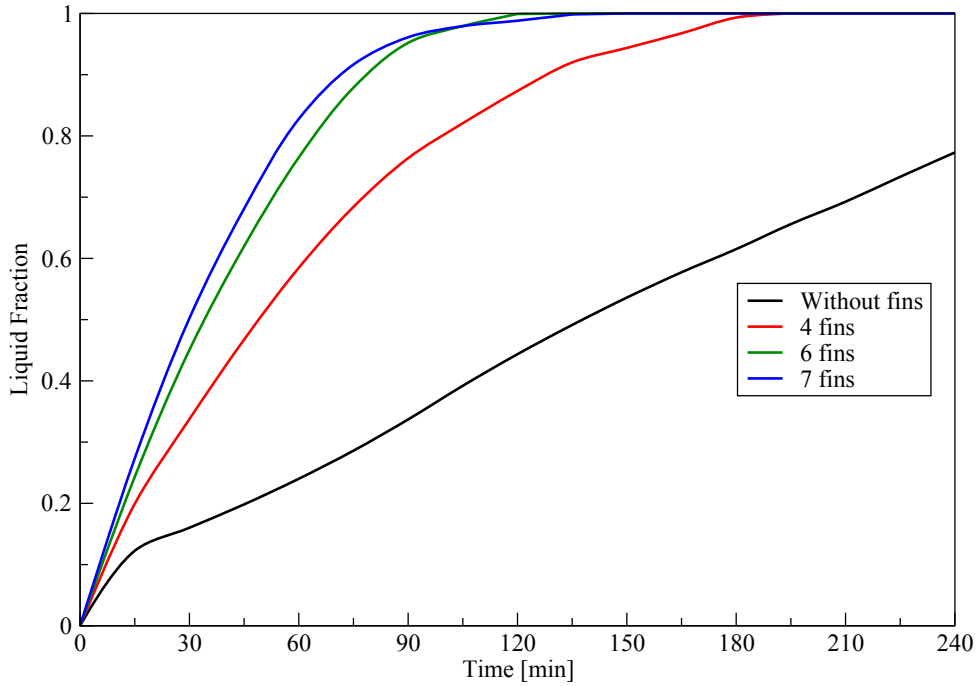

Figure 4.19: Liquid fraction comparison for melting process for different numbers of plus fins.

Table 4.5: Melting time and melting time reduction for different numbers of plus fins

Number of fins	**Melting time (min)**	**Reduction (%)**
4 fins (base case)	180	—
6 fins	120	33
7 fins	138	23

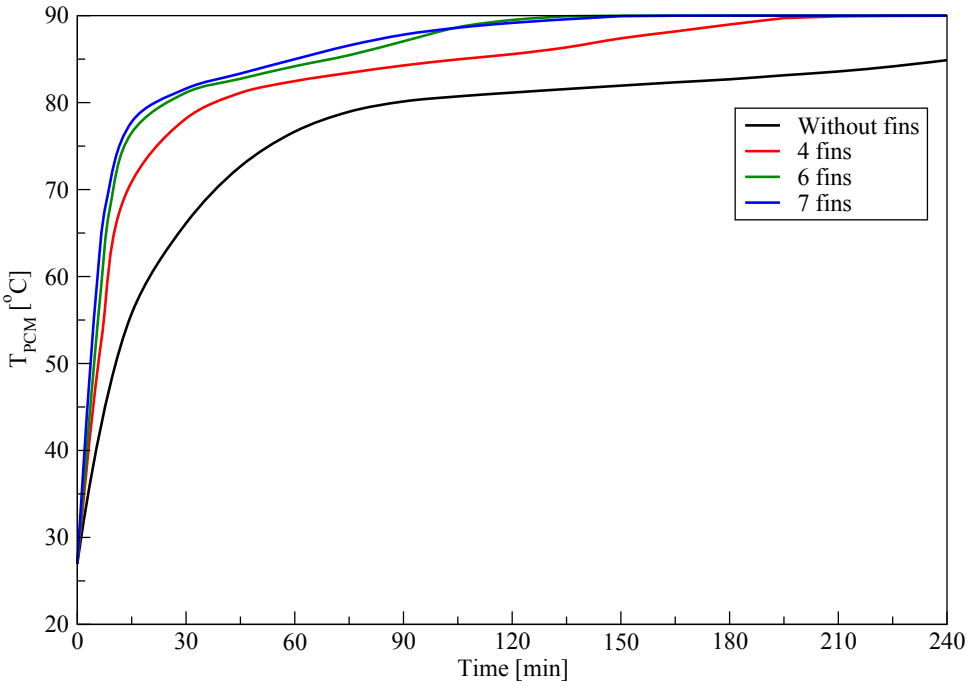

Figure 4.20: Average PCM temperature comparison for the melting process for various numbers of plus fins.

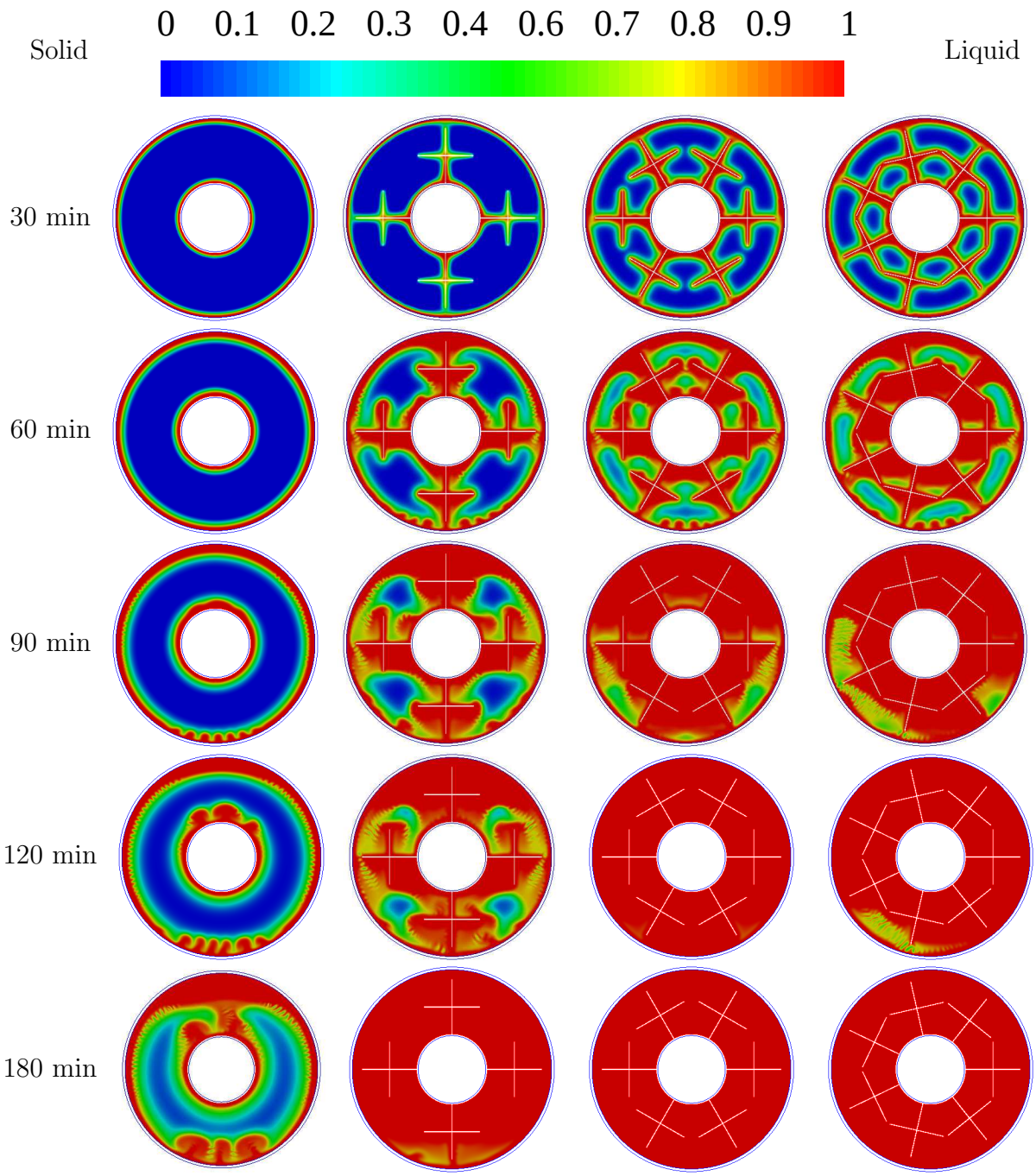

Figure 4.21: Liquid fraction contours at different times for melting process for different plus fin numbers configurations': first from the left without fins, second 4 fins, third 6 fins, and fourth 7 fins.

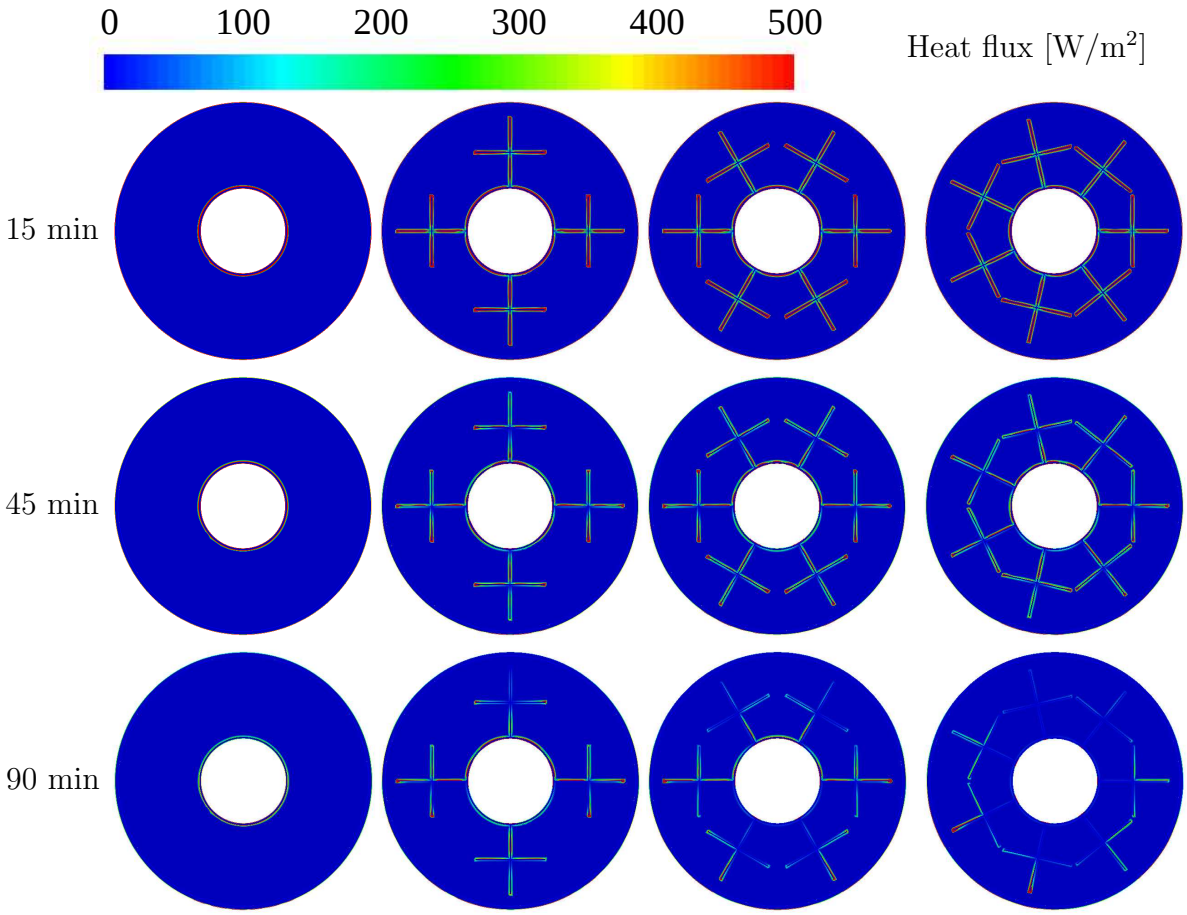

Figure 4.22: Surface heat flux contours at different times for melting process for different plus fin numbers configurations': first from the left without fins, second 4 fins, third 6 fins, and fourth 7 fins.

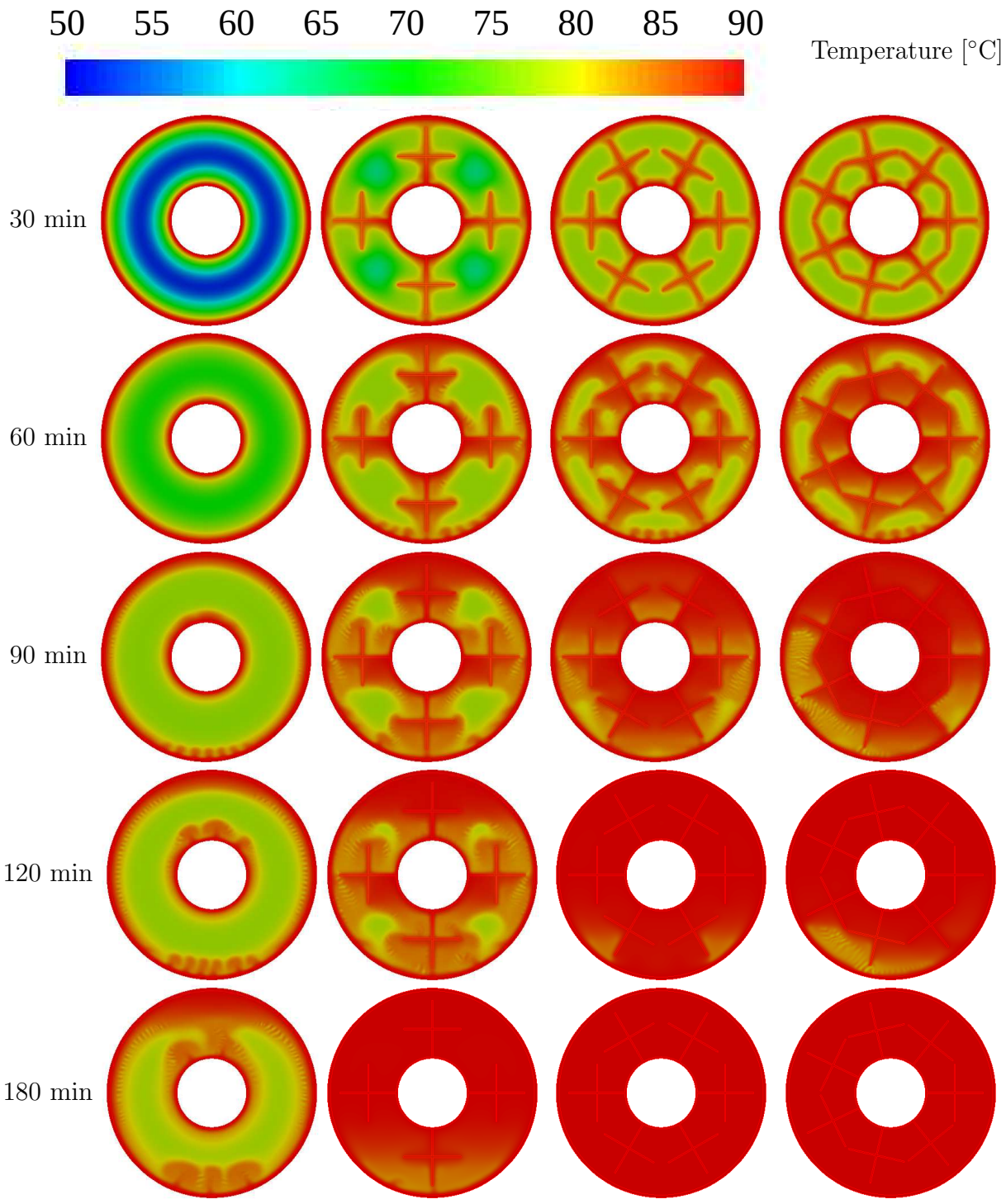

Figure 4.23: Temperature contours at different times for melting process for different numbers of plus fins configurations: first from the left without fins, second 4 fins, third 6 fins, and fourth 7 fins.

4.4.2 Solidification process

Fig. 4.24 shows the liquid fraction for the case without fins and the different number of fins cases. This figure shows that in the case without fins the PCM did not complete solidification after 4 hours. When utilizing six fins, the PCM total solidification time decreased to about 1.5 hours, compared to about 3 hours when using four fins. As such, the total PCM solidification time reduced by about 50% if the fins' number increased from four to six. There was no clear difference in PCM liquid fraction if the fin numbers increased from six to seven, so the case with six fins is the optimum one. In the case of utilizing more fins, the solidification rate increases owing to the increase in the heat exchange area. The total solidification time and solidification time reductions for different numbers of plus fins are shown in Table 4.6.

The average PCM temperature for different fin numbers' cases is shown in Fig. 4.25. As can be seen, increasing fin numbers increase the heat transfer rate, thereby reducing the PCM average temperature and this accelerates the solidification process to enhance the thermal energy release from the PCM.

Liquid fraction contours for various numbers of fins at different times are shown in Fig. 4.26. It is clear from this figure that increasing the fin numbers accelerates the solidification process. This due to the increase of the heat transfer area between the HTF tube and the PCM which improves the conduction heat transfer process.

Contours of surface heat flux for different fins numbers' configuration at different times are shown in Fig. 4.27. From this figure, it can be seen that increasing fin numbers increases the thermal penetration depth. Contours of temperature for the different number of fins at different times are in Fig. 4.28, which shows that increasing fin numbers decreases the PCM temperature owing to the increase of the heat exchange area.

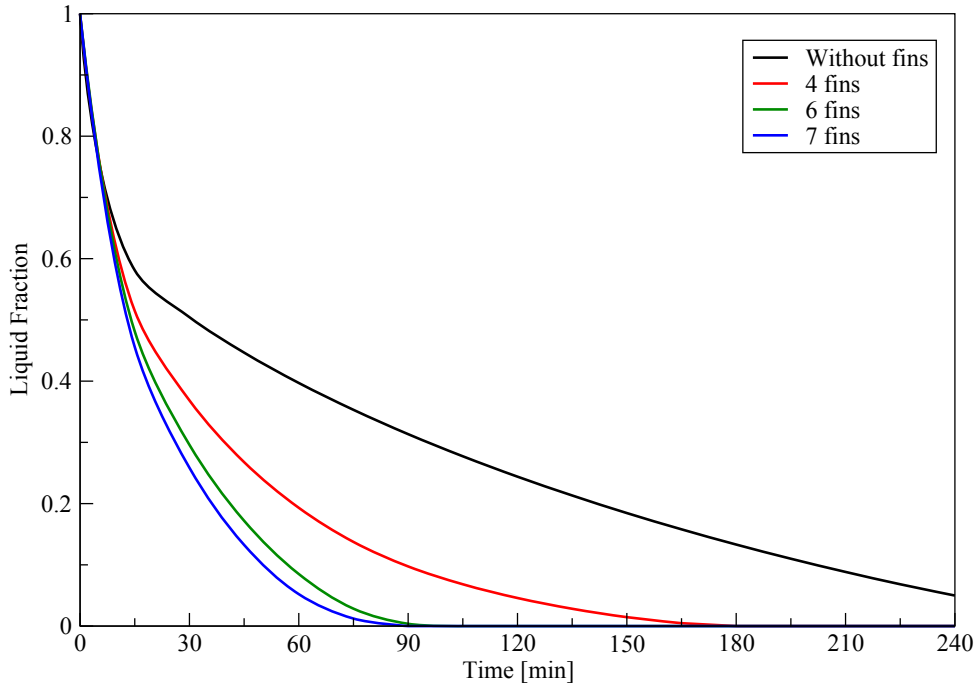

Figure 4.24: Liquid fraction comparison for solidification process for various numbers of plus fins.

Table 4.6: Solidification time and solidification time reduction for different numbers of plus fins

Number of fins	**Solidification time (min)**	**Reduction (%)**
4 fins (base case)	182	—
6 fins	91	50
7 fins	89	51

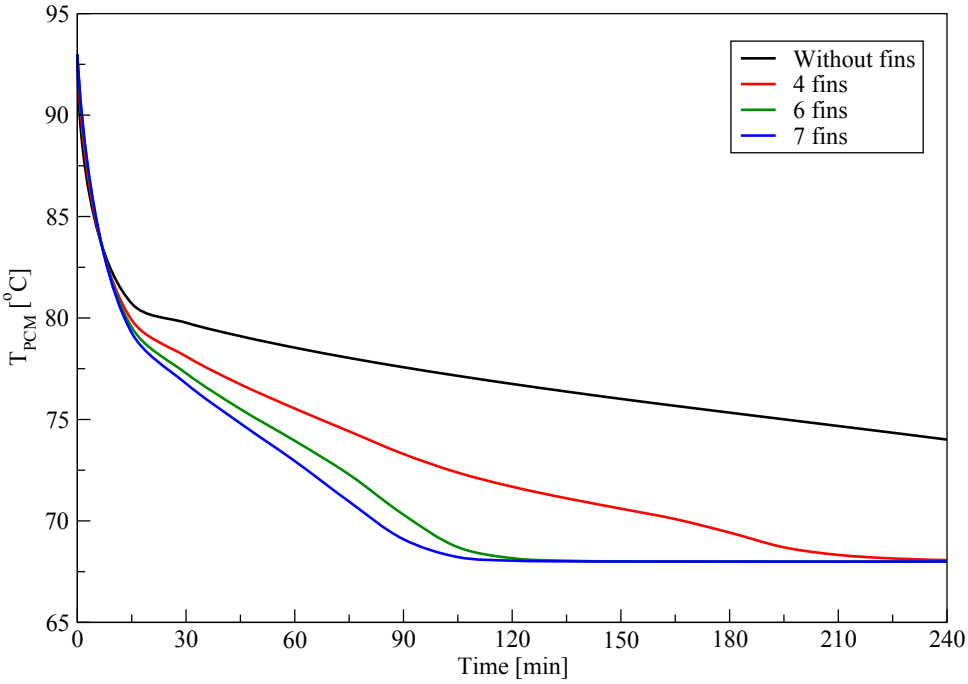

Figure 4.25: PCM average temperature comparison for solidification process for various numbers of plus fins.

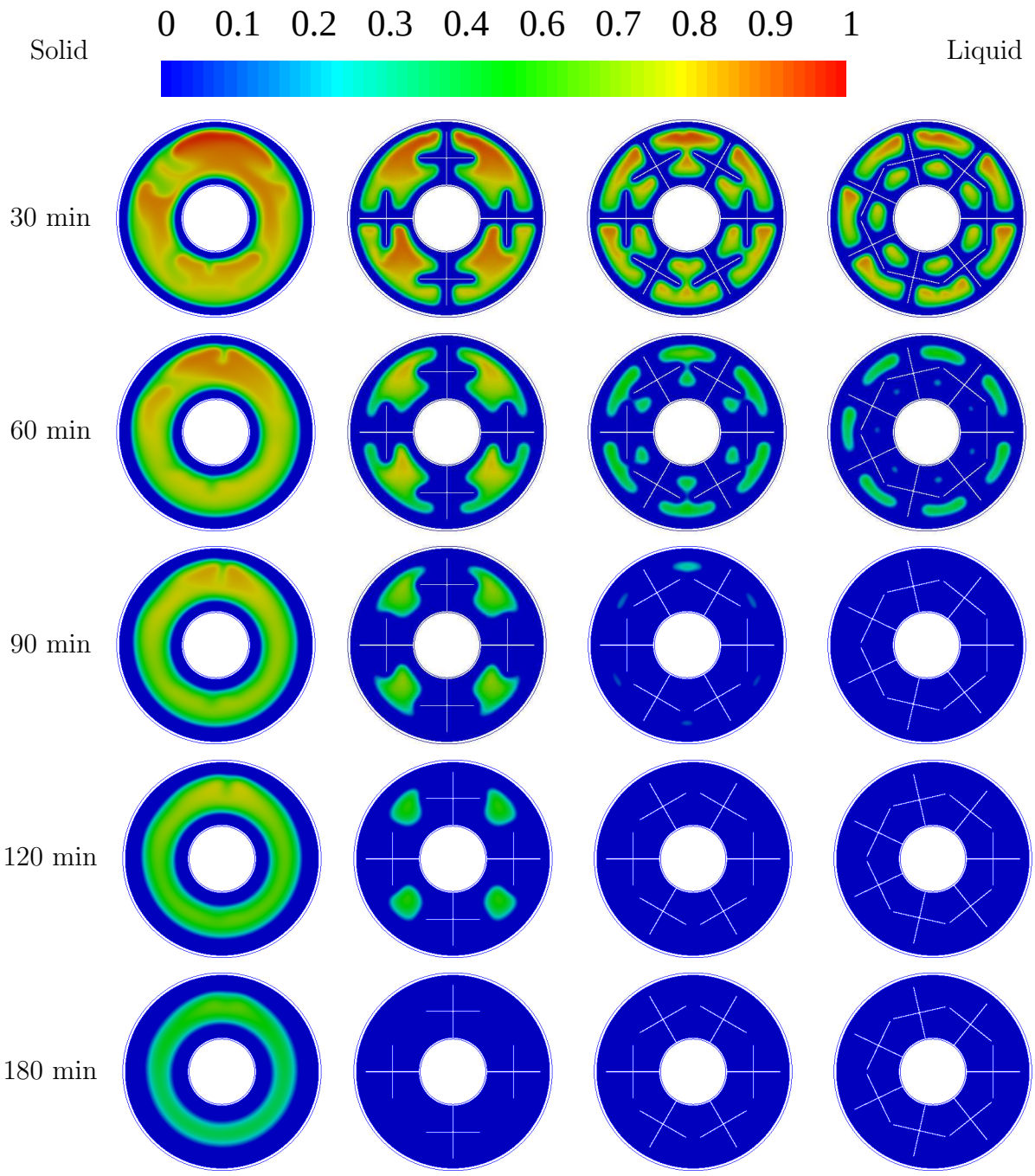

Figure 4.26: Contours of liquid fraction at various times for solidification process for the various numbers of plus fins: first from the left without fins, second 4 fins, third 6 fins, and fourth 7 fins.

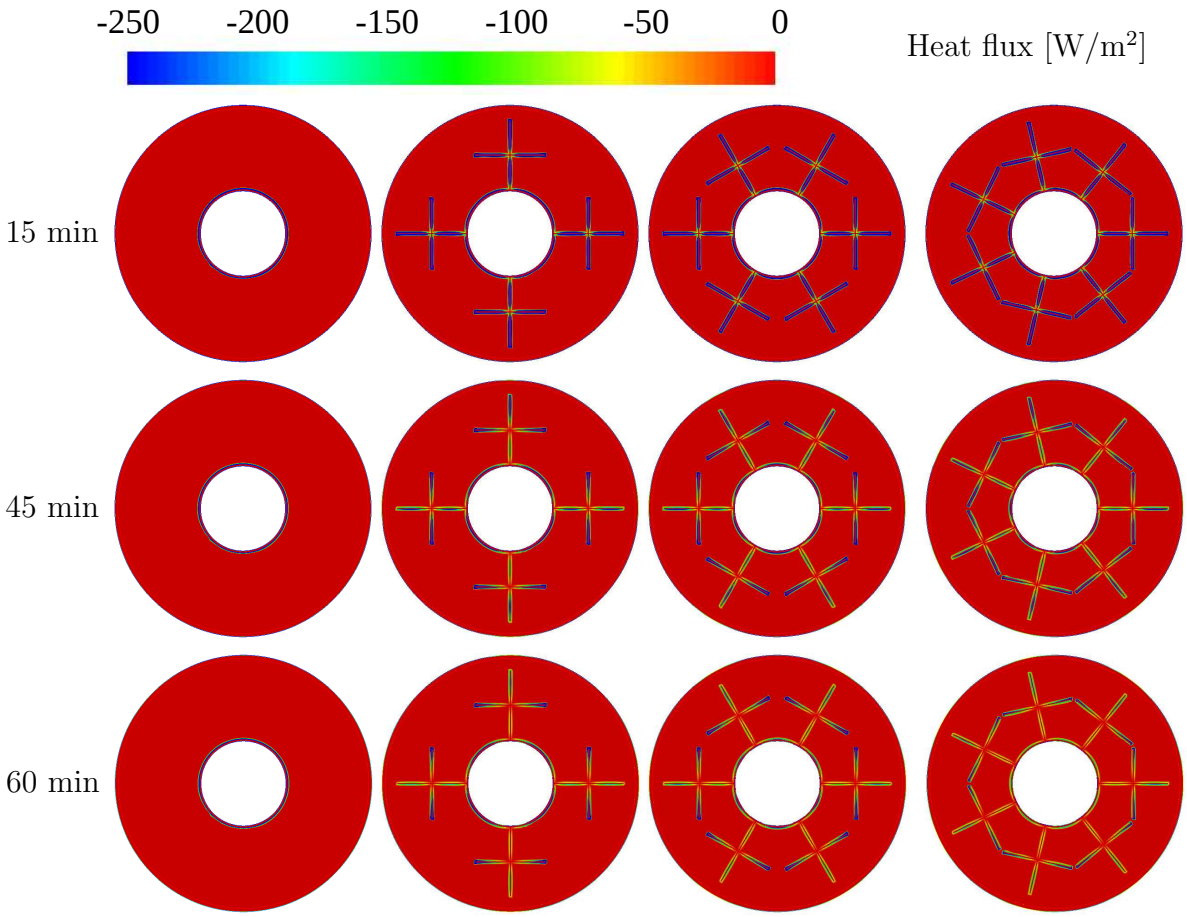

Figure 4.27: Surface heat flux contours at different times for solidification process for different plus fin numbers configurations': first from the left without fins, second 4 fins, third 6 fins, and fourth 7 fins.

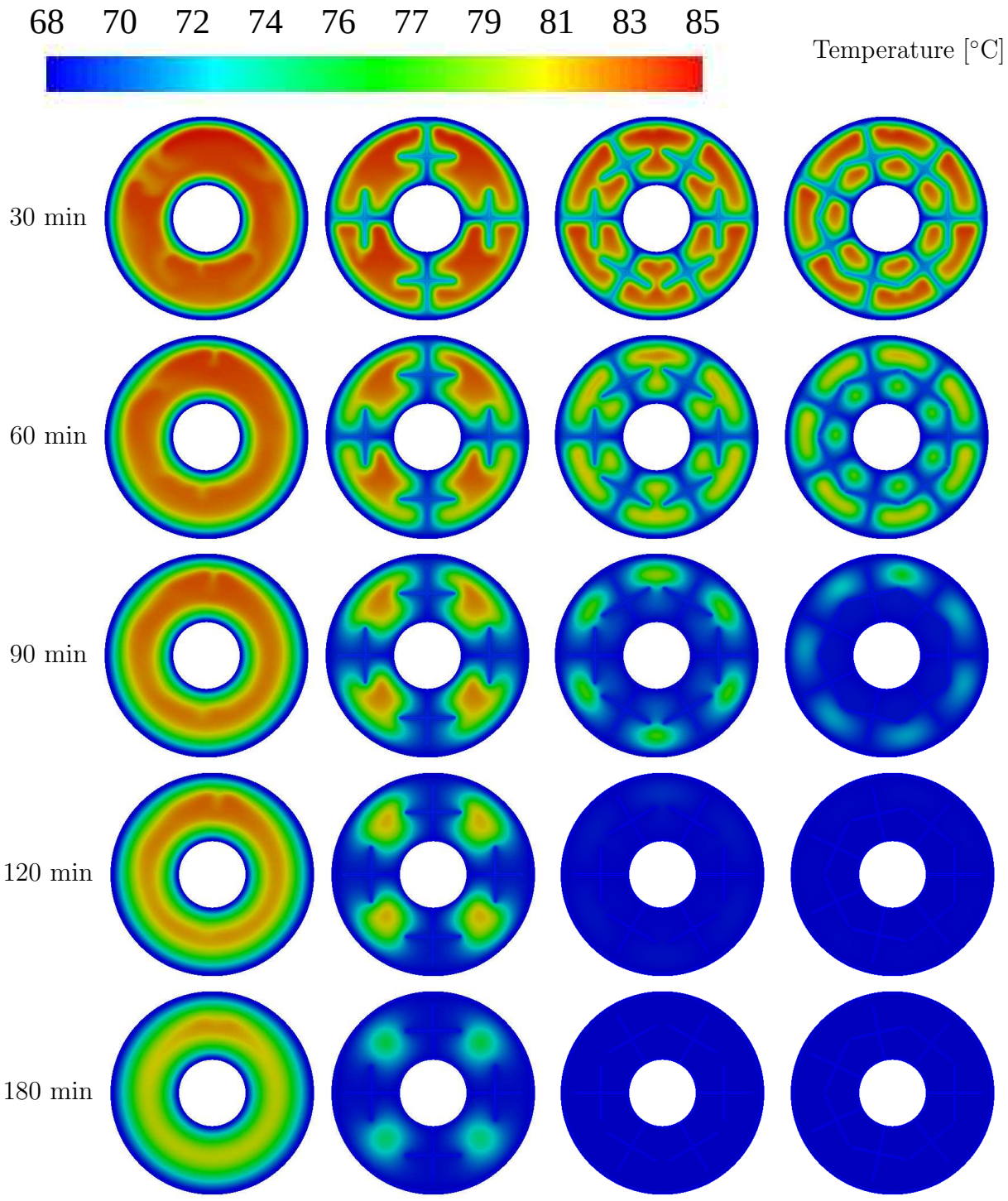

Figure 4.28: Contours of temperature at different times for solidification process for various numbers of plus fins: first from the left without fins, second 4 fins, third 6 fins, and fourth 7 fins.

4.5 Influence of plus fins dimensions on the TTHX thermal performance

For this test, TTHX with six plus fins welded to the external surface of the inner HTF tube wall was utilized to study the influence of fins' dimensions: length (L), width (W) and thickness (t).

4.5.1 Effect of fin length

The influence of fins' lengths on the solidification and melting of PCM in the TTHX were investigated. Various fin lengths were tested without changing the fin's width and thickness. The fin lengths tested were 25 mm, 30 mm, 35 mm, and 42 mm. The dimensions of different fin length cases are shown in Table 4.7 and Fig. 4.8c.

Table 4.7: Dimensions of different fin length cases

Fin case	**Length (L) (mm)**	**Width (W) (mm)**	**Thickness (t) (mm)**
Case 1	25	42	1
Case 2	30	42	1
Case 3	35	42	1
Case 4	42	42	1

Melting process

Fig. 4.29 illustrates the liquid fraction for different fin length cases. It is obvious from this figure that increasing the length of fins improves the melting rate. When fins' length was 42 mm the PCM completely melted after 2 hours compared to 3 hours in the case when the fins' length was 25 mm. Hence, the total PCM melting time decreased by 33% when

the fins' length increased from 25 mm to 42 mm. The total melting time and melting time reductions for different plus fins' lengths are shown in Table 4.8.

The average PCM temperature for various fin length cases is shown in Fig. 4.30. It is obvious from this figure that the PCM temperature increased by increasing the length of fins due to the increase of the heat transfer rate, thereby accelerating the PCM melting process. Contours of liquid fraction for various fin lengths are shown in Fig. 4.31. It is clear from this figure that employing longer fins of high conductivity increases the PCM melting rate due to increasing the conduction heat transfer, due to the increase of the heat transfer area and thermal penetration depth. Contours of temperature for various fin lengths are shown in Fig. 4.32. It is seen from this figure that increasing the length of fins increases PCM temperature owing to the increase in conduction heat transfer rate, thus accelerating the melting process.

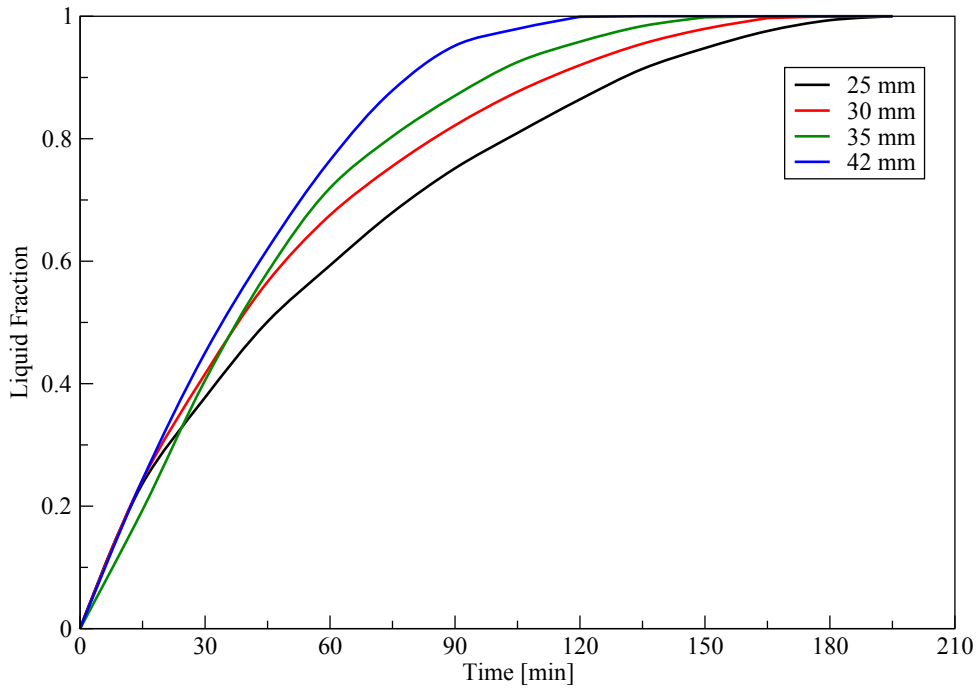

Figure 4.29: PCM liquid fraction comparison for melting process for different plus fins' lengths.

Table 4.8: Melting time and melting time reduction for different plus fins' lengths

Fin length (mm)	**Melting time (min)**	**Reduction (%)**
25 (base case)	180	—
30	167	7
35	151	16
42	120	33

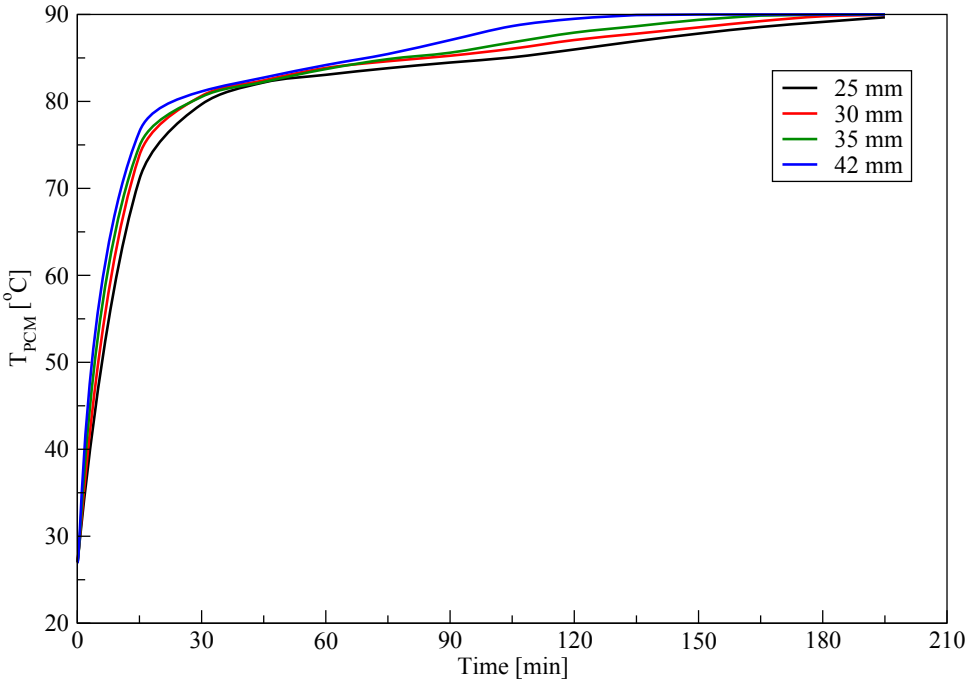

Figure 4.30: PCM average temperature comparison for melting process for various plus fins' lengths.

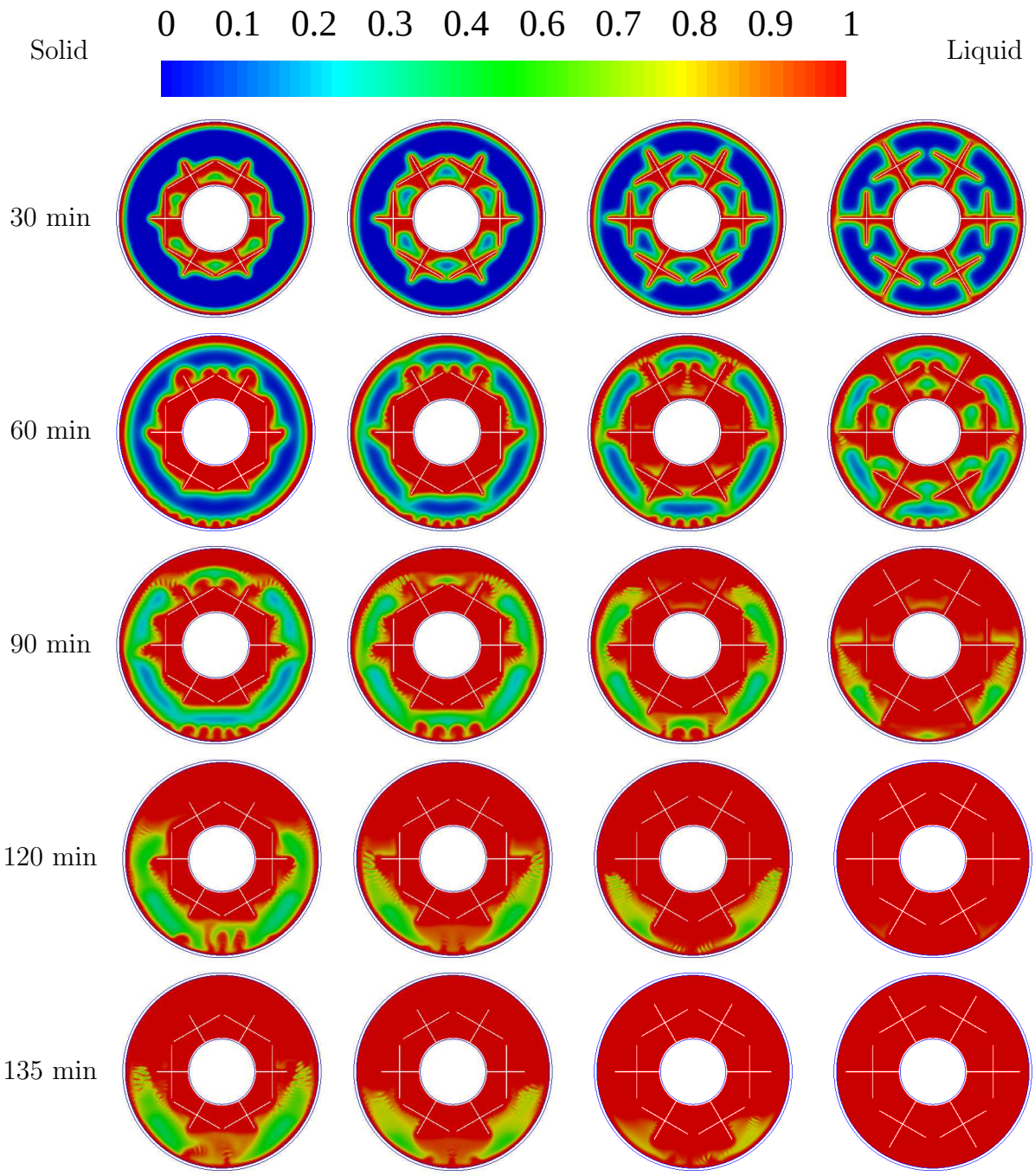

Figure 4.31: Liquid fraction contours at different times for the melting process for various plus fins' lengths: first from left 25 mm, second 30 mm, third 35 mm, and fourth 42 mm.

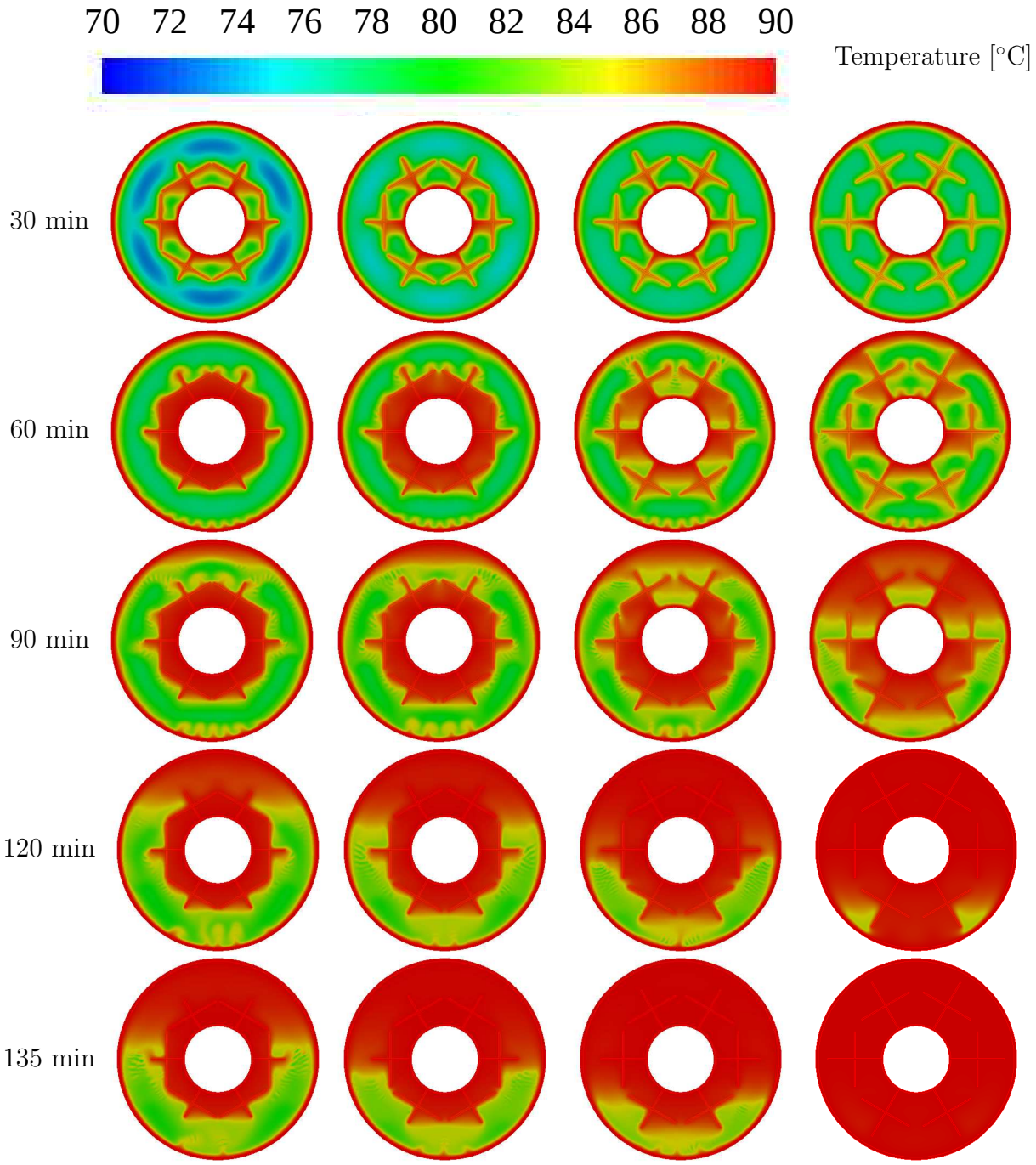

Figure 4.32: Contours of temperature at different times for the melting process for various plus fins' lengths: first from left 25 mm, second 30 mm, third 35 mm, and fourth 42 mm.

Solidification process

Fig. 4.33 shows the liquid fraction versus time for various fin length configurations. It is clear from this that the solidification rate increased by utilizing longer fins. When the length of fins was 42 mm the PCM completely solidified after 1.5 hours, compared to 2.25 hours when the length of fins was 25 mm. As such, the total PCM solidification time decreased by about 33% if the fins' length increased from 25 mm to 42 mm. The total solidification time and solidification time reductions for different plus fins' lengths are shown in Table 4.9.

The average PCM temperature for various fins lengths cases is illustrated in Fig. 4.34. It is clear from this figure that utilizing longer fins increases the heat transfer rate and decreases the PCM temperature, thereby accelerating the solidification process.

Liquid fraction contours for different fins lengths are shown in Fig. 4.35. The PCM solidification process accelerated by increasing the length of fins owing to the increase of the thermal penetration depth. Contours of temperature for different fin lengths are shown in Fig. 4.36. It is obvious from this figure that employing longer fins enhances the conduction heat transfer rate, thus decreasing the PCM temperature and accelerating the solidification process.

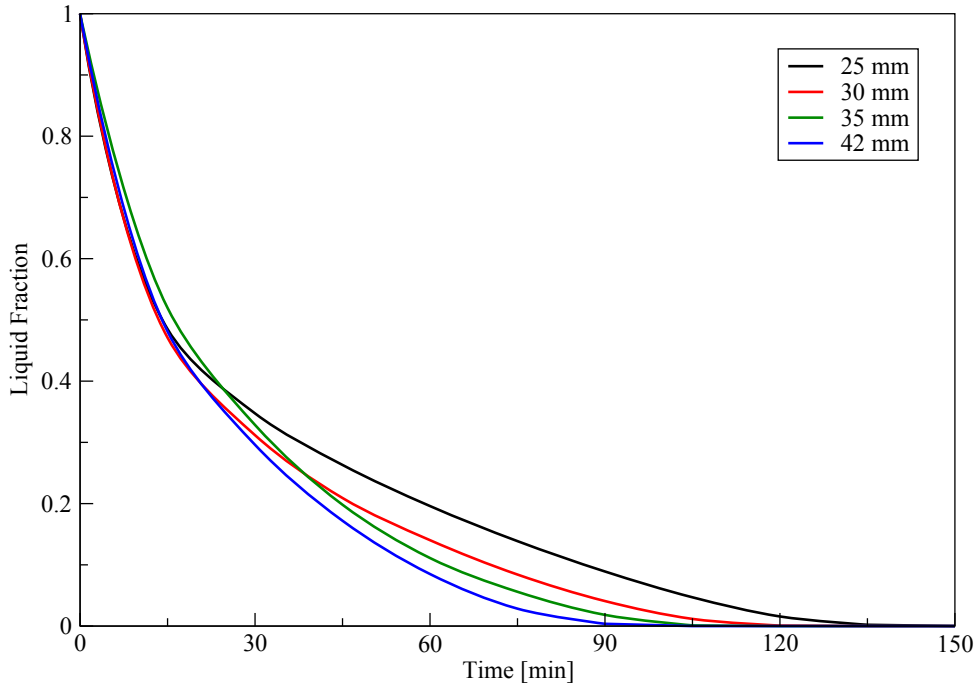

Figure 4.33: PCM liquid fraction comparison for solidification process for different plus fins' lengths.

Table 4.9: Solidification time and solidification time reduction for different plus fins' lengths

Fin length (mm)	**Solidification time (min)**	**Reduction (%)**
25 (base case)	135	—
30	121	10
35	107	20
42	90	33

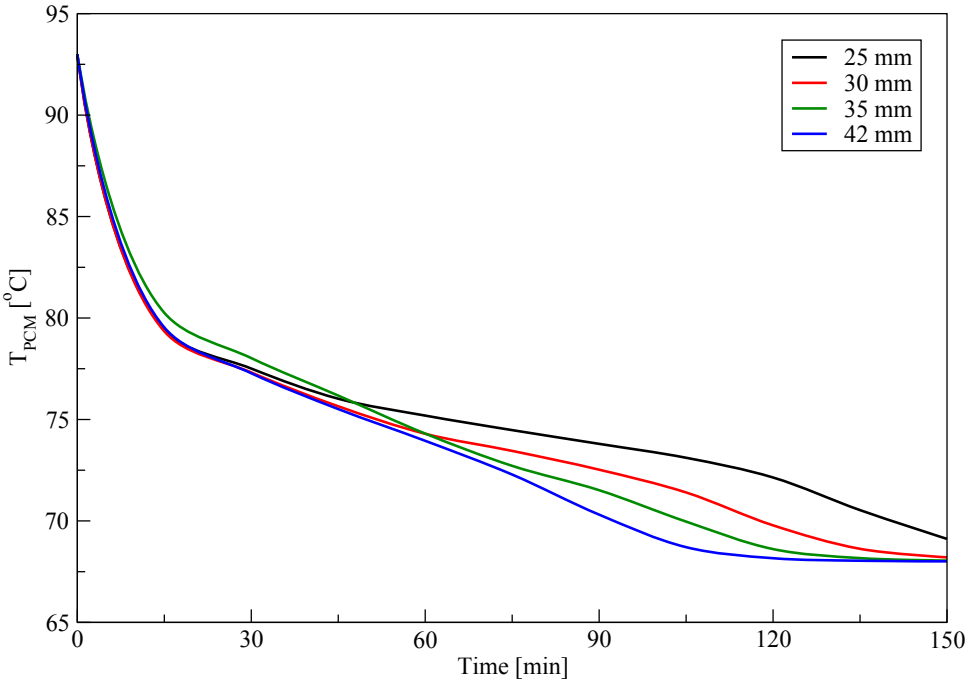

Figure 4.34: PCM average temperature comparison for solidification process for various plus fins' lengths.

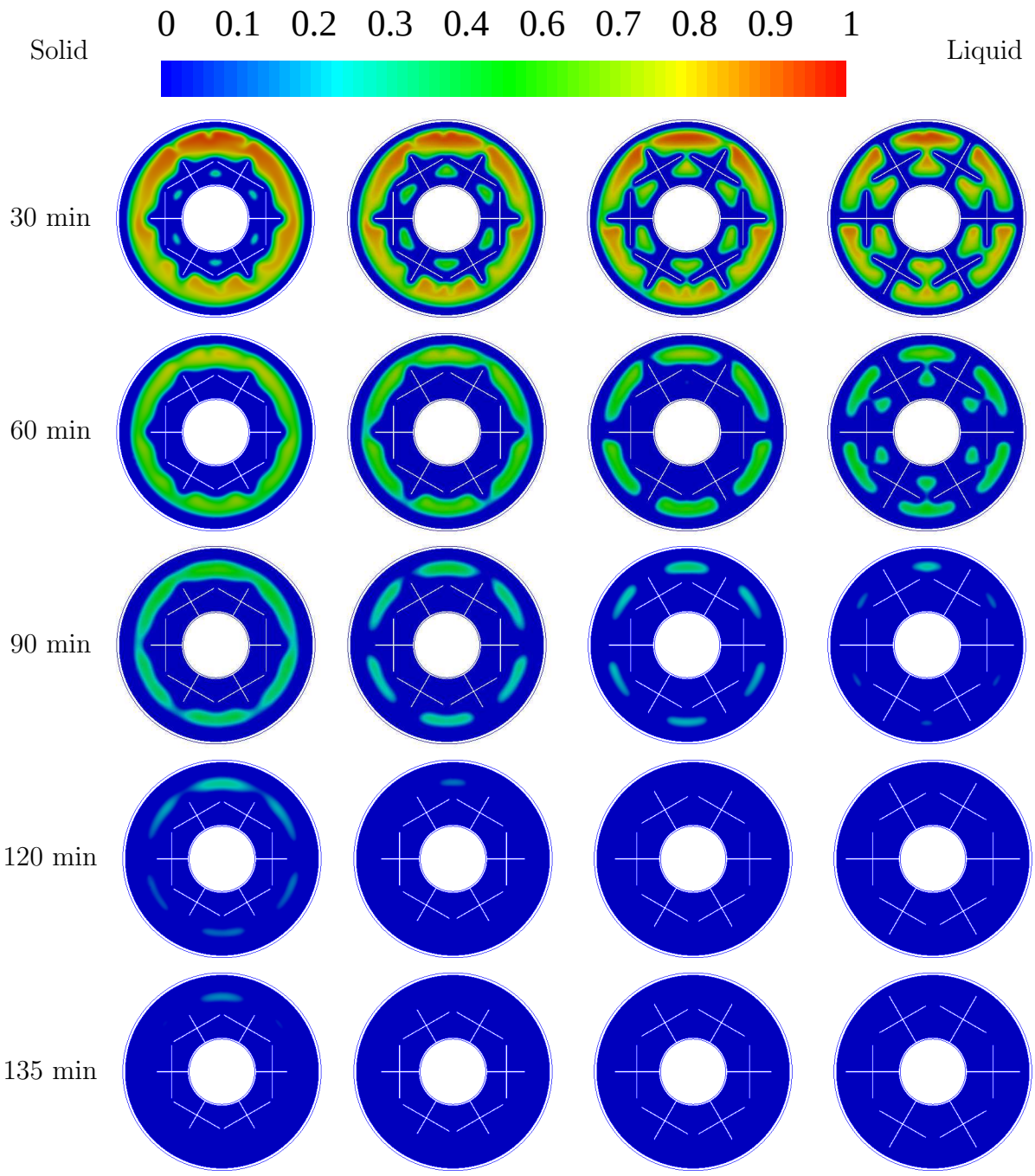

Figure 4.35: Liquid fraction contours at different times for solidification process for different plus fins' lengths: first from left 25 mm, second 30 mm, third 35 mm, and fourth 42 mm.

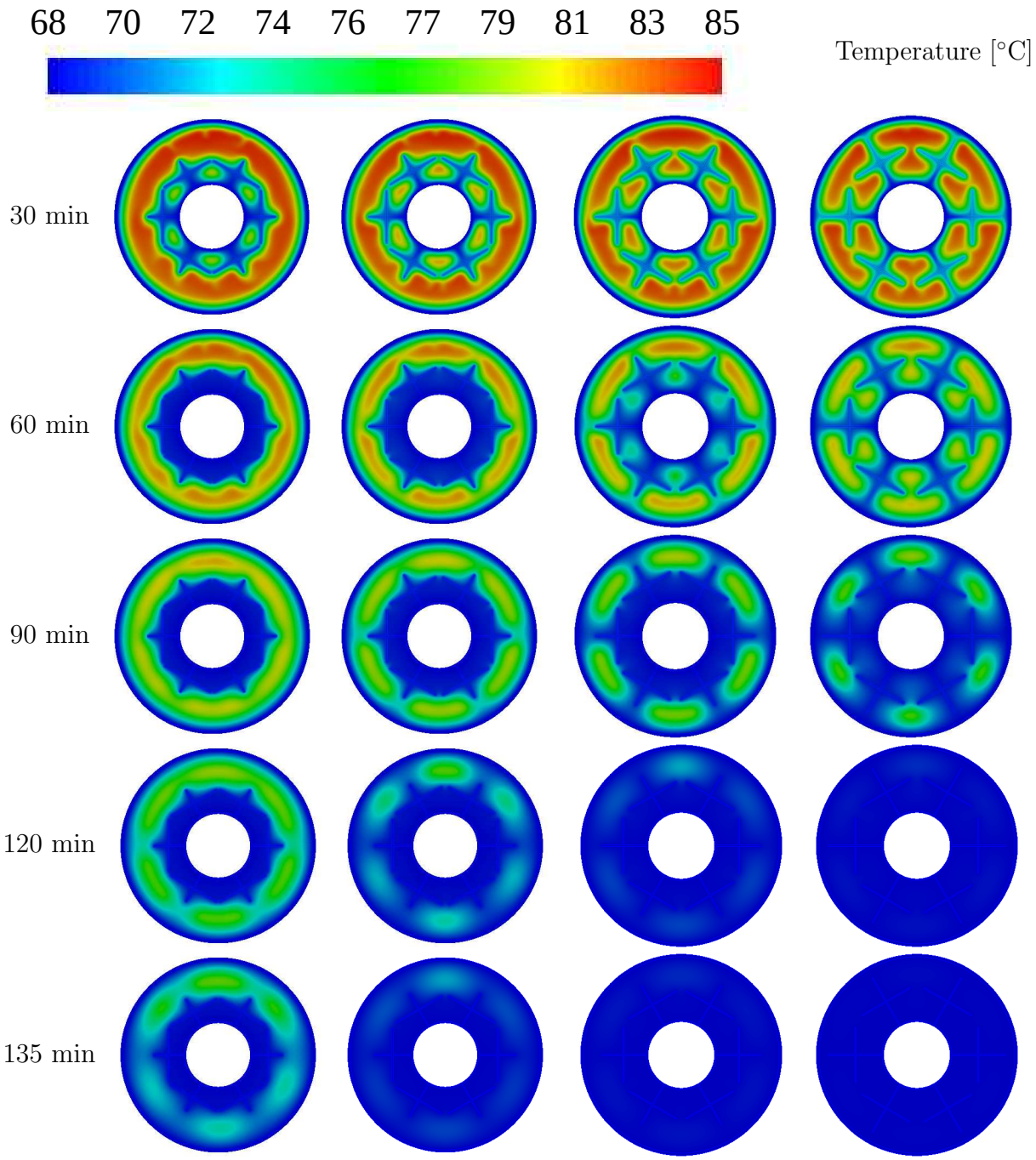

Figure 4.36: Contours of temperature at different times for solidification process for different plus fins' lengths: first from left 25 mm, second 30 mm, third 35 mm, and fourth 42 mm.

4.5.2 Effect of fins width

Different fin widths were tested without changing the length and thickness of fins. The widths tested were 15 mm, 25 mm, 35 mm, and 50 mm. The dimensions of different fin width cases are shown in Table 4.10.

Table 4.10: Dimensions of various fin width cases

Fin case	**Length (L) (mm)**	**Width (W) (mm)**	**Thickness (t) (mm)**
Case 1	42	15	1
Case 2	42	25	1
Case 3	42	35	1
Case 4	42	50	1

Melting process

Fig. 4.37 shows the PCM liquid fraction for various fin width cases. It is clear from this figure that increasing fin width increases the melting rate. When fin width was 50 mm the PCM completely melted after 1.75 hours, compared to 2.5 hours when fin width was 15 mm. Thus, the total PCM melting time decreased by about 30% if the fin width increased from 15 mm to 50 mm. The total melting time and melting time reductions for different plus fins' widths are shown in Table 4.11.

The average PCM temperature for various fins' configurations is shown in Fig. 4.38. It is obvious from this figure that the heat transfer rate increased by increasing the width of the fins, thereby increasing the PCM temperature and accelerating the melting process.

Liquid fraction contours for different fin widths are shown in Fig. 4.39. The melting process accelerated by increasing the width of the fins is due to increasing heat transfer area. Contours of temperature for various fin widths are shown in Fig. 4.40. As is seen from this figure, increasing fin width improves heat transfer rate, which accelerates the PCM

melting process.

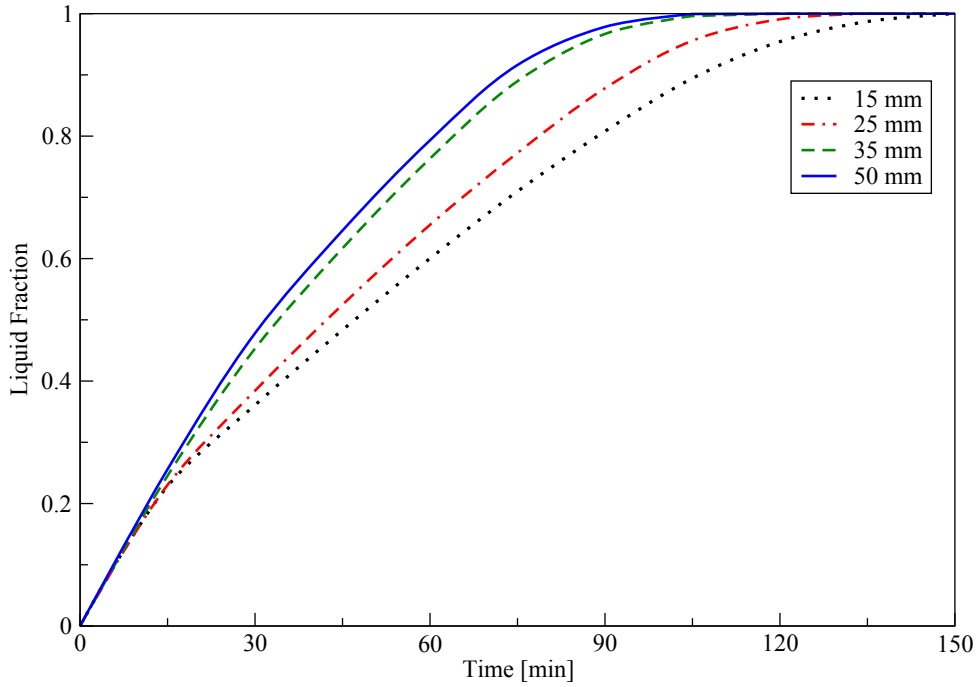

Figure 4.37: PCM liquid fraction comparison for melting process for different plus fins' widths.

Table 4.11: Melting time and melting time reduction for different plus fins' widths

Fin width (mm)	**Melting time (min)**	**Reduction (%)**
15 (base case)	150	—
25	127	15
35	107	28
50	105	30

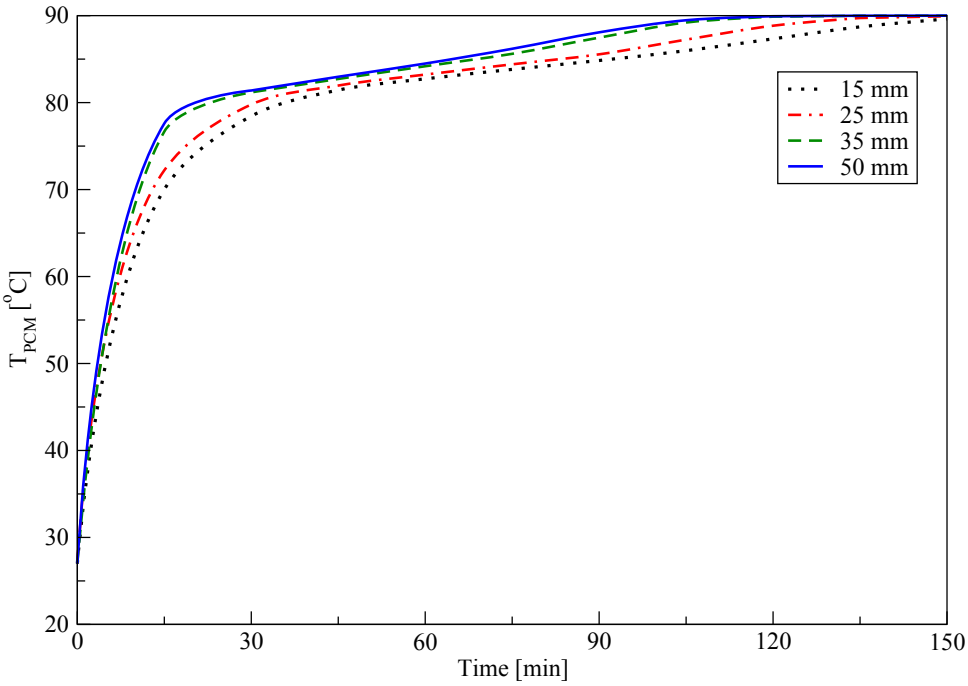

Figure 4.38: PCM average temperature comparison for melting process for various plus fins' widths.

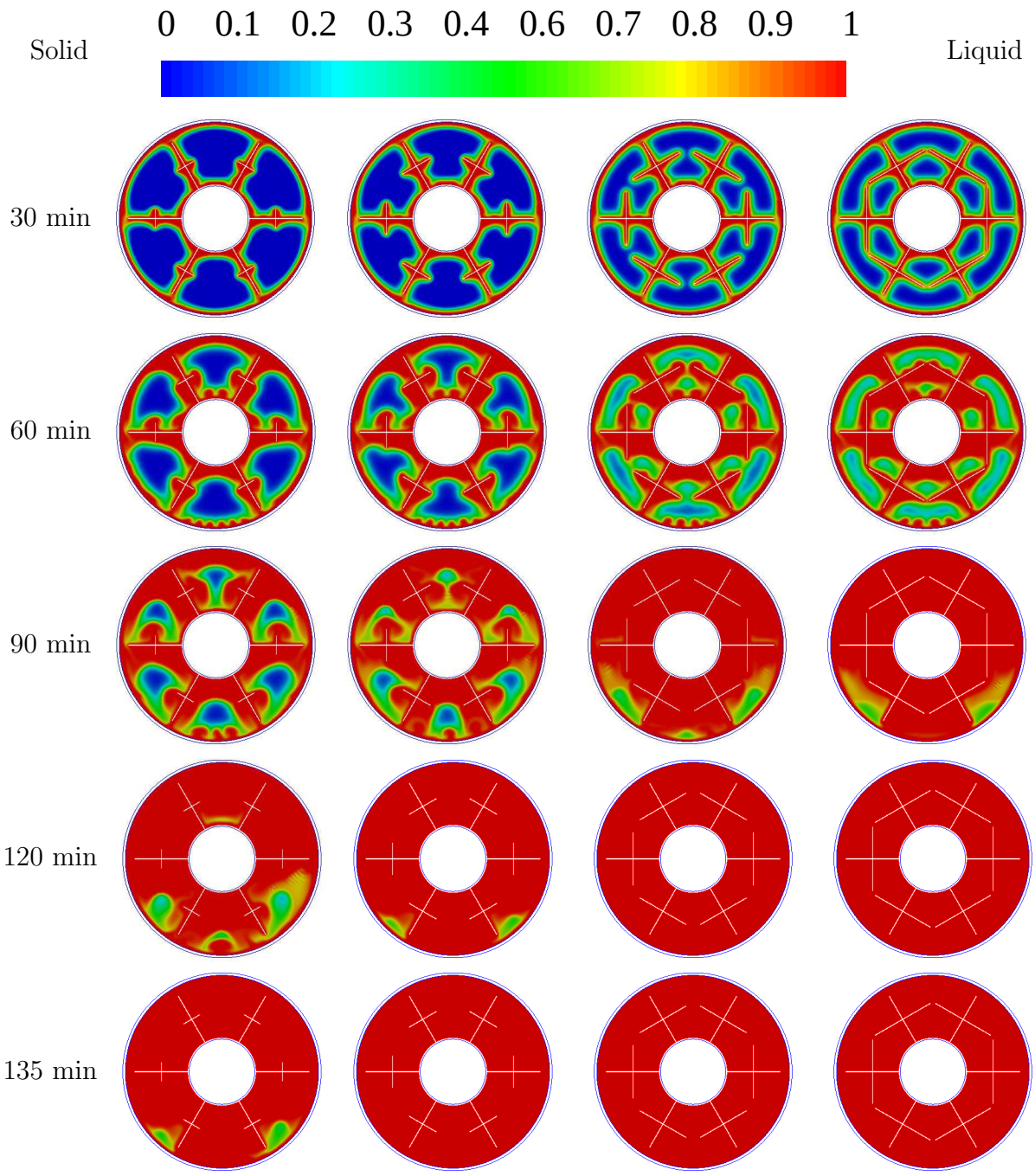

Figure 4.39: Liquid fraction contours at different times for melting process for various plus fins' widths: first from left 15 mm, second 25 mm, third 35 mm and fourth 50 mm.

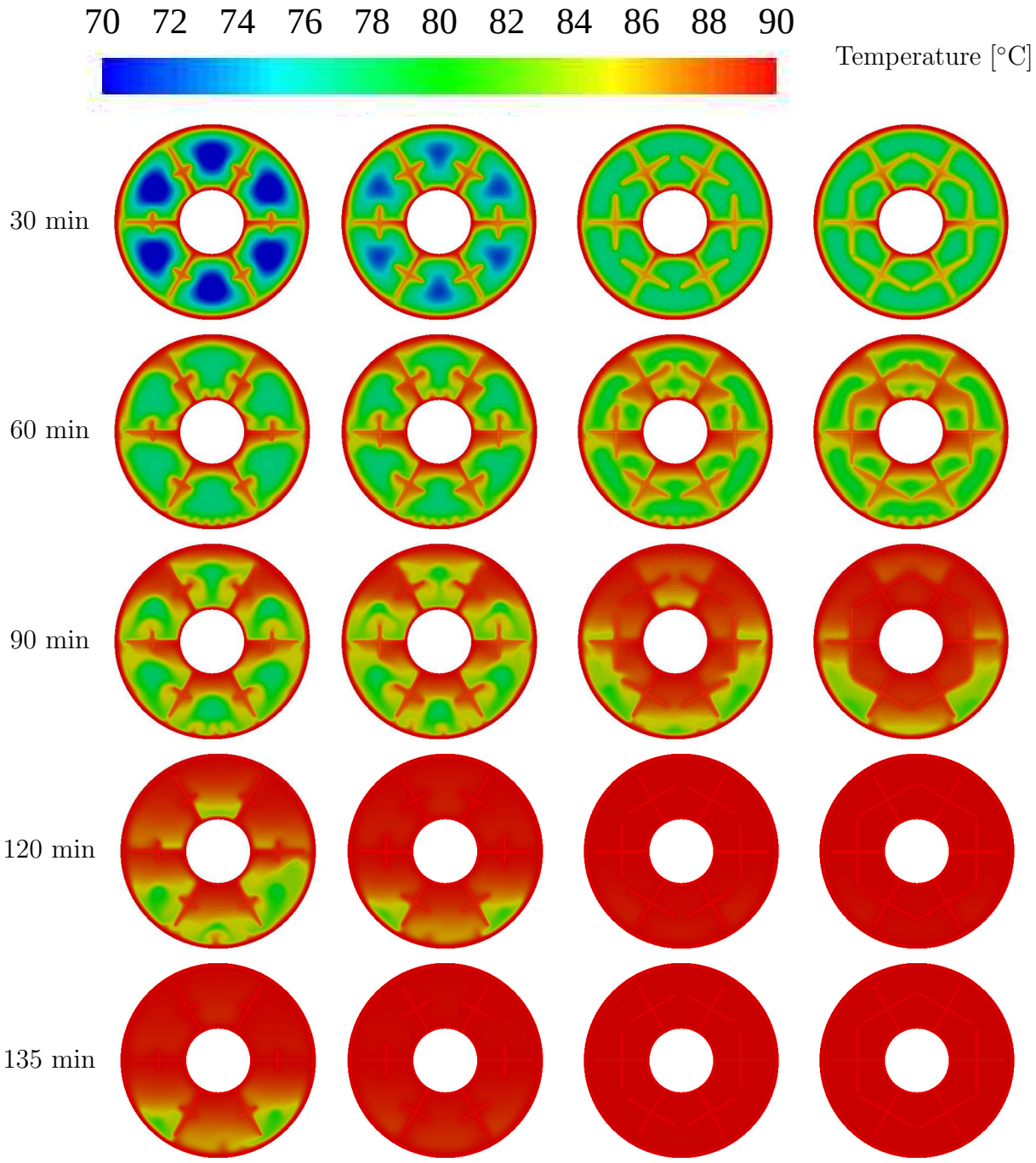

Figure 4.40: Contours of temperature at different times for melting process for different plus fins' widths: first from left 15 mm, second 25 mm, third 35 mm, and fourth 50 mm.

Solidification process

Fig. 4.41 presents the liquid fraction versus time for various fin width configurations. It can be seen from this figure that the solidification process is significantly accelerated by increasing the fins' width. When the width was 50 mm the PCM completely solidified after 1.5 hours, compared to 2.5 hours when the fins width was 15 mm. Given this, the total PCM solidification time decreased by about 40% if the fins' width increased from 15 mm to 50 mm. It is also clear from Fig. 4.41 that the melting rate of PCM after a 30-minute increased significantly by increasing the fins' width due to the increase of heat conduction due to the increase of heat transfer surface area. The total solidification time and solidification time reductions for different plus fins' widths are shown in Table 4.12. The average PCM temperature for various fin width configurations is shown in Fig. 4.42. It is seen that by increasing the width of fins the PCM temperature decreased due to the increase of the heat transfer rate, thereby accelerating the solidification process. Liquid fraction contours for different fins' widths are shown in Fig. 4.43. It can be observed that the PCM solidification rate increased by increasing the width of fins due to increasing the heat transfer area and thermal penetration depth. By increasing the fins' width, the high thermal conductivity fins reached more regions of PCM which has low thermal conductivity, hence the melting rate increases. Contours of temperature for various fins' widths are shown in Fig. 4.44. It is seen that increasing the width of fins decreases the PCM temperature and accelerates the PCM solidification process.

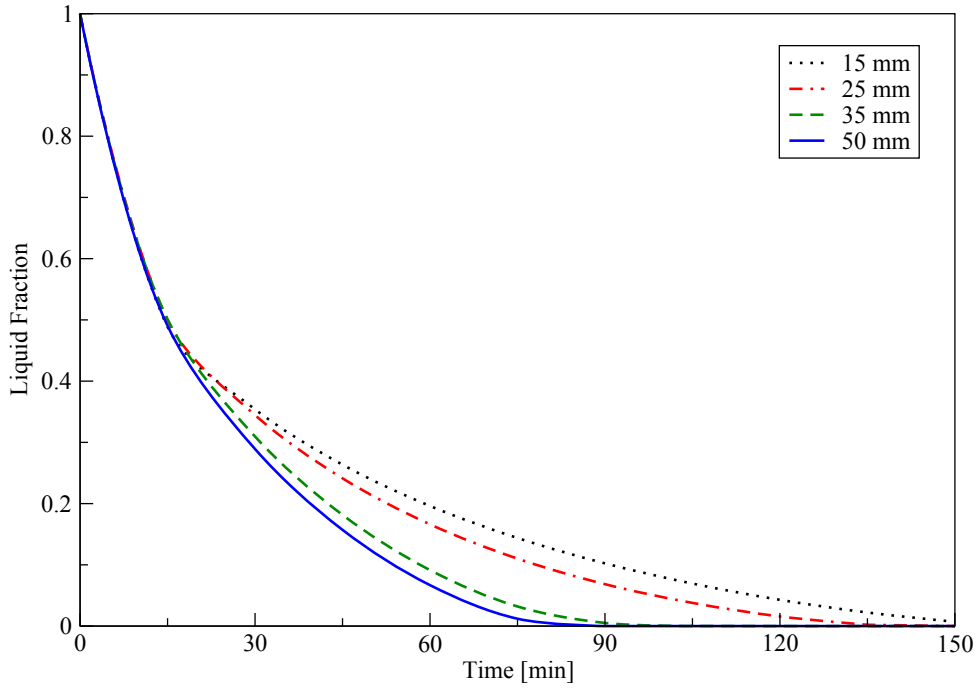

Figure 4.41: PCM liquid fraction comparison for solidification process for different plus fin widths.

Table 4.12: Solidification time and solidification time reduction for different plus fins' widths

Fin width (mm)	**Solidification time (min)**	**Reduction (%)**
15 (base case)	150	—
25	136	9
35	98	34
50	90	40

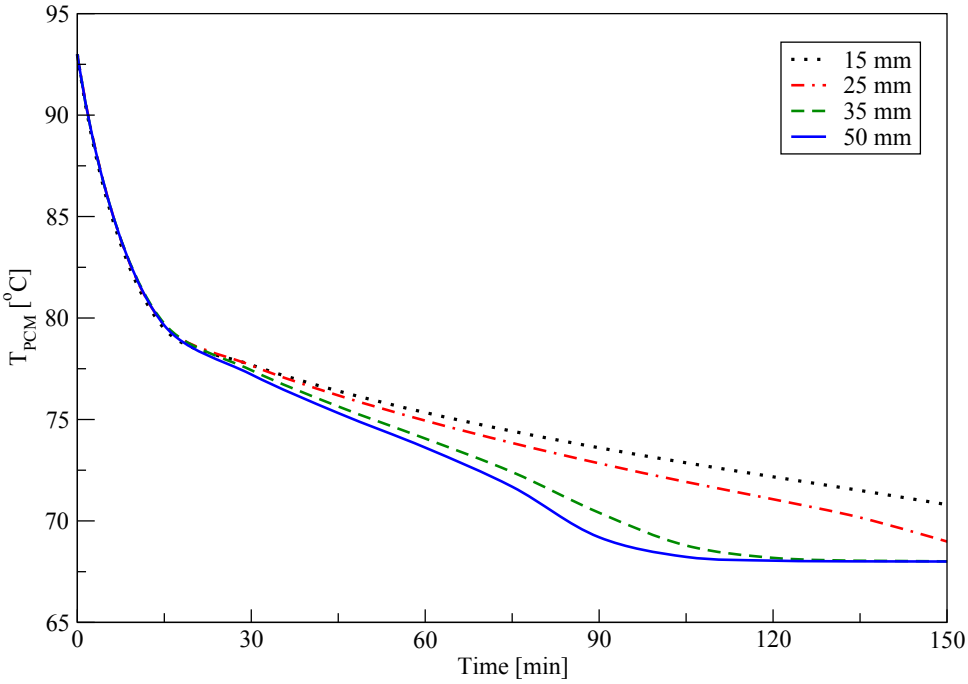

Figure 4.42: PCM average temperature comparison for solidification process for various plus fin widths.

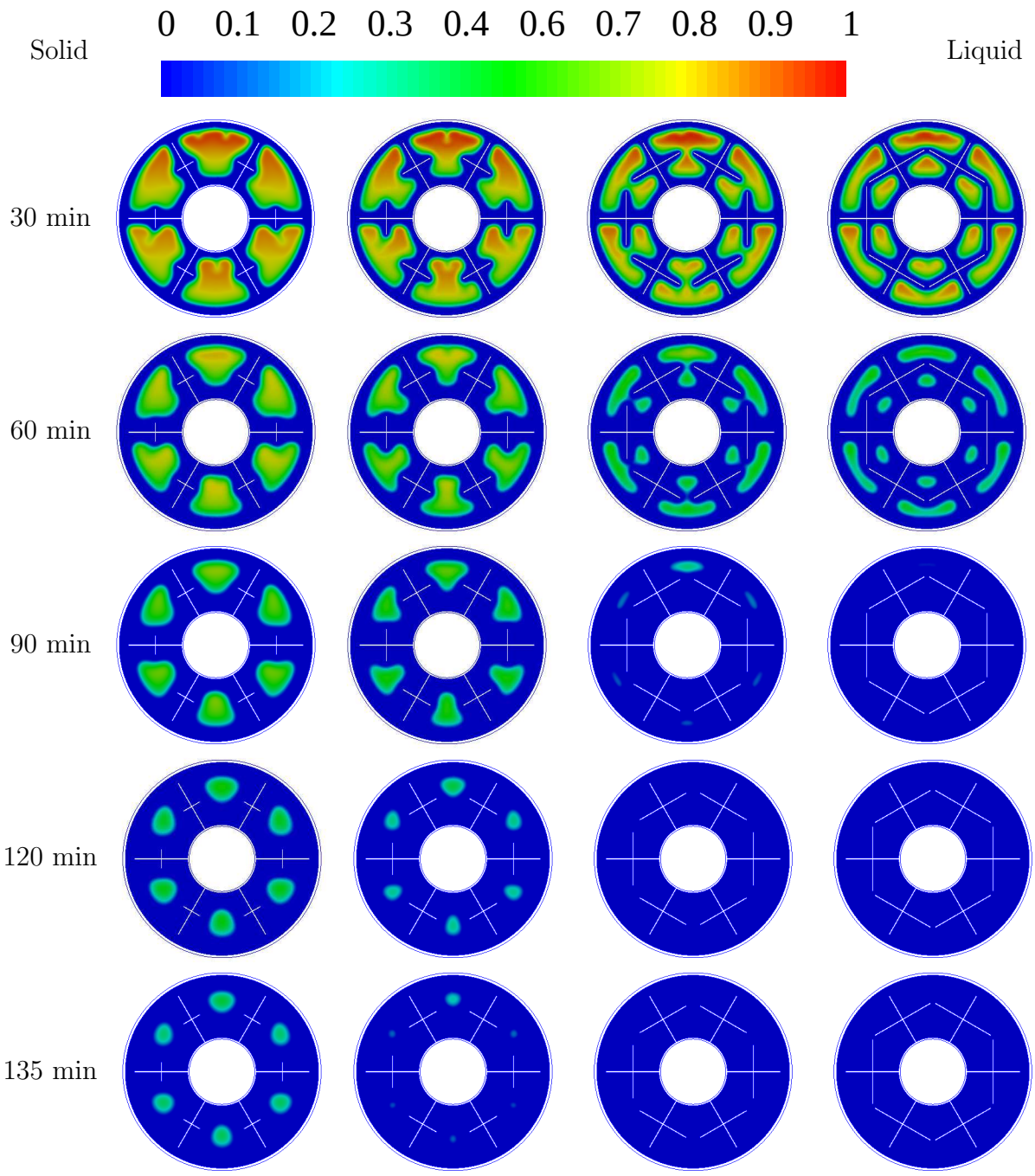

Figure 4.43: Liquid fraction contours at different times for solidification process for different plus fin widths: first from left 15 mm, second 25 mm, third 35 mm, and fourth 50 mm.

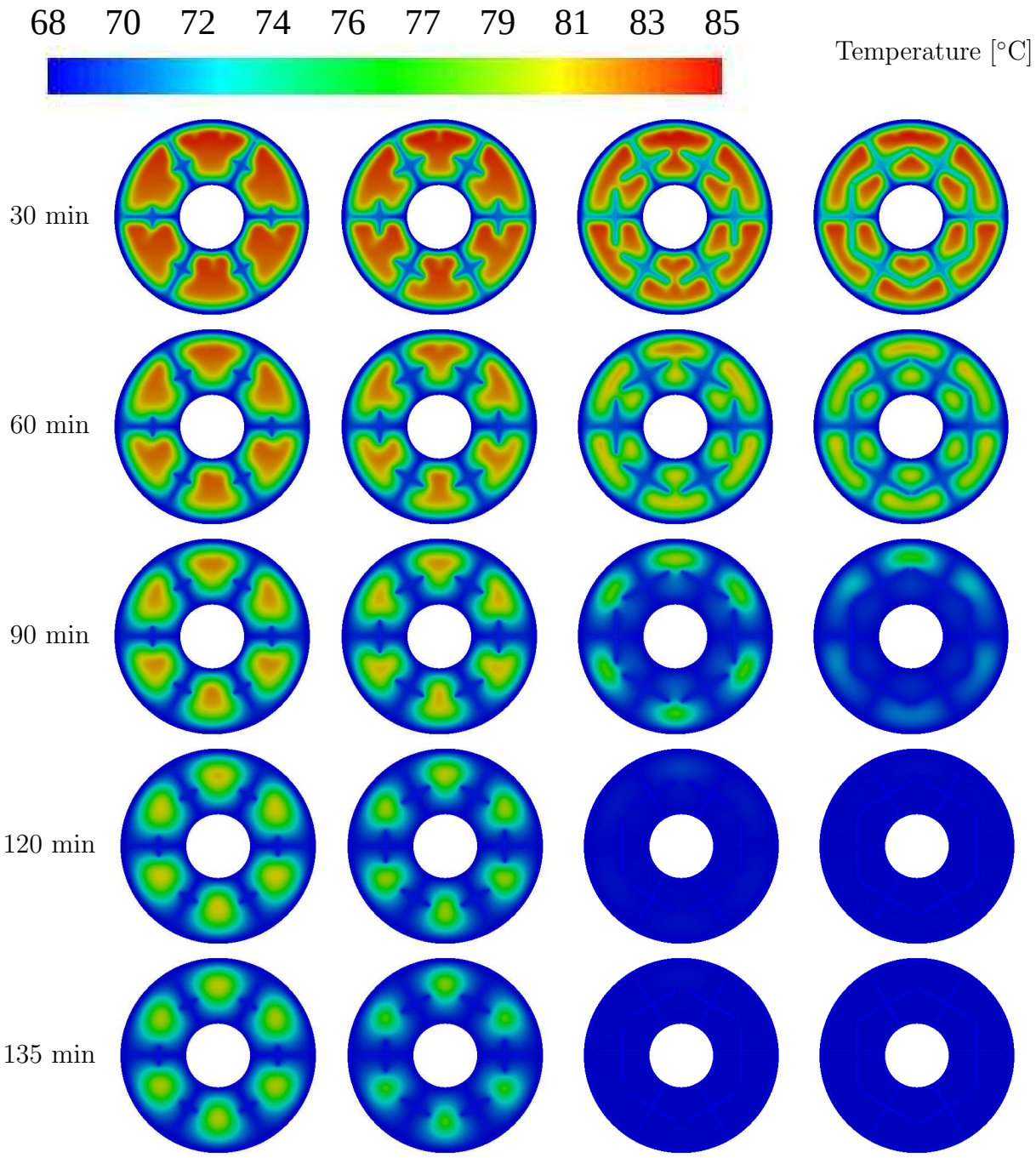

Figure 4.44: Contours of temperature at different times for solidification process for different plus fin widths: first from left 15 mm, second 25 mm, third 35 mm, and fourth 50 mm.

4.5.3 Effect of fins thickness

Different fins' thickness was tested without changing the length and width of fins. The thickness tests were for 0.5 mm, 1 mm, 2 mm and 3 mm. The dimensions of various fins' thickness cases are shown in Table 4.13.

Table 4.13: Dimensions of various fins' thickness cases

Fin case	**Length (L) (mm)**	**Width (W) (mm)**	**Thickness (t) (mm)**
Case1	42	42	0.5
Case2	42	42	1
Case3	42	42	2
Case4	42	42	3

Melting process

Fig. 4.45 presents the liquid fraction for different fins' thickness cases. It is obvious from this figure that the PCM melting process accelerated by increasing the thickness of the fins. When the thickness of fins was 3 mm the PCM completely melted after 1.5 hours as compared to 2.25 hours when the fins' thickness was 0.5 mm. Hence, the total PCM melting time decreases by about 33% if the fins' thickness increased from 0.5 mm to 3 mm. The total melting time and melting time reductions for different plus fins' thickness are shown in Table 4.14.

The average PCM temperature for various configurations is illustrated in Fig. 4.46. It is obvious that increasing fins' thickness improves the heat transfer rate and increases the PCM temperature, hence accelerating the melting process. Liquid fraction contours for various fins' thickness are displayed in Fig. 4.47. It is clear that the PCM melting rate increased by increasing the thickness of the fins. Contours of temperature for different fins' thickness are shown in Fig. 4.48. It is clear that by increasing the fins' thickness the

conduction heat transfer rate increased owing to the increase of the heat exchange area.

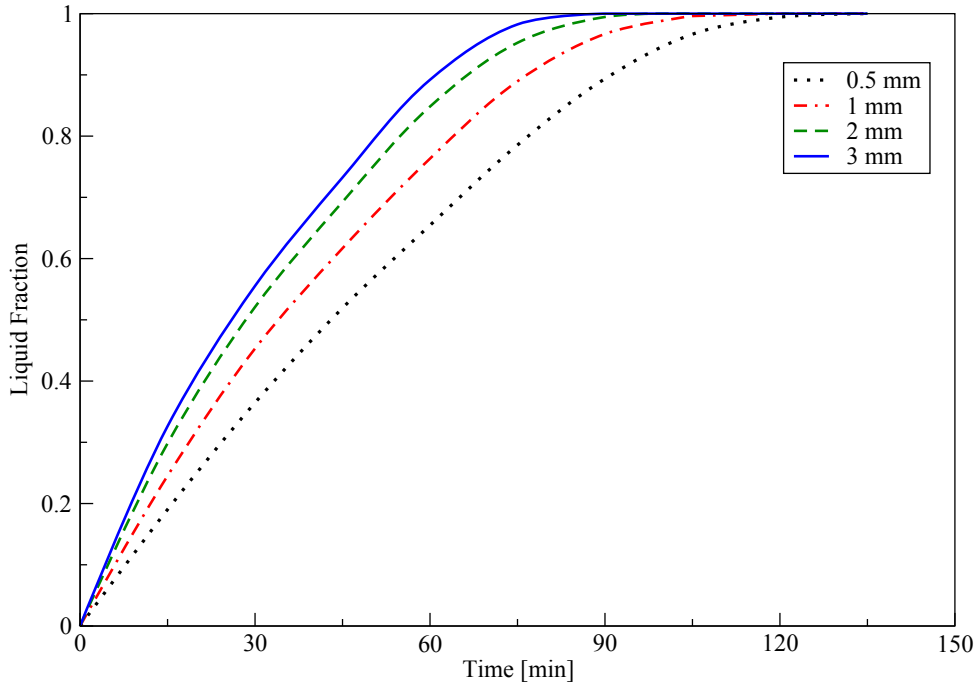

Figure 4.45: PCM liquid fraction comparison for melting process for different plus fins' thickness.

Table 4.14: Melting time and melting time reduction for different plus fins' thickness

Fin width (mm)	**Melting time (min)**	**Reduction (%)**
0.5 (base case)	135	—
1	118	12
2	102	24
3	90	33

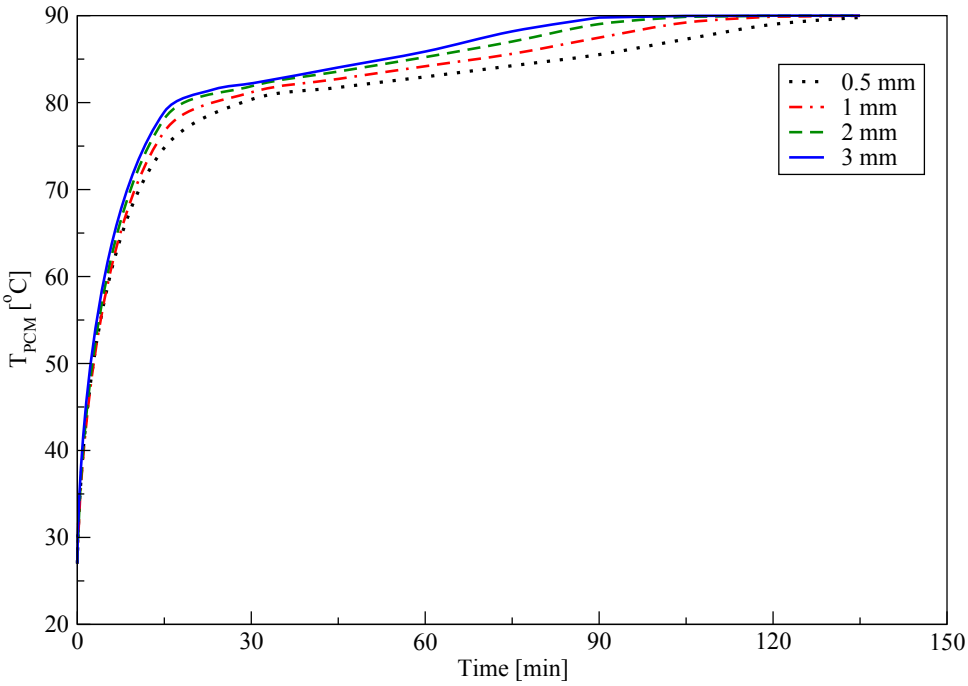

Figure 4.46: PCM average temperature comparison for melting process for various plus fins' thickness.

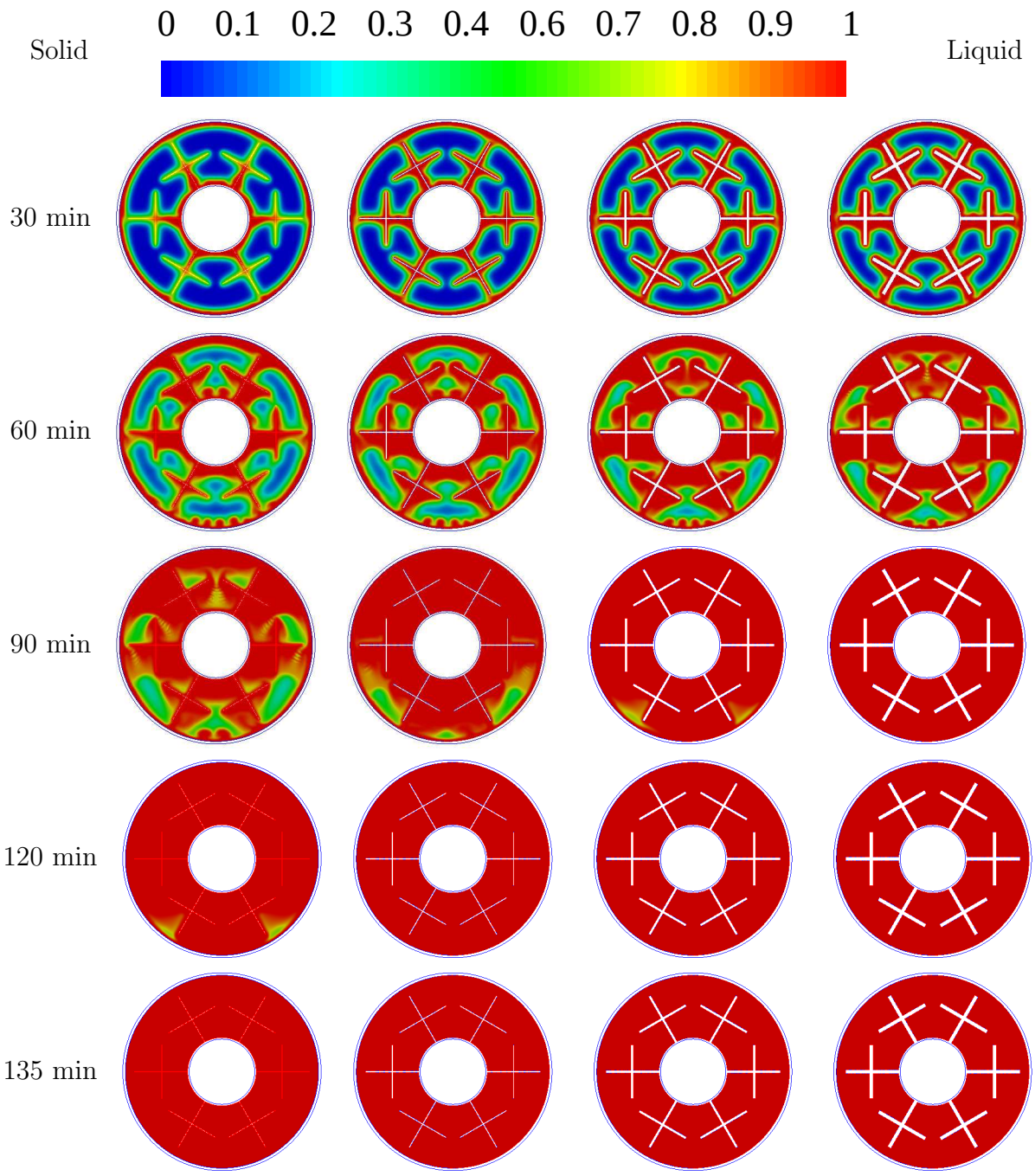

Figure 4.47: Liquid fraction contours at different times for melting process for various plus fins' thickness: first from left 0.5 mm, second 1 mm, third 2 mm, and fourth 3 mm.

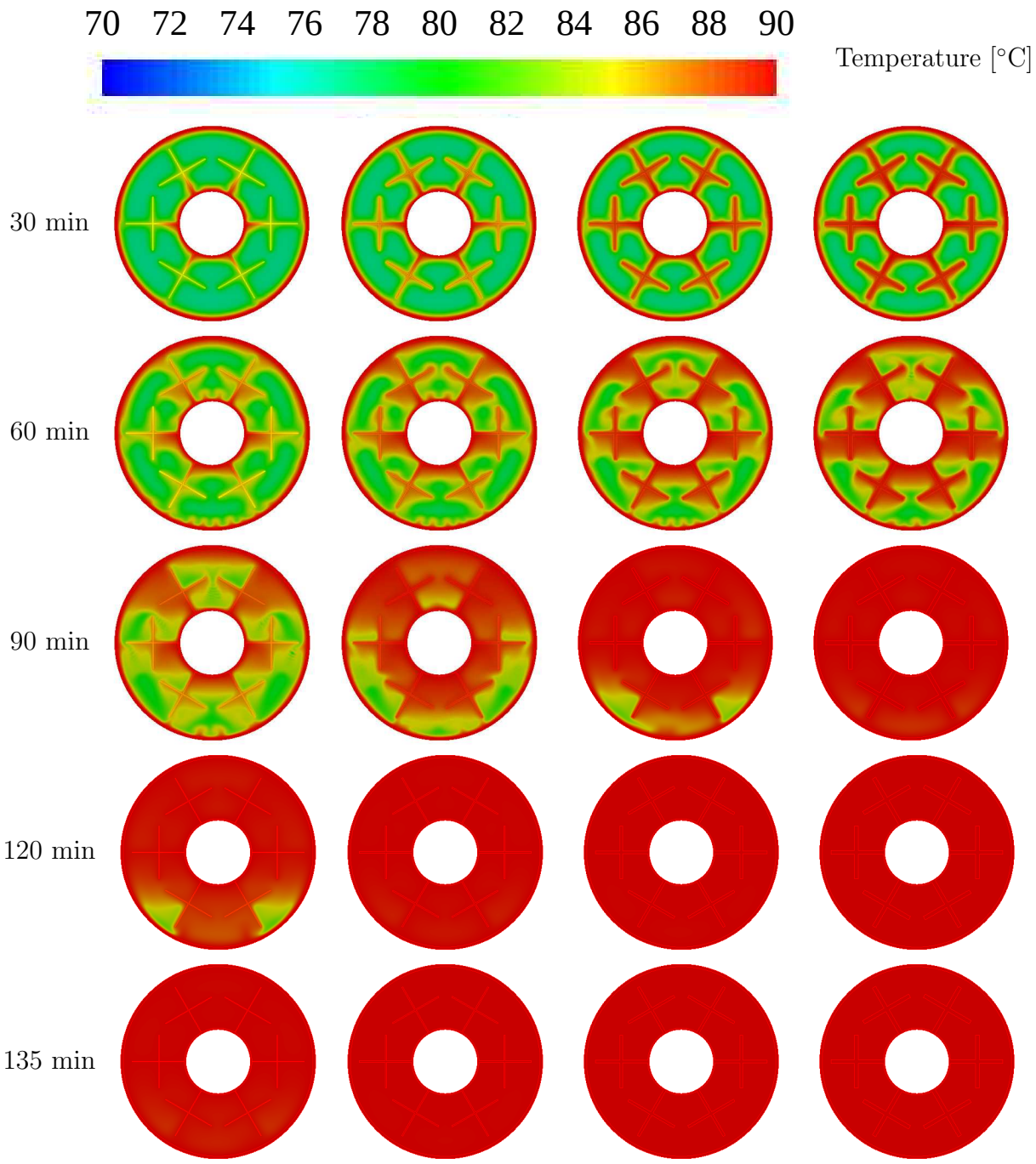

Figure 4.48: Contours of temperature at different times for melting process for different plus fins' thickness: first from left 0.5 mm, second 1 mm, third 2 mm, and fourth 3 mm.

Solidification process

Fig. 4.49 illustrates liquid fraction for different fin thickness cases. It is clear that increasing the thickness of fins accelerates the PCM solidification process. When fins' thickness was 3 mm the PCM completely solidified after 1.25 hours, compared to 1.75 hours in the case when fins' thickness was 0.5 mm. Hence, the total PCM solidification time decreased by about 28% if the fins' thickness increased from 0.5 mm to 3 mm. The average PCM temperature for various fin thickness configurations is exhibited in Fig. 4.50. It obvious from this figure that increasing fin thickness increases the heat transfer rate and decreases the PCM temperature. The total solidification time and solidification time reductions for different plus fins' thickness are shown in Table 4.15.

Liquid fraction contours for the various thickness of fins are shown in Fig. 4.51. The increase in the thickness of fins increases the solidification rate due to increasing the heat transfer area. Contours of PCM temperature at different times for different thickness of fins are displayed in Fig. 4.52. It is obvious that increasing fins' thickness decreases the PCM temperature and accelerates the PCM solidification process.

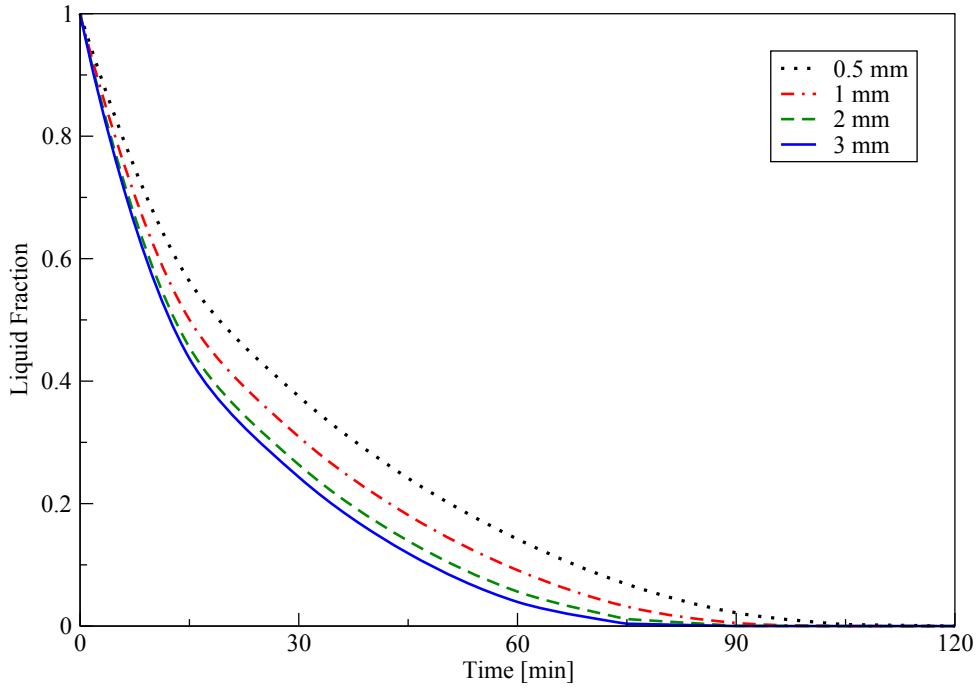

Figure 4.49: PCM liquid fraction comparison for solidification process for different plus fins' thickness.

Table 4.15: Solidification time and solidification time reduction for different plus fins' thickness

Fin width (mm)	**Solidification time (min)**	**Reduction (%)**
0.5 (base case)	105	—
1	96	8
2	89	15
3	75	28

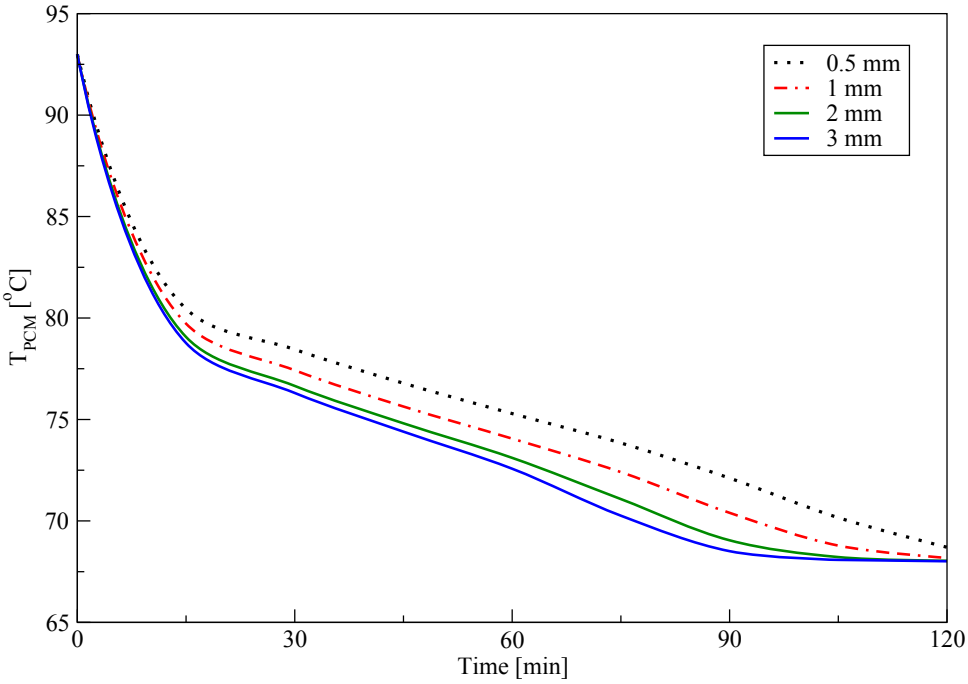

Figure 4.50: PCM average temperature comparison for solidification process for various plus fins' thickness.

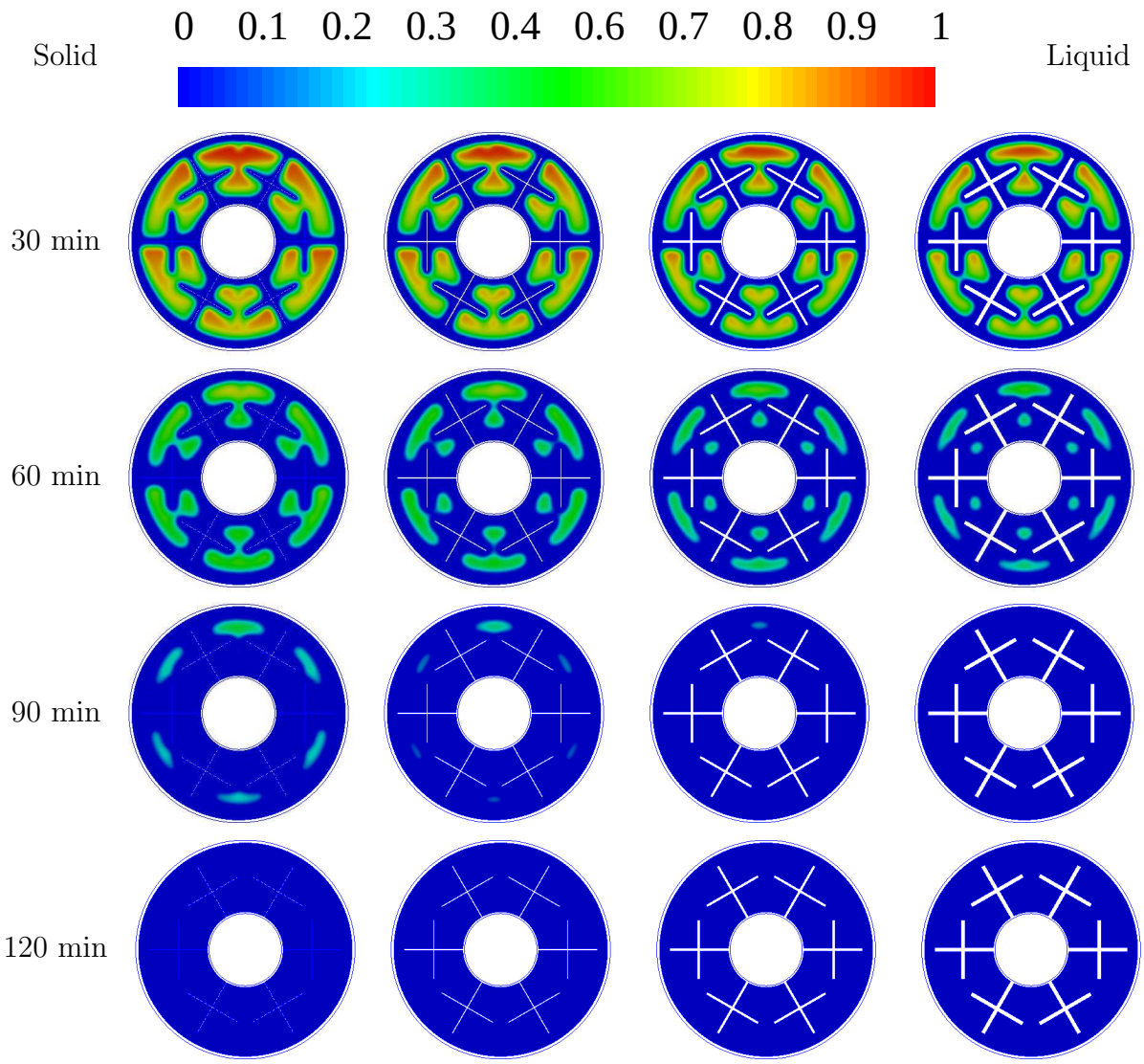

Figure 4.51: Liquid fraction contours at different times for solidification process for different plus fins' thickness: first from left 0.5 mm, second 1 mm, third 2 mm, and fourth 3 mm.

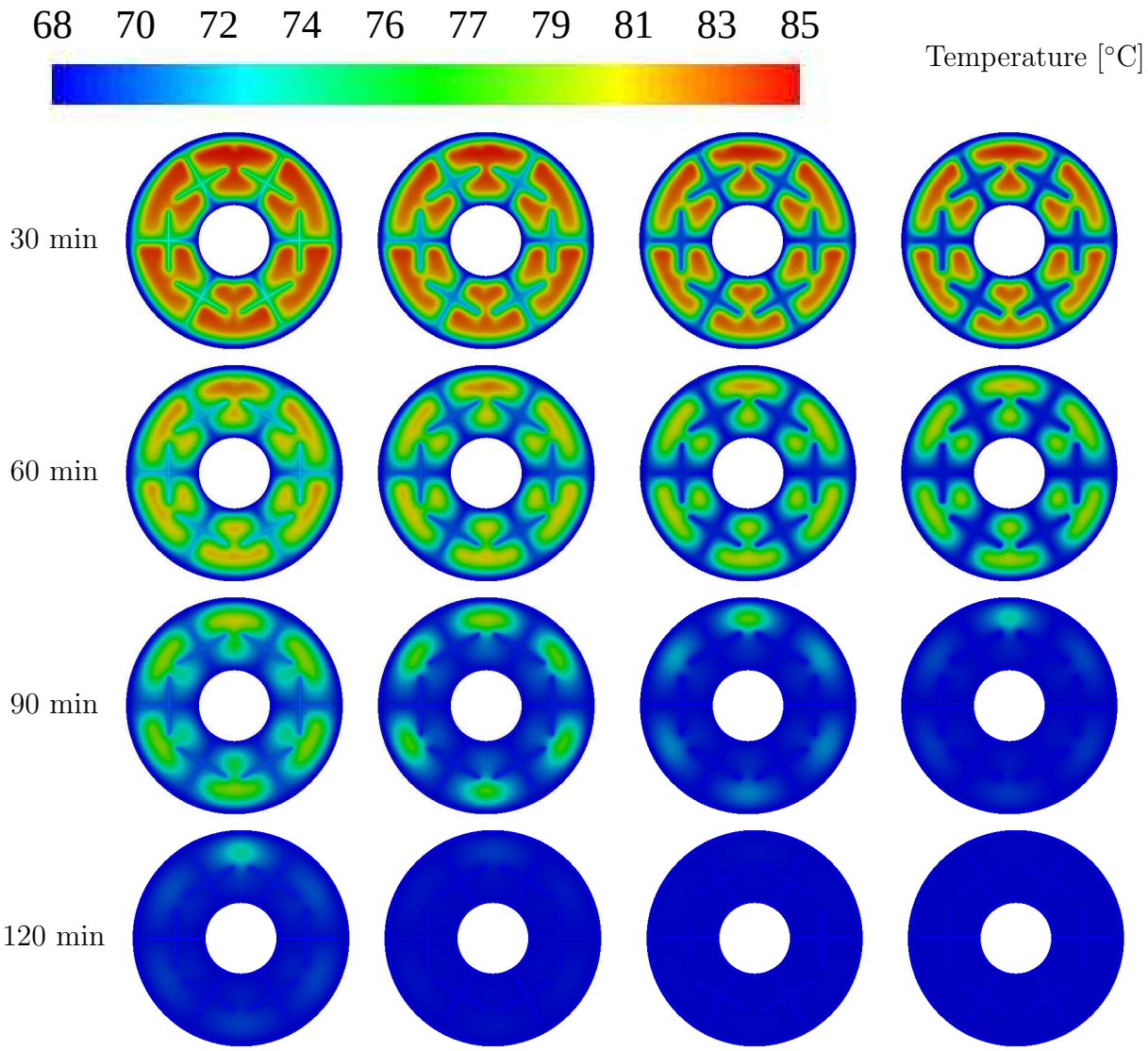

Figure 4.52: Contours of temperature at different times for the solidification process for different plus fins' thickness: first from left 0.5 mm, second 1 mm, third 2 mm, and fourth 3 mm.

4.6 Optimization by utilizing the response surface method

4.6.1 The influence of the shape of fins and the number of fins

For this test, the effect of changing fin numbers and changing fin shapes on the melting process of PCM in the TTHX was studied. Different numbers of fins were tested which were: 2 fins, 3 fins, 4 fins, 5 fins, and 6 fins. Then the shape of the fin was changed by changing the dimension (L1) see Fig. 4.53. The L1 dimensions tested were: 10.5 mm, 21 mm, 31.5 mm, and 42 mm. The new fin shapes that were produced by changing the dimension L1 are shown in Fig. 4.54.

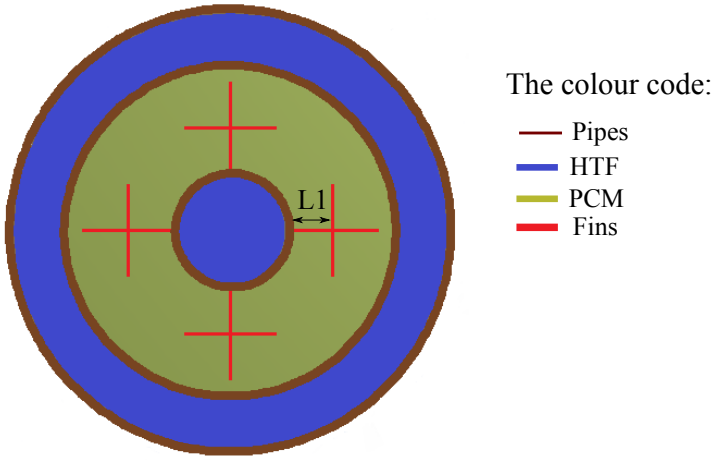

Figure 4.53: Changing the dimension of fin (L1).

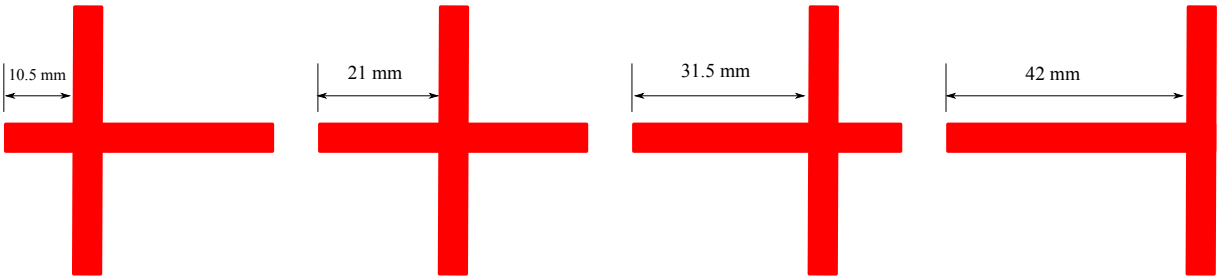

Figure 4.54: Different fin shapes produced by changing the dimension of fin (L1).

The response surface for the total melting time for different values of L1 and the different number of fins is shown in Fig. 4.55. It is obvious that changing the shape of fins has a significant influence on the PCM melting process. Moreover, the number and direction of fins also have a strong effect on PCM melting. In response surface method, the optimum value is determined using a parameter called desirability. It is a function with values between zero and one, and in the optimization procedure, it is tried to reach its value close to one. For multi-objective problems, all objectives are converted to one objective and the optimization is applied to the calculated desirability. The desirability for the melting process for different numbers of fins and different values of L1 is shown in Fig. 4.56.

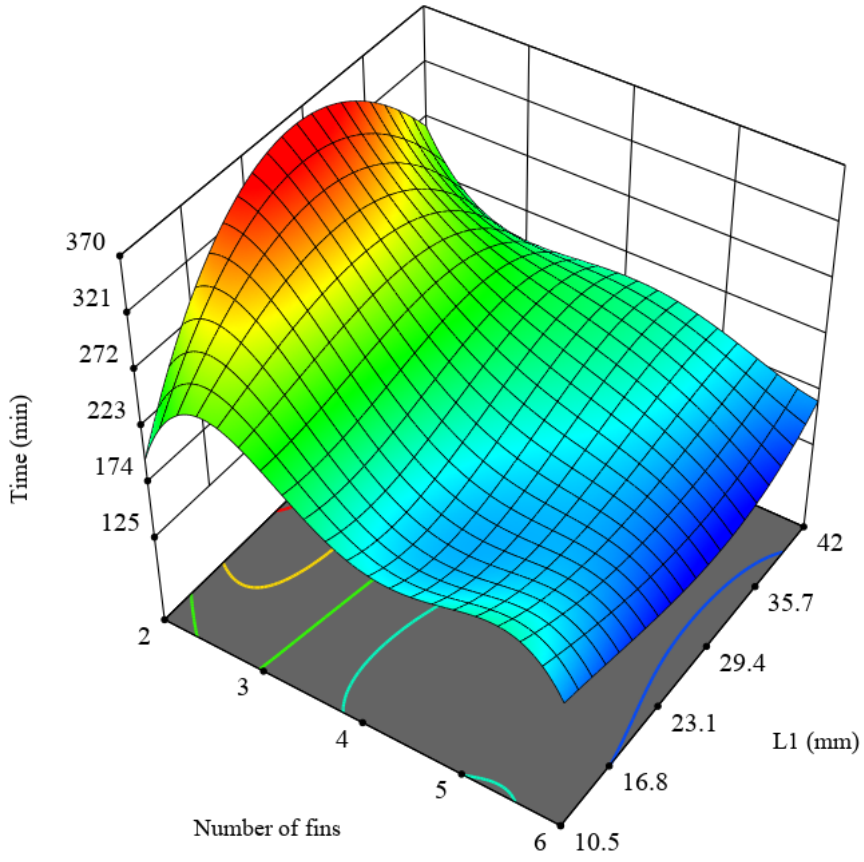

Figure 4.55: The response surface for the total melting time for different values of L1 and the different number of fins for the PCM melting process in the TTHX.

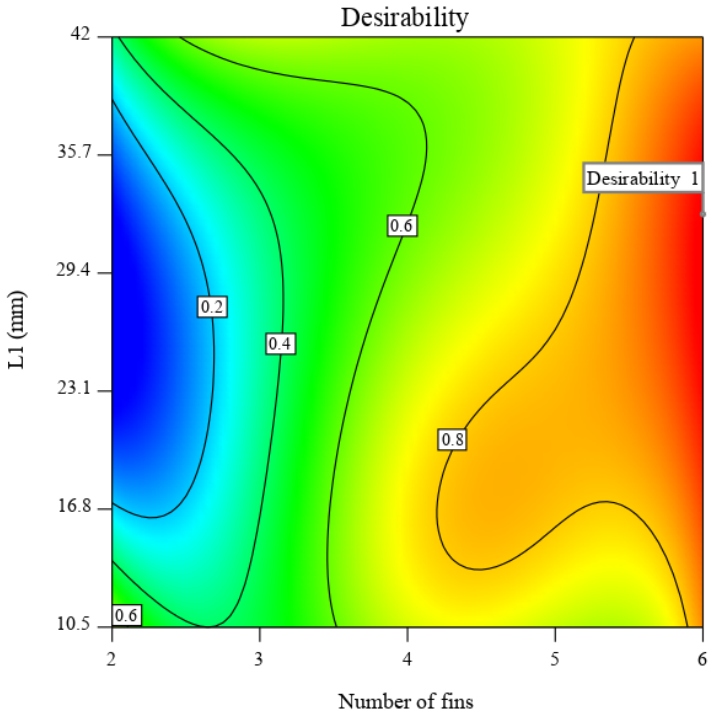

Figure 4.56: The desirability of the PCM melting process in the TTHX for the different number of fins and different values of L1.

4.6.2 The effect of changing the initial PCM temperature and the HTF temperature

For this test, the effect of changing the HTF temperature and the initial PCM temperature on the melting process of PCM in the TTHX without fins was studied. Three HTF temperatures were tested, which were: 87 °C, 90 °C and 93 °C. Additionally, three initial PCM temperatures were tested, which were: 27 °C, 30 °C and 33 °C. Fig. 4.57 shows the response surface of the total PCM melting time for different values of HTF temperature and initial PCM temperature. It clear from this figure, that changing the HTF temperature has a significant influence on the PCM melting process while changing the initial PCM temperature has a weak influence. The total PCM melting time decreased by 29% by increasing the HTF temperature from 87 °C to 93 °C.

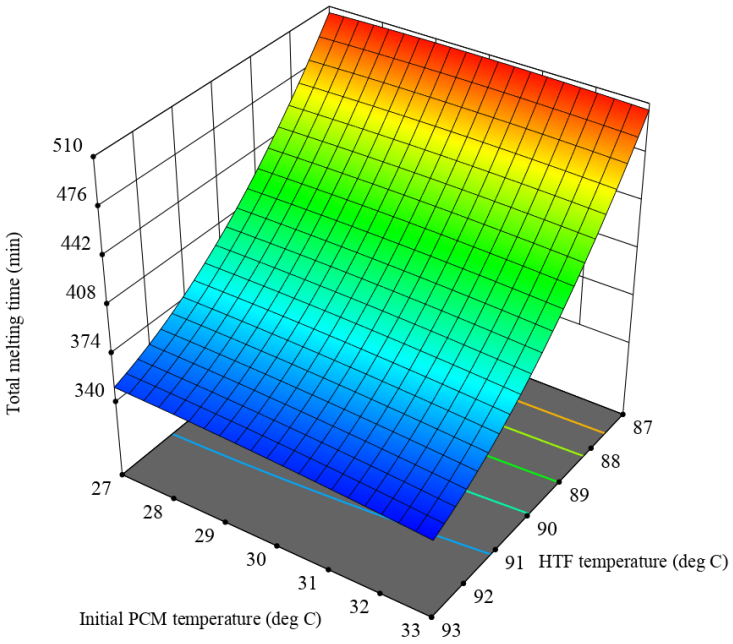

Figure 4.57: The response surface of the total melting time for different values of initial PCM temperature and HTF temperature for melting process for the TTHX.

Chapter 5

Using Fins to Enhance the Thermal Performance of PCM in a Shell and Tube Heat Exchanger

The low thermal conductivity of PCMs leads to a poor heat transfer rate and limits the widespread utilization of PCMs. There are various techniques to enhance the thermal conductivity of PCMs such as employing fins or metal foams, adding nanoparticles and using multiple PCMs. In this chapter, several fin shapes are introduced to improve the thermal performance of PCM in a shell and tube heat exchanger (STHX). To evaluate the performance of the suggested fin shapes, comparisons were made with conventional longitudinal fins.

5.1 Shell and tube heat exchanger with fins

5.1.1 Model description and dimensions

For the STHX the heat transfer fluid (HTF) passes through the inner tube, while the PCM is contained in the shell side. In this test, a novel tee fin shape was introduced to improve the poor thermal performance of PCM. Six tee fins were connected to the outer surface of the inner HTF tube. The PCM used in this test is (RT82) paraffin (manufactured by RUBITHERM GmbH-Germany). The thermophysical properties of PCM (RT82) are shown in Table 4.1.

The STHX physical model is shown in Fig. 5.1. This model has an inner tube diameter of $d_i = 50.8$ mm and 1.2 mm thickness, the outer tube has an inner diameter $d_o = 150$ mm and thickness of 2 mm. The dimensions of the tee fins used are shown in Table 5.1. The computational domain with the indicated boundary conditions is shown in Fig. 5.2.

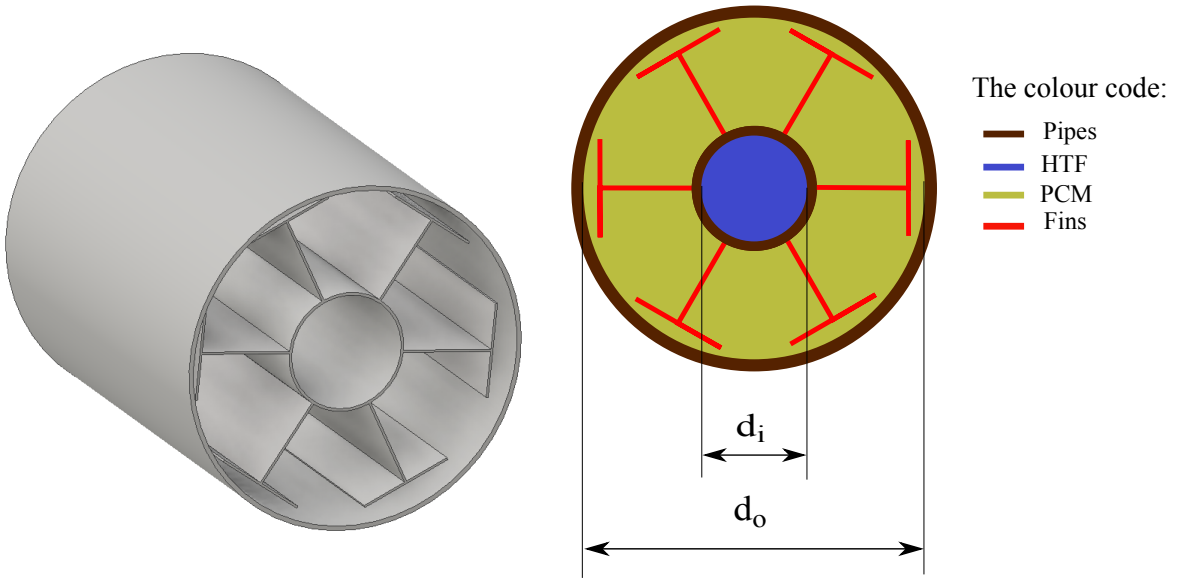

Figure 5.1: The physical model of the shell and tube heat exchanger with the major dimensions, left 3D, right the cross-sectional area.

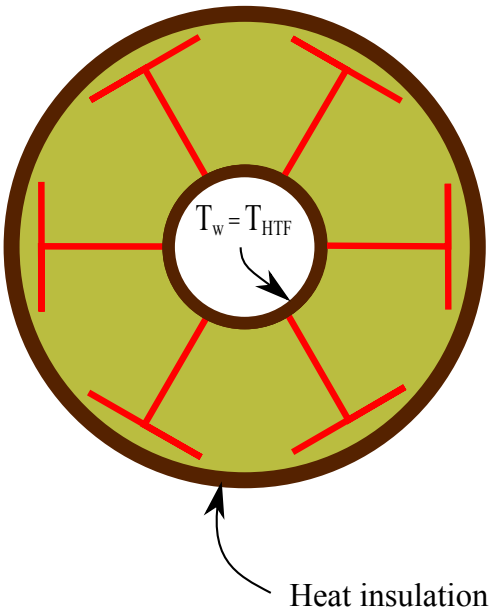

Figure 5.2: The computational domain with the indicated boundary conditions for the STHX with six tee fins.

5.2 Validation of numerical model

To validate the present numerical model, a comparison was made with experimental work carried out by Ismail *et al.* [61] and numerical work carried out by Sciacovelli *et al.* [57]. The model used for validation is a shell and tube heat exchanger with four longitudinal fins on the shell side. The PCM fills the shell side, while the HTF (water) passes through the inner tube. The shell has an internal diameter of 73 mm, while the inner tube has an external diameter of 21 mm. The fins' dimensions were length 10 mm and thickness 1 mm. The PCM used in this test has a melting temperature of 55.8 °C. The solidification process was considered for the validation purpose. The initial liquid PCM temperature used was 65 °C. The boundary condition used was the HTF temperature of 21 °C, imposed along the HTF tube wall. For the outer wall of the PCM shell, an adiabatic boundary condition was used.

A quarter of the heat exchanger model was used for the validation and is shown in Fig. 5.3.

The results of the validation for the solidification front are shown in Fig. 5.4. As can be seen from Fig. 5.4, there is good agreement between the current CFD model results and the experimental data of Ismail *et al.* [61] and the numerical data from Sciacovelli *et al.* [57].

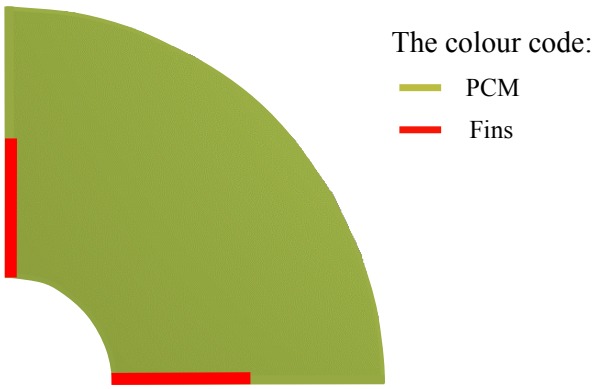

Figure 5.3: Two dimensional model used in validation with Ismail *et al.* [61] and Sciacovelli *et al.* [57].

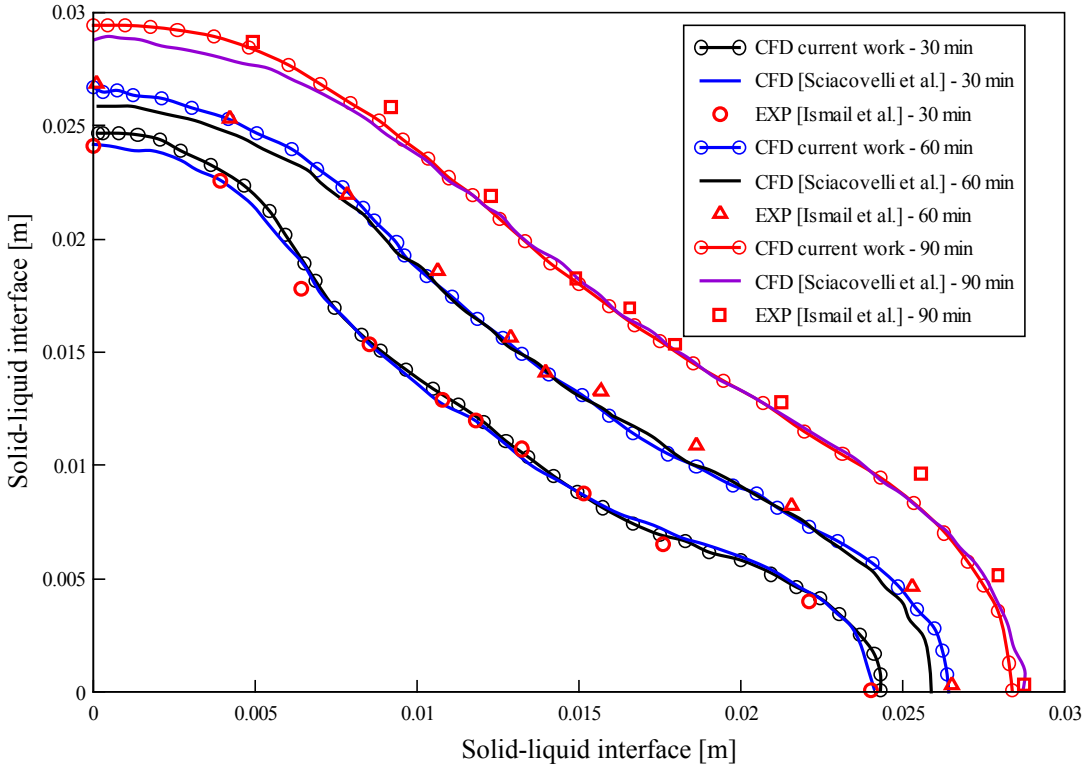

Figure 5.4: Validation of the present study with the experimental work carried out by Ismail *et al.* [61] and numerical work carried out by Sciacovelli *et al.* [57] solidification front.

5.3 Numerical procedure

ANSYS Fluent 15 software was used in the simulations. Fluent utilizes the finite volume method and the enthalpy-porosity technique to solve the continuity, momentum and energy equations. The solidification and melting model was used to model the PCM melting/solidification process. Two-dimensional computational domains were used in the simulations. A Transient Pressure-Based solver was employed to solve the governing equations for incompressible flow. The SIMPLE scheme was utilized for pressure-velocity coupling. The PRESTO scheme was employed for pressure discretization, which is recommended for solving natural convection flow [15, 98]. The second order upwind scheme was

employed for solving the energy and momentum equations. The under-relaxation factors for momentum, pressure, liquid fraction and energy were 0.7, 0.3, 0.9 and 1 respectively. The convergence criterion for energy equation was set to 10^{-6} and 10^{-4} for continuity and momentum equations.

5.4 Mesh and time step independent test

The mesh and time step independent tests were performed for the solidification process for the STHX model with 6 tree fins. Fig. 5.5 presents the mesh independence test results. To validate the grid independent test, four different grid systems were tested, which included 5339 cells, 10679 cells, 21396 cells, and 30701 cells. As can be seen from Fig. 5.5 there is an identical result between 21396 cells and 30701 cells. Therefore, 21396 cells will be used in the following simulation. This mesh is shown in Fig. 5.6.

The time step independence test was performed with four different time steps and the result is shown in Fig. 5.7. It can be seen from this figure that there is an identical result between time step 0.5 s and 1 s. Therefore 1 s time step will be used in the following simulation.

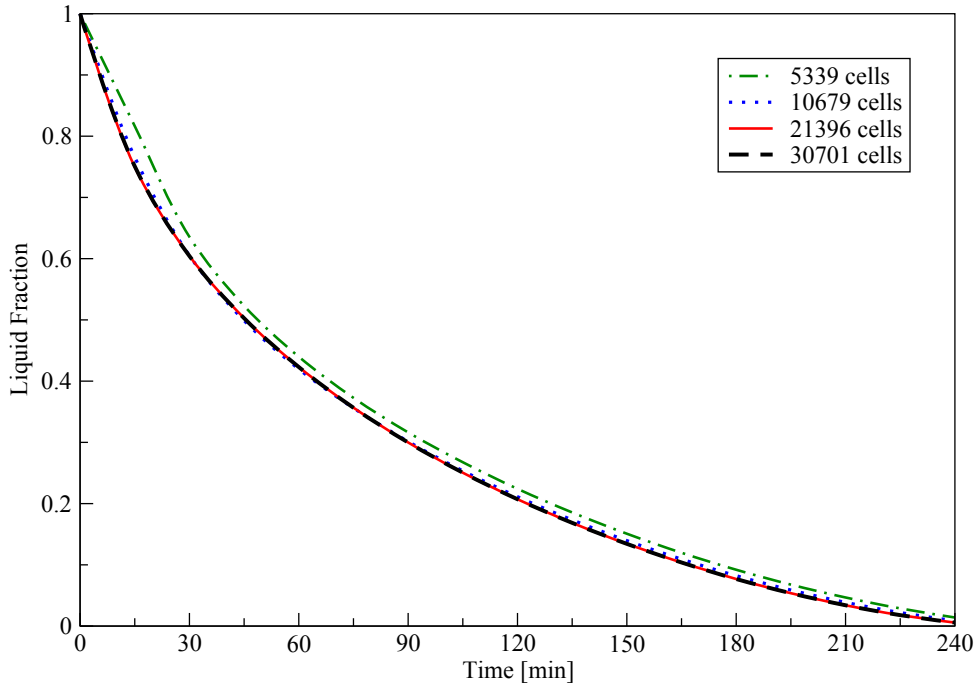

Figure 5.5: Mesh independence test, liquid fraction

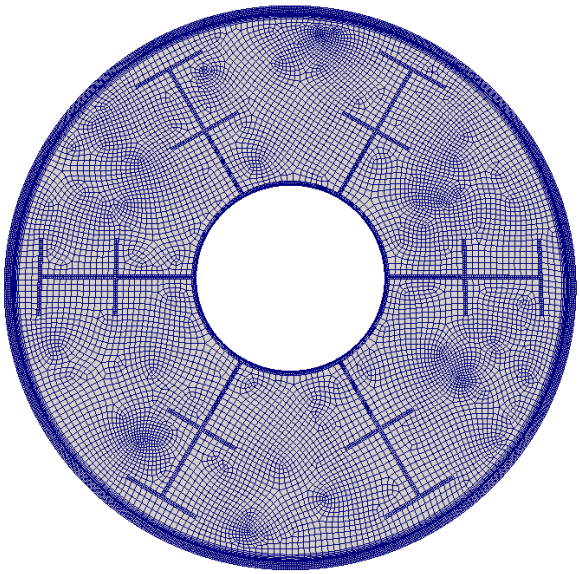

Figure 5.6: The mesh of the 2D model (21396 cells).

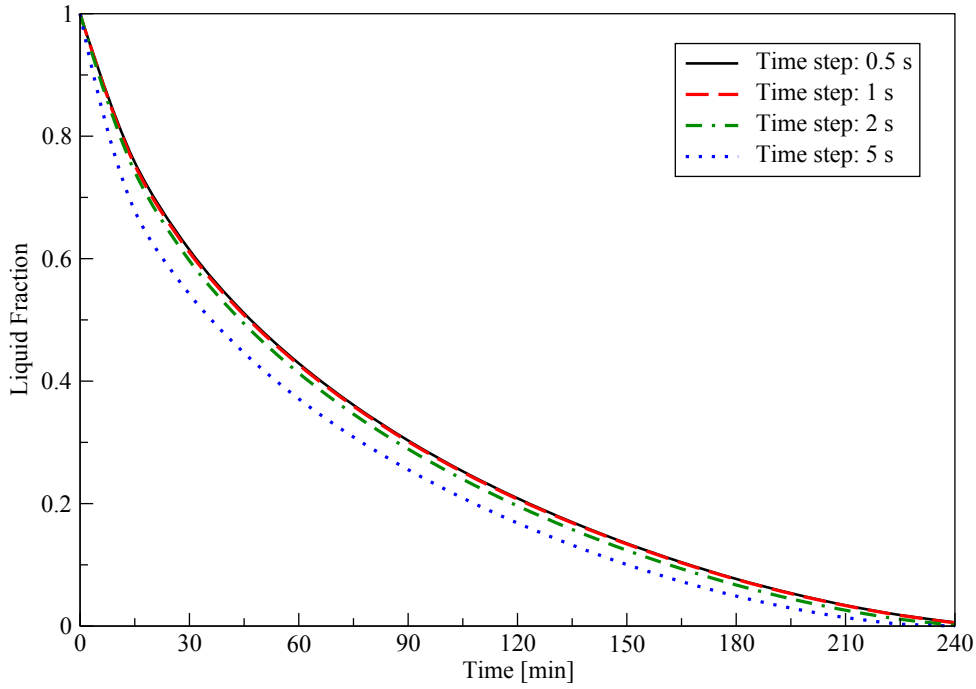

Figure 5.7: Time step independence test, liquid fraction

5.5 Initial and boundary conditions

5.5.1 Melting process

At the initial time (t = 0), the PCM was in the solid state, with its temperature at 27 °C which is below its melting temperature. The HTF had a constant temperature ($T_w = T_{HTF} = 90$ °C), which is higher than the PCM melting temperature. This temperature was imposed along the inner tube wall and the external wall is assumed to be adiabatic as shown in Fig. 5.2. Therefore, the initial and boundary conditions can be listed as

$T = T_{initial} = 27$ °C at (t = 0).

At $d = d_i$, $T = T_{HTF} = 90$ °C.

At $d = d_o$, wall insulated (adiabatic).

5.5.2 Solidification process

At the initial time (t = 0), the PCM was in the liquid state, hence its temperature was 93 °C, which is above its solidification temperature. The HTF had a constant temperature ($T_w = T_{HTF} = 68$ °C), which is lower than the PCM solidification temperature. This temperature was imposed along the inner tube wall and the external wall is assumed to be adiabatic as shown in Fig. 5.2. Therefore, the initial and boundary conditions can be listed as

$T = T_{initial} = 93$ °C at (t = 0).

At $d = d_i$, $T = T_{HTF} = 68$ °C.

At $d = d_o$, wall insulated (adiabatic).

5.6 Comparisons between STHX with different fins shapes and without fins

Various fin shapes were considered in the analysis to enhance the thermal performance of PCM and to find the best fin shape to reduce the solidification/melting times of PCM. Different fins' configurations are shown in Fig. 5.8. Three fin shapes were tested which were: longitudinal fin Fig. 5.8a, tee fin Fig. 5.8b and tree fin Fig. 5.8c.

The plus fin's shape which introduced in Chapter 4 with the TTHX, and showed good thermal performance, is not used here with the STHX because there is a need to a fin shape that reached the isolated region of the PCM and increases the thermal penetration depth near the inner wall of the outer shell. In this test, many heat exchangers with various fin shapes were tested and compared, to study the effect of utilizing fins. These heat exchangers were: heat exchanger without fins, heat exchanger with six tee fins, heat exchanger with six longitudinal fins and heat exchanger with six tree fins. The total cross-section area of all fins' types was kept constant to compare different fins' thermal performance. To achieve this, the dimensions of the fins were carefully chosen. The

dimensions of the various fins' shapes are shown in Table 5.1. For different fins' systems, the same amount of PCM was used in all cases, so that the same amount of energy could be stored in all systems. Copper was used for pipes and fins. The computational domains for the various heat exchangers used in the simulations are shown in Fig. 5.9. The convection and conduction heat transfer mechanisms were taken in to account during the numerical simulations.

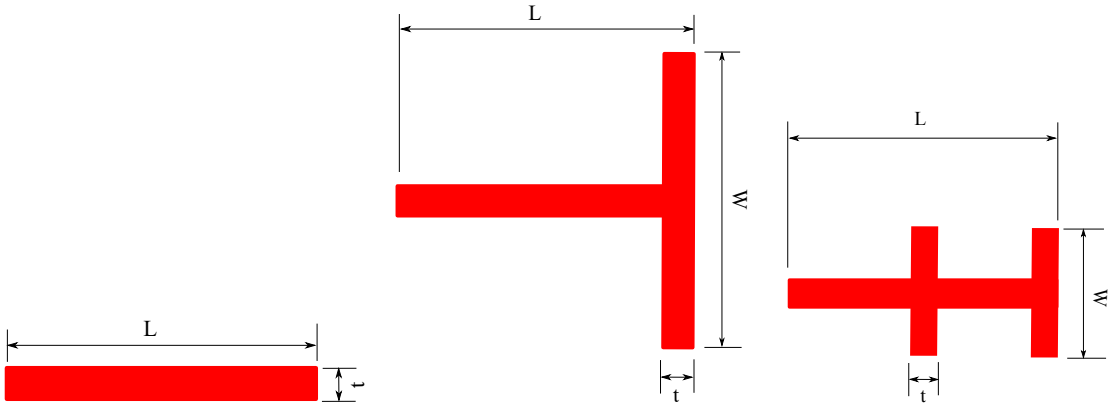

(a) Longitudinal fin (b) tee fin (c) tree fin

Figure 5.8: Different fins' configurations and dimensions: (a) longitudinal fin, (b) tee fin and (c) tree fin.

Table 5.1: The dimensions of various fin shapes

Fin shape	**Length (L) (mm)**	**Width (W) (mm)**	**Thickness (t) (mm)**
Longitudinal fin	42	0	2
Tee fin	42	42	1
Tree fin	42	21	1

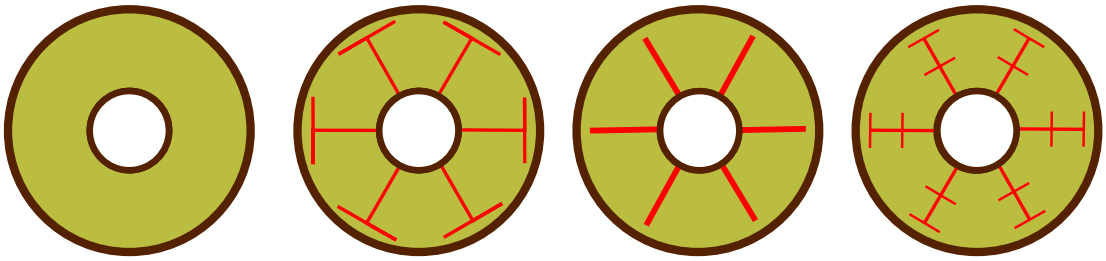

(a) without fins (b) tee fins (c) longitudinal fins (d) tree fins

Figure 5.9: The computational domains for the various heat exchangers with different fin configurations: (a) without fins, (b) tee fins, (c) longitudinal fins and (d) tree fins.

5.6.1 Melting process

Fig. 5.10 shows the liquid fraction of PCM for the various heat exchangers with different fins. It is clear from this figure that at all time intervals the liquid fraction for tee fins case is more than the longitudinal fins and tree fins cases. This figure also shows that the case without fins had about 15% of the PCM melted after 6 hours, while, with the tee fins the PCM completely melted after 3.5 hours. The total PCM melting time reduced by 33% when using the tee fins, as compared to when the longitudinal fins were used. It is observed that the geometry of the fins has a significant effect on the PCM melting process. The total melting time and melting time reductions for the various fins' configurations are shown in Table 5.2.

The average PCM temperature for the various heat exchangers with different fins is shown in Fig. 5.11. It is clear, that the PCM temperature increased by using the fins, owing to the increase of the heat exchange area. It is clear that by employing the tee fins there is a significant enhancement in the heat transfer rate, compared to the cases utilizing tree fins or the longitudinal fins. Hence, the average PCM temperature increased when compared to cases utilizing the longitudinal fins or the tree fins. As such, the total charging time was decreased when employing tee fins compared to other cases.

Fig. 5.12 shows the liquid fraction contours for the various fins at different moments. It is clear from this figure that the melting front appeared at different times at positions

close to the HTF tube and fins and progressing at different rates outwards. Moreover, the melting rate for the tee fins is higher when compared to longitudinal or tree fins. The melting process accelerated in the case of the use of tee fins design because these fins reached the isolated areas of the PCM near the isolated outer tube wall. As time passes the PCM melting process is largely influenced by natural convection.

Fig. 5.13 shows the surface heat flux contours for the various fins at different moments. It can be seen from this figure that the thermal penetration depth increased by using the tee fins and the tree fins. Fig. 5.14 shows the temperature contours for various fins at different moments. It is clear from this figure that employing tee fins greatly enhances the heat transfer rate, compared to using longitudinal fins and tree fins. During the PCM melting process, the heat transfer to the PCM followed three regimes which are: conduction, mixed conduction and convection, and convection. At the early stage of the melting process, the heat transfer process is controlled by pure conduction. When the PCM start to melt, the conduction domination was gradually replaced by convection. Moreover, the buoyancy effect due to the PCM density variation enhances the convection.

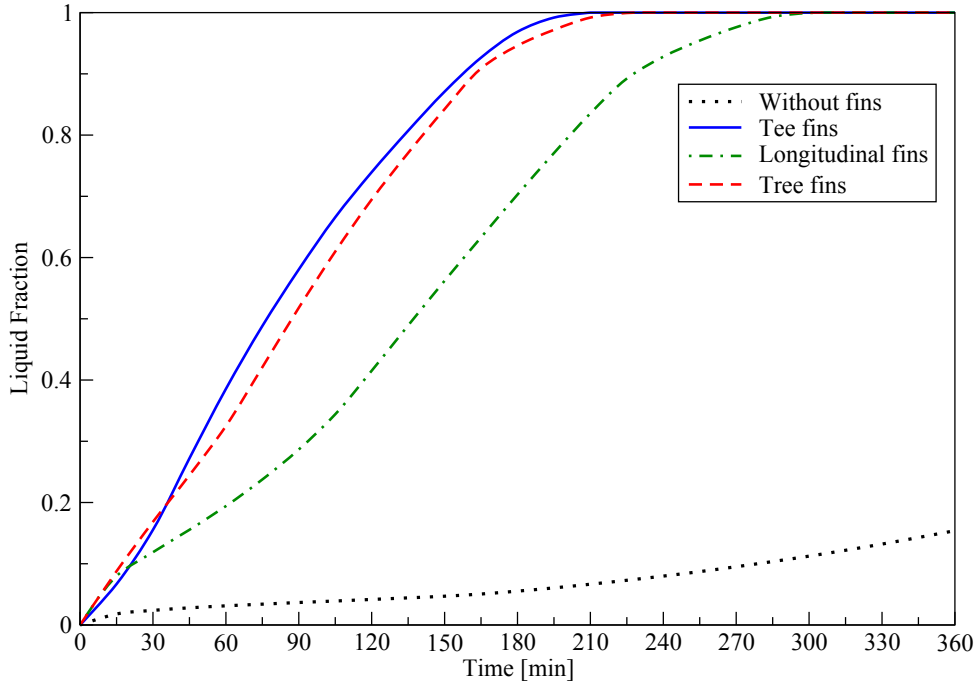

Figure 5.10: Liquid fraction comparison for melting process between heat exchangers with various fin shapes and without fins.

Table 5.2: Melting time and melting time reduction for various fins' shapes

Fin shape	**Melting time (min)**	**Reduction (%)**
Longitudinal (base case)	315	—
Tree	240	24
Tee	210	33

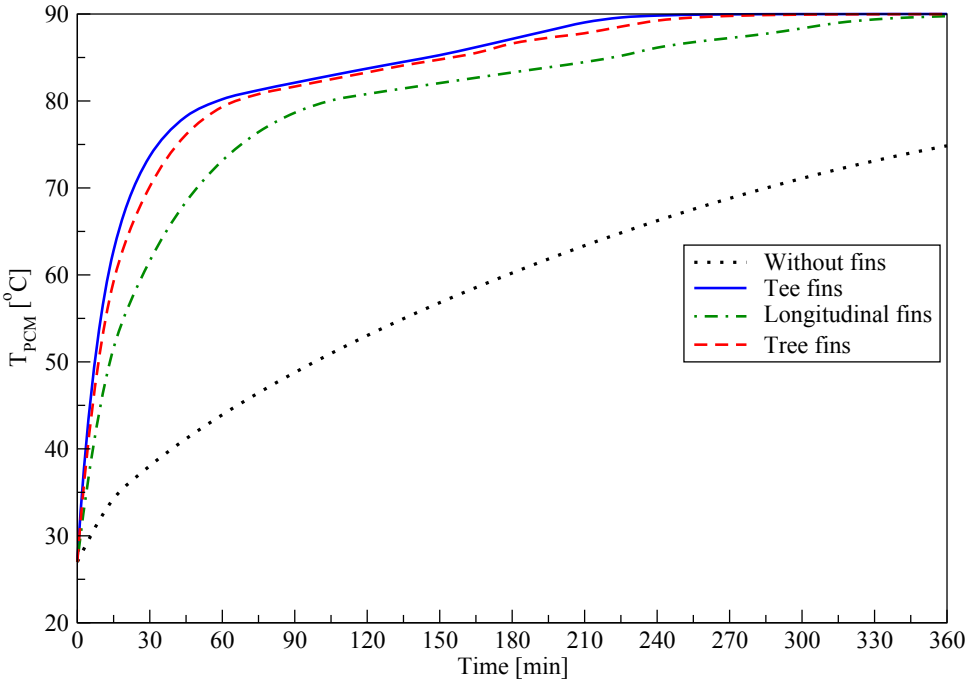

Figure 5.11: Average PCM temperature comparison for melting process between heat exchangers with various fin shapes and without fins.

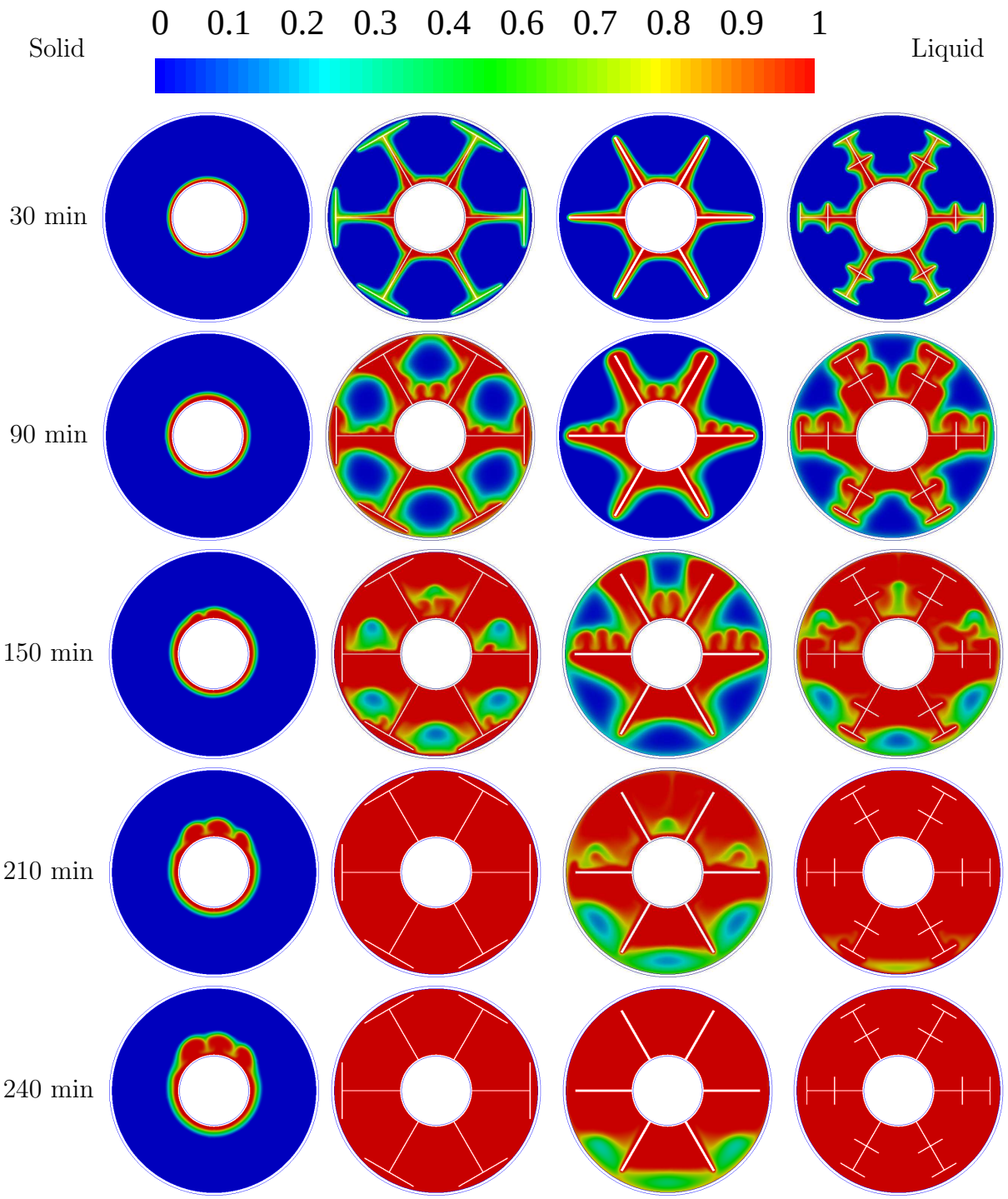

Figure 5.12: Liquid fraction contours at different times for melting process comparison for various fins shapes. From left: first without fins, second tee fins, third longitudinal fins, and fourth tree fins.

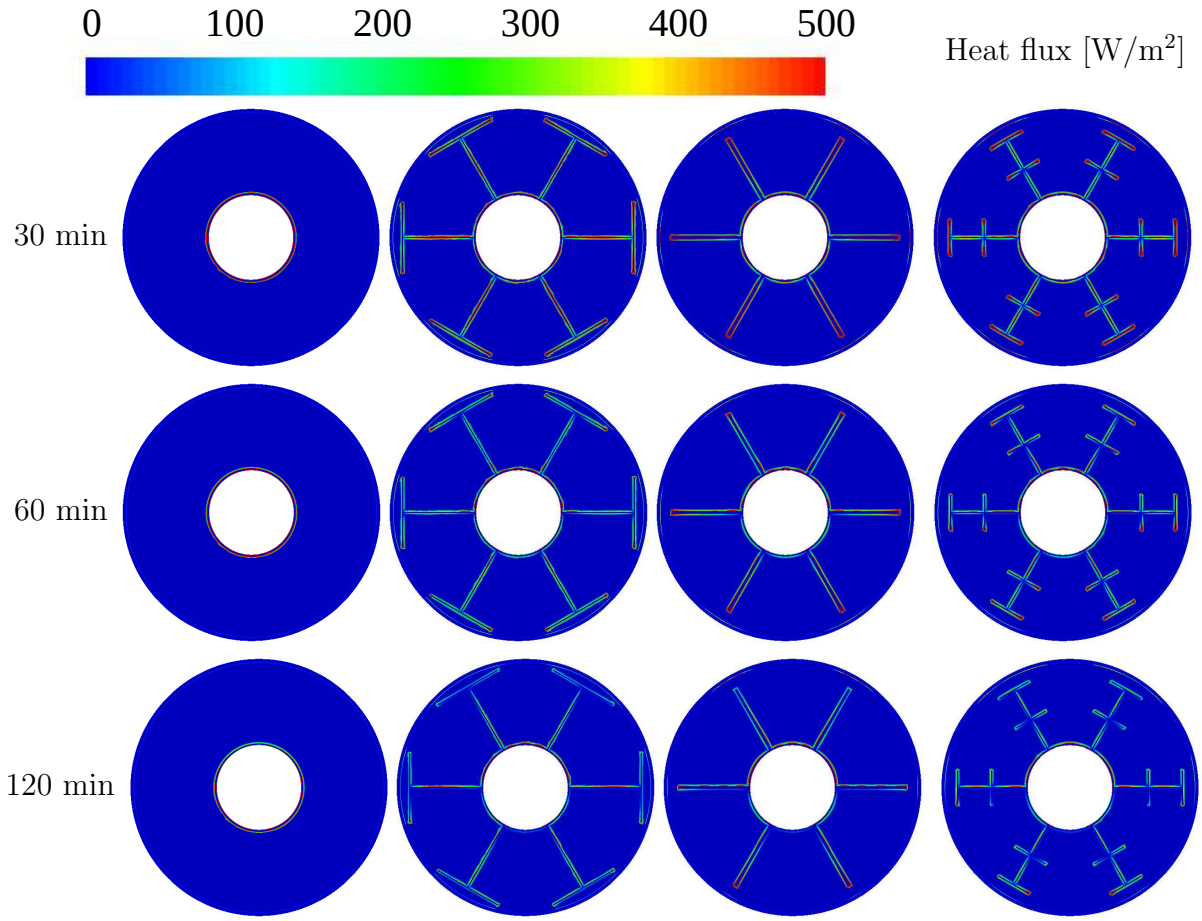

Figure 5.13: Surface heat flux contours at different times for melting process comparison for various fins shapes. From left: first without fins, second tee fins, third longitudinal fins, and fourth tree fins.

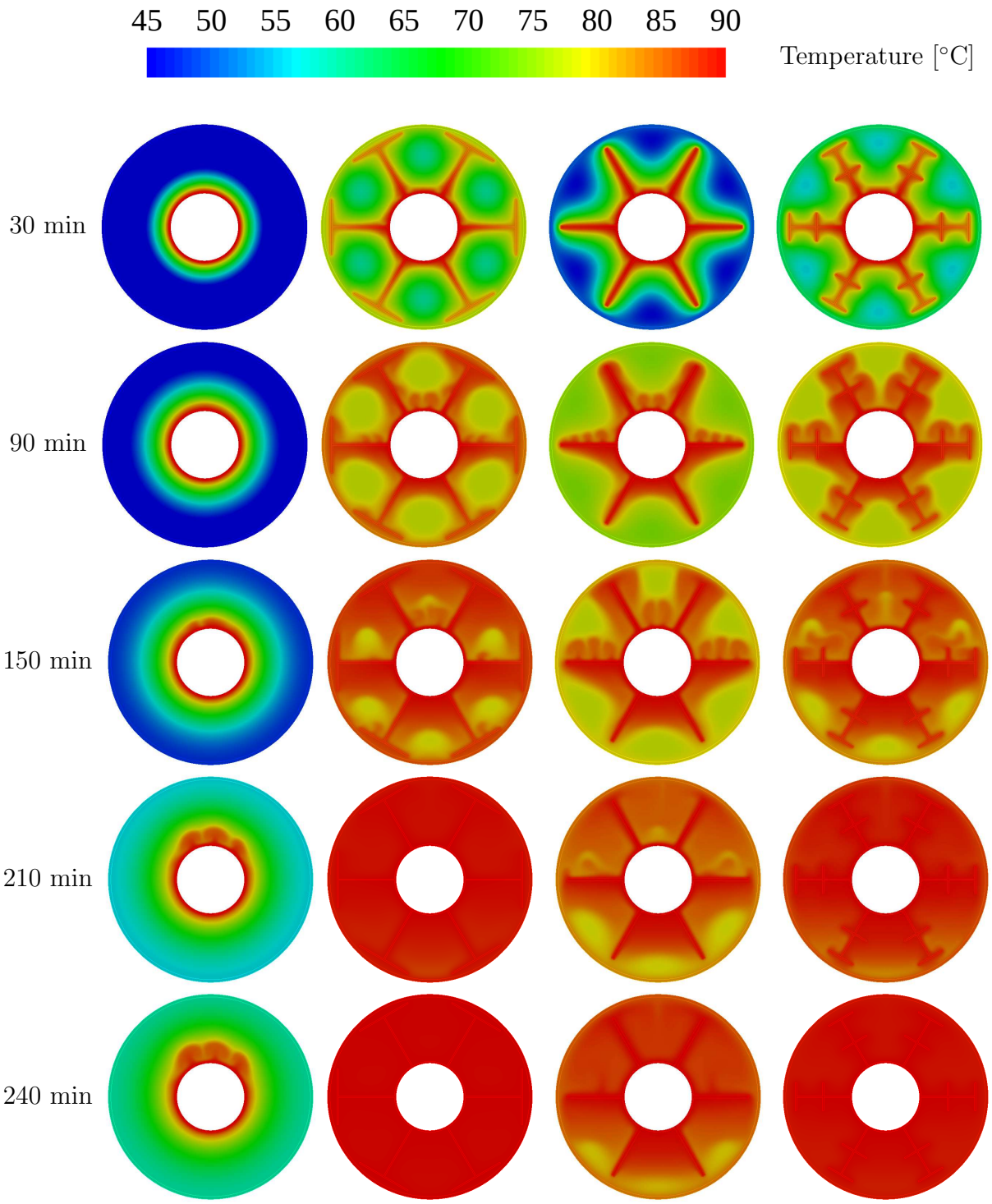

Figure 5.14: Contours of temperature at different times for melting process comparison for different fin shapes. From left: first without fins, second tee fins, third longitudinal fins, and fourth tree fins.

5.6.2 Solidification process

Fig. 5.15 presents the liquid fraction for the various heat exchangers with different fin shapes. It is clear from this figure that at all time intervals the liquid fraction for the heat exchanger with the tee fins is less than the heat exchangers with longitudinal fins or the tree fins. This figure also shows that when using a heat exchanger without fins only about 37% of PCM solidified after 6 hours, while, in the heat exchanger with the tee fins, the PCM completely solidified after 4 hours. The total PCM solidification time reduced by 33% when employing the tee fins, compared to employing the longitudinal fins. The total solidification time and solidification time reductions for the various fins' configurations are shown in Table 5.3.

Fig. 5.16 shows the average PCM temperature for the various heat exchangers with different fins shapes. It is clear from this figure that the tee fins' design has a high heat transfer rate compared to the cases employing the tree fins or the longitudinal fins. Hence, the average PCM temperature reduced and the solidification rate increased compared to cases with longitudinal fins or tree fins.

Fig. 5.17 shows liquid fraction contours for the various heat exchangers with different fin shapes at different times. It is clear from this figure that the heat exchanger with tee fins has a higher solidification rate at all time intervals, compared to the heat exchanger with longitudinal fins. This was due to the increase of the heat exchange area when employing tee fins and increase the thermal penetration, where the fins reached the isolated PCM regions near the outer shell.

Fig. 5.18 shows the surface heat flux contours for the various fins at different moments. It can be seen from this figure that the thermal penetration depth increased by using the tee fins and the tree fins. Fig. 5.17 shows temperature contours at different times. It is obvious from this figure that the heat exchanger with the tee fins shows a lower temperature, compared to the other fins' cases, at all time intervals. This happened due to the increase in heat transfer rate owing to the increase in the heat exchange area when employing tee fins. It is clear from Fig. 5.17 that the temperature rapidly rises in the area close to the fins and HTF tube. By utilizing the tee fins the temperature distribution is

more homogeneous compared to longitudinal and tree fins cases. This leads to a faster solidification rate specially in the PCM regions near the outer shell.

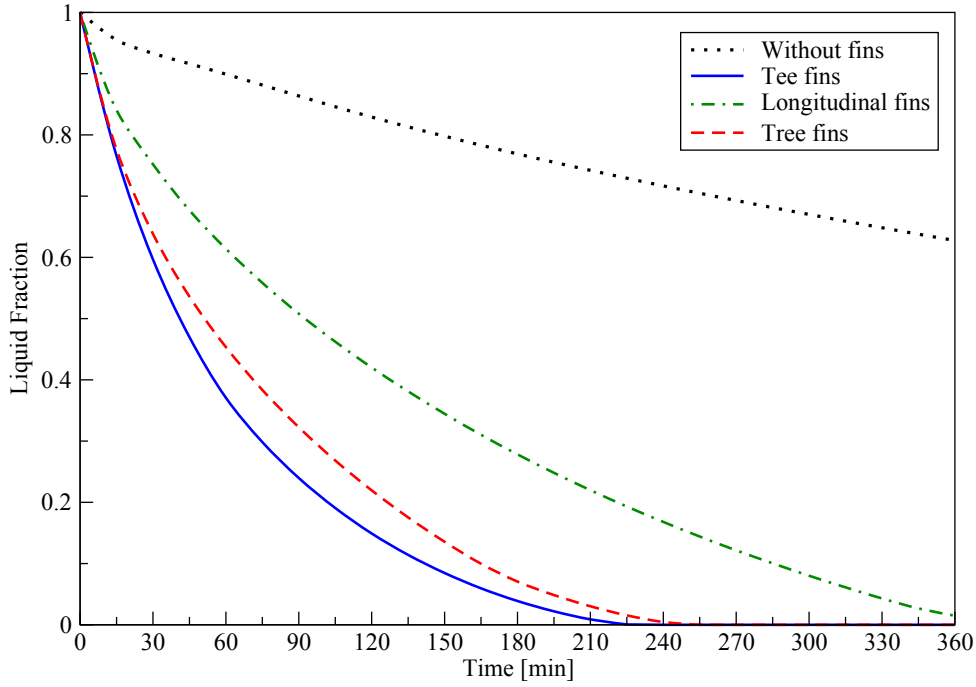

Figure 5.15: Liquid fraction comparison for solidification process between heat exchanger with various fin shapes and without fins.

Table 5.3: Solidification time and solidification time reduction for various fins' shapes

Fin shape	**Solidification time (min)**	**Reduction (%)**
Longitudinal (base case)	360	—
Tree	253	29
Tee	240	33

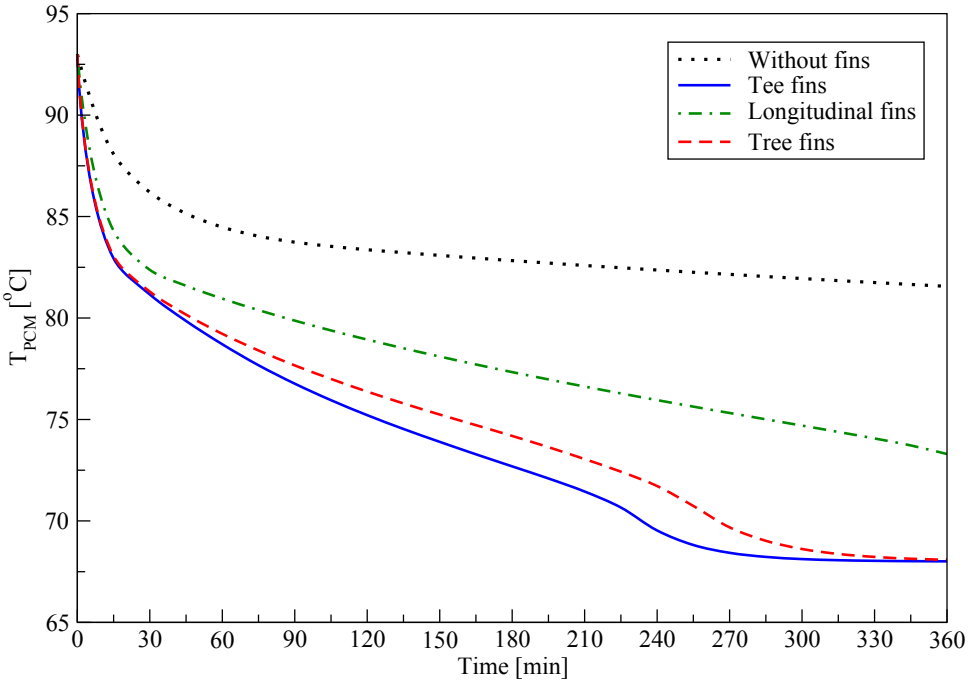

Figure 5.16: Average PCM temperature comparison for solidification process between heat exchanger with various fin shapes and without fins.

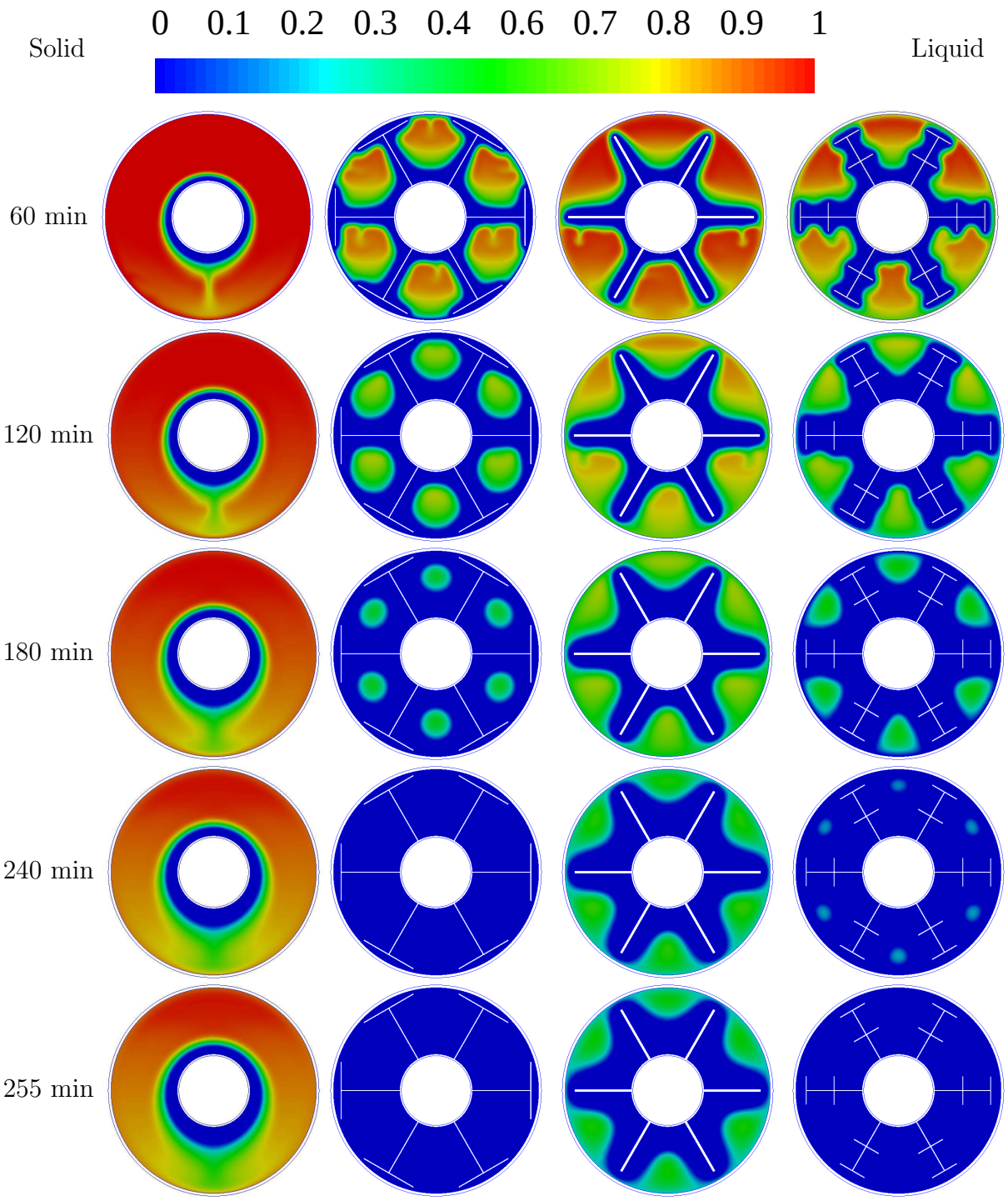

Figure 5.17: Contours of liquid fraction at different moments for solidification process comparison for various heat exchangers with different fin shapes. From left: first without fin, second tee fins, third longitudinal fins and fourth tree fins.

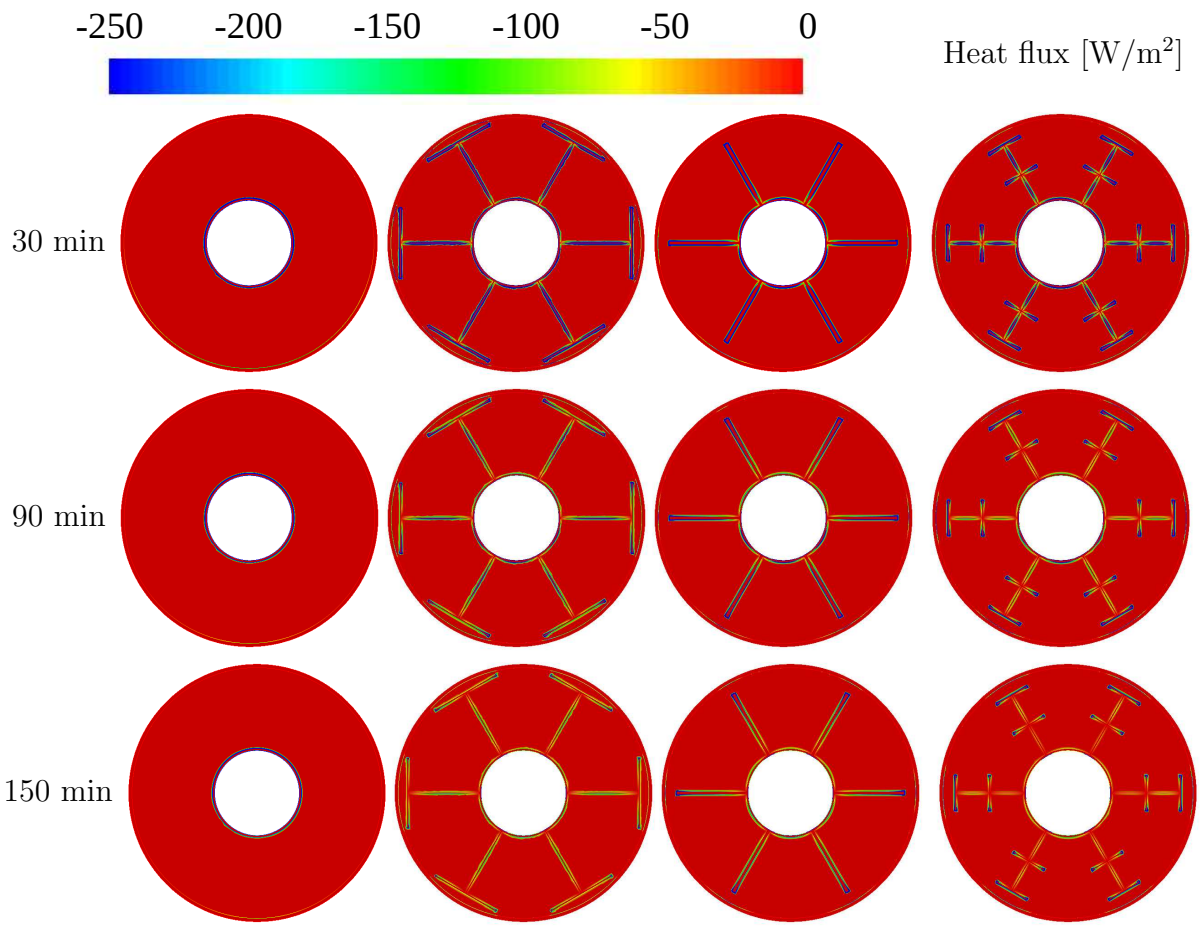

Figure 5.18: Surface heat flux contours at different times for solidification process comparison for various fins shapes. From left: first without fins, second tee fins, third longitudinal fins, and fourth tree fins.

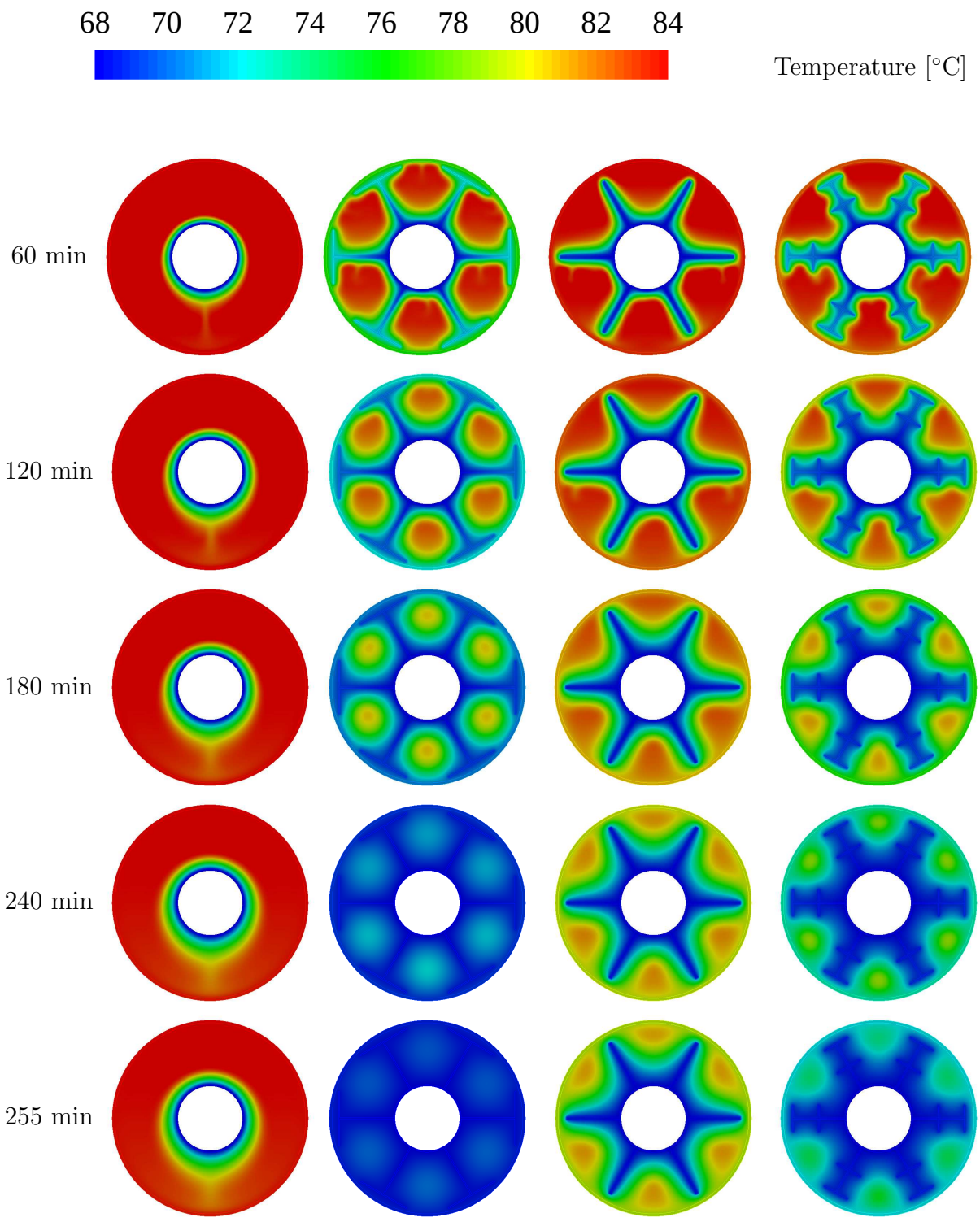

Figure 5.19: Contours of temperature at different times for solidification process comparison for various heat exchangers with different fin shapes. From left: first without fin, second tee fins, third longitudinal fins and fourth tree fins.

5.7 The effect of changing the HTF temperature

The difference between the HTF temperature and the phase transition temperature of the PCM is the driving force for the heat transfer process between the HTF and the PCM. Given this, the HTF temperature has a significant influence on the PCM solidification/melting process. The influence of changing the HTF temperature on the PCM solidification and melting process was tested. The STHX model with six tee fins was used for this test; the computational domain is shown in Fig. 5.9b.

5.7.1 Melting process

In this test, the influence of changing the HTF temperature on the PCM melting process was studied. Various HTF temperatures were tested, which were: 87 °C, 90 °C, 93 °C and 96 °C. Fig. 5.20 shows the liquid fraction for different HTF temperatures. It is clear from this figure that increasing the difference between the HTF temperature and the PCM melting temperature, increases the heat transfer rate, thereby accelerating the PCM melting process. The total melting time decreased by 58% with the increase of the HTF temperature from 87 °C to 96 °C. The total melting time and melting time reductions for the various HTF temperatures are shown in Table 5.4.

Average PCM temperature versus time for different HTF temperatures is shown in Fig. 5.21. The increase in the HTF temperature increases the PCM temperature, and this decreases the PCM total melting time. Fig. 5.21 shows three stages of the PCM temperature before reaching steady state: quick increase, slow increase, and a slower increase in PCM temperature.

Liquid fraction contours for various HTF temperatures at different times are shown in Fig. 5.22. This figure shows that increasing the HTF temperature accelerates the PCM melting process. At the beginning stages, the dominant heat transfer mechanism between the heat transfer surfaces and the solid surface of the PCM is conduction. As time passes, the liquid PCM increases; due to the natural convection effects the hotter part of the

PCM is raised upward, whereas the solid part of the PCM sticks to the lower part of the tube due to its high density. The rate of heat transfer increases by increasing the HTF temperature. The reason for this, that the temperature difference is the driving power for any heat transfer process. Contours of temperature for the various HTF temperatures at different times are shown in Fig. 5.23. It is obvious from this figure that increasing the HTF temperature increases the PCM temperature and decreases the total melting time.

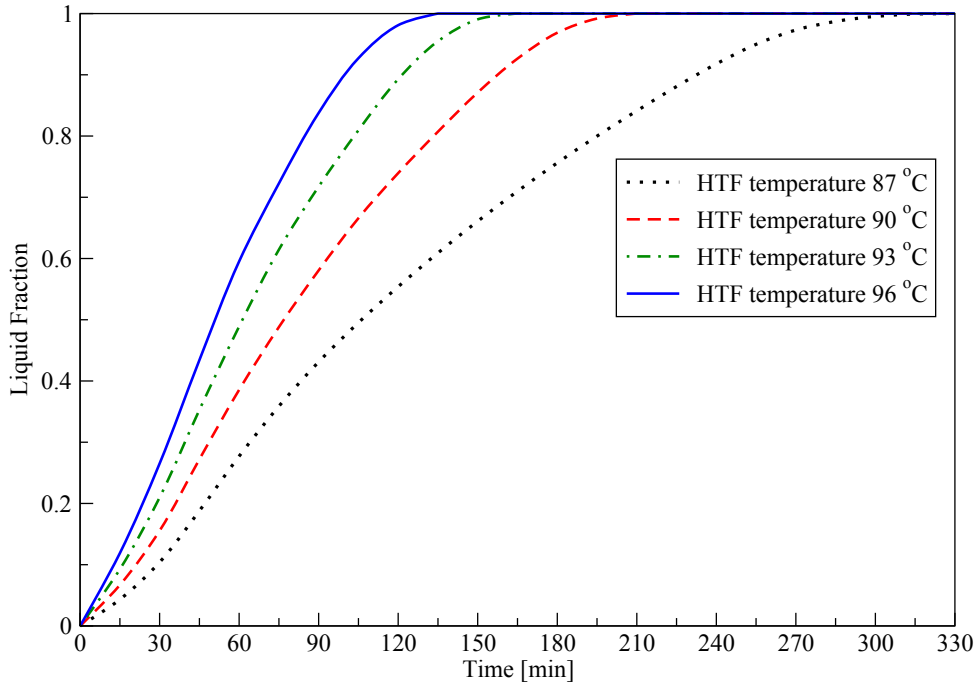

Figure 5.20: Liquid fraction comparison for the melting process with different HTF temperatures.

Table 5.4: Melting time and melting time reduction for various HTF temperatures

HTF temperature (°C)	**Melting time (min)**	**Reduction (%)**
87 (base case)	322	—
90	209	35
93	162	49
96	134	58

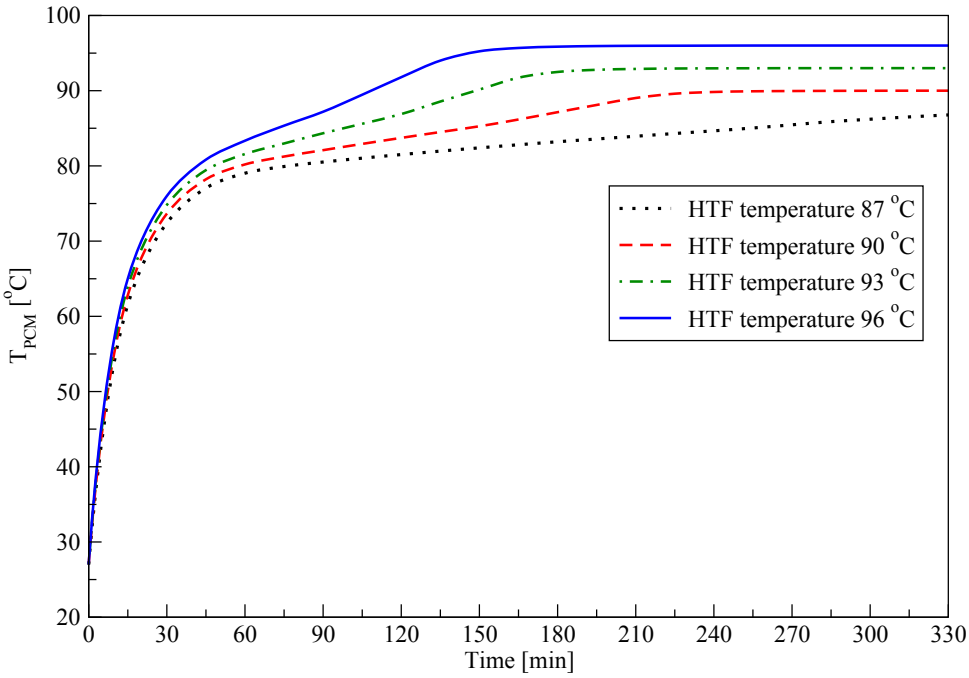

Figure 5.21: Average PCM temperature comparison for the melting process with different HTF temperatures.

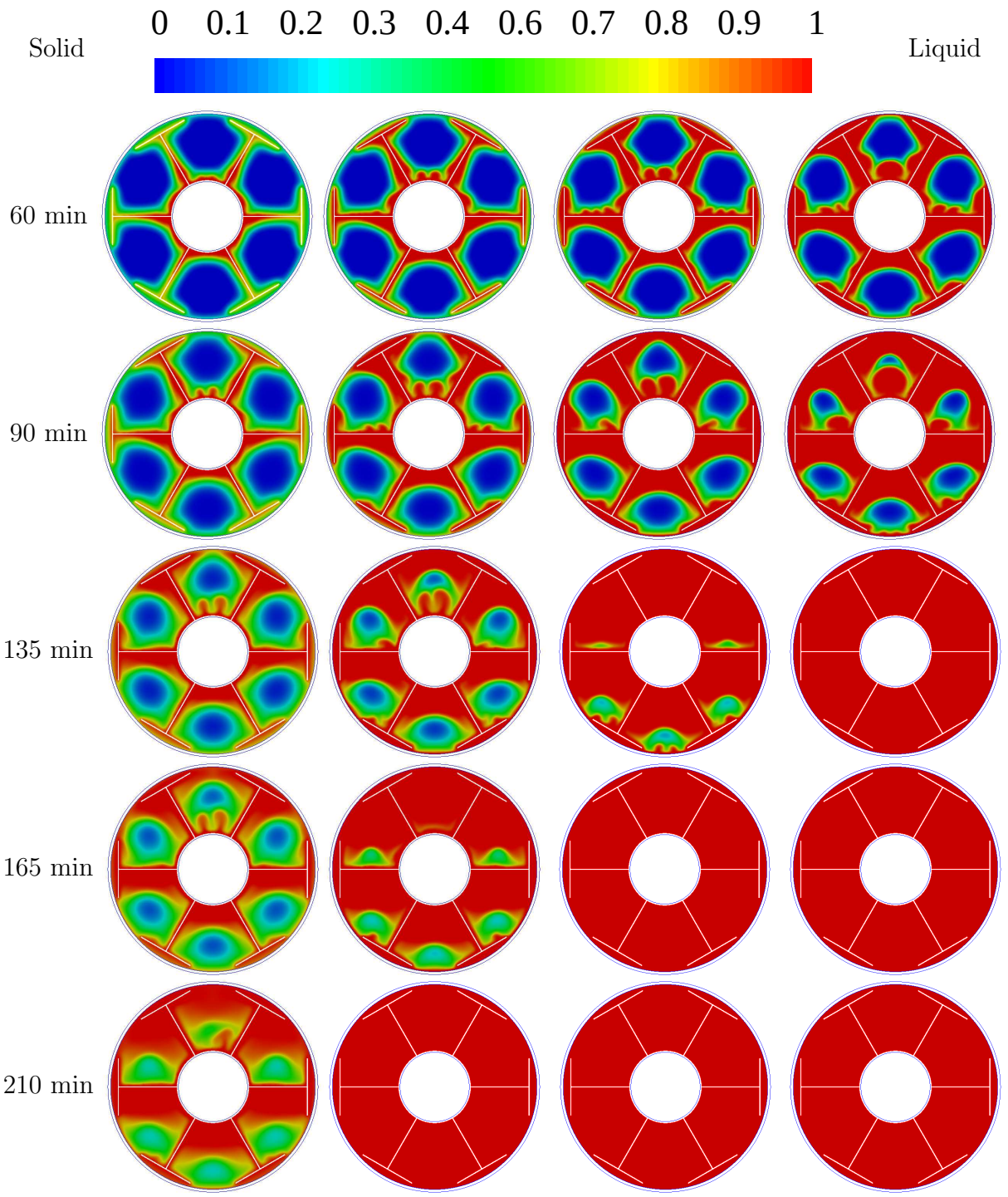

Figure 5.22: Liquid fraction contours at different times for melting process for various HTF temperatures. From left: first HTF temperature 87 °C, second HTF temperature 90 °C, third HTF temperature 93 °C and fourth HTF temperature 96 °C.

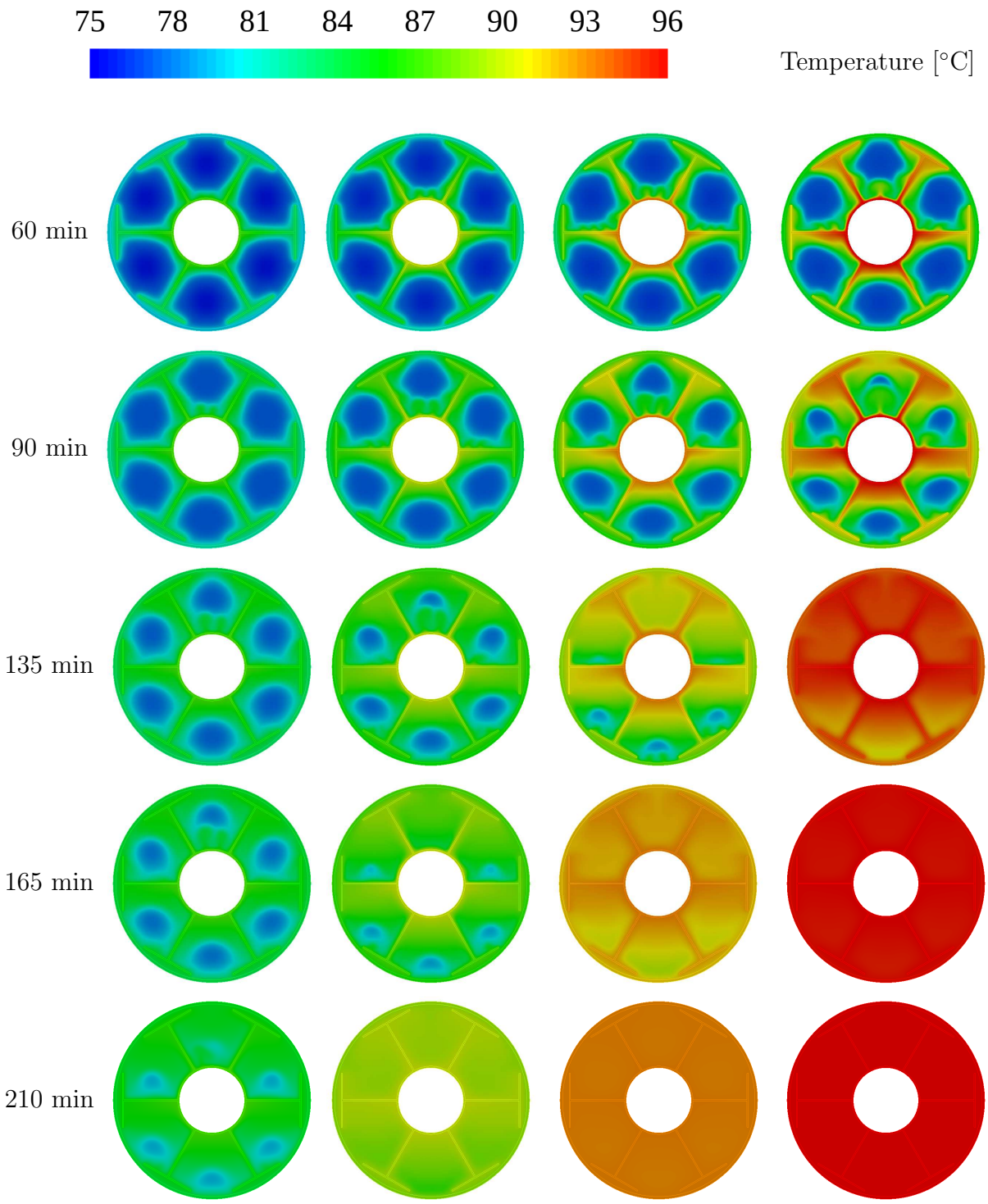

Figure 5.23: Contours of temperature at various times for melting process with different HTF temperatures. From left: first HTF temperature 87 °C, second HTF temperature 90 °C, third HTF temperature 93 °C and fourth HTF temperature 96 °C.

5.7.2 Solidification process

In this test, the influence of changing the HTF temperature on the PCM solidification process was studied. Various HTF temperatures were studied, which were: 60 °C, 64 °C, 68 °C and 72 °C. Fig. 5.24 presents the liquid fraction for different HTF temperatures. It can be seen from this figure that increasing the difference between the PCM solidification temperature and the HTF temperature increases the heat transfer rate, which accelerates the PCM solidification process. If the HTF temperature decreases from 72 °C to 60 °C the total solidification time reduces by 50%.

Fig. 5.25 shows the average PCM temperature as a function of time for different HTF temperatures. Reducing the HTF temperature decreases the PCM temperature and this reduces the PCM total solidification time.

Liquid fraction contours for different HTF temperatures at different times are shown in Fig. 5.26. It can be seen from this figure that the decrease in the HTF temperature accelerates the PCM solidification process. Contours of temperature for different HTF temperatures at different times are shown in Fig. 5.27. It is obvious from this figure that the decrease in the HTF temperature decreases the PCM temperature and accelerates the solidification process.

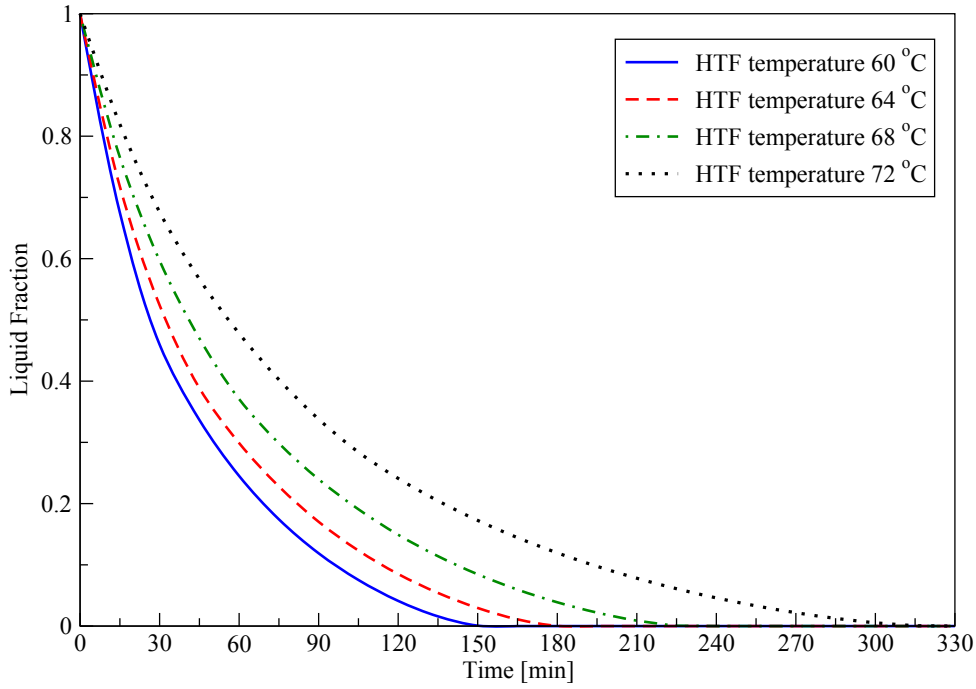

Figure 5.24: Liquid fraction comparison for solidification process with different HTF temperatures.

Table 5.5: Solidification time and solidification time reduction for various HTF temperatures

HTF temperature (°C)	**Solidification time (min)**	**Reduction (%)**
72 (base case)	314	—
68	226	28
64	182	42
60	157	50

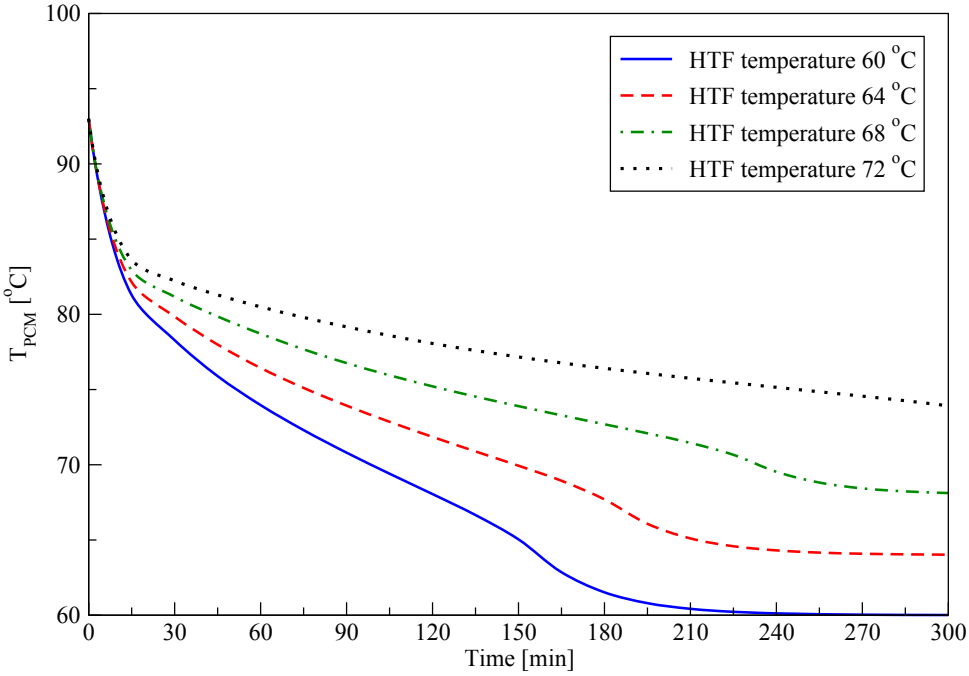

Figure 5.25: Average PCM temperature comparison for solidification process with different HTF temperatures.

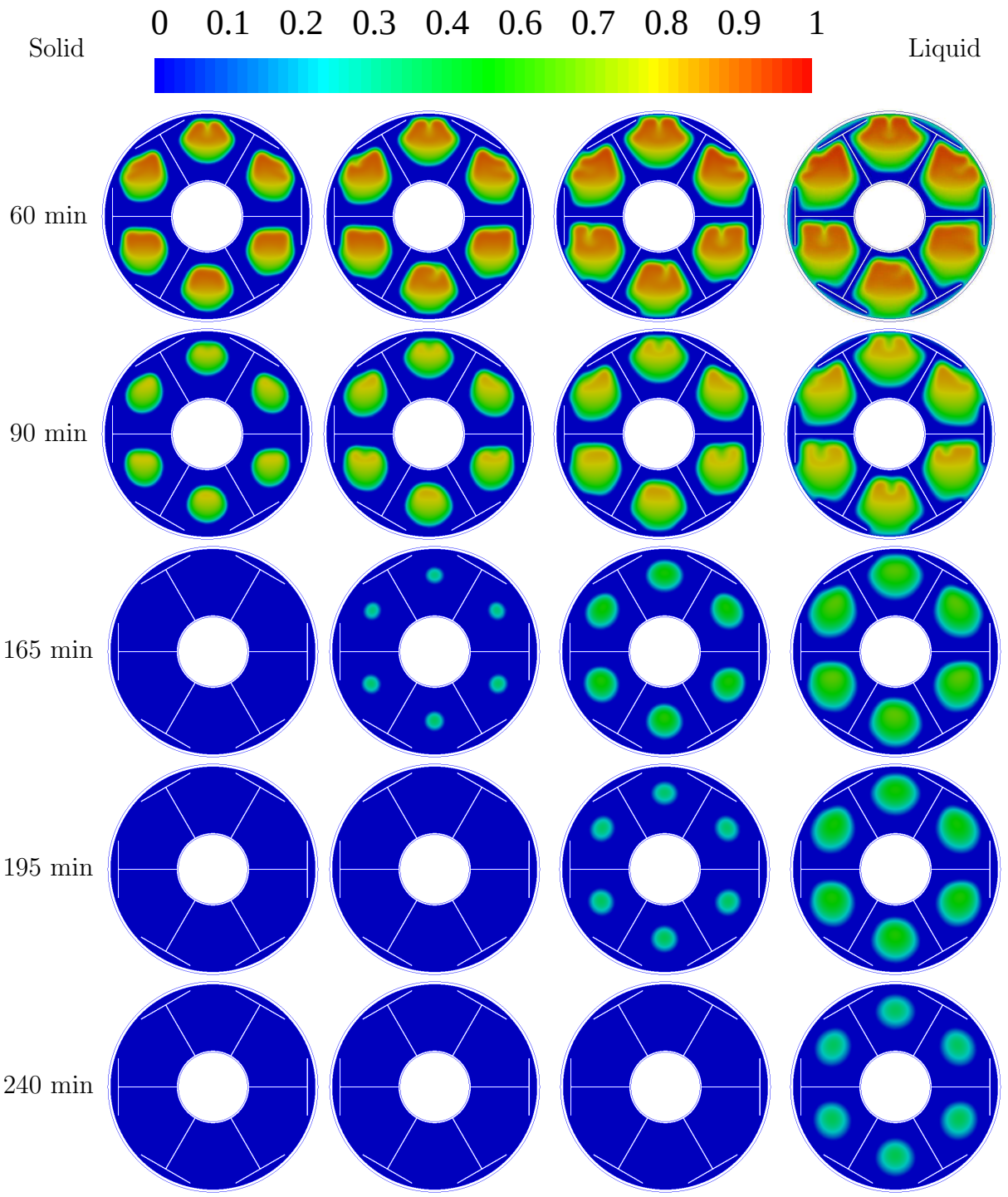

Figure 5.26: Liquid fraction contours at various times for solidification process for different HTF temperatures. From left: first HTF temperature 60 °C, second HTF temperature 64 °C, third HTF temperature 68 °C and fourth HTF temperature 72 °C.

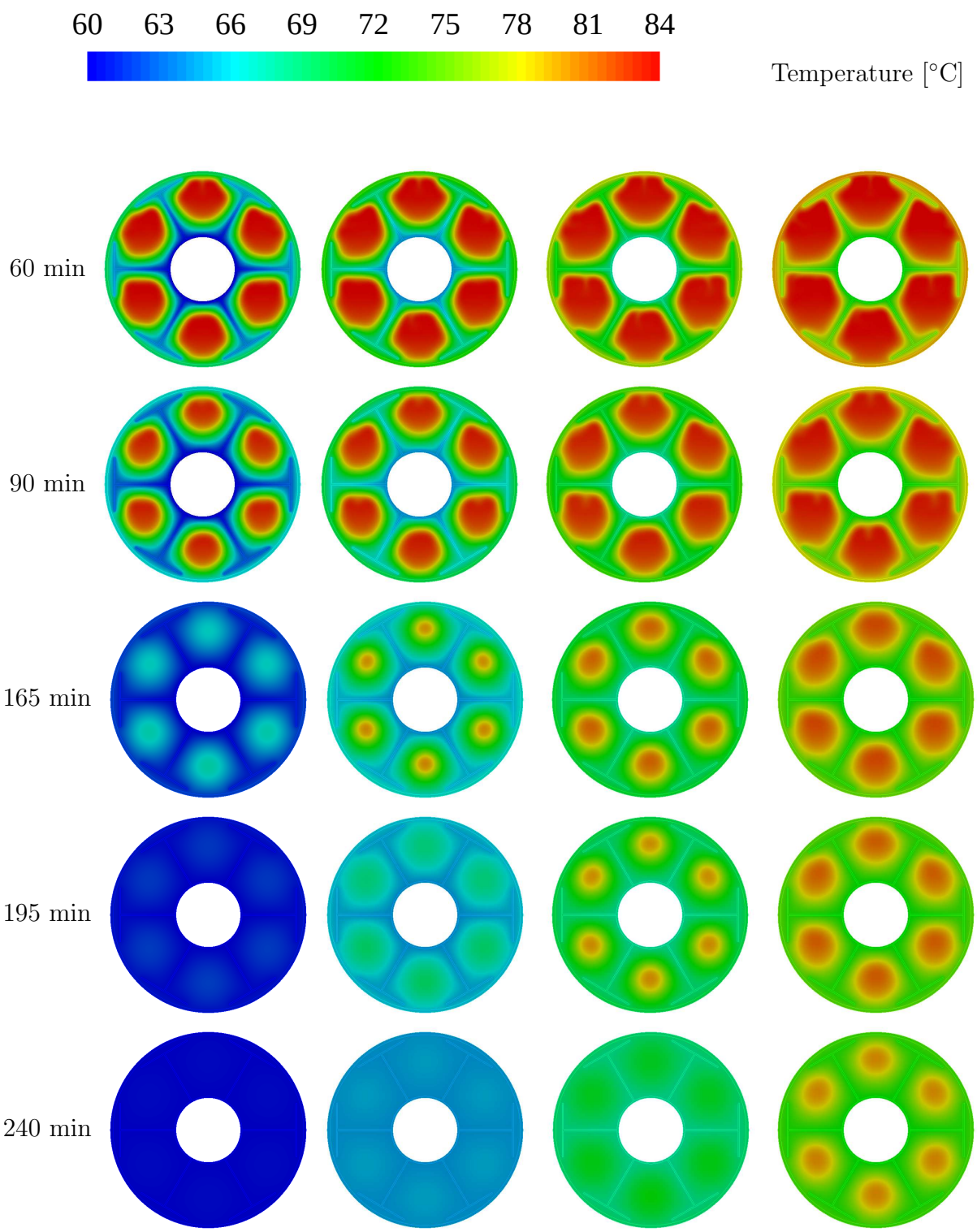

Figure 5.27: Contours of temperature at various times for solidification process for different HTF temperature. From left: first HTF temperature 60 °C, second HTF temperature 64 °C, third HTF temperature 68 °C and fourth HTF temperature 72 °C.

Chapter 6

Utilizing a Webbed Tube Heat Exchanger to Improve the Thermal Performance of PCM

In this chapter, an innovative heat exchanger design (webbed tube heat exchanger) is introduced to improve the thermal performance of PCM. Then, to demonstrate the value of the webbed tube heat exchanger design, its thermal performance was compared against the traditional heat exchangers.

6.1 Physical model

The design of the webbed tube heat exchanger (WTHX) is taken from the shell and tube heat exchanger (STHX) design which studied in Chapter 5, where the inner HTF tube was replaced by small four inner HTF tubes with the same cross-sectional area. This means that each inner HTF tube in the WTHX has a cross-sectional area equal to a quarter of the cross-sectional area of the inner HTF of the STHX. While, the inner diameter of the outer shell of the WTHX is the same as the inner diameter of the outer shell of the STHX,

for more detail about the dimensions see Table 6.1.

To increase the heat transfer surface area and accelerate PCM melting and solidification processes, metal plates were used to connect the inner HTF tubes together. The WTHX consisted of four horizontal inner tubes and an outer shell. The inner tubes were connected together using many metal plates that were welded to these tubes. The HTF (water) flows through the inner tubes, and the PCM is placed on the shell's side. The PCM used in this study was (RT82). The thermal and physical properties of PCM (RT82) are shown in Table 4.1. The WTHX was tested as a novel design to reduce the charging and discharging time for the TES systems, based on PCMs. The WTHX physical model with the major dimensions is shown in Fig. 6.1. This model has four inner tubes with an inner diameter of $d_i = 20$ mm and 3 mm thickness, the outer shell has an inner diameter of $d_o = 150$ mm and thickness of 2 mm. The centres of the inner tubes were drawn on a circle with 100 mm diameter. The angular distance between the inner tubes was equally distributed. The plates' dimensions were 144 mm (L), 144 mm (W1), 26.5 mm (W2) and 3 mm thickness see Fig. 6.1. Copper was utilized for tubes and plates.

The tee fin was not used with the WTHX, because there is another heat transfer enhancement technique which included utilizing metal plates to increase the heat transfer surface area will be tested as another heat transfer enhancement option.

The schematic diagram of the computational domain used in the numerical simulations with the indicated boundary conditions is shown in Fig. 6.2.

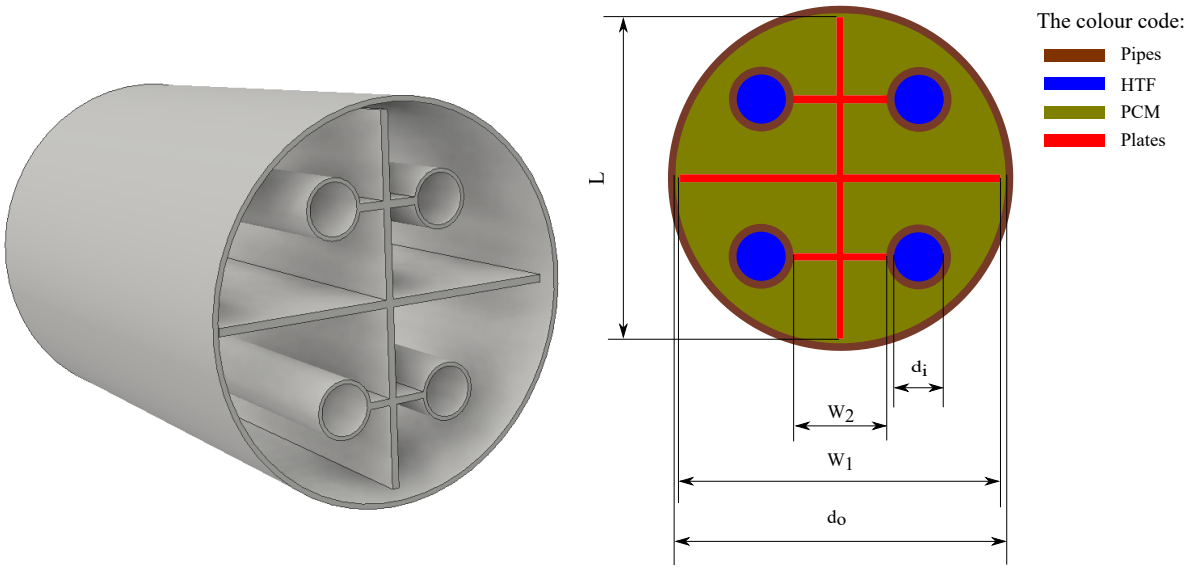

Figure 6.1: Webbed tube heat exchanger physical model with the major dimensions, left: 3D, right: cross-sectional area.

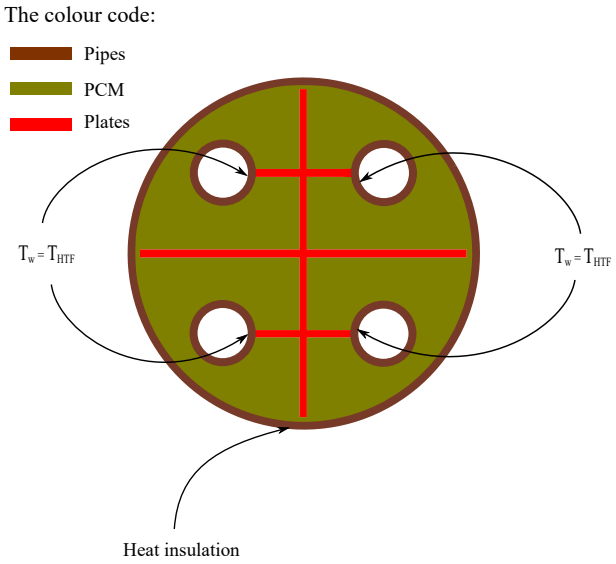

Figure 6.2: Webbed tube heat exchanger computational domain with the indicated boundary conditions.

6.2 Numerical procedure

ANSYS Fluent 15 software was used in the simulation. Fluent employs the finite volume method and uses the enthalpy-porosity technique to solve the continuity, momentum and energy equations. The solidification and melting model was used to model the PCM melting and solidification process. Two-dimensional computational domains were used in the simulations. A Transient Pressure-Based solver was employed to solve the governing equations for incompressible flow. The SIMPLE scheme was used for pressure-velocity coupling. The PRESTO scheme was utilized for pressure discretization, which is recommended for solving natural convection flow [15]. The second order upwind scheme was employed for solving the momentum and energy equations. The under-relaxation factors for momentum, pressure, liquid fraction and energy were 0.7, 0.3, 0.9 and 1 respectively. The convergence criterion for energy equation was set to 10^{-6} and 10^{-4} for continuity and momentum equations.

6.3 Mesh and time step independent test

For this test, the WTHX model was used. The model is shown in Fig. 6.2. The melting process was considered for this test. Many mesh numbers were tested which included: 15241 cells, 39721 cells, 59372 cells, and 68821 cells. The mesh independent test result is shown in Fig. 6.3. A 5 s time step was used in this test. Its clear from this figure that the results were identical between 59372 cells and 68821 cells. Given this, mesh consisting of 59372 cells will be used in the following simulations and is shown in Fig. 6.4. The result of the time step independent test is shown in Fig. 6.5. The mesh used for this test was 59372 cells. It is clear from this figure that there are identical results for time steps 1 s, 5 s, and 10 s. As such, a 10 s time step will be used in the following simulations.

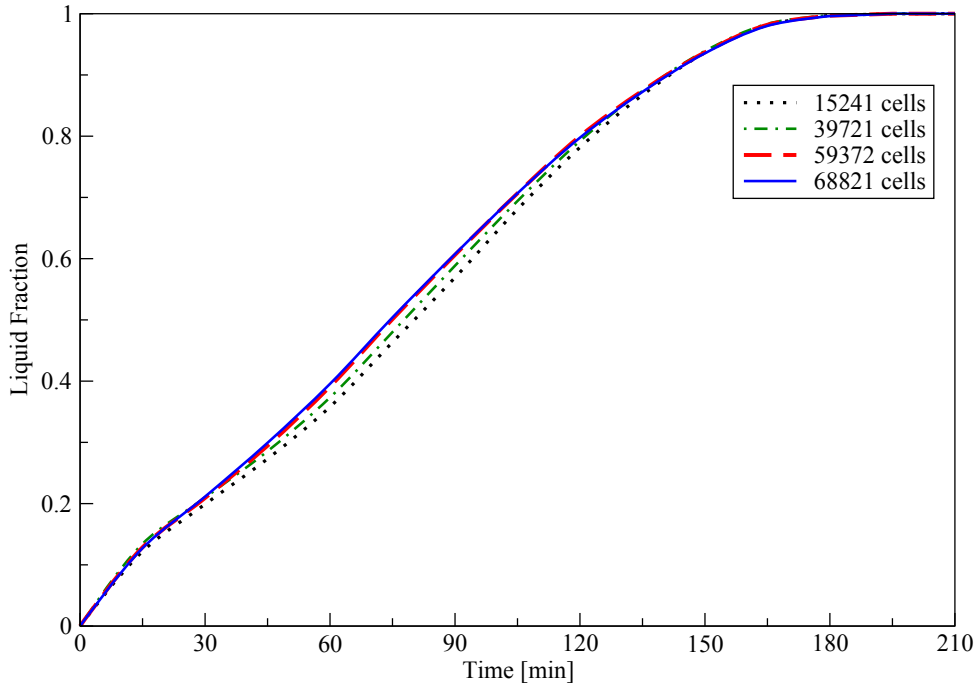

Figure 6.3: WTHX mesh independent test, liquid fraction.

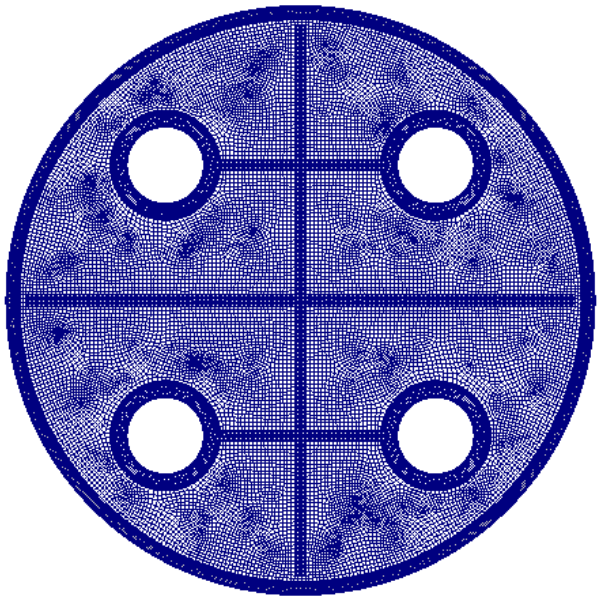

Figure 6.4: WTHX mesh (59372 cells).

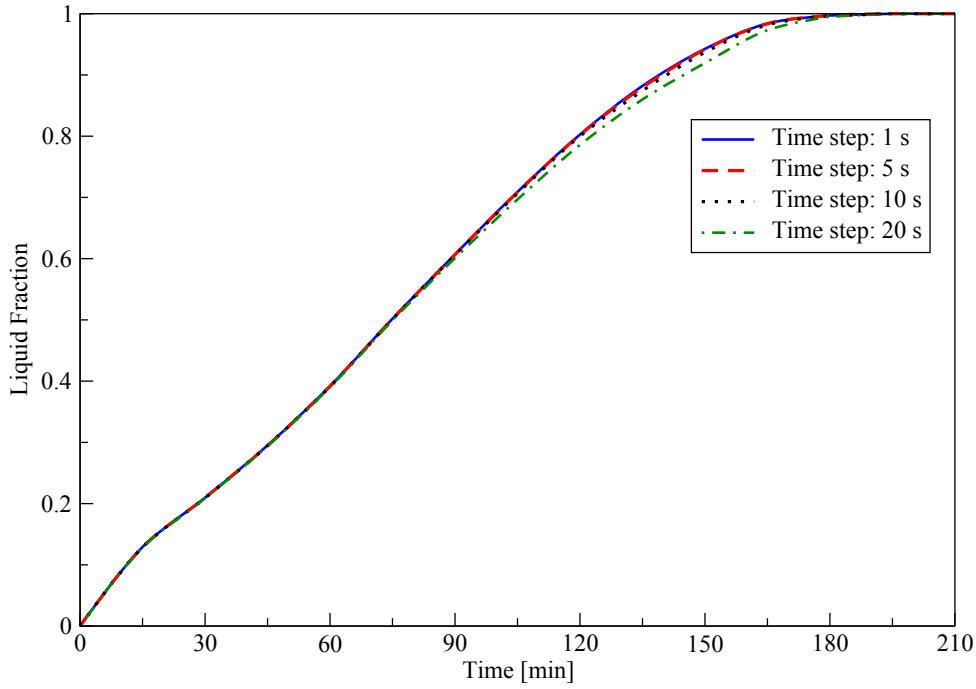

Figure 6.5: WTHX time step independent test, liquid fraction.

6.4 Comparison between webbed tube heat exchanger with conventional heat exchangers types

To demonstrate the value of the webbed tube heat exchanger (WTHX) design, its thermal performance was compared with the shell and tube heat exchanger (STHX), the triple tube heat exchanger (TTHX) and the multi-tube heat exchanger (MTHX). The cross-sectional areas of the physical heat exchanger models are illustrated in Fig. 6.6. The dimensions of the various heat exchangers are illustrated in Table 6.1. To make a fair comparison the same amount of the PCM was used for the STHX, the TTHX, and the MTHX, so the same amount of energy could be stored in all these heat exchangers. The WTHX has a slightly lower amount of PCM compared to the other heat exchanger types due to the usage of the metal plates. However, the usage of the metal plates reduces the volume of the PCM by less than 4% but significantly enhances the thermal performance of the WTHX compared

to the other heat exchangers. This enhancement in the WTHX thermal performance due to the usage of metal plates compensates the slight change in PCM compared to other heat exchangers. The computational domains for the various heat exchangers with the indicated boundary conditions are shown in Fig. 6.7. These heat exchangers included: shell and tube heat exchanger (STHX) as shown in Fig. 6.7a, triple tube heat exchanger (TTHX) as shown in Fig. 6.7b, multitube heat exchanger (MTHX) as shown in Fig. 6.7c and webbed tube heat exchanger (WTHX) as shown in Fig. 6.7d. For the STHX the HTF passes through the inner tube and the PCM was placed in the shell side. For the TTHX the HTF passes through the inner and outer tubes while the PCM was placed in the middle annular. For the MTHX and the WTHX the HTF passes through the inner tubes and the PCM was placed in the shell side. Many metal plates were used in the WTHX and were welded to the HTF tubes to increase the heat transfer surface area and enhance the PCM thermal performance.

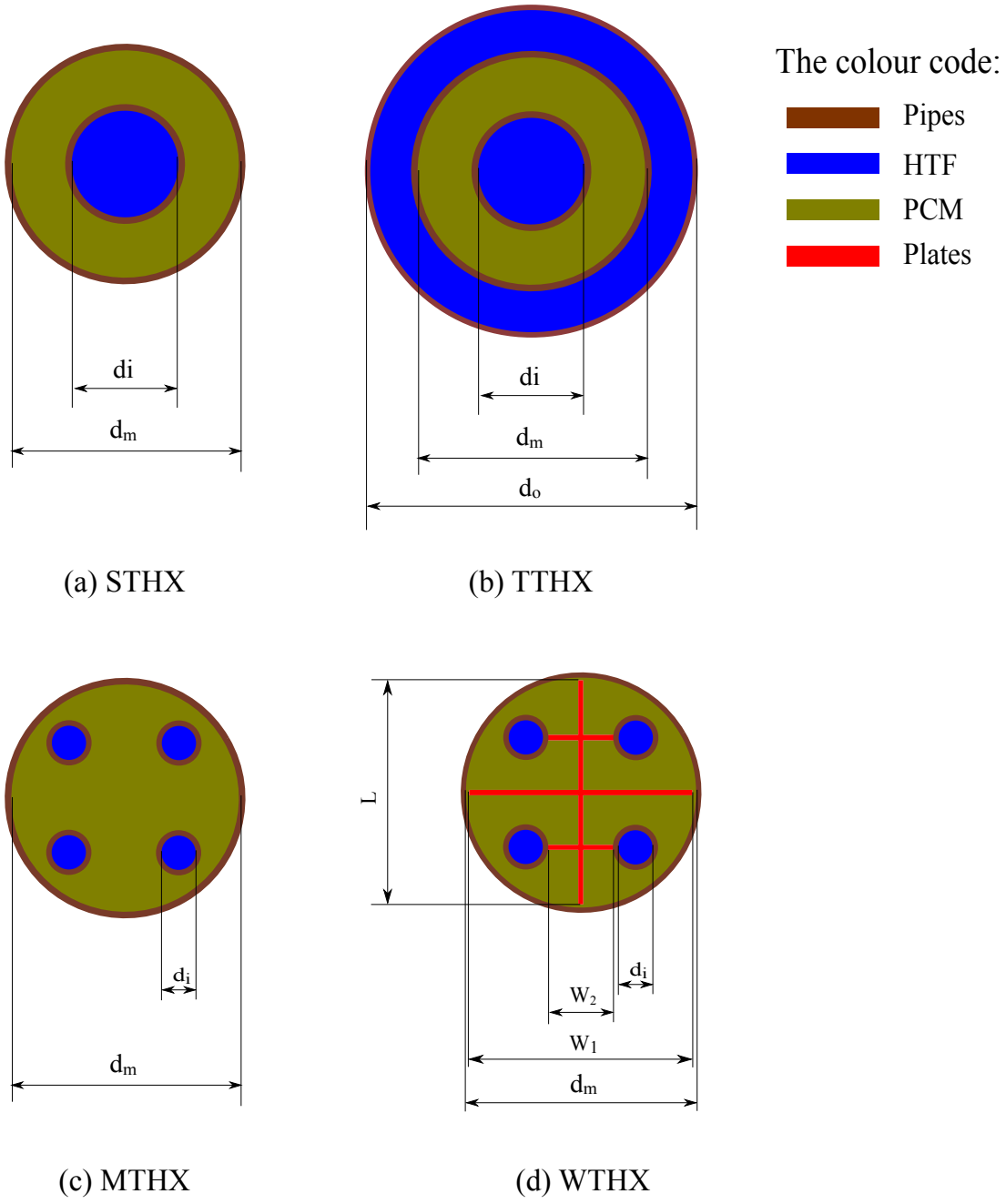

(a) STHX (b) TTHX

(c) MTHX (d) WTHX

Figure 6.6: The cross-sectional area for various heat exchangers' configurations. (a) STHX, (b) TTHX, (c) MTHX, and (d) WTHX..

Table 6.1: Geometrical dimensions of different heat exchangers types

Heat exchanger type	d_i (mm)	d_m (mm)	d_o (mm)	W_1 (mm)	W_2 (mm)	L (mm)
STHX	50.8	150	——	——	——	——
TTHX	50.8	150	200	——	——	——
MTHX	20	150	——	——	——	——
WTHX	20	150	——	144	26.5	144

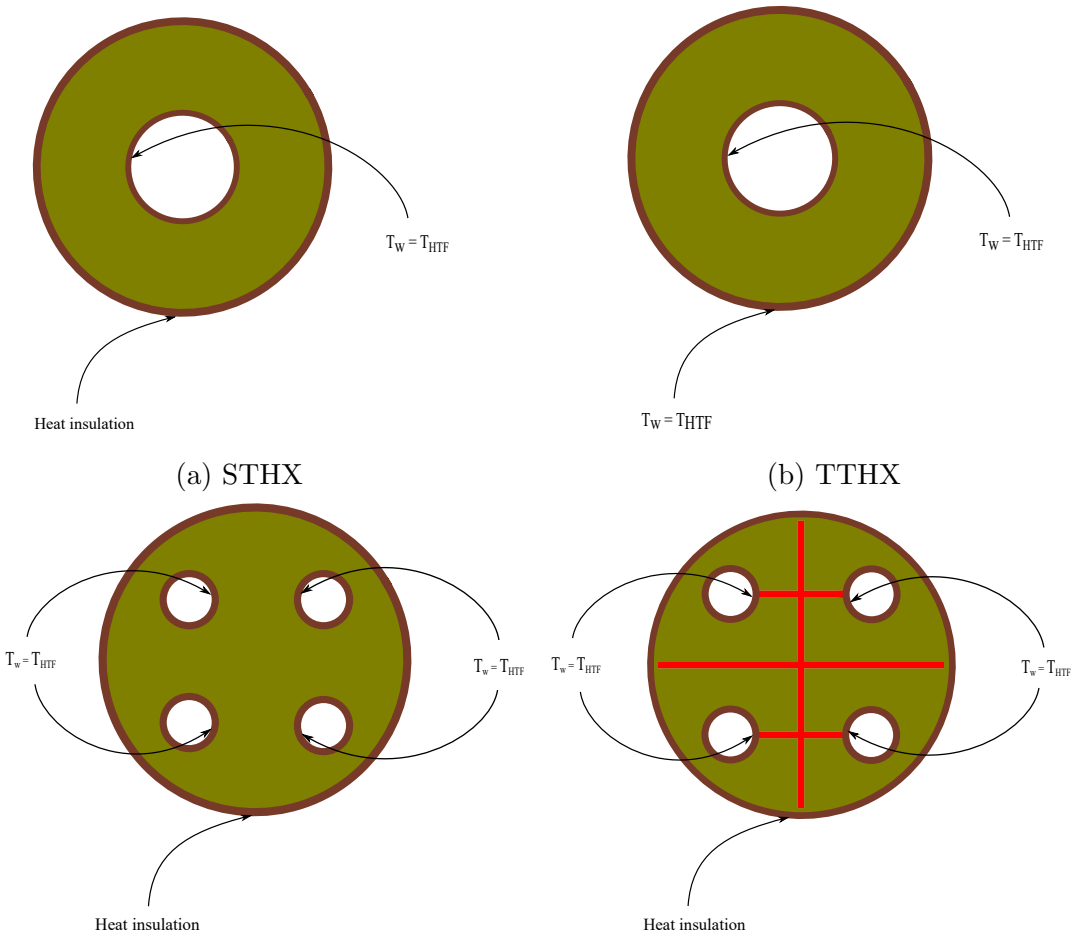

(a) STHX (b) TTHX

(c) MTHX (d) WTHX

Figure 6.7: Computational domains with the indicated boundary conditions for various heat exchangers' configurations. (a) STHX, (b) TTHX, (c) MTHX, and (d) WTHX.

6.4.1 Initial and boundary conditions

Melting process

At the initial time (t = 0), the PCM was in the solid state, hence its temperature was 27 °C, below its melting temperature. The HTF has a constant temperature ($T_w = T_{HTF} = 90$ °C), which is higher than the PCM melting temperature. This temperature was imposed along the inner tubes walls when using the MTHX (Fig. 6.7c) or the WTHX (Fig. 6.7d), imposed along inner tube wall when using the STHX (Fig. 6.7a),and imposed along inner and outer tubes walls when using the TTHX (Fig. 6.7b). Therefore, the initial and boundary conditions can be listed as:

$T = T_{initial} = 27$ °C at (t = 0).

At $d = d_i$, $T = T_{HTF} = 90$ °C.

At $d = d_o$, wall insulated (adiabatic) in cases of using STHX, MTHX, and WTHX.

Or at $d = d_o$, $T = T_{HTF} = 90$ °C at case of using TTHX.

Solidification process

At the initial time (t = 0), the PCM was in the liquid state, hence its temperature was 93 °C, which is above its solidification temperature. The HTF has a constant temperature ($T_w = T_{HTF} = 68$ °C), which is lower than the PCM solidification temperature. This temperature is imposed along the inner tubes walls when using the MTHX (Fig. 6.7c) or the WTHX (Fig. 6.7d), imposed along inner tube wall when using the STHX (Fig. 6.7a), and imposed along inner and outer tubes walls when using the TTHX (Fig. 6.7b). Therefore, the initial and boundary conditions can be listed as:

$T = T_{initial} = 93$ °C at (t = 0).

At $d = d_i$, $T = T_{HTF} = 68$ °C.

At $d = d_o$, wall insulated (adiabatic) in cases of using STHX, MTHX, and WTHX.

Or at $d = d_o$, $T = T_{HTF} = 68$ °C at case of using TTHX.

6.4.2 Melting process

Fig. 6.8 shows the liquid fraction for the various heat exchangers. It is clear from this figure that by utilizing the WTHX the total melting time decreased significantly compared to the other heat exchangers. The PCM completely melted after 180 minutes when utilizing the WTHX, while for the same amount of time only around 10%, 30% and 60% of PCM melted in the cases of STHX, MTHX, and TTHX respectively. The total PCM melting time reduced by 50% when utilizing the WTHX compared to the TTHX. Moreover, the total PCM melting time decreased by 72% when using the WTHX as compared to the MTHX. This acceleration in the melting process when using the WTHX occurred because of the increase of the heat transfer area and increase heat penetration due to using the metal plates. The total melting time and melting time reductions for the various heat exchanger configurations are shown in Table 6.2.

The average PCM temperature versus time for the various heat exchangers is shown in Fig. 6.9. It is obvious from this figure that the PCM average temperature when using the WTHX was higher at all time intervals compared to the other heat exchangers. This demonstrates the significant improvement in the PCM thermal performance when utilizing the WTHX. Contours of liquid fraction for various heat exchanger configurations at various time intervals are shown in Fig. 6.10. It is clear from this figure that the PCM melted faster when utilizing the WTHX compared to the other heat exchangers, which was due to the increase of the heat transfer area. It can be seen in all heat exchangers types, that the PCM at top position melt quickly compared to the bottom position. This due to the natural convection and upward rise of high-temperature liquid PCM. At an early stage, the conduction is the dominant heat transfer mechanism. When the liquid fraction increases, natural convection become the dominant heat transfer mechanism. It is clear that by increasing the heat transfer area the melting rate increase. In case of utilizing the WTHX, the conduction heat transfer increased by using the metal plates. In the MTHX the melting rate increased compared to the STHX, this happens due to increase heat transfer area due to the use of small HTF tubes, moreover, these tubes were distributed on the isolated regions of PCM. It can be seen in all heat exchangers cases, that at initial

stages the melting process concentrated near the heat transfer walls (tubes and plates). With the increase of the liquid percentage of PCM, the convection heat transfer increased and the liquid PCM pushed upward due to the buoyancy effect while the solid part of the PCM sticks down to the bottom of the middle tube due to its high density.

Contours of surface heat flux for various heat exchanger configurations at various time intervals are shown in Fig. 6.11. It is clear from this figure that by utilizing the WTHX the surface heat flux increased significantly compared to the other heat exchangers. Contours of temperature for various heat exchanger configurations at different times are shown in Fig. 6.12. The WTHX shows higher temperatures compared to other heat exchangers' configurations, this reduces the total PCM melting time. It can be seen from Fig. 6.12 that for the STHX, the isotherms of the upper half of the PCM-shell is high deformed compared to the lower half. This implies that the annulus is dominated by convection at the upper half and by conduction at the lower half.

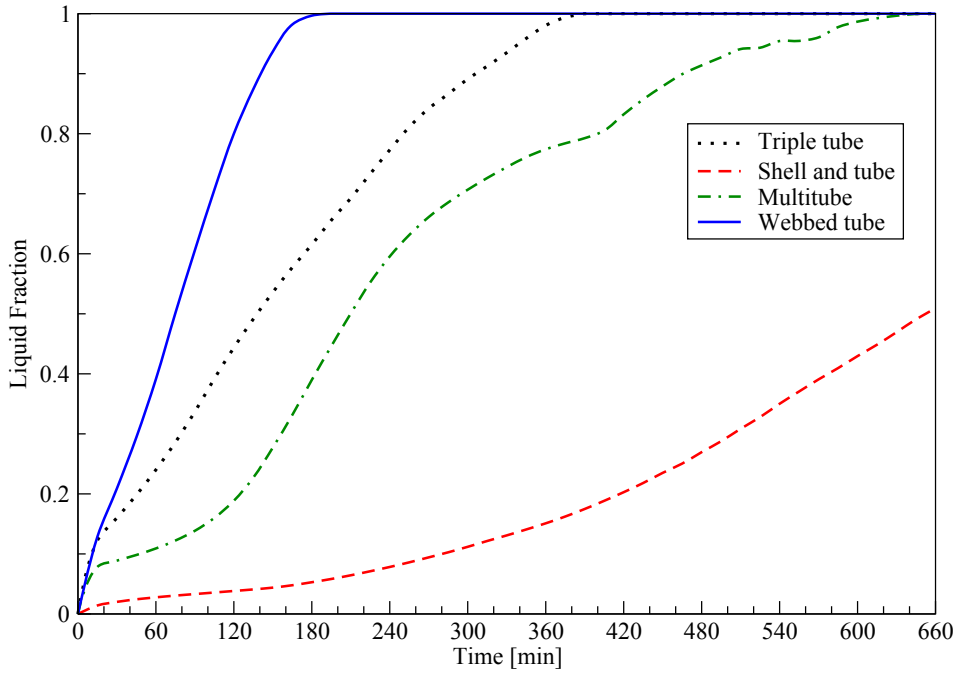

Figure 6.8: Liquid fraction comparison for melting process for WTHX, TTHX, STHX, and MTHX.

Table 6.2: Melting time and melting time reduction for various heat exchangers

Heat exchanger type	**Melting time (min)**	**Reduction (%)**
MTHX (base case)	647	—
TTHX	360	44
WTHX	180	72

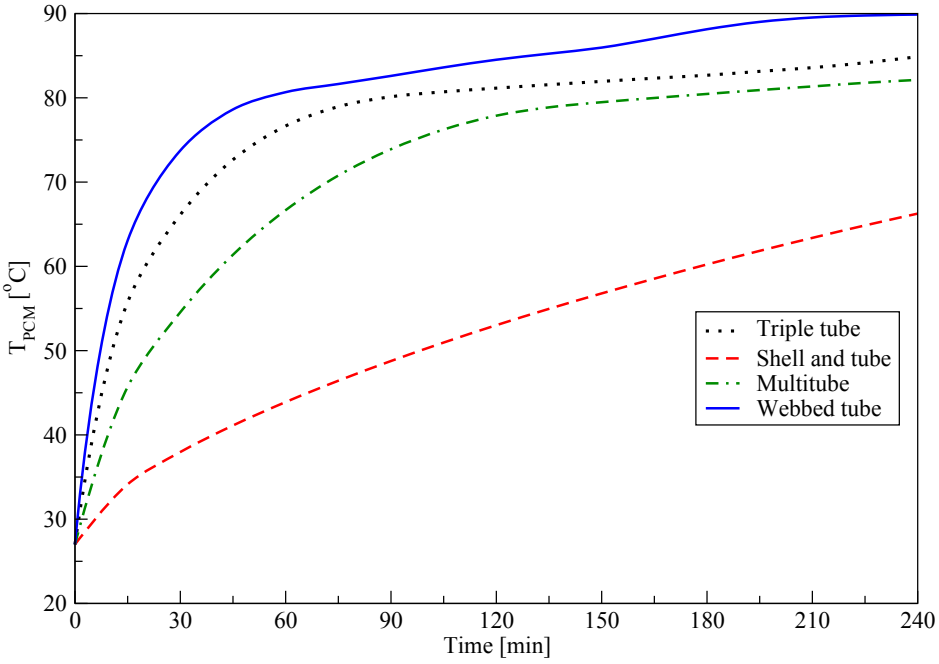

Figure 6.9: Average PCM temperature comparison for melting process for WTHX, TTHX, STHX, and MTHX.

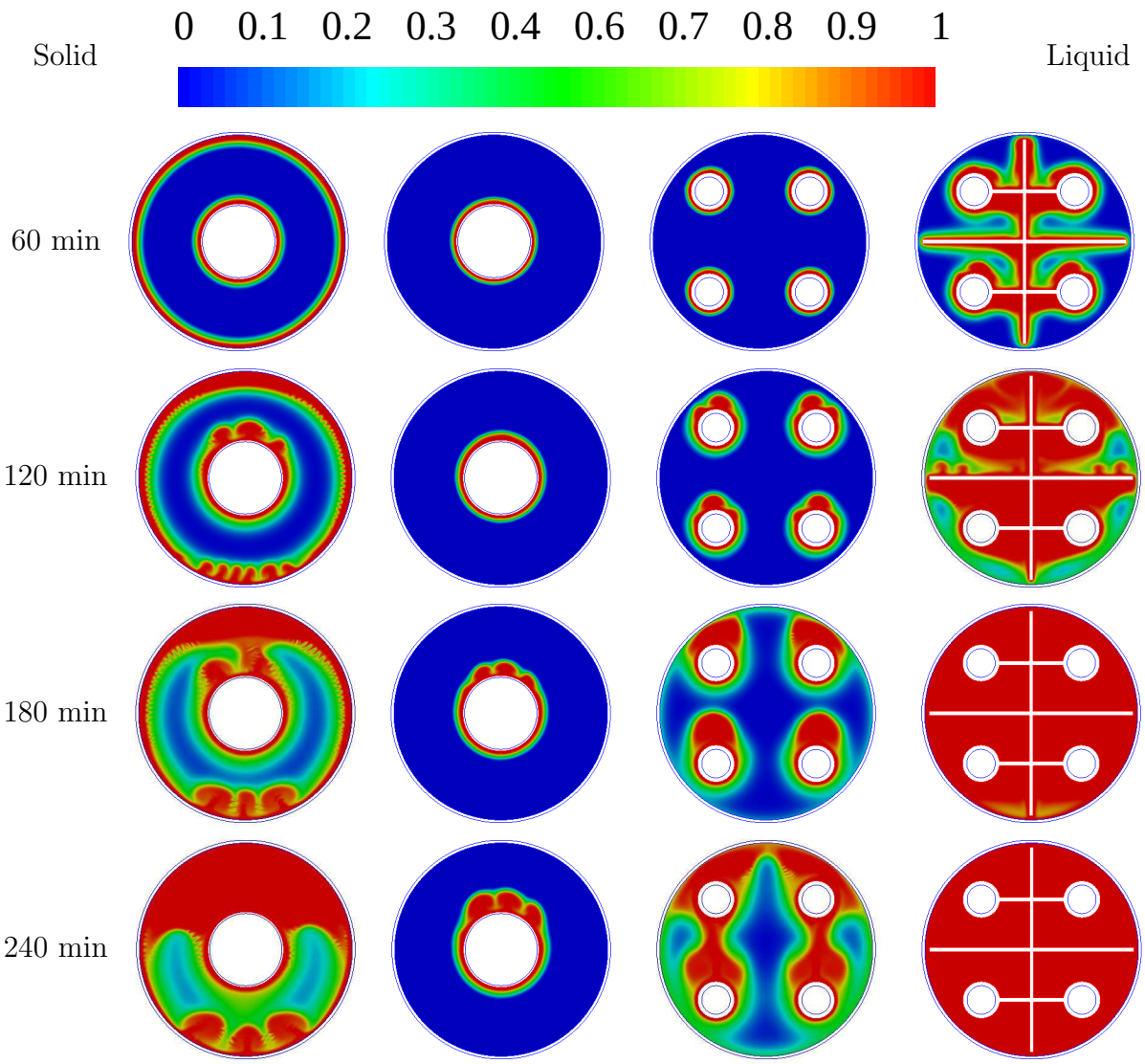

Figure 6.10: Liquid fraction contours at different times for melting process for various heat exchangers: first from left TTHX, second STHX, third MTHX, and fourth WTHX.

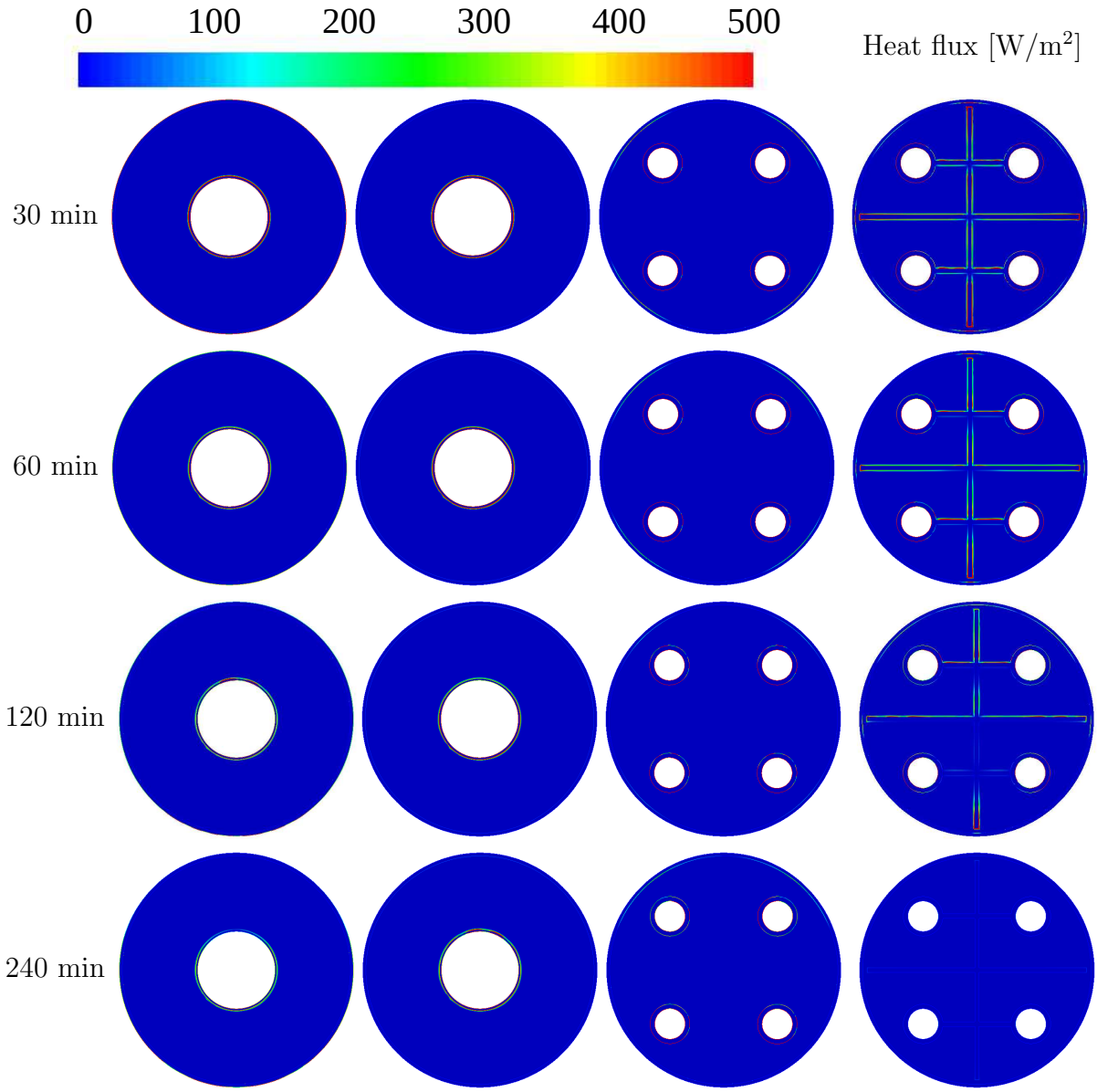

Figure 6.11: Surface heat flux contours at different times for melting process for various heat exchangers: first from left TTHX, second STHX, third MTHX, and fourth WTHX.

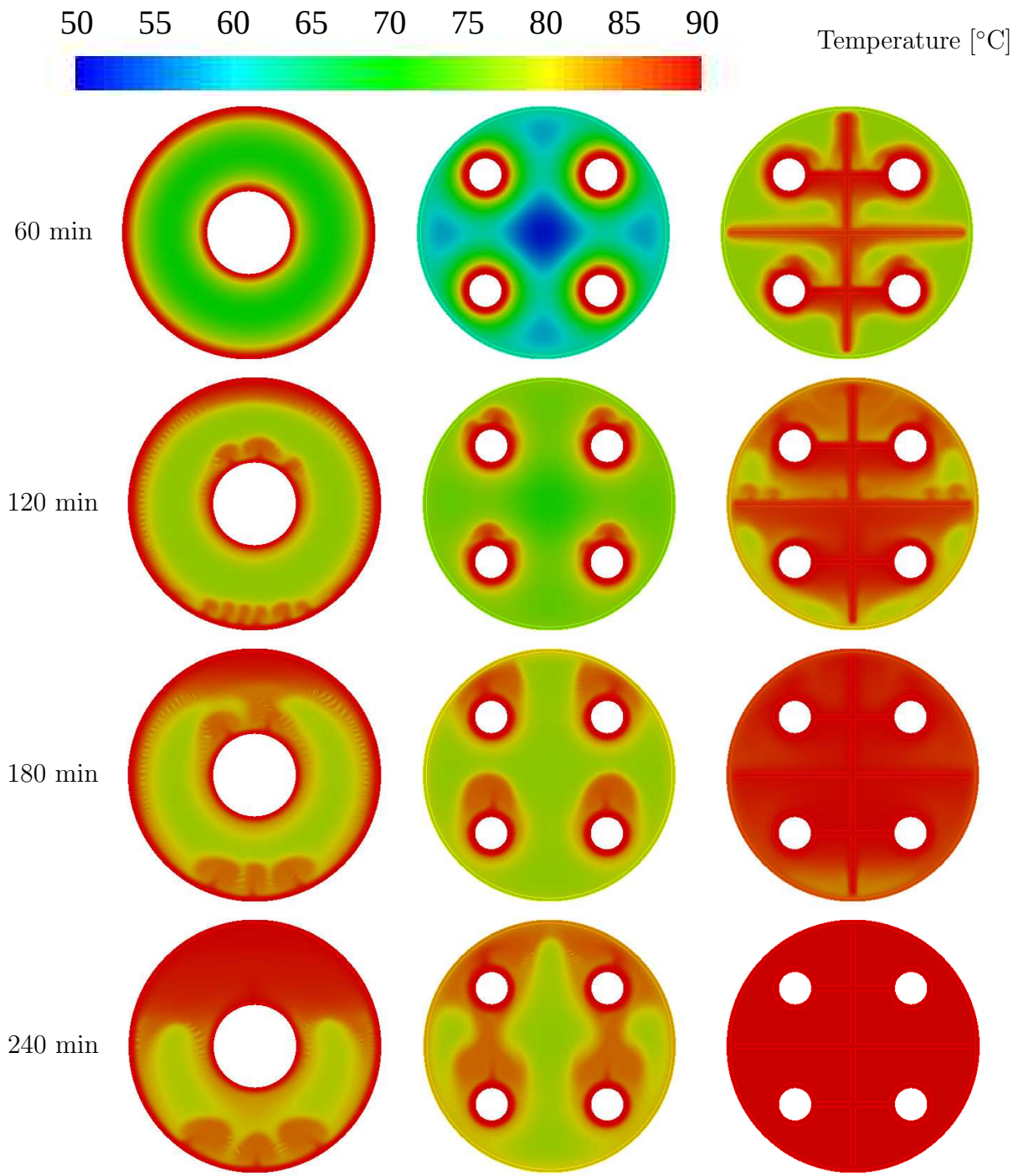

Figure 6.12: Contours of temperature at different times for melting process for various heat exchangers: first from left TTHX, second MTHX, and third WTHX.

6.4.3 Solidification process

Fig. 6.13 shows the liquid fraction for various heat exchangers. It is clear from this figure that the PCM completely solidified in a shorter time when using the WTHX compared to other heat exchangers. When using the WTHX, the PCM completely solidified after 165 minutes, while for the same amount of time only around 90%, 60% and 25% of the PCM solidified when using the TTHX, MTHX, and STHX respectively. The total PCM solidification time reduced by 45% when utilizing the WTHX compared to the TTHX. Moreover, the total PCM solidification time decreased by 66% when using the WTHX compared to the MTHX. The total solidification time and solidification time reductions for the various heat exchanger configurations are shown in Table 6.3.

The average PCM temperature versus time for various heat exchangers is illustrated in Fig. 6.14. It can be observed from this figure that after 60 minutes using the WTHX the PCM temperature was lower compared to the other heat exchangers' configurations, thus accelerating the PCM solidification process. Contours of liquid fraction for various heat exchangers at different times are represented in Fig. 6.15. It is obvious from this figure that the worst heat exchanger type was the STHX, owing to the lower heat transfer area. As the heat transfer area increases the solidification process accelerates, so the MTHX showed better performance compared to the STHX. Additionally, if the heat transfer area further increased when using the WTHX the total solidification time reduced. By utilizing the WTHX the solidification finishes at a lower time due to enhancement of thermal penetration depth due to the use of metal plates.

Contours of surface heat flux for various heat exchanger configurations at various time intervals are shown in Fig. 6.16. It is clear from this figure that by utilizing the WTHX the heat transfer surface area increased significantly compared to the other heat exchangers. Contours of temperature for different heat exchangers at different times are shown in Fig. 6.17. It is obvious from this figure that the WTHX has a low PCM temperature at all time intervals compared to the other heat exchangers' configurations, so the solidification process in the WTHX was completed in a shorter time.

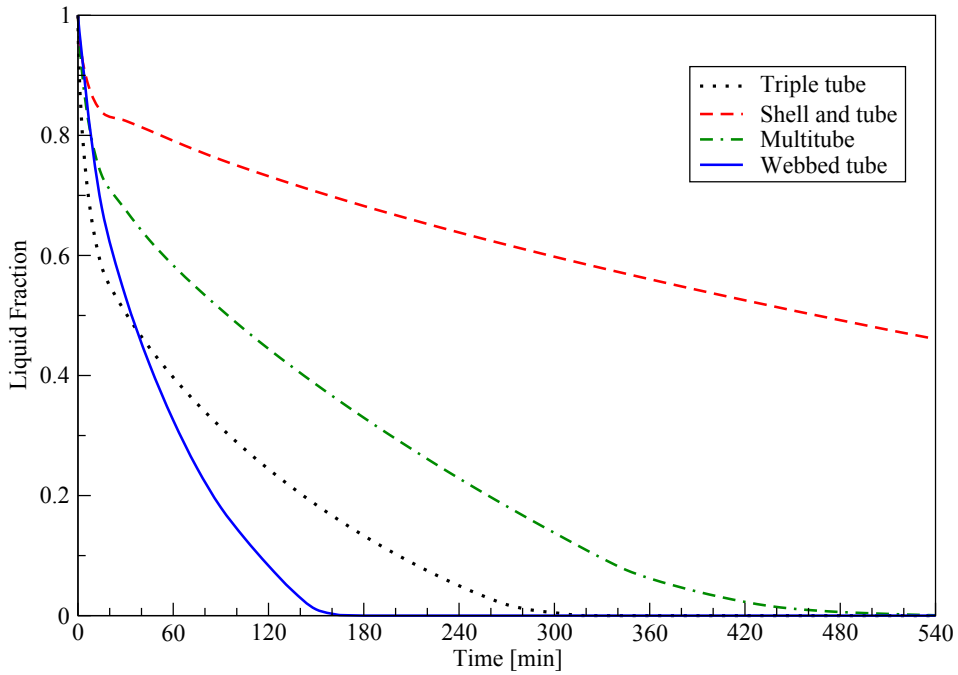

Figure 6.13: Liquid fraction comparison for solidification process for WTHX, TTHX, STHX, and MTHX.

Table 6.3: Solidification time and solidification time reduction for various heat exchangers

Heat exchanger type	**Solidification time (min)**	**Reduction (%)**
MTHX (base case)	485	—
TTHX	302	0.37
WTHX	165	66

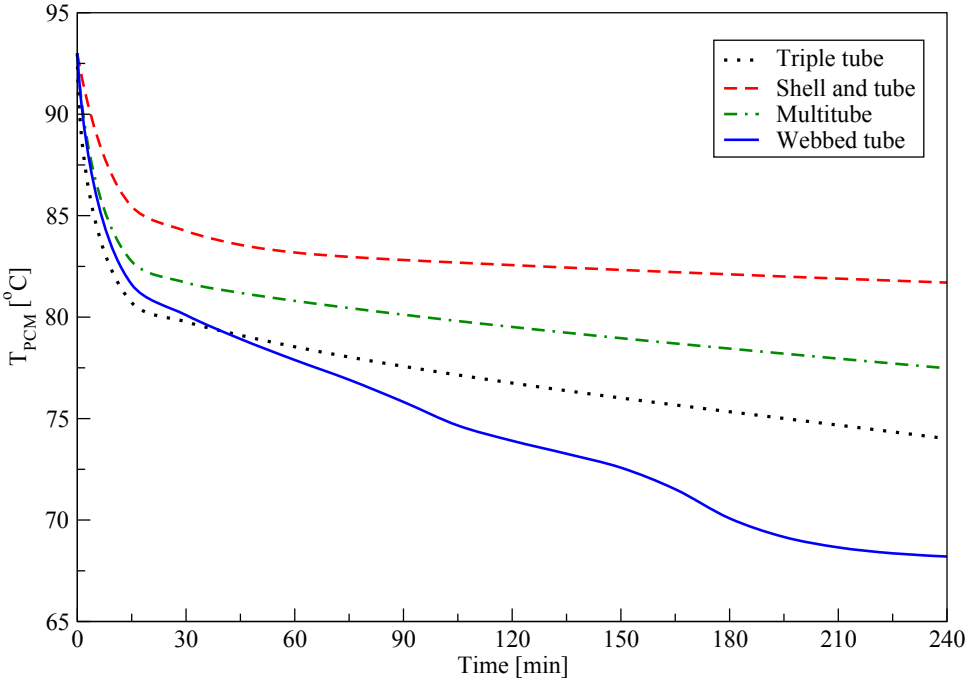

Figure 6.14: Average PCM temperature comparison for solidification process for WTHX, TTHX, STHX, and MTHX.

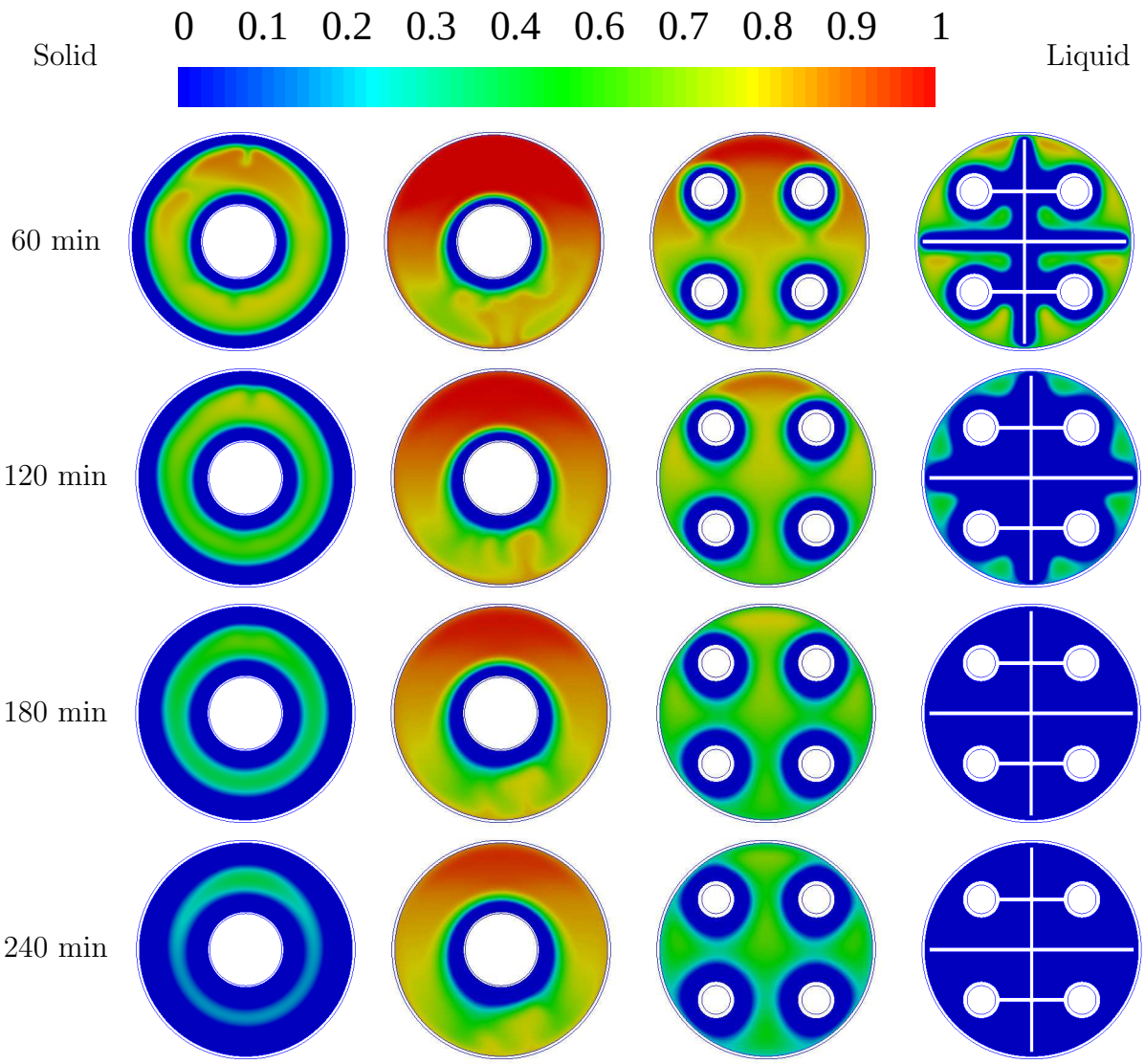

Figure 6.15: Liquid fraction contours at different times for solidification process for various heat exchanger types: first from left TTHX, second STHX, third MTHX, and fourth WTHX.

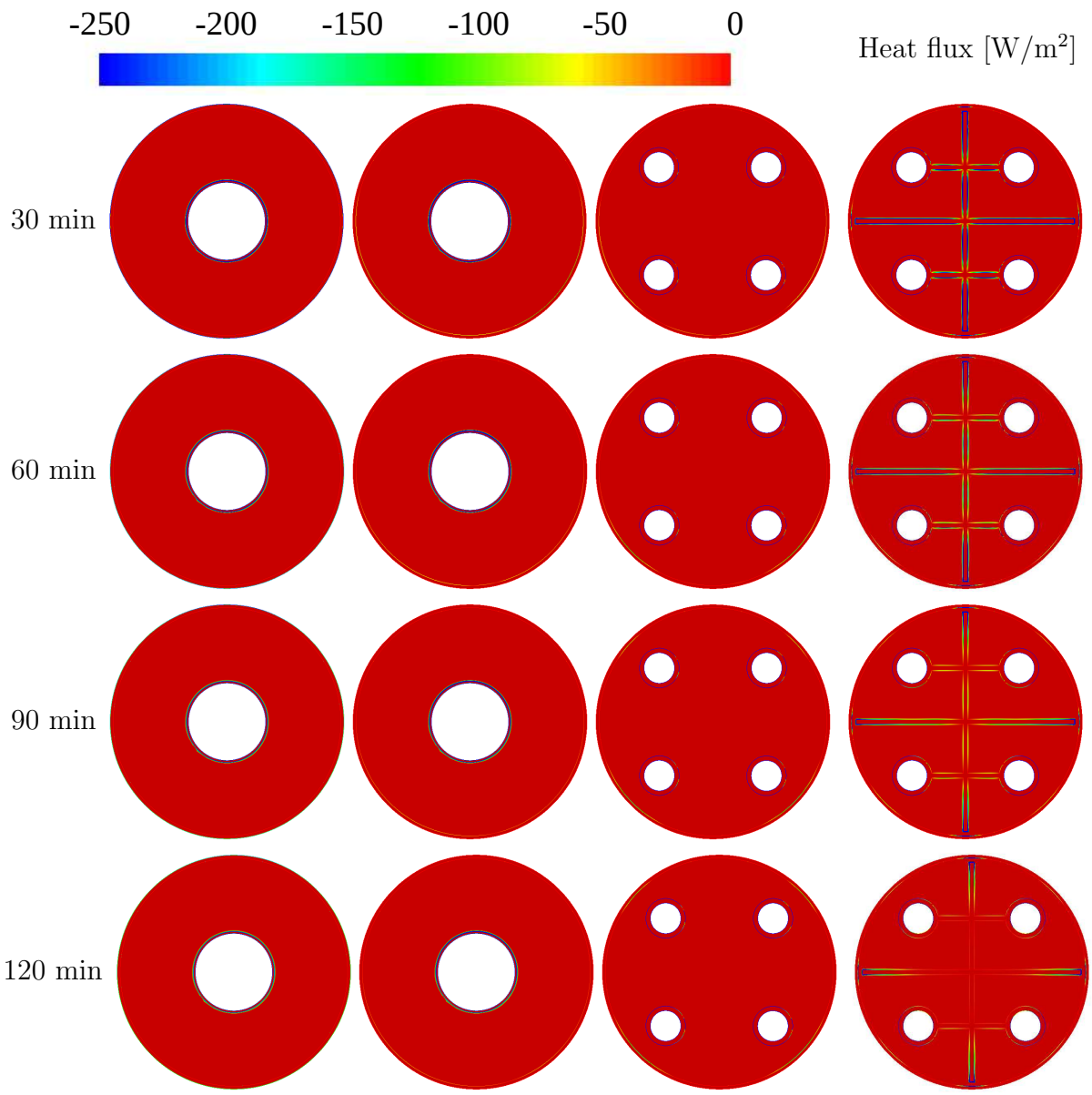

Figure 6.16: Surface heat flux contours at different times for solidification process for various heat exchangers: first from left TTHX, second STHX, third MTHX, and fourth WTHX.

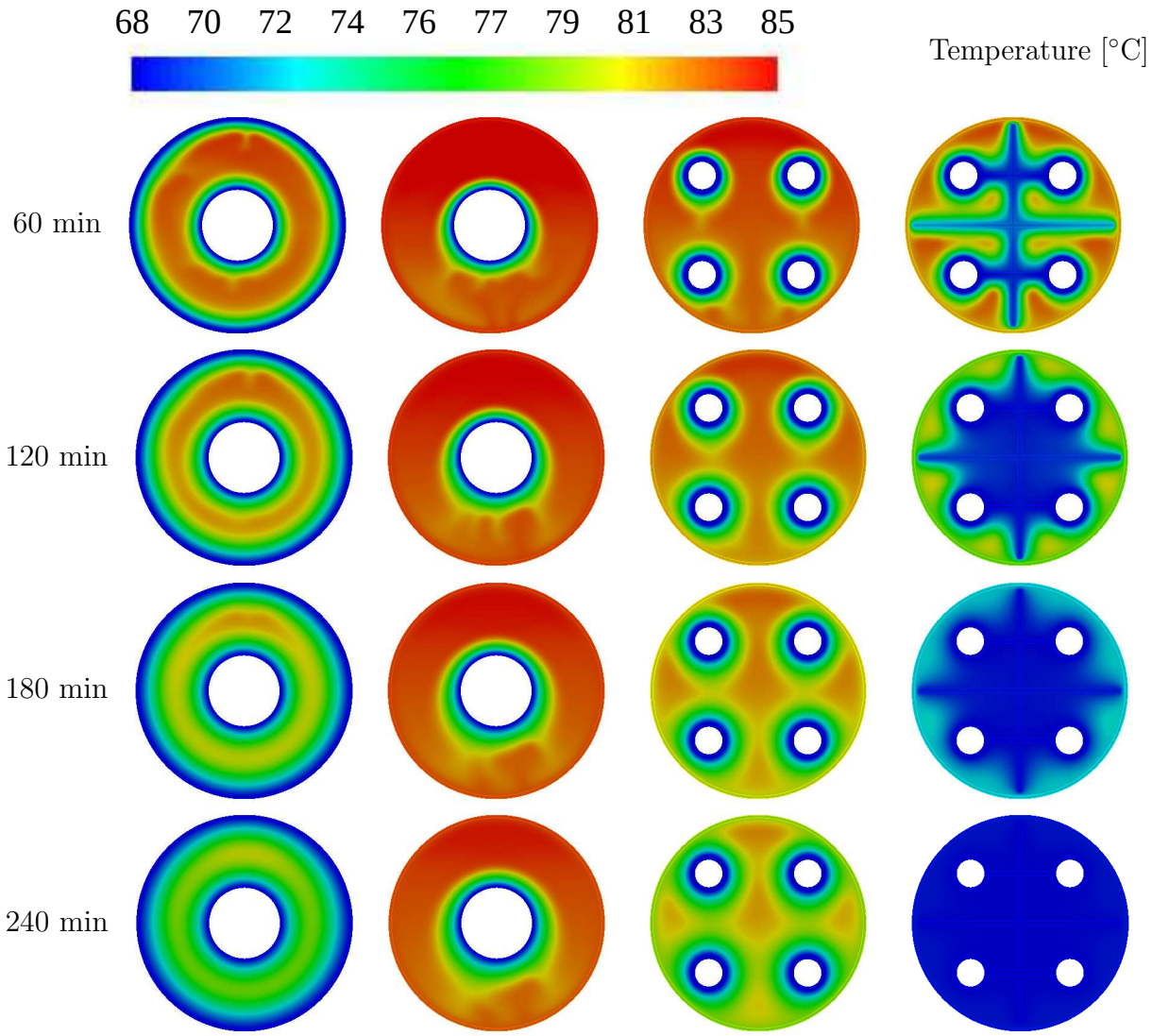

Figure 6.17: Contours of temperature at different times for solidification process for various heat exchanger types: first from left TTHX, second STHX, third MTHX, and fourth WTHX.

6.5 Effect of changing the HTF temperature on the WTHX performance

6.5.1 Melting process

In this test, the influence of changing the HTF temperature on the PCM melting process was studied. Various HTF temperatures were investigated, which were: 87 °C, 90 °C, 93 °C and 96 °C. Fig. 6.18 shows the liquid fraction for different HTF temperatures. It is clear from this figure that the melting process was significantly accelerated by increasing the HTF temperature. If the HTF temperature increased from 87 °C to 96 °C the total melting time reduced by about 50%. The increase of the HTF temperature increases the temperature difference between the PCM and the HTF and consequently the heat transfer rate increased. Hence the melting rate of PCM increased. The response surface of the total melting time for different values of the HTF temperature and the initial PCM temperature for the melting process is illustrated in Fig. 6.19. It is obvious from this figure that changing the HTF temperature has a strong influence on the PCM melting process, while changing the initial PCM temperature has a weak influence on the PCM melting process. The total melting time and melting time reductions for the various HTF temperatures are shown in Table 6.4.

Fig. 6.20 presents the average PCM temperature for different HTF temperatures. The increase of the HTF temperature enhances the heat transfer rate and this accelerates the PCM melting process.

Contours of liquid fraction for the various HTF temperatures at different times are represented in Fig. 6.21. It is obvious from this figure that increasing the HTF temperature accelerates the PCM melting process. Contours of temperature for the various HTF temperatures at different times are shown in Fig. 6.22. It is clear from this figure that the heat transfer rate increased by increasing the temperature of HTF hence, the PCM melting rate increased.

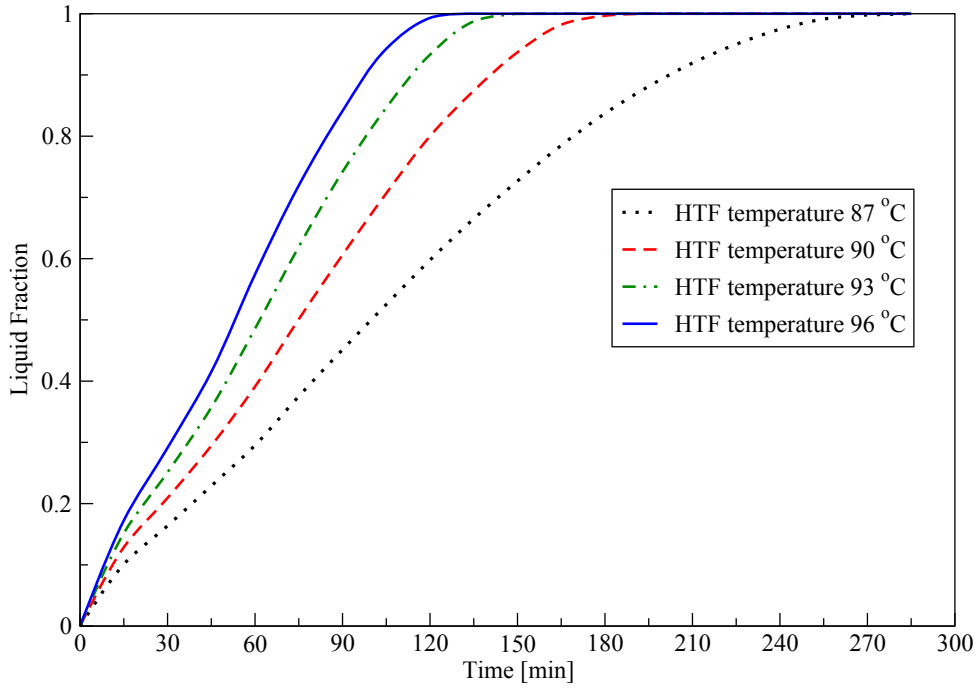

Figure 6.18: Liquid fraction versus time for melting process in the WTHX with different HTF temperatures.

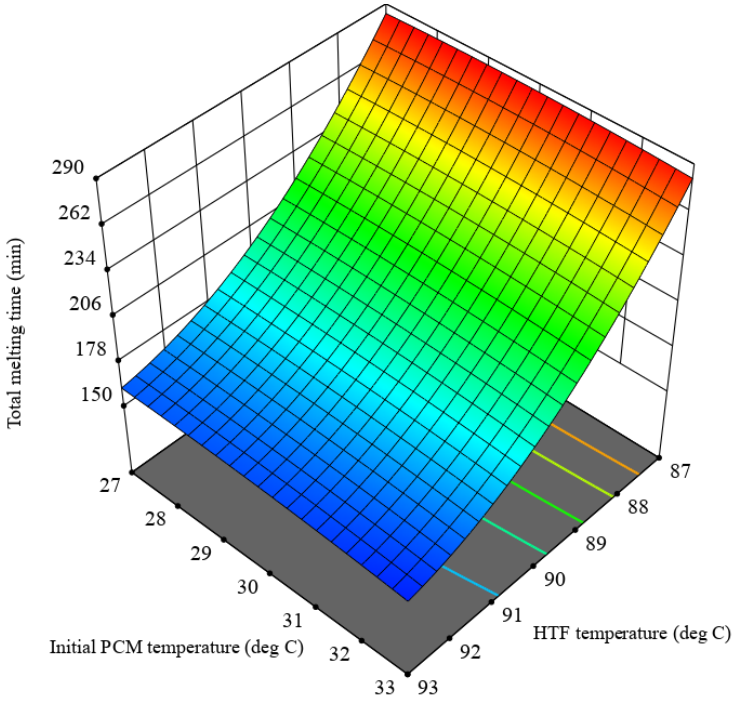

Figure 6.19: The response surface of the total melting time for different values of initial PCM temperature and HTF temperature for the melting process in the WTHX.

Table 6.4: Melting time and melting time reduction for various HTF temperatures

HTF temperature (°C)	**Melting time (min)**	**Reduction (%)**
87 (base case)	272	—
90	183	32
93	149	45
96	136	50

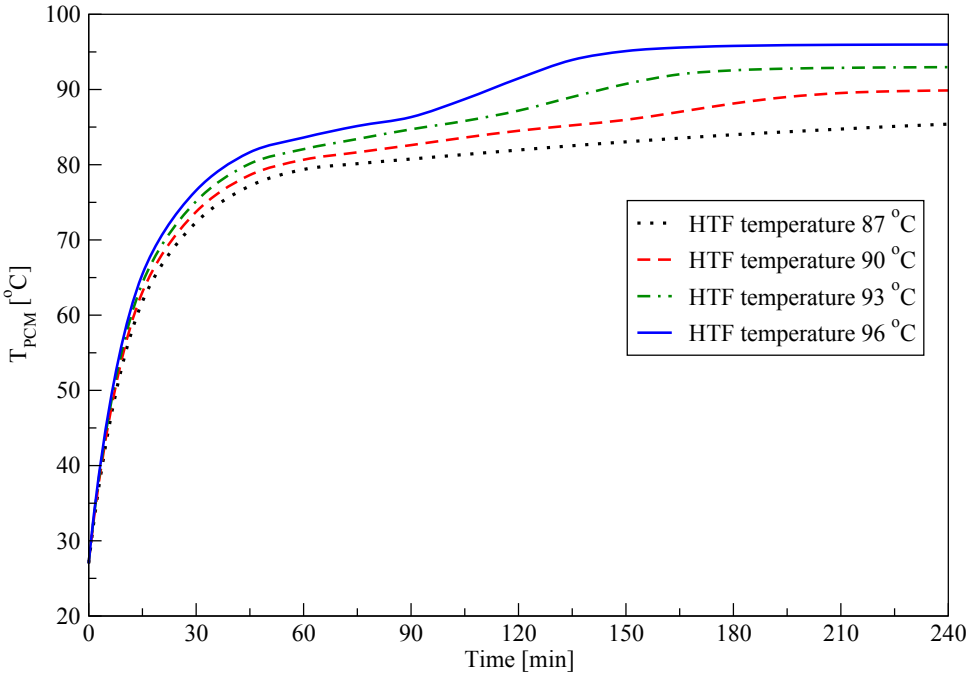

Figure 6.20: Average PCM temperature versus time for the melting process in the WTHX with different HTF temperatures.

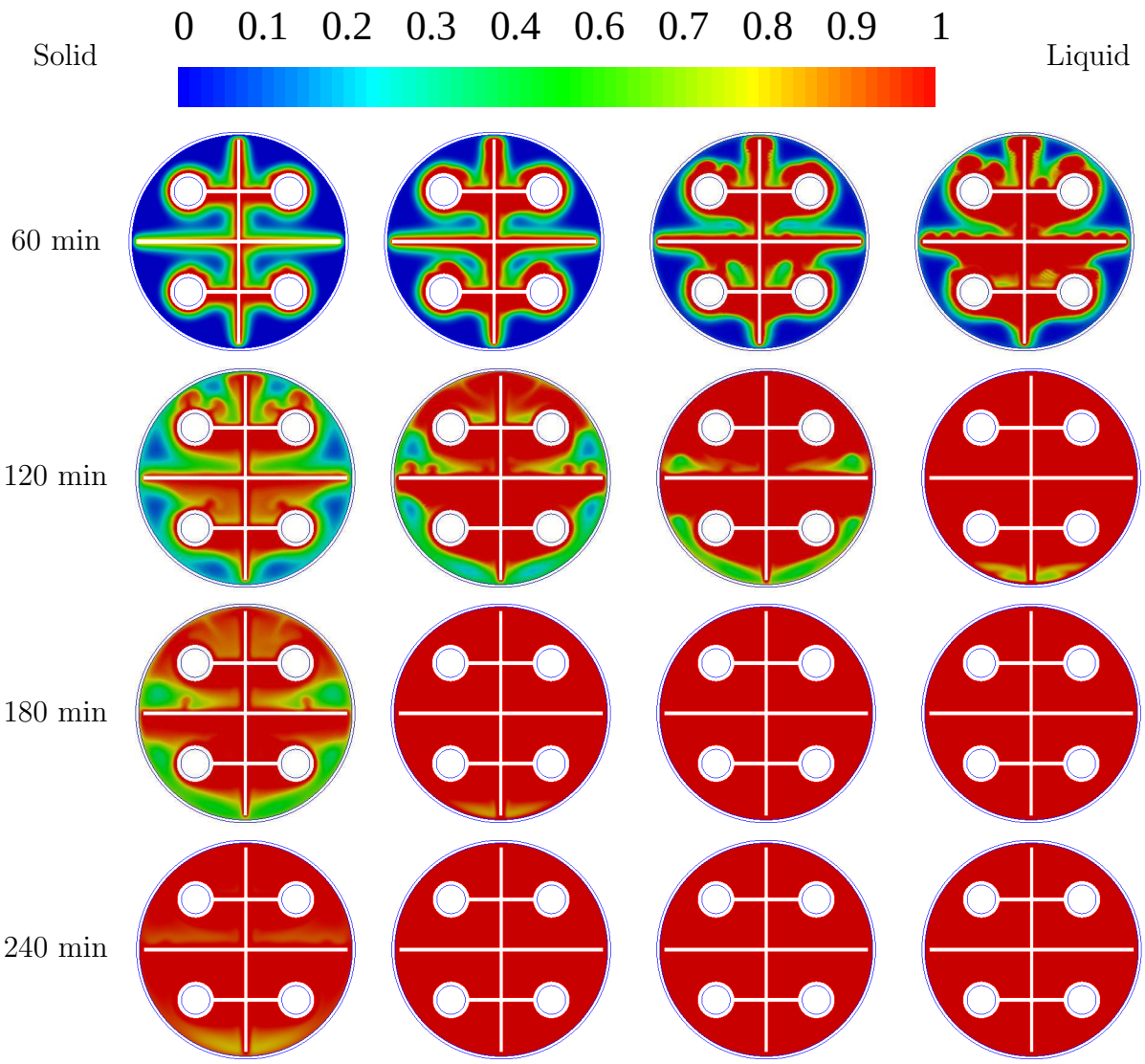

Figure 6.21: Liquid fraction contours at different times for the melting process for various values of the HTF temperature: first from left HTF temperature 87 °C, second HTF temperature 90 °C, third HTF temperature 93 °C and fourth HTF temperature 96 °C.

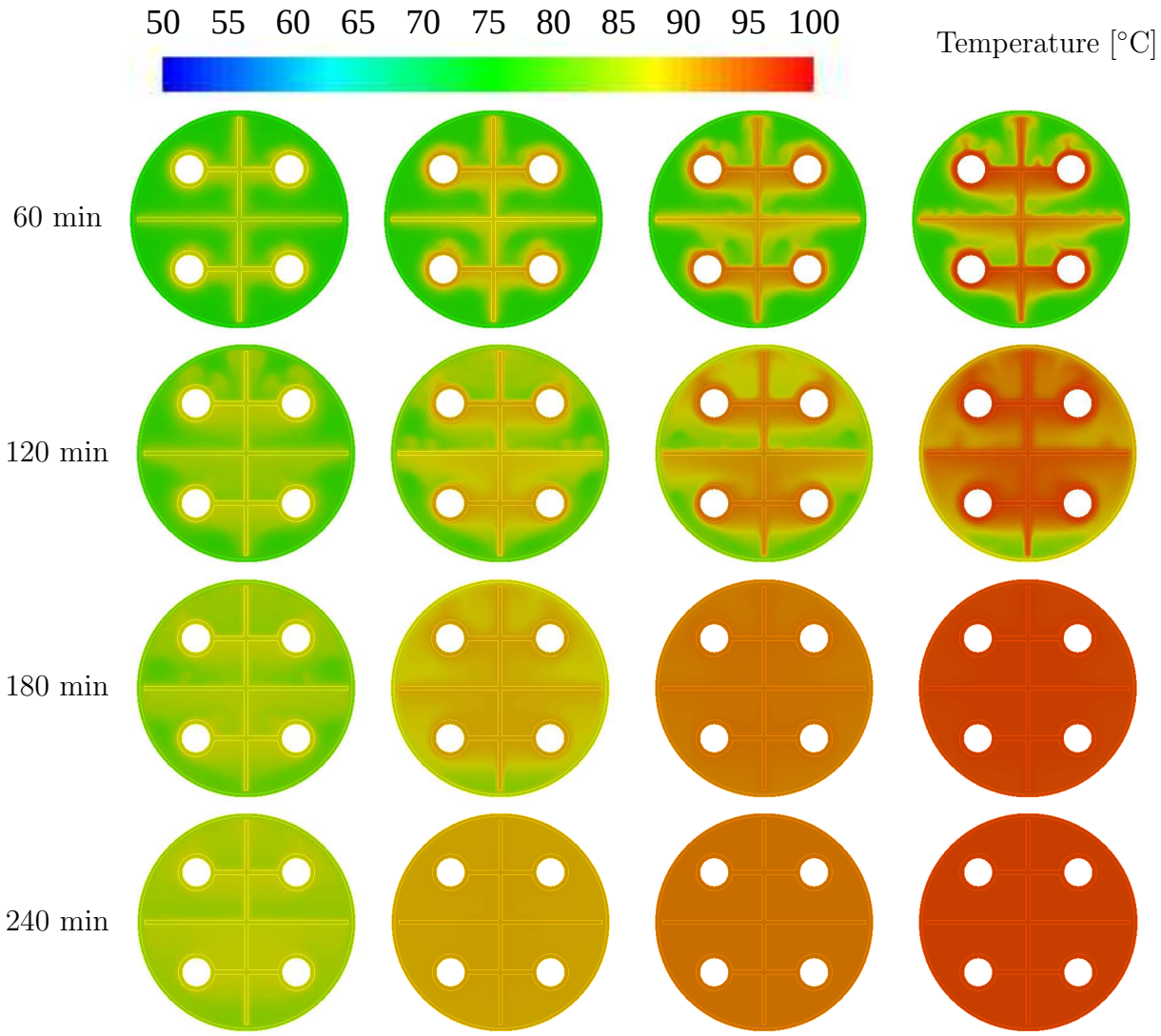

Figure 6.22: Temperature contours at different times for the melting process for various values of the HTF temperature: first from left HTF temperature 87 °C, second HTF temperature 90 °C, third HTF temperature 93 °C and fourth HTF temperature 96 °C.

6.5.2 Solidification process

In this test, the influence of changing the HTF temperature on the PCM solidification process was studied. Different values of the HTF temperatures were investigated, which were: 62 °C, 65 °C, 68 °C and 71 °C. Fig. 6.23 shows the liquid fraction versus time for

various values of the HTF temperatures. It can be seen from this figure that decreasing the temperature of the HTF increases the solidification rate and reduces the solidification time. If the HTF temperature decreased from 71 °C to 62 °C the total PCM solidification time reduced by about 40%. The total solidification time and solidification time reductions for the various HTF temperatures are shown in Table 6.5.

Fig. 6.24 shows the average PCM temperature for different values of the HTF temperatures. The decrease of the HTF temperature decreases the PCM temperature and this reduces the total solidification time.

Contours of liquid fraction for the various values of the HTF temperatures at different times are presented in Fig. 6.25. It is obvious from this figure that the decrease in the temperature of the HTF accelerates the PCM solidification. Contours of temperature for the various values of the HTF temperatures are shown in Fig. 6.26. It can be seen from this figure that the decrease in temperature of the HTF reduces the PCM temperature due to the increased heat transfer rate.

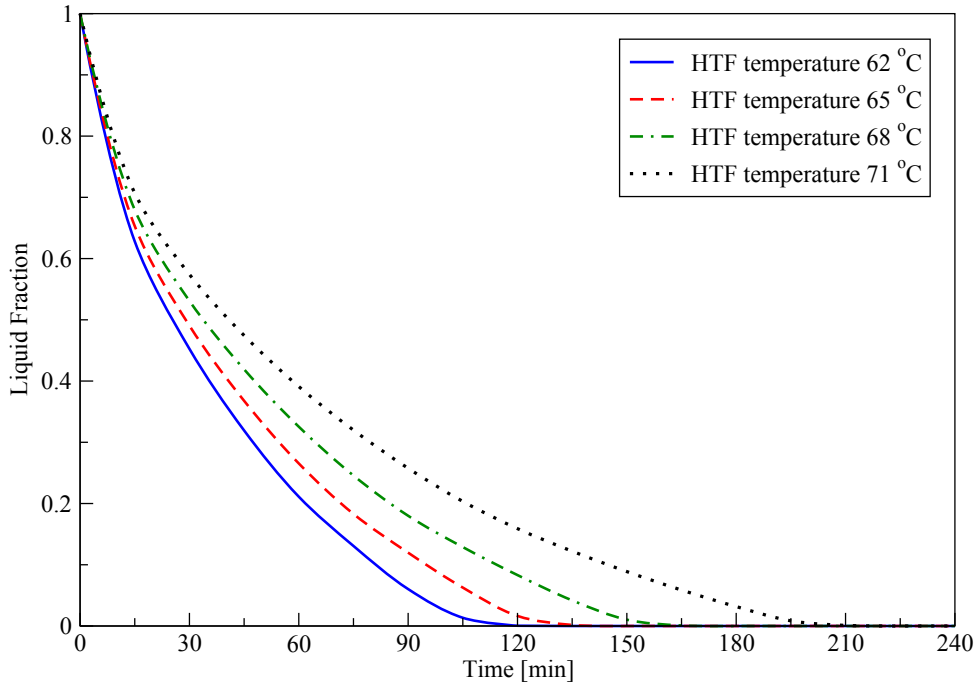

Figure 6.23: Liquid fraction versus time for solidification process in the WTHX with different values of the HTF temperatures.

Table 6.5: Solidification time and solidification time reduction for various HTF temperatures

HTF temperature (°C)	**Solidification time (min)**	**Reduction (%)**
71 (base case)	200	—
68	166	17
65	137	31
62	120	40

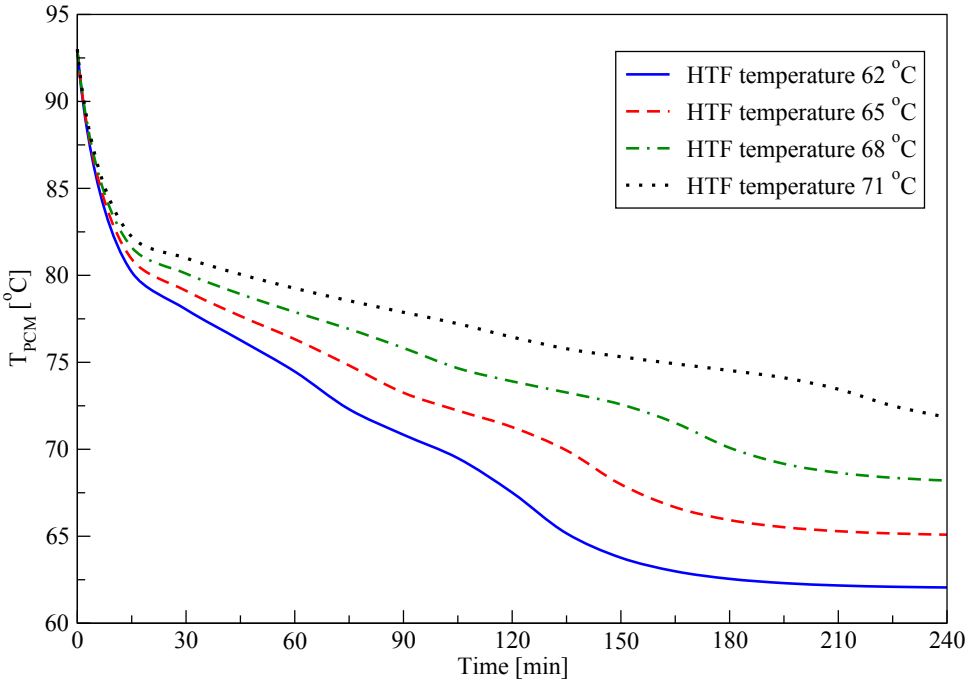

Figure 6.24: Average PCM temperature versus time for solidification process in the WTHX with different values of the HTF temperatures.

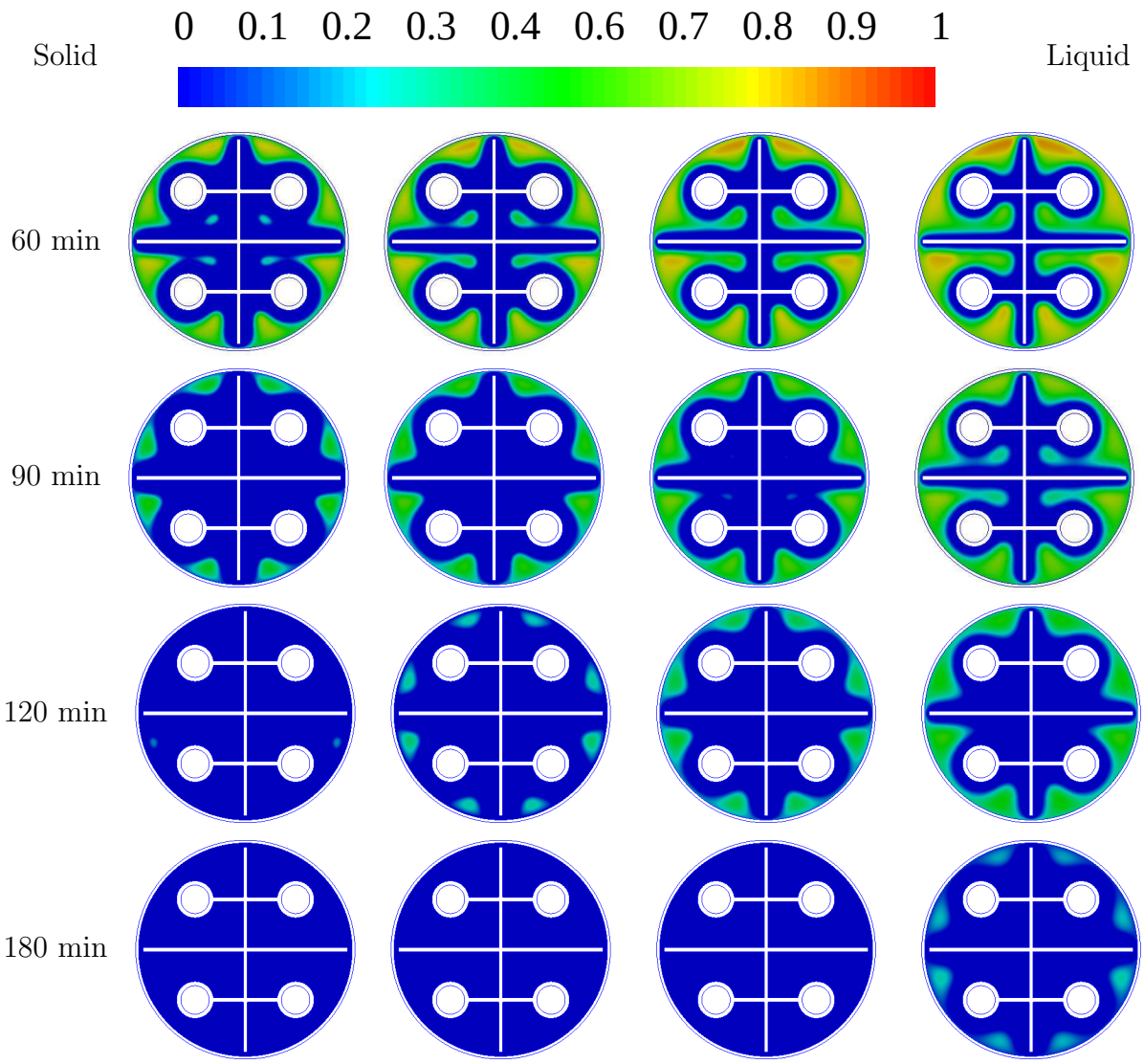

Figure 6.25: Liquid fraction contours at different times for solidification process for different values of the HTF temperatures: first from left HTF temperature 62 °C, second HTF temperature 65 °C, third HTF temperature 68 °C and fourth HTF temperature 71 °C.

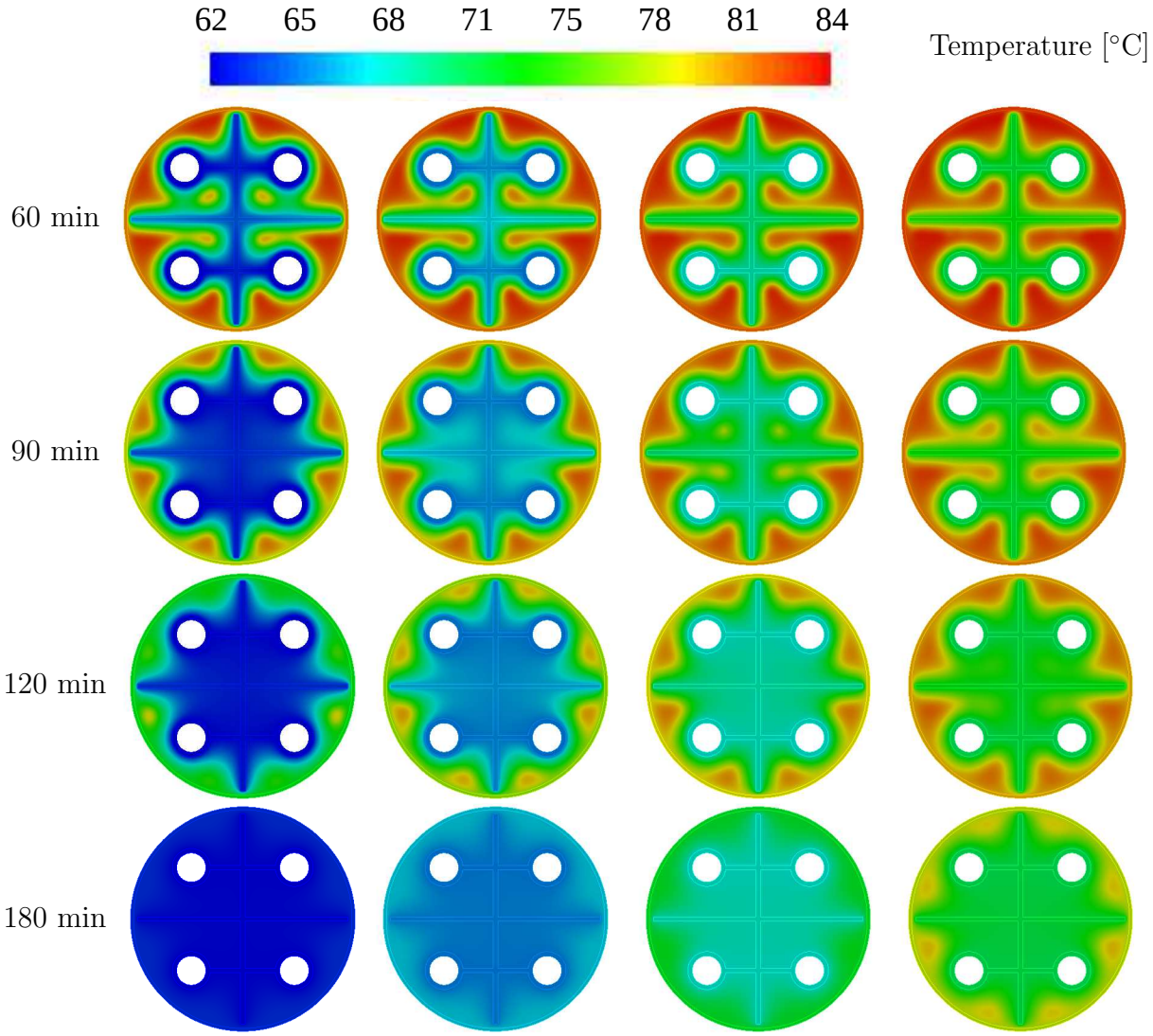

Figure 6.26: Temperature contours at different times for solidification process for various values of the HTF temperatures: first from left HTF temperature 62 °C, second HTF temperature 65 °C, third HTF temperature 68 °C and fourth HTF temperature 71 °C.

6.6 Effect of the dimensions of the metal plates on the WTHX thermal performance

6.6.1 Effect of vertical plate length

In this test, the influence of changing the vertical plate length (L) on the PCM thermal performance was studied. Four lengths were tested:- 80 mm, 100 mm, 120 mm, and 140 mm.

Melting process

Fig. 6.27 shows the liquid fraction for different vertical plate lengths. It is obvious from this figure that the PCM melts faster by employing a longer vertical plate. When using a 140 mm vertical plate length the PCM had completely melted after 180 minutes, while when using an 80 mm plate length the PCM melting was complete after 270 minutes. If the vertical plate length increased from 80 mm to 140 mm the total PCM melting time decreased by 33%. The total melting time and melting time reductions for different vertical plate lengths are shown in Table 6.6.

The average PCM temperature versus time for various plate lengths is illustrated in Fig. 6.28. As can be seen from this figure, increasing the vertical plate length increases the PCM temperature and enhances the heat transfer rate. Liquid fraction contours for various vertical plate lengths at different times are shown in Fig. 6.29. It can be observed from this figure that the increase of the vertical plate length accelerates the melting process due to the increase of the heat exchange area. By increasing the vertical plate length the thermal conduction enhances due to the increase of heat transfer area and consequently, the overall heat transfer improves. Contours of temperature for various values of the vertical plate lengths at different times are presented in Fig. 6.30. It is obvious from this figure that as the plate length increased the PCM temperature increased, due to the increased

conduction heat transfer rate. It is clear from Fig. 6.30 that the temperature distribution is significantly improved by increasing plate length.

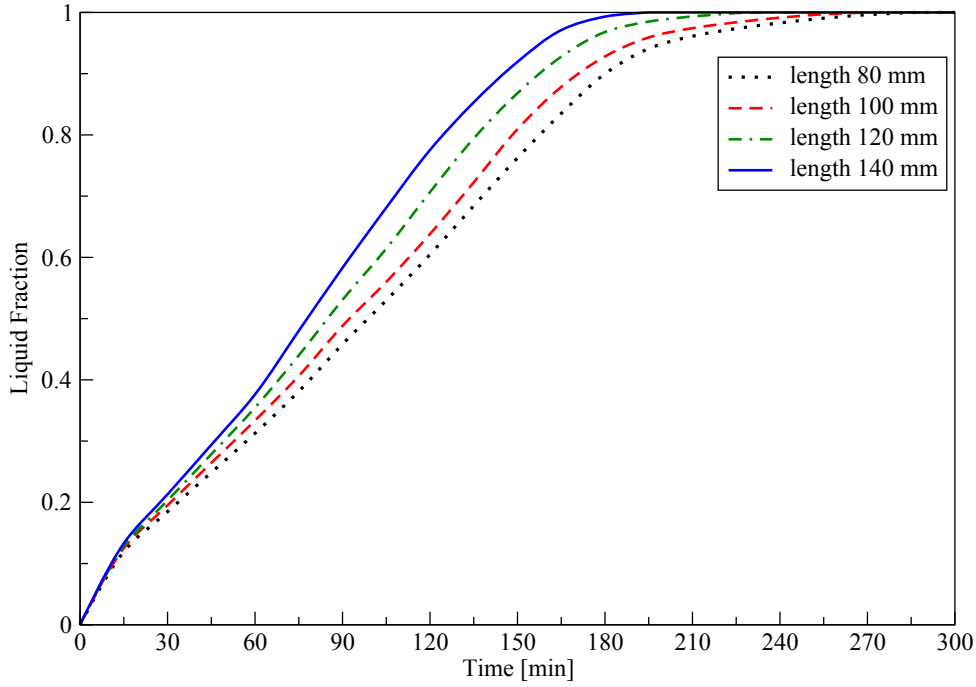

Figure 6.27: Liquid fraction versus time for the melting process for the WTHX with different vertical plate lengths.

Table 6.6: Melting time and melting time reduction for different vertical plate lengths

Vertical plate length (mm)	**Melting time (min)**	**Reduction (%)**
80 (base case)	270	—
100	256	5
120	230	14
140	180	33

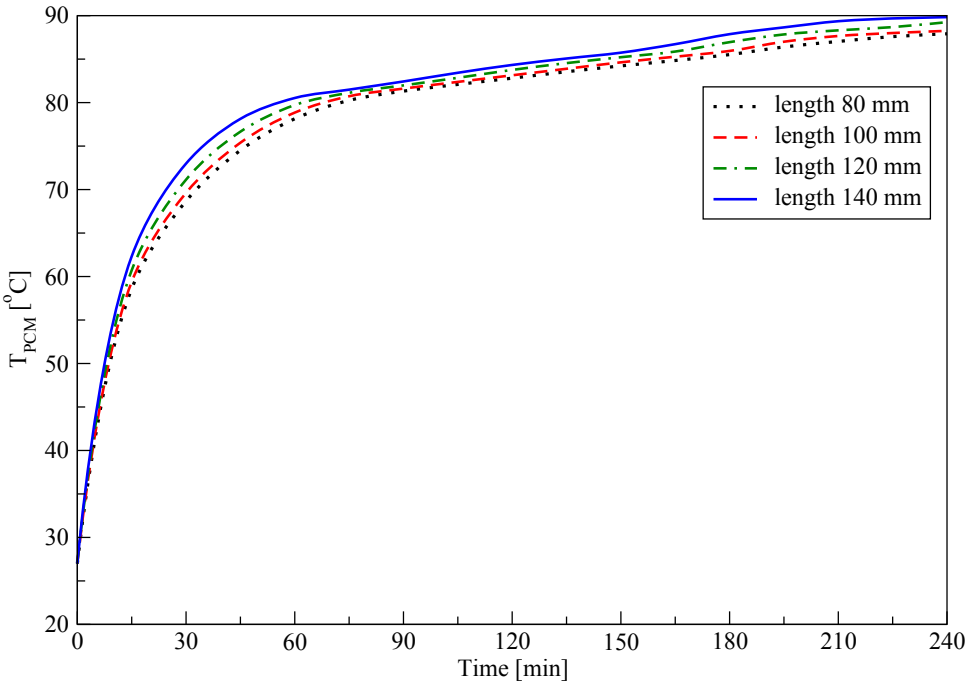

Figure 6.28: Average PCM temperature versus time for the melting process for the WTHX with different vertical plate lengths.

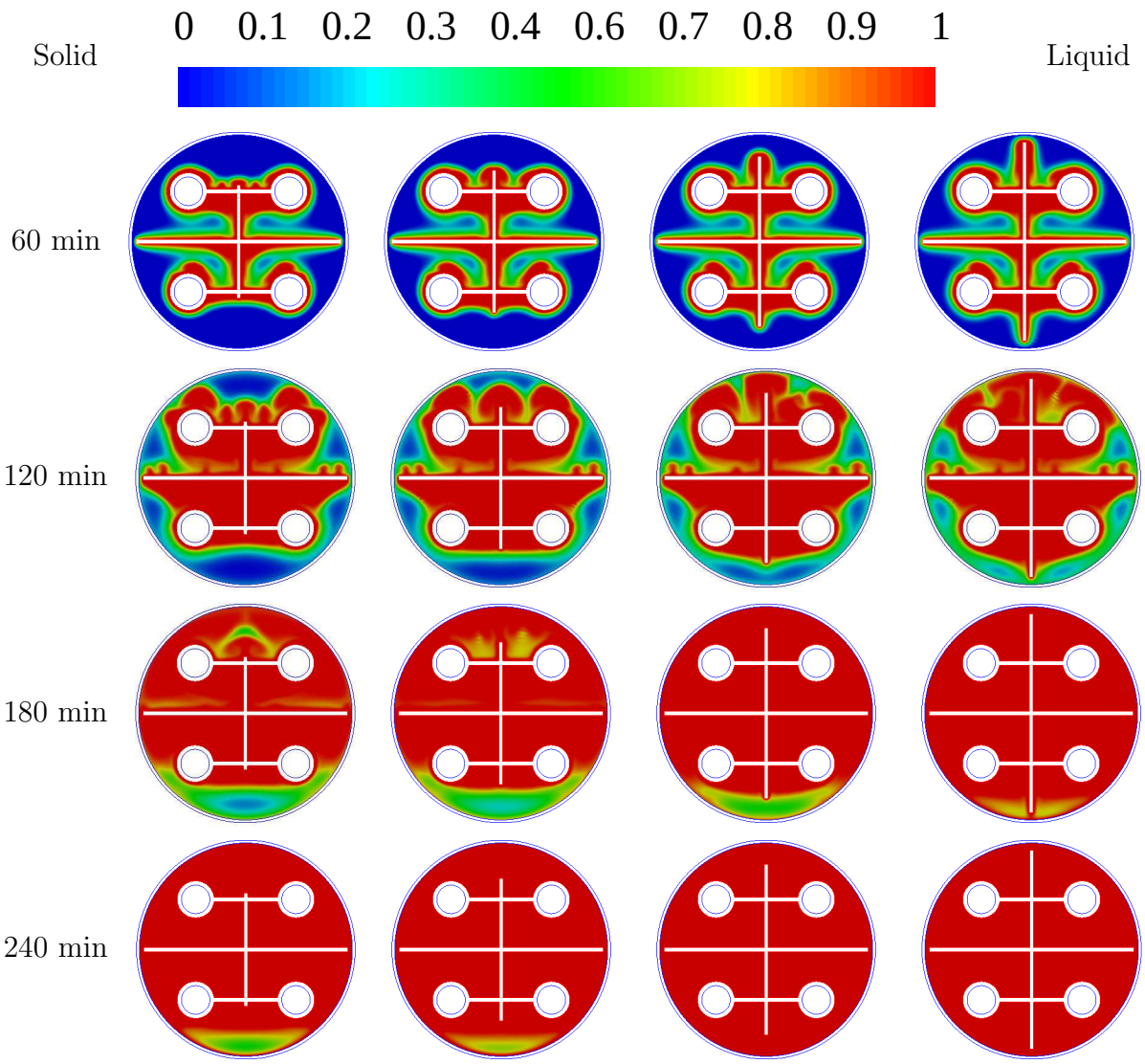

Figure 6.29: Liquid fraction contours at different times for the melting process for various vertical plate lengths: first from left length 80 mm, second length 100 mm, third length 120 mm, and fourth length 140 mm.

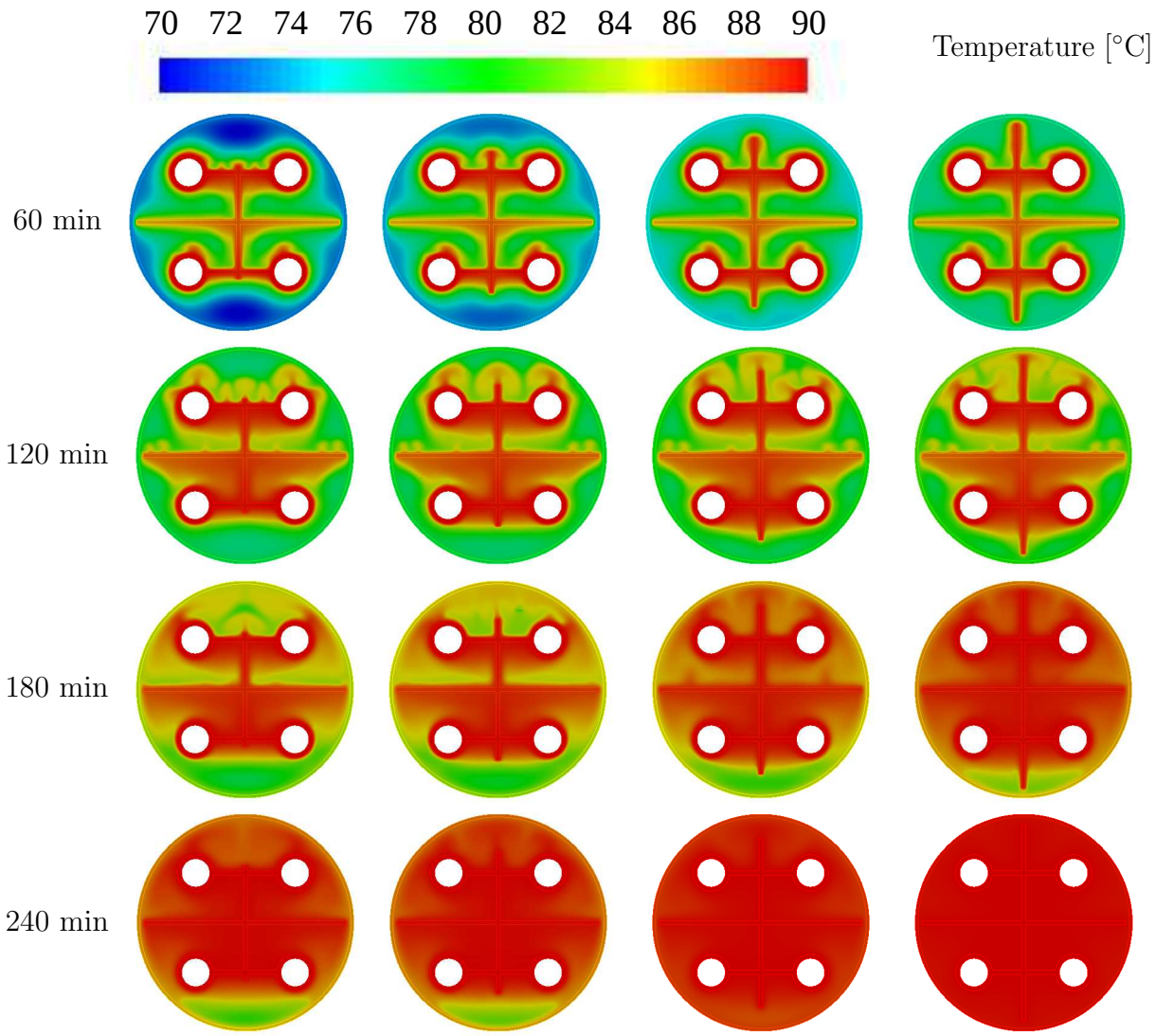

Figure 6.30: Contours of temperature at different times for melting process for the different vertical plate lengths: first from left length 80 mm, second length 100 mm, third length 120 mm, and fourth length 140 mm.

Solidification process

Fig. 6.31 shows the liquid fraction for various vertical plate lengths. It is obvious from this figure that the PCM solidification rate increases when employing a longer vertical plate. When utilizing a 140 mm vertical plate length the PCM completely solidified after 180 minutes. When using an 80 mm plate length the PCM completely solidified after

270 minutes. If the vertical plate length increased from 80 mm to 140 mm the total PCM solidification time reduced by 33%. The total solidification time and solidification time reductions for different vertical plate lengths are shown in Table 6.7.

The average PCM temperature versus time for various plate lengths is illustrated in Fig. 6.32. It can be seen from this figure that increasing the vertical plate length decreases the PCM temperature due to the increased heat transfer rate. Liquid fraction contours for various vertical plate lengths at different times are presented in Fig. 6.33. It is clear from this figure that increasing the vertical plate length accelerated the solidification process owing to the increased heat transfer area. Moreover, the heat penetration depth increase by increasing the length of the vertical plate and this enhances the heat transfer process and accelerates the solidification process.

Contours of temperature for different values of the vertical plate lengths at different times are shown in Fig. 6.34. It is obvious from this figure that the heat transfer rate is enhanced by utilizing longer vertical plates, this is due to the increase in the heat exchange area.

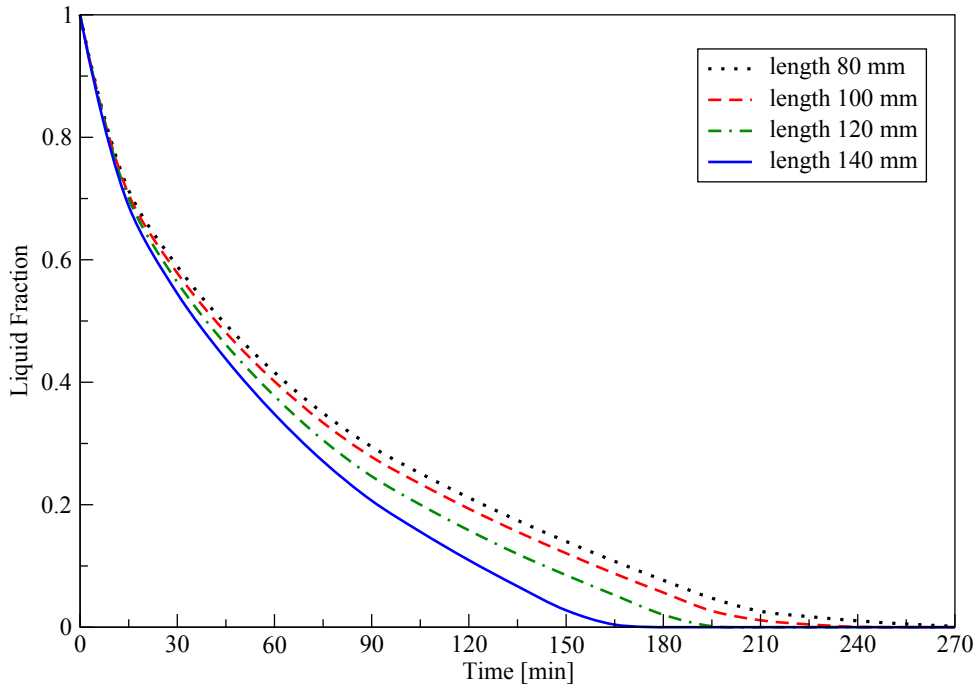

Figure 6.31: Liquid fraction versus time for the solidification process for the WTHX with different vertical plate lengths.

Table 6.7: Solidification time and solidification time reduction for different vertical plate lengths

Vertical plate length (mm)	**Solidification time (min)**	**Reduction (%)**
80 (base case)	270	—
100	241	10
120	196	27
140	180	33

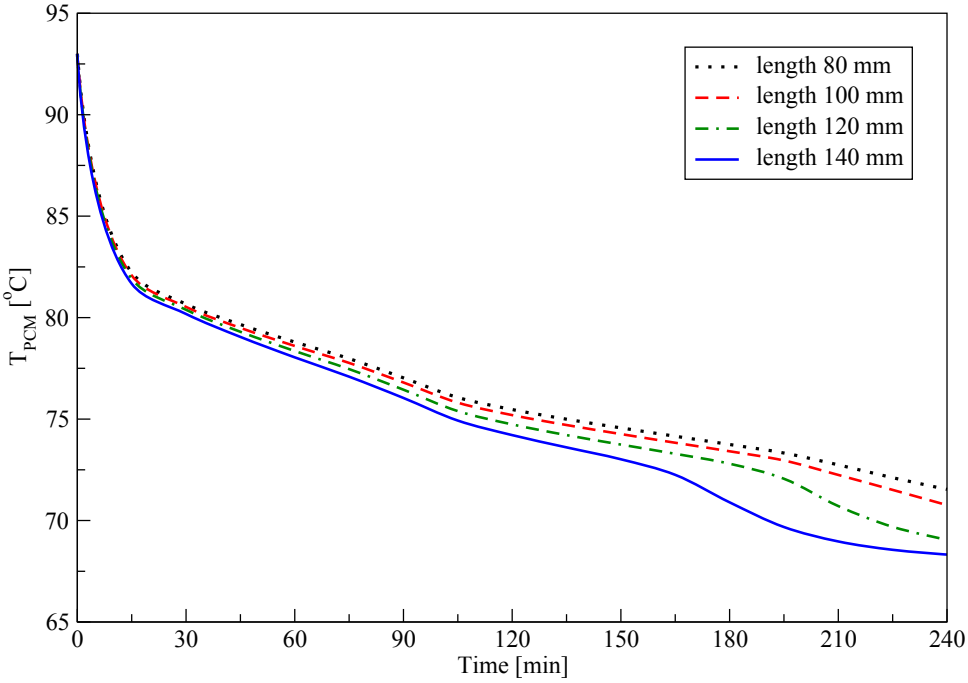

Figure 6.32: Average PCM temperature versus time for the solidification process for the WTHX with different vertical plate lengths.

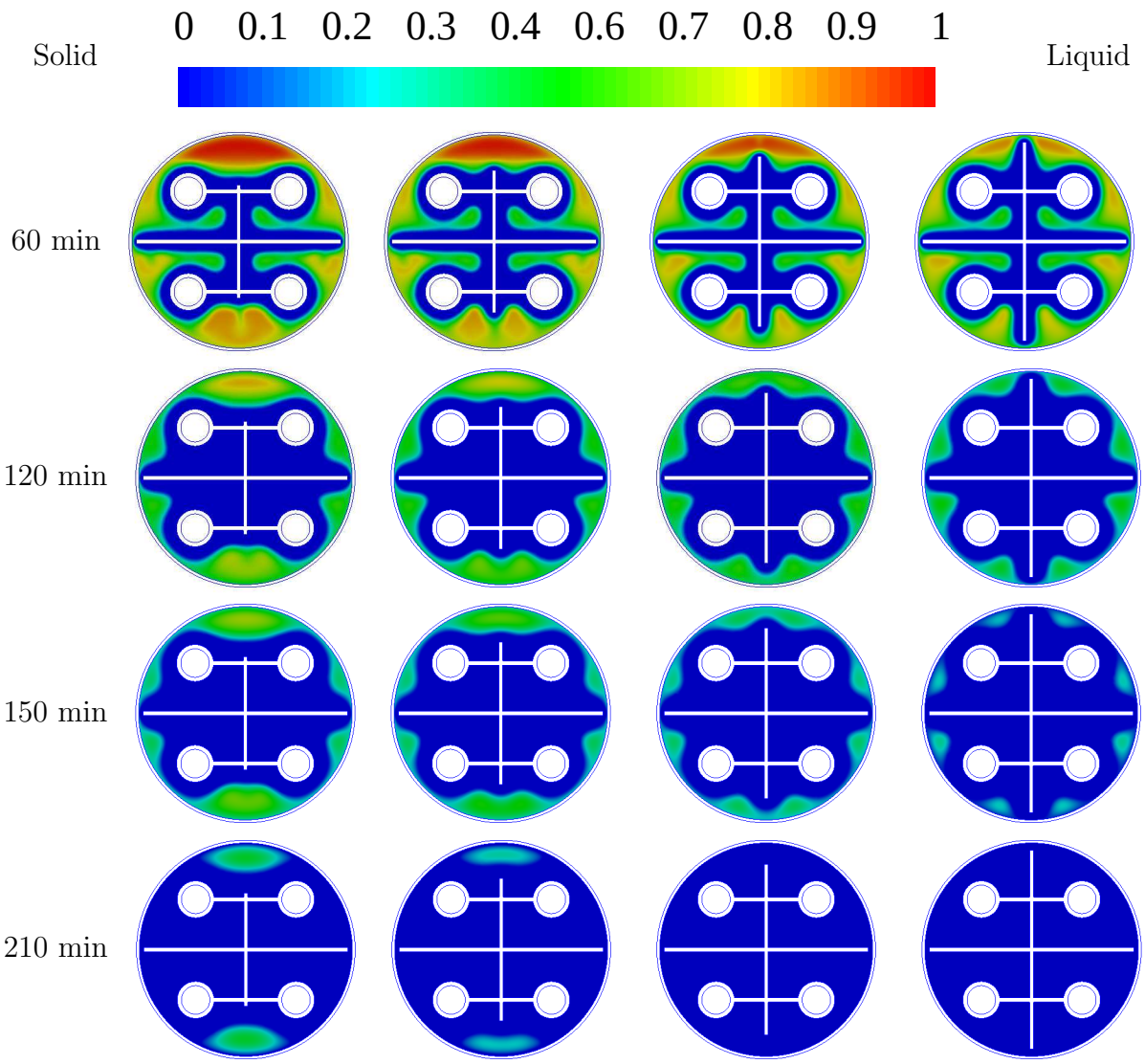

Figure 6.33: Liquid fraction contours at different times for the solidification process for various vertical plate lengths: first from left length 80 mm, second length 100 mm, third length 120 mm, and fourth length 140 mm.

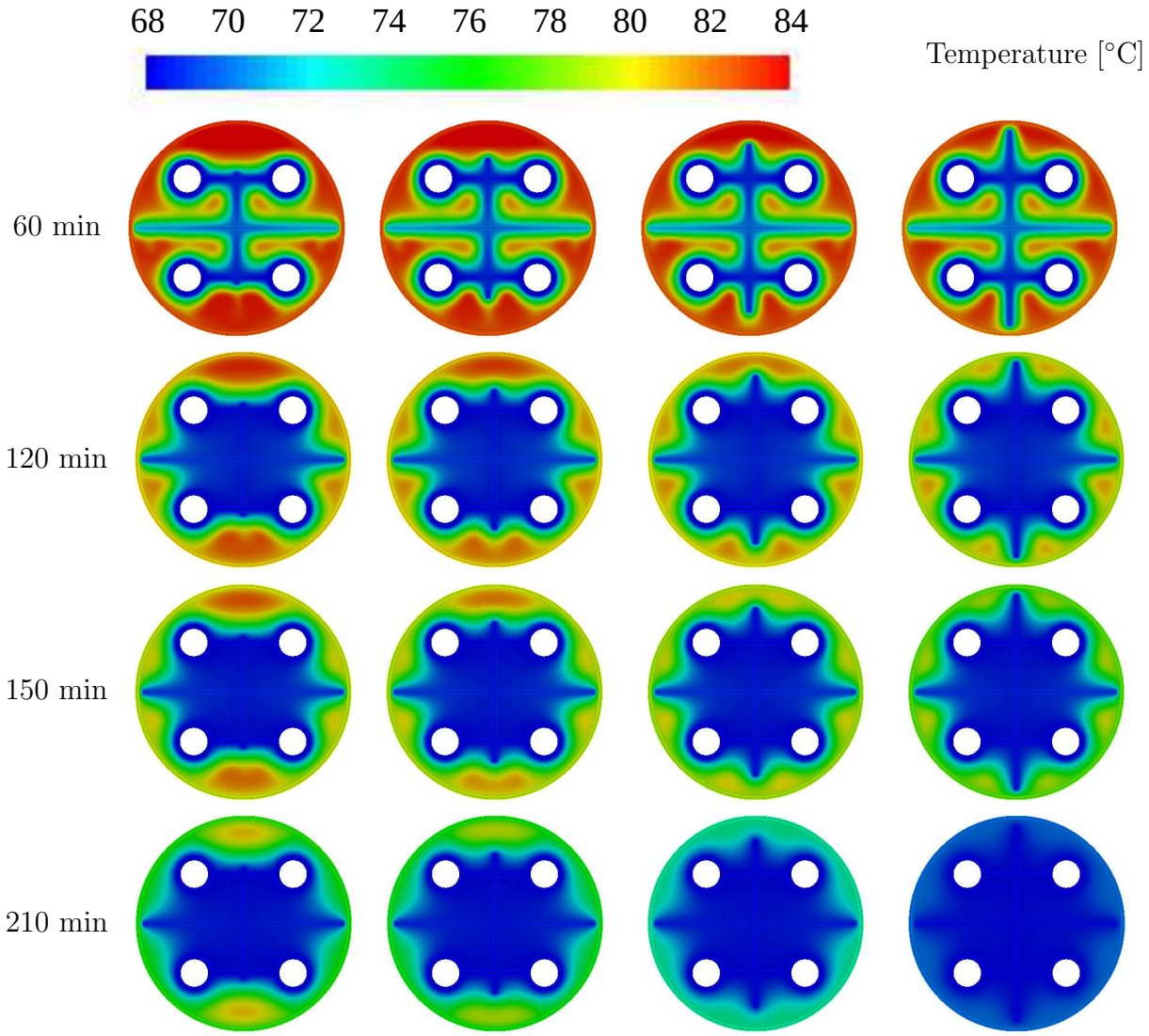

Figure 6.34: Contours of temperature at different times for the solidification process for different vertical plate lengths: first from left length 80 mm, second length 100 mm, third length 120 mm, and fourth length 140 mm.

6.6.2 The effect of horizontal plate length

In this test, the influence of changing the horizontal plate length (W1) on the PCM thermal performance was studied. Four lengths were tested:- 80 mm, 100 mm, 120 mm, and 140 mm.

Melting process

Fig. 6.35 shows the liquid fraction for different horizontal plate lengths. It is clear from this figure that the PCM melts faster by utilizing longer horizontal plates owing to the increase of the heat exchange area. When using a 140 mm horizontal plate length the PCM completely melted after 180 minutes. However, when utilizing an 80 mm horizontal plate length the PCM completely melted after 255 minutes. If the horizontal plate length increased from 80 mm to 140 mm the total PCM melting time reduced by about 29%. The total melting time and melting time reductions for different horizontal plate lengths are shown in Table 6.8.

The average PCM temperature for different values of the horizontal plate length is shown in Fig. 6.36. It can be seen from this figure that increasing the horizontal plate length increases the PCM temperature and accelerates the PCM melting process. Contours of liquid fraction for the various horizontal plate lengths at different times are shown in Fig. 6.37. It is clear from this figure that increasing the horizontal plate length accelerates the melting process due to the increase in the heat exchange area. Contours of temperature for different values of the horizontal plate lengths at different times are shown in Fig. 6.38. As can be seen from this figure, as the plate length increased the PCM temperature increased, so the PCM melting process was completed in a shorter time.

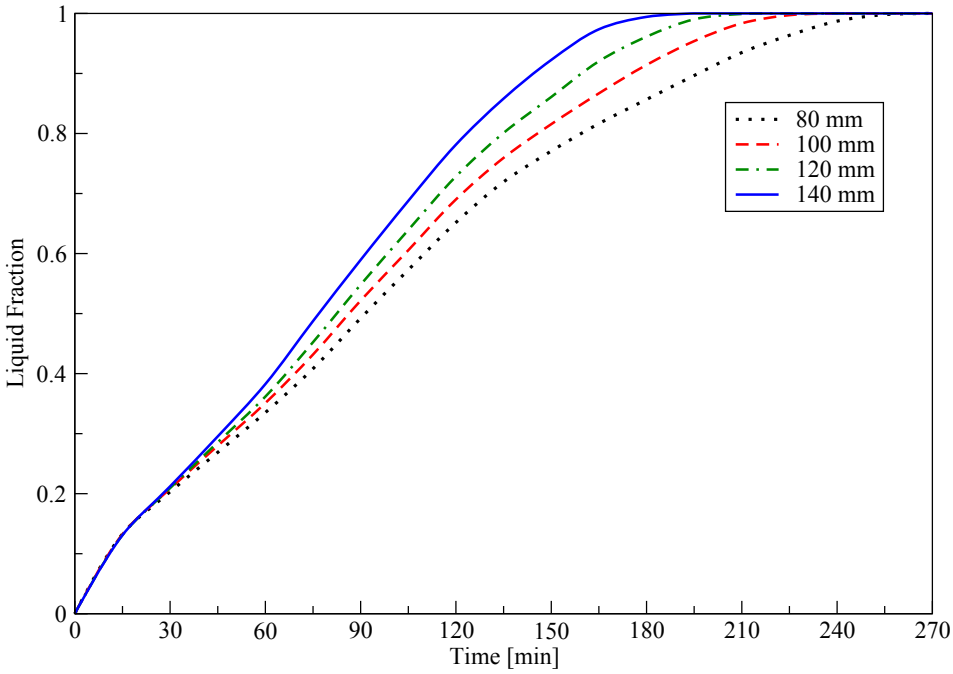

Figure 6.35: Liquid fraction versus time for the melting process for the WTHX with different horizontal plate lengths.

Table 6.8: Melting time and melting time reduction for different horizontal plate lengths

Horizontal plate length (mm)	**Melting time (min)**	**Reduction (%)**
80 (base case)	255	—
100	228	10
120	212	16
140	180	29

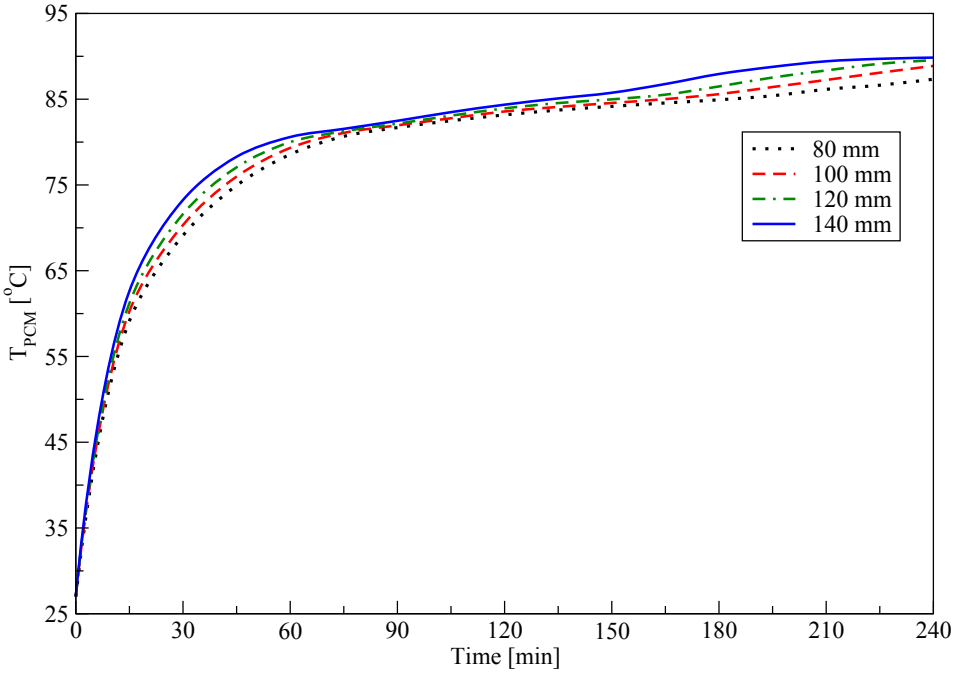

Figure 6.36: Average PCM temperature versus time for the melting process for the WTHX with different horizontal plate lengths.

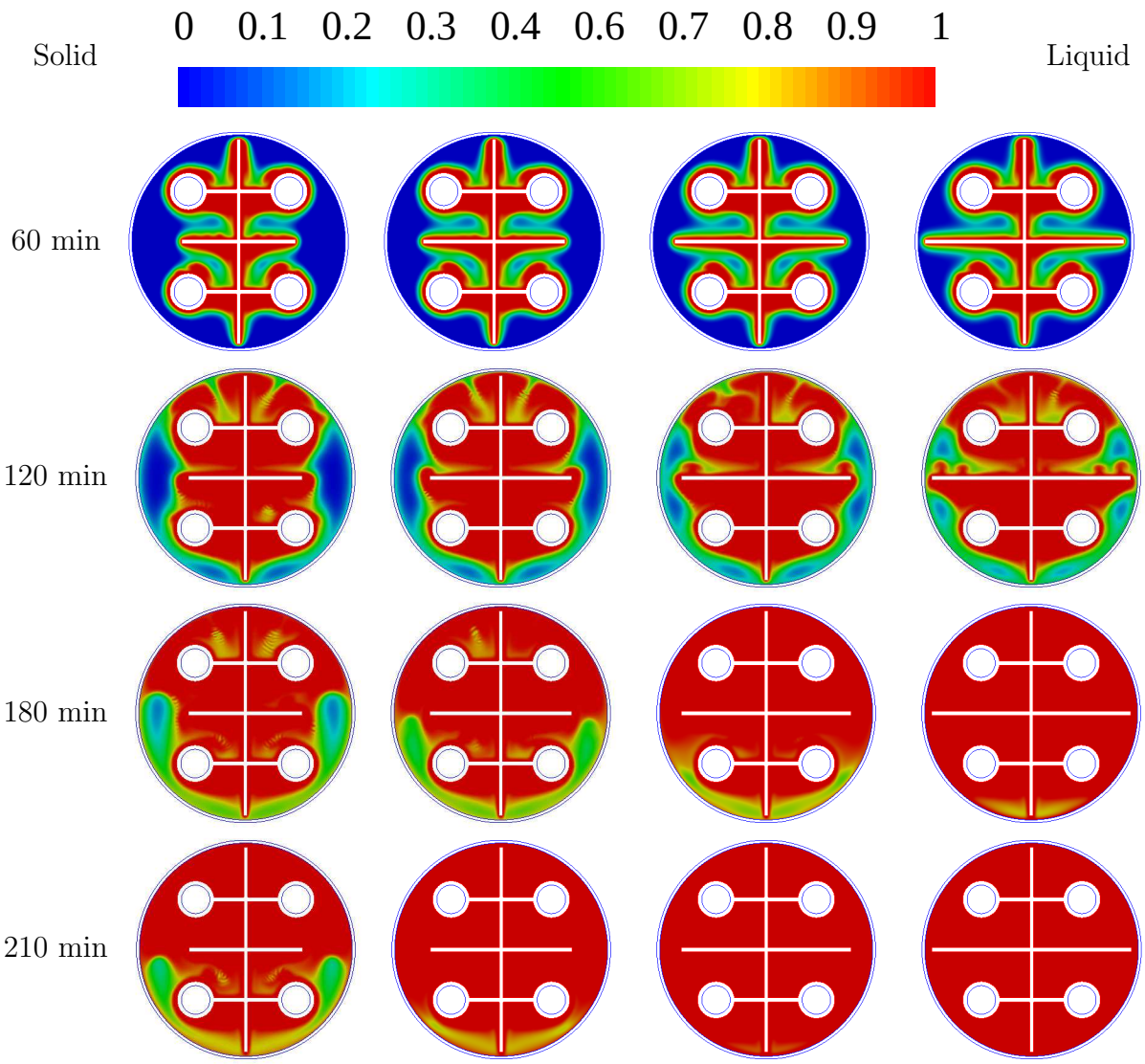

Figure 6.37: Liquid fraction contours at different times for the melting process for various horizontal plate lengths: first from left length 80 mm, second length 100 mm, third length 120 mm, and fourth length 140 mm.

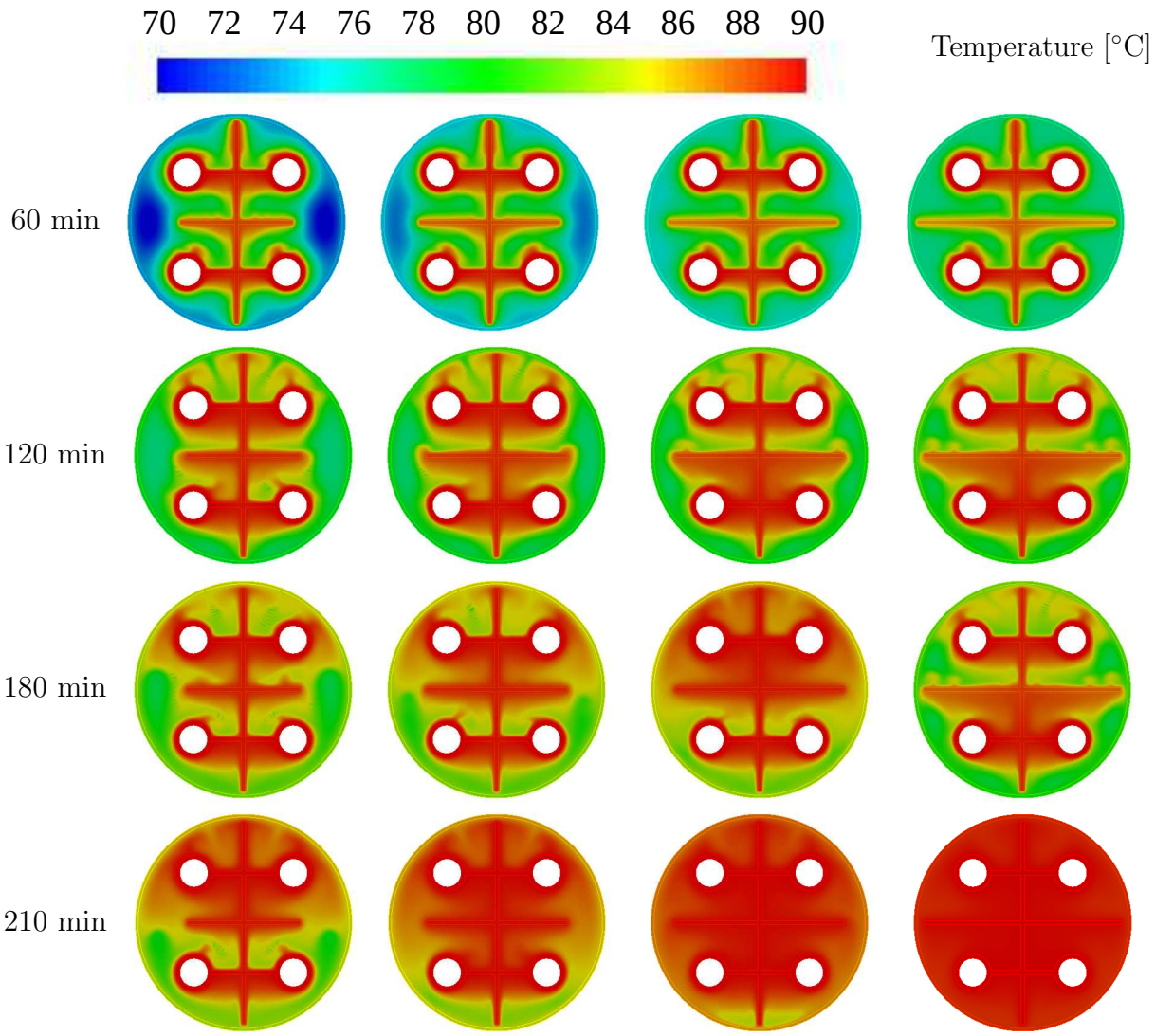

Figure 6.38: Contours of temperature at different times for the melting process for different horizontal plate lengths: first from left length 80 mm, second length 100 mm, third length 120 mm, and fourth length 140 mm.

Solidification process

Fig. 6.39 shows the liquid fraction for various horizontal plates lengths. It is clear from this figure that the PCM completely solidified at an earlier time when using a horizontal plate length of 140 mm, compared to other lengths. When using a 140 mm horizontal plate length the PCM completely solidified after 165 minutes. However, when using an

80 mm plate length the PCM completely solidified after 255 minutes. If the horizontal plate length increased from 80 mm to 140 mm the total PCM solidification time reduced by about 35%. The total solidification time and solidification time reductions for different horizontal plate lengths are shown in Table 6.9.

The average PCM temperature versus time for various horizontal plate lengths is shown in Fig. 6.40. It is clear from this figure that increasing the horizontal plate length decreases the PCM temperature and accelerates the solidification process. Liquid fraction contours for various horizontal plate lengths at different times are presented in Fig. 6.41. It is obvious from this figure that the increase of horizontal plate length accelerates the solidification process owing to the increase of the heat exchange area. The solidification process is mainly influenced by conduction, hence using a longer horizontal plate increases thermal penetration which accelerates the solidification process. Contours of temperature for different horizontal plate lengths at different times are shown in Fig. 6.42. It can be seen from this figure that as the plate length increased the PCM temperature decreased, so the solidification process was completed in a shorter time.

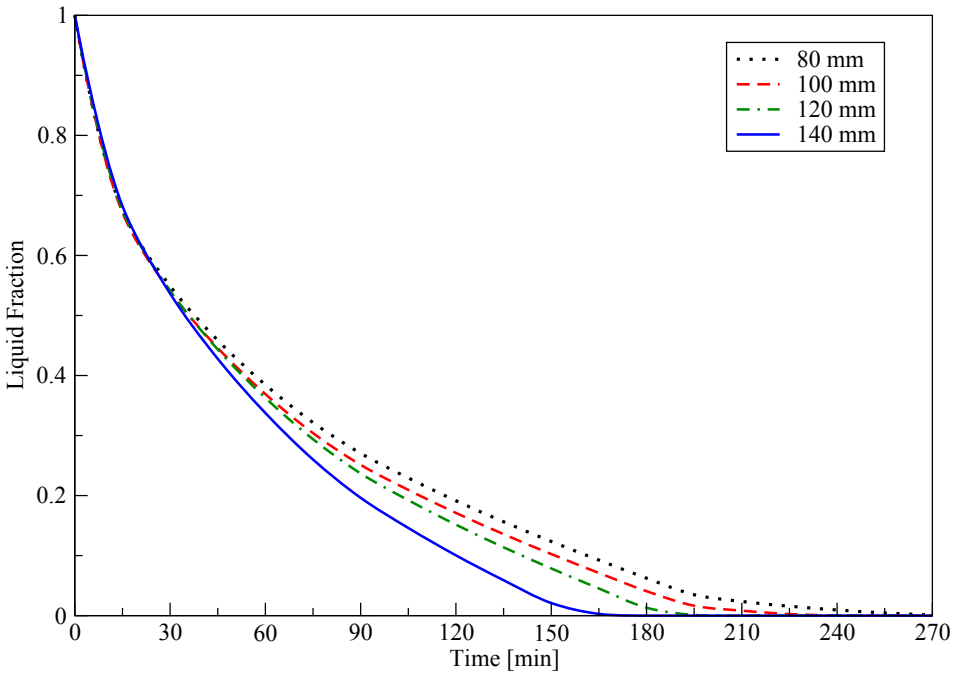

Figure 6.39: Liquid fraction versus time for the solidification process for the WTHX with different horizontal plate lengths.

Table 6.9: Solidification time and solidification time reduction for different horizontal plate lengths

Horizontal plate length (mm)	**Solidification time (min)**	**Reduction (%)**
80 (base case)	255	—
100	228	10
120	193	24
140	165	35

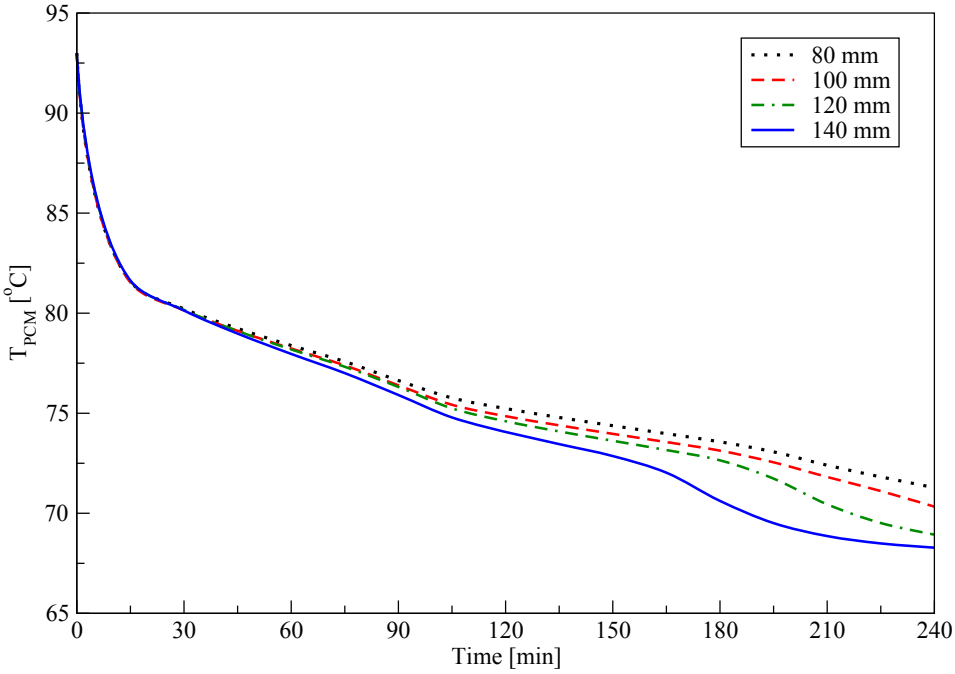

Figure 6.40: Average PCM temperature versus time for the solidification process for the WTHX with different horizontal plate lengths.

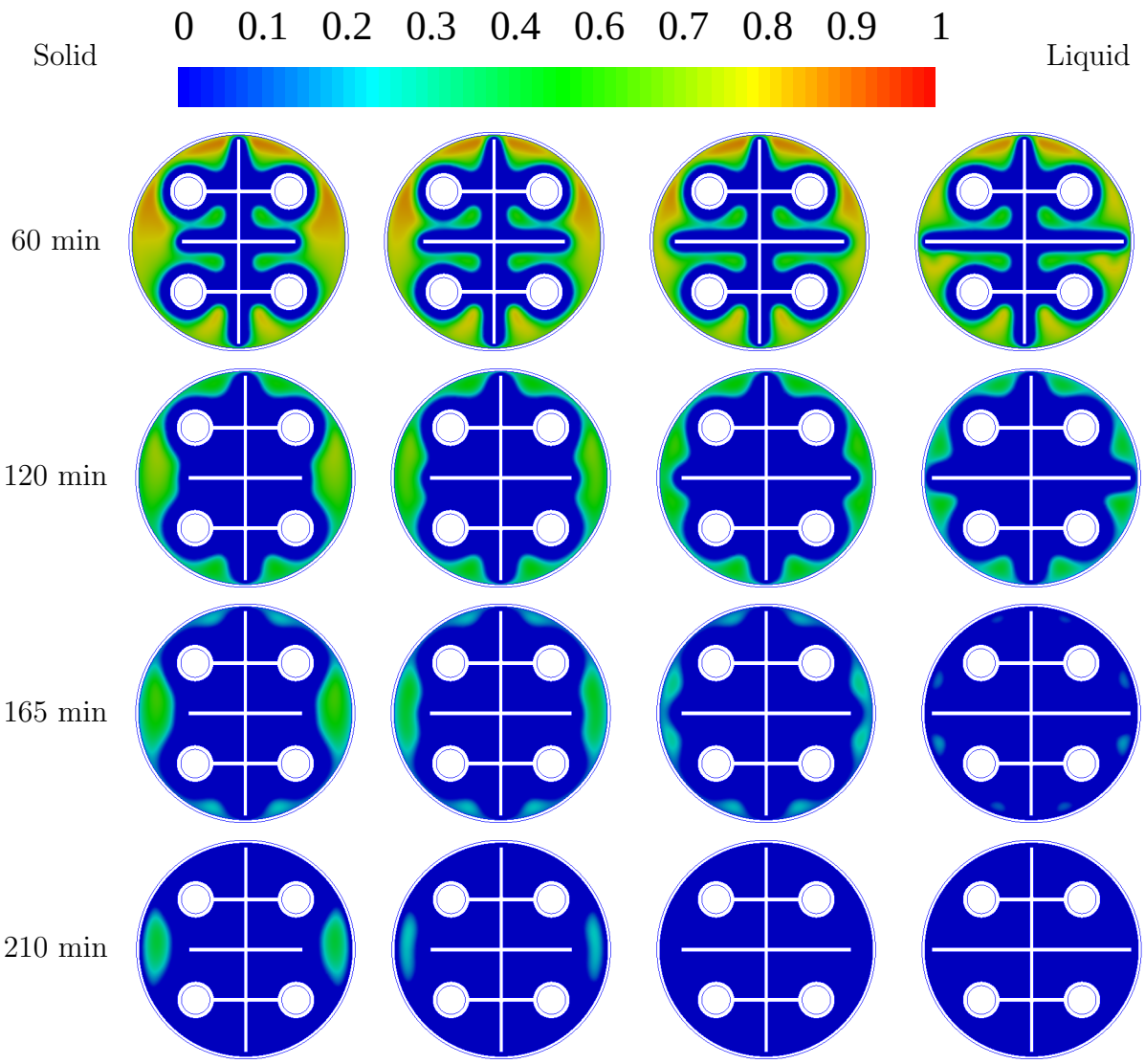

Figure 6.41: Liquid fraction contours at different times for the solidification process for different horizontal plate lengths: first from left length 80 mm, second length 100 mm, third length 120 mm, and fourth length 140 mm.

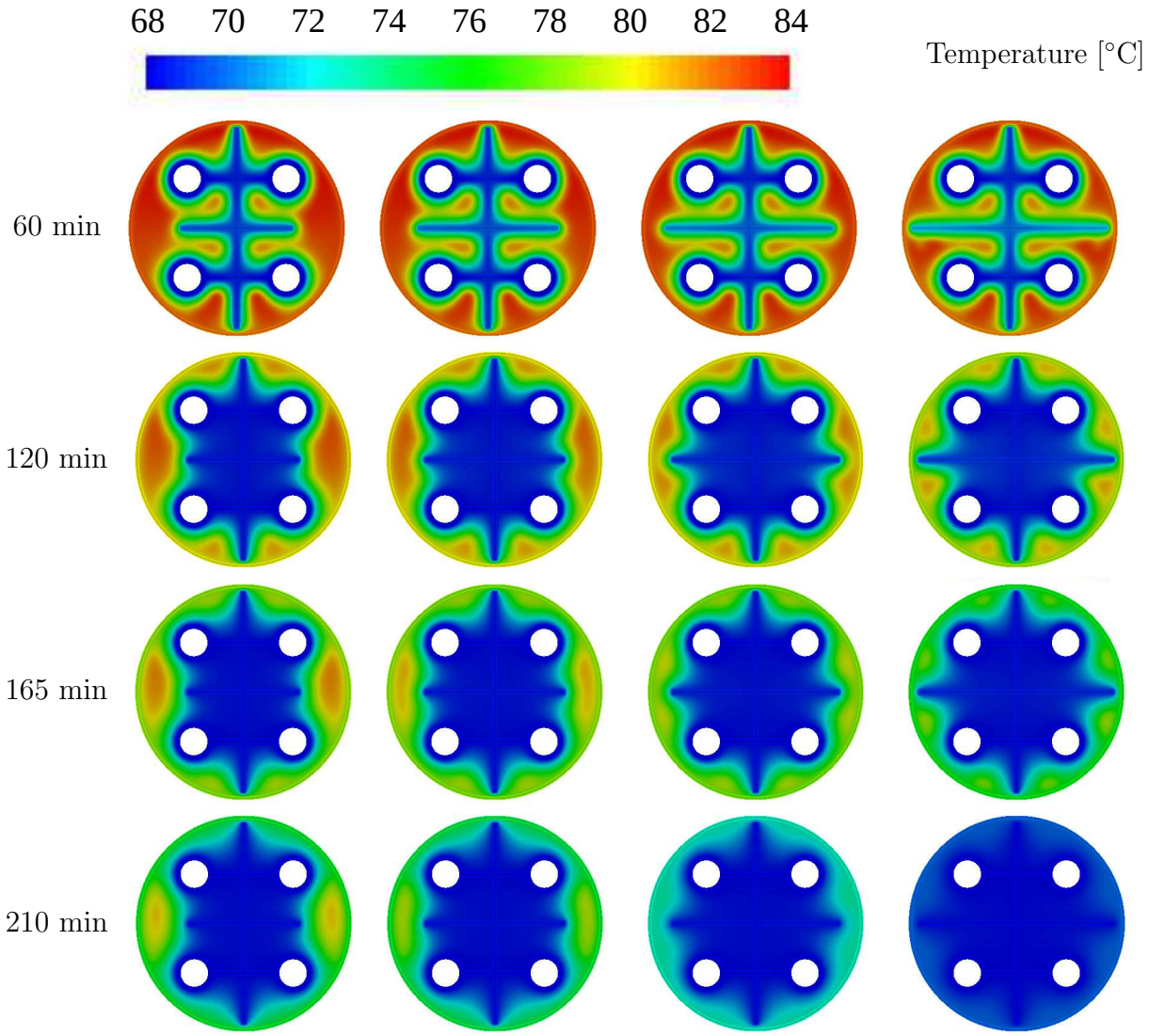

Figure 6.42: Contours of temperature at different times for the solidification process for different horizontal plate lengths: first from left length 80 mm, second length 100 mm, third length 120 mm, and fourth length 140 mm.

6.7 Optimization by utilizing the response surface method

6.7.1 The effect of changing the HTF temperature and the vertical plate length

For this test, the WTHX with different vertical plates lengths and different HTF temperatures was tested. Three vertical plate lengths were tested: 100 mm, 120 mm, 140 mm. Additionally, three HTF temperatures were tested: 87 °C, 90 °C and 93 °C. For this test, the melting process was considered. The response surface for the total melting time for different values of the HTF temperature and different values of the vertical plate length is illustrated in Fig. 6.43. It is obvious from this figure that changing the HTF temperature has a strong effect on the PCM melting process. Moreover, increasing the vertical plate length accelerates the PCM melting process due to the increase of the heat exchange area. The desirability of the melting process for the various vertical plate lengths and different values of HTF temperatures is shown in Fig. 6.44.

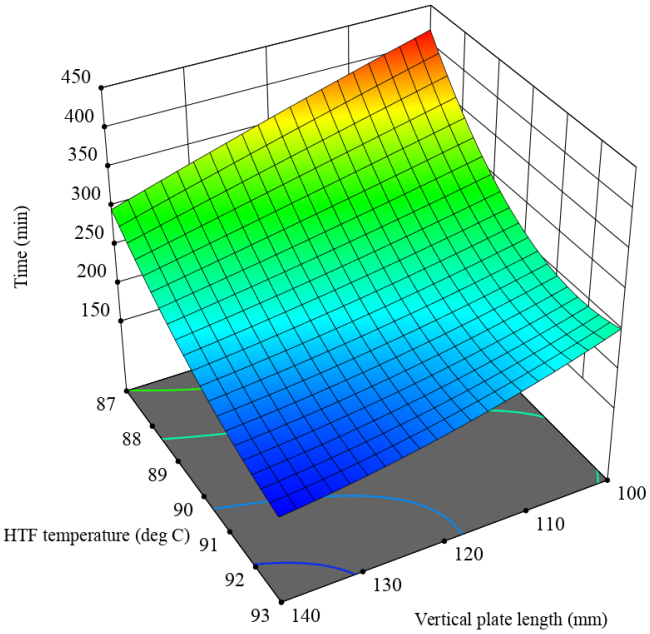

Figure 6.43: The response surface of the total PCM melting time for different values of vertical plate length and HTF temperature.

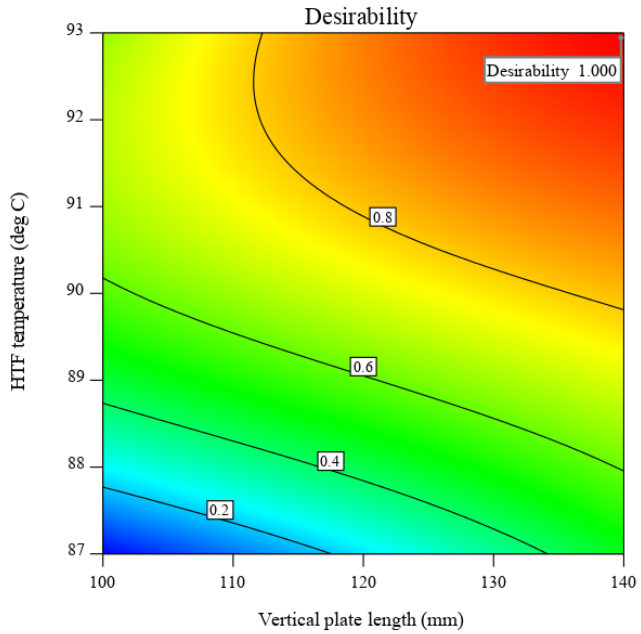

Figure 6.44: The desirability for different values of vertical plate length and HTF temperature for the melting process.

Chapter 7

Modified Webbed Tube Heat Exchanger

According to the literature reviewed, there has no simultaneous study on a triple tube heat exchanger (TTHX) and a webbed tube heat exchanger (WTHX). By combining these two heat exchangers, a new heat exchanger is found. This new heat exchanger may improve the thermal performance of the LHTES systems based on PCMs. In this chapter the webbed tube heat exchanger, introduced in Chapter 6, is employed instead of the inner and middle tube of the triple tube heat exchanger to produce the modified webbed tube heat exchanger (MWTHX). The MWTHX is suggested as a novel heat exchanger design to enhance the thermal performance of the LHTES systems based on PCMs. In the MWTHX the HTF passes through the inner tubes and outer tube, while the PCM is placed in the middle tube. In the MWTHX design, the heat transfer area is higher when compared to the TTHX or the WTHX. Hence, the PCM thermal performance could be enhanced, which would lead to accelerating the PCM melting and solidification process. To evaluate the thermal performance of the MWTHX, its thermal performance was compared with the TTHX and the WTHX.

7.1 Physical model

The MWTHX consisted of four horizontal inner tubes, a middle tube and an outer tube. The inner webbed tubes were connected together by utilizing several metal plates that were welded to the external surface of the inner tubes. The MWTHX physical model and its dimensions are shown in Fig. 7.1. This model has four inner tubes with inner diameters of d_i = 20 mm and 3 mm thickness, the middle tube has an inner diameter of d_m = 150 mm and thickness of 2 mm, the outer tube has an inner diameter d_o = 200 mm and thickness of 2 mm. The centres of the inner tubes were drawn on a circle with a 100 mm diameter. The angular distance between the inner tubes was equally distributed. The plates, dimensions were 144 mm (W1), 26.5 mm (W2), 144 mm (L) and 3 mm thickness (see Fig. 7.1). Copper was used for plates and pipes. The schematic diagram of the domain utilized in the numerical simulations with the indicated boundary conditions is shown in Fig. 7.2. The PCM was placed in the middle tube, while the HTF (water) passed through the inner tubes and outer tube. The PCM utilized in this study is (RT82). The thermal and physical properties of the PCM (RT82) are shown in Table 4.1.

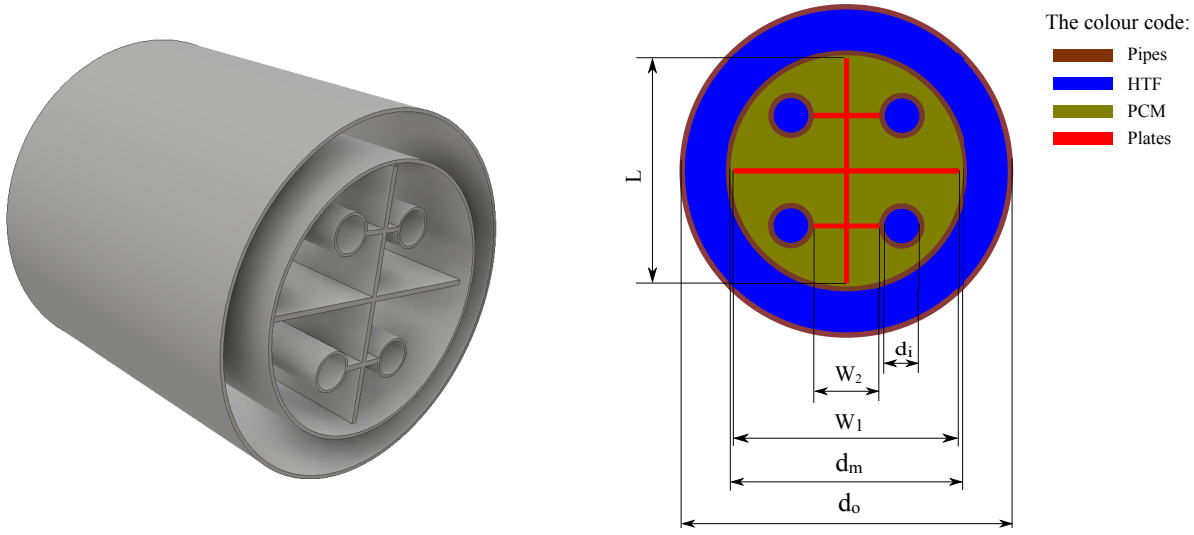

Figure 7.1: The modified webbed tube heat exchanger physical model with the major dimensions, left: 3D, right: the cross-sectional area.

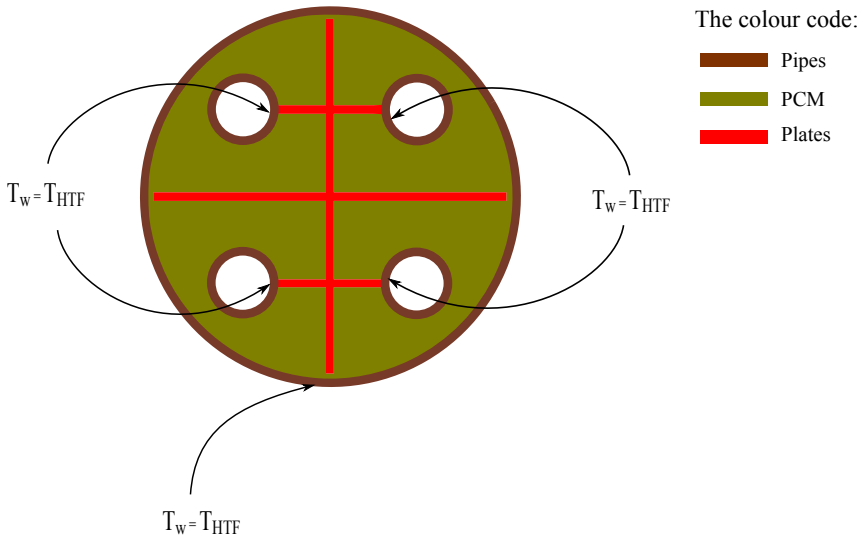

Figure 7.2: The computational domain of the modified webbed tube heat exchanger with the indicated boundary conditions.

7.2 Comparing the modified webbed tube heat exchanger with the TTHX and the WTHX

In this test, the modified webbed tube heat exchanger (MWTHX) is compared with the triple tube heat exchanger (TTHX) and the webbed tube heat exchanger (WTHX) to test its thermal performance. The cross-sectional areas of the physical heat exchanger models are illustrated in Fig. 7.3. The dimensions of the various heat exchangers are illustrated in Table 7.1. The same amount of the PCM was used for both the WTHX and the MWTHX, so the same amount of energy could be stored in both heat exchangers. The computational domains of these heat exchangers with the indicated boundary conditions are shown in Fig. 7.4. For the WTHX, the HTF flows through the inner tubes and the PCM is placed in the shell side. For TTHX, the HTF flows through the inner and outer tube while the PCM is placed in the middle tube. For the MWTHX, the HTF flows through the inner tubes and outer tube, while the PCM is placed in the middle tube (see Fig. 7.3).

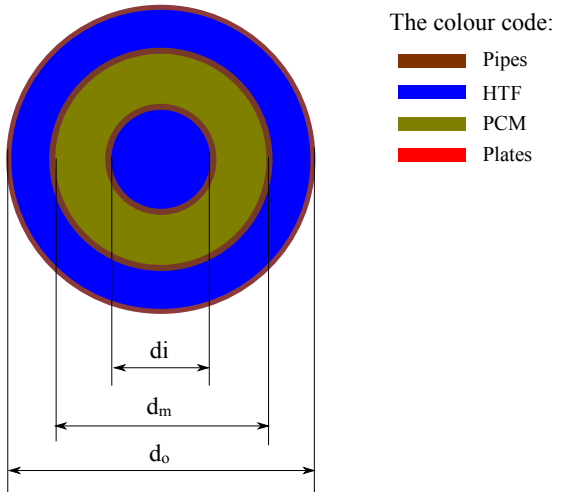

(a) TTHX

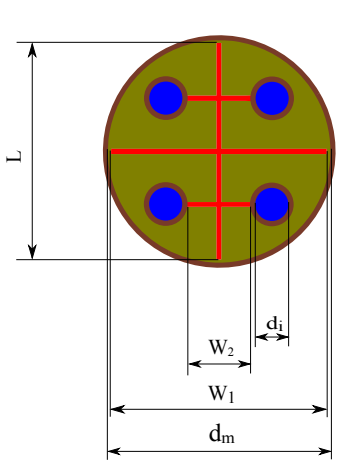

(b) WTHX

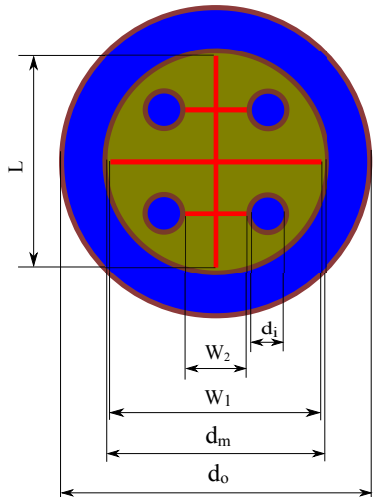

(c) MWTHX

Figure 7.3: The cross-sectional area of the various heat exchangers. (a) Triple tube heat exchanger (TTHX). (b) Webbed tube heat exchanger (WTHX). (c) Modified webbed tube heat exchanger (MWTHX).

Table 7.1: Geometrical dimensions of different heat exchangers types

Heat exchanger type	d_i (mm)	d_m (mm)	d_o (mm)	W_1 (mm)	W_2 (mm)	L (mm)
TTHX	50.8	150	200	—	—	—
WTHX	20	150	—	144	26.5	144
MWTHX	20	150	200	144	26.5	144

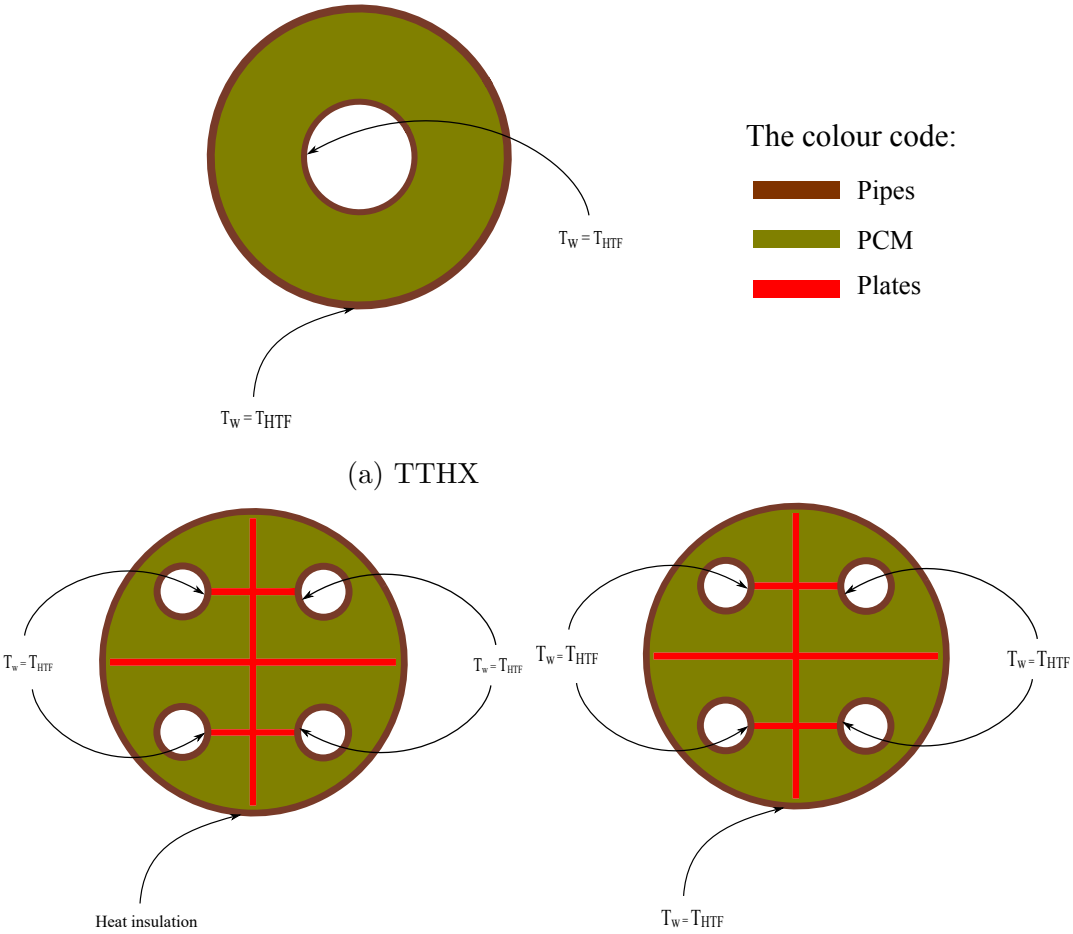

(a) TTHX

(b) WTHX

(c) MWTHX

Figure 7.4: The computational domains with the indicated boundary conditions for the various heat exchangers. (a) Triple tube heat exchanger (TTHX). (b) Webbed tube heat exchanger (WTHX). (c) Modified webbed tube heat exchanger (MWTHX).

7.2.1 Initial and boundary conditions

Melting process

At the initial time (t = 0), the PCM was in the solid state, hence its temperature was 27 °C, below its melting temperature. The HTF has a constant temperature ($T_w = T_{HTF} = 90$ °C), which is higher than the PCM melting temperature. This temperature is imposed along the inner tube and middle tube walls when using the TTHX (Fig. 7.4a), imposed along inner tubes walls when using the WTHX (Fig. 7.4b), and imposed along inner tubes and middle tube walls when using the MWTHX (Fig. 7.4c). Therefore, the initial and boundary conditions can be listed as:

$T = T_{initial} = 27$ °C at (t = 0).

At $d = d_i$, $T = T_{HTF} = 90$ °C

At $d = d_m$, wall insulated (adiabatic) when using the WTHX.

Or at $d = d_m$, $T = T_{HTF} = 90$ °C when using the TTHX or the MWTHX.

Solidification process

At the initial time (t = 0), the PCM was in the liquid state, hence its temperature was 93 °C, which is above its solidification temperature. The HTF has a constant temperature ($T_w = T_{HTF} = 68$ °C), which is lower than the PCM solidification temperature. This temperature is imposed along the inner tube and middle tube walls when using the TTHX (Fig. 7.4a), imposed along inner tubes walls when using the WTHX (Fig. 7.4b), and imposed along inner tubes and middle tube walls when using the MWTHX (Fig. 7.4c). Therefore, the initial and boundary conditions can be listed as:

$T = T_{initial} = 93$ °C at (t = 0).

At $d = d_i$, $T = T_{HTF} = 68$ °C.

At $d = d_m$, wall insulated (adiabatic) when using the WTHX.

Or at $d = d_m$, $T = T_{HTF} = 68$ °C when using the TTHX or the MWTHX.

7.2.2 Melting process

Fig. 7.5 shows the liquid fraction versus time for various heat exchanger types. It is clear from this figure that by utilizing the MWTHX the total melting time decreased significantly compared to the other heat exchangers. The PCM completely melted after 106 minutes when utilizing the MWTHX, while at the same time only around 39% and 70% of PCM melted when using the TTHX and the WTHX respectively. This acceleration of the melting process when using the MWTHX occurred because of the increase of the heat transfer area due to the heating from the outer tube and utilizing the metal plates. The total PCM melting time decreased by 41% when utilizing the MWTHX compared to the WTHX. The total melting time and melting time reductions for the various heat exchanger configurations are shown in Table 7.2.

The average PCM temperature versus time for the various heat exchangers is shown in Fig. 7.6. It is obvious from this figure that the PCM average temperature when using the MWTHX is higher at all time intervals compared to the WTHX and the TTHX. This proves the enhancement of the thermal performance of PCM in the MWTHX compared to the WTHX or the TTHX.

Contours of liquid fraction for the various heat exchangers at different times are presented in Fig. 7.7. It is obvious from this figure that the melting rate increased when utilizing the MWTHX, compared to the TTHX and the WTHX; this was due to the increase of the heat transfer area. Initially, the melting process concentrated near the heat transfer surfaces is dominated by conduction. As time passes, the melted PCM increase, hence, the natural convection dominates the heat transfer process due to the buoyancy effect. In case of utilizing the MWTHX, the melting rate increase near the metal plates, because these plates reached the isolated parts of PCM. The melting rate in the case of using the MWTHX is high compared to the WTHX, due to the heating from the outer HTF tube. In the case of utilizing the TTHX, the heat transfer process in concentrated around the inner and outer HTF tubes, while the middle part of the PCM, which is relatively remote from the hot walls of the HTF tubes is remained for long period without melting. This happens due to the poor heat transfer process through the solid PCM, which has low

thermal conductivity.

Contours of surface heat flux for the various heat exchangers at different times are presented in Fig. 7.8. It is clear from this figure that by utilizing the WTHX and the MWTHX the surface heat flux increased significantly compared to the TTHX due to the increase of heat transfer surface area. Temperature contours for various heat exchanger configurations at different times are illustrated in Fig. 7.9. As can be seen from this figure, by utilizing the MWTHX the heat transfer rate increased compared to the other heat exchangers' configurations, thereby reducing the total PCM melting time.

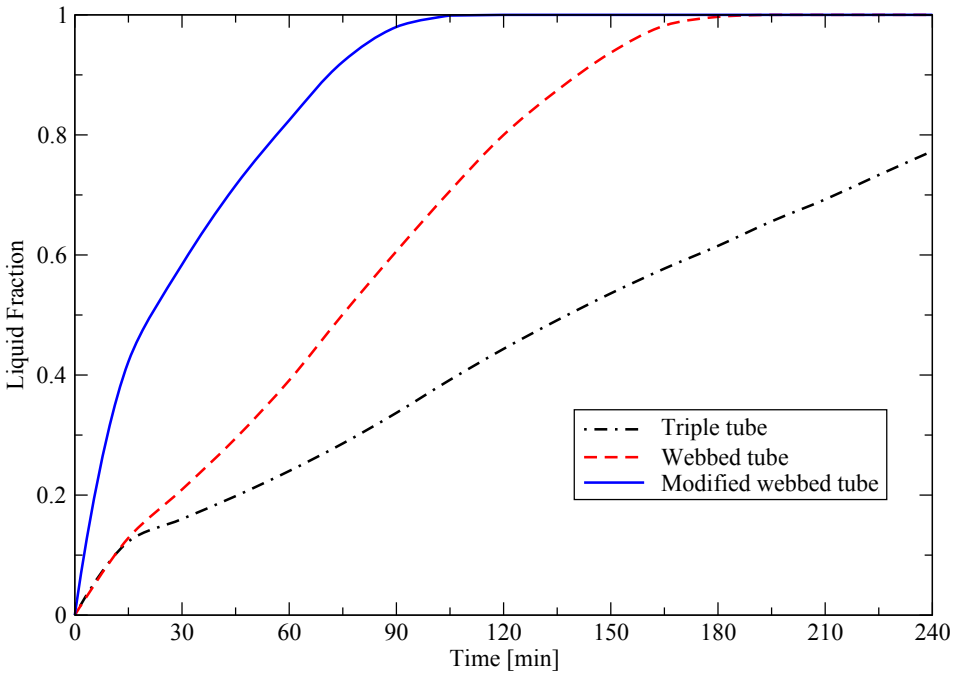

Figure 7.5: Liquid fraction comparison for melting process for MWTHX, WTHX, and TTHX.

Table 7.2: Melting time and melting time reduction for various heat exchangers

Heat exchanger type	**Melting time (min)**	**Reduction (%)**
TTHX (base case)	360	—
WTHX	180	50
MWTHX	106	70

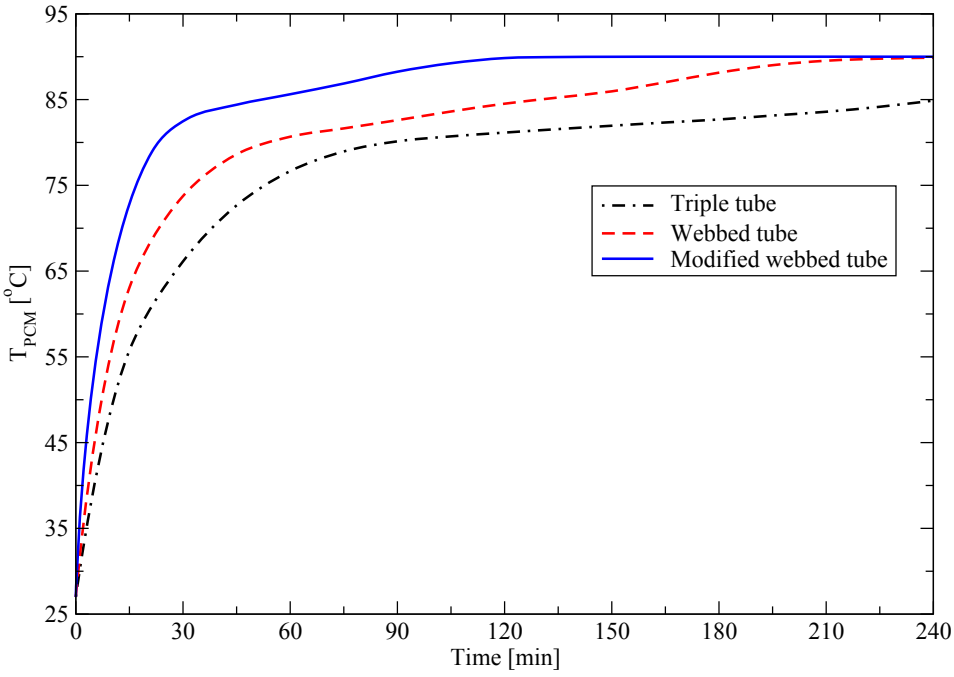

Figure 7.6: Average PCM temperature comparison for melting process for MWTHX, WTHX, and TTHX.

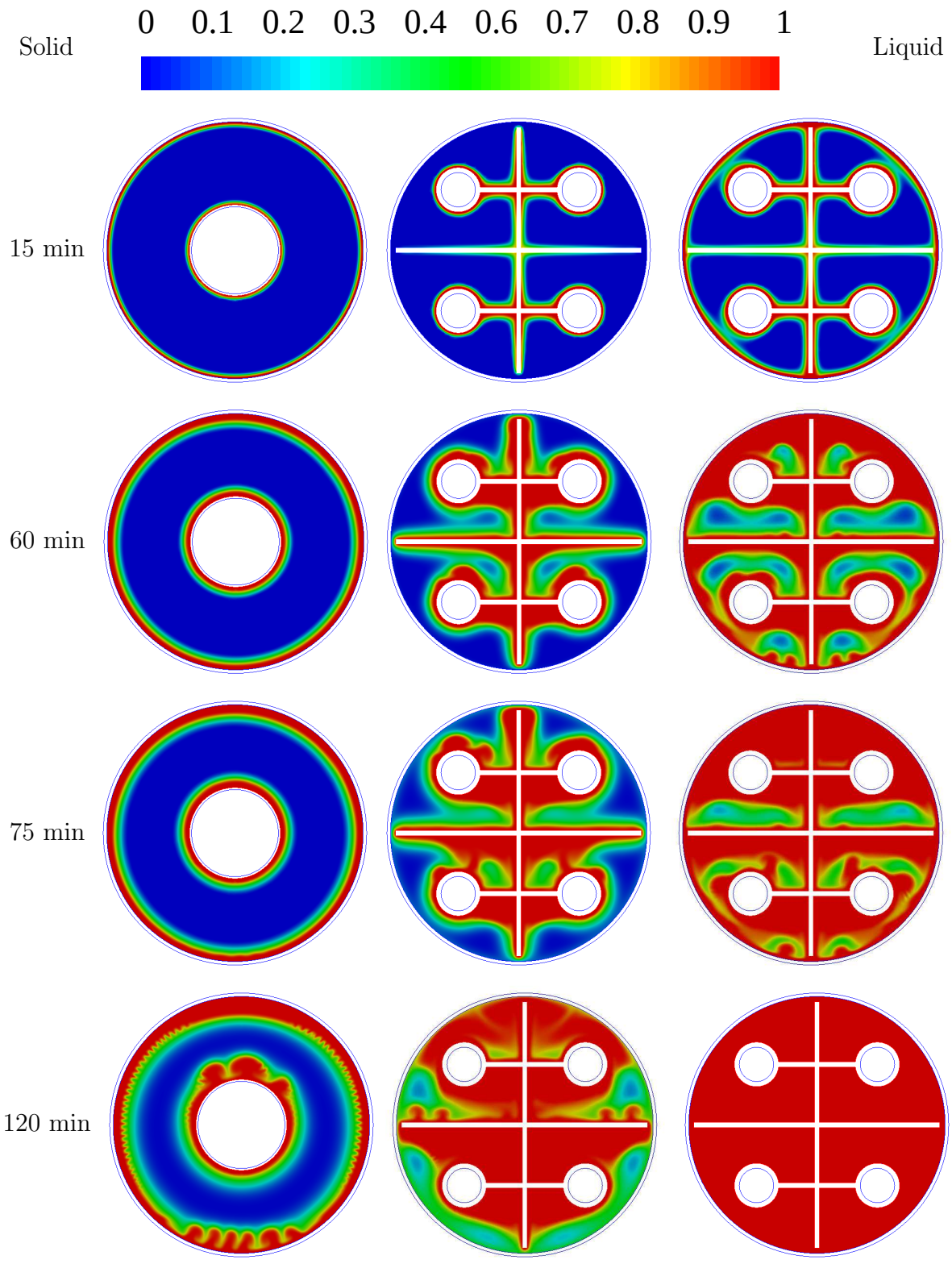

Figure 7.7: Liquid fraction contours at different times for melting process for various heat exchangers: first from left TTHX, second WTHX, and third MWTHX.

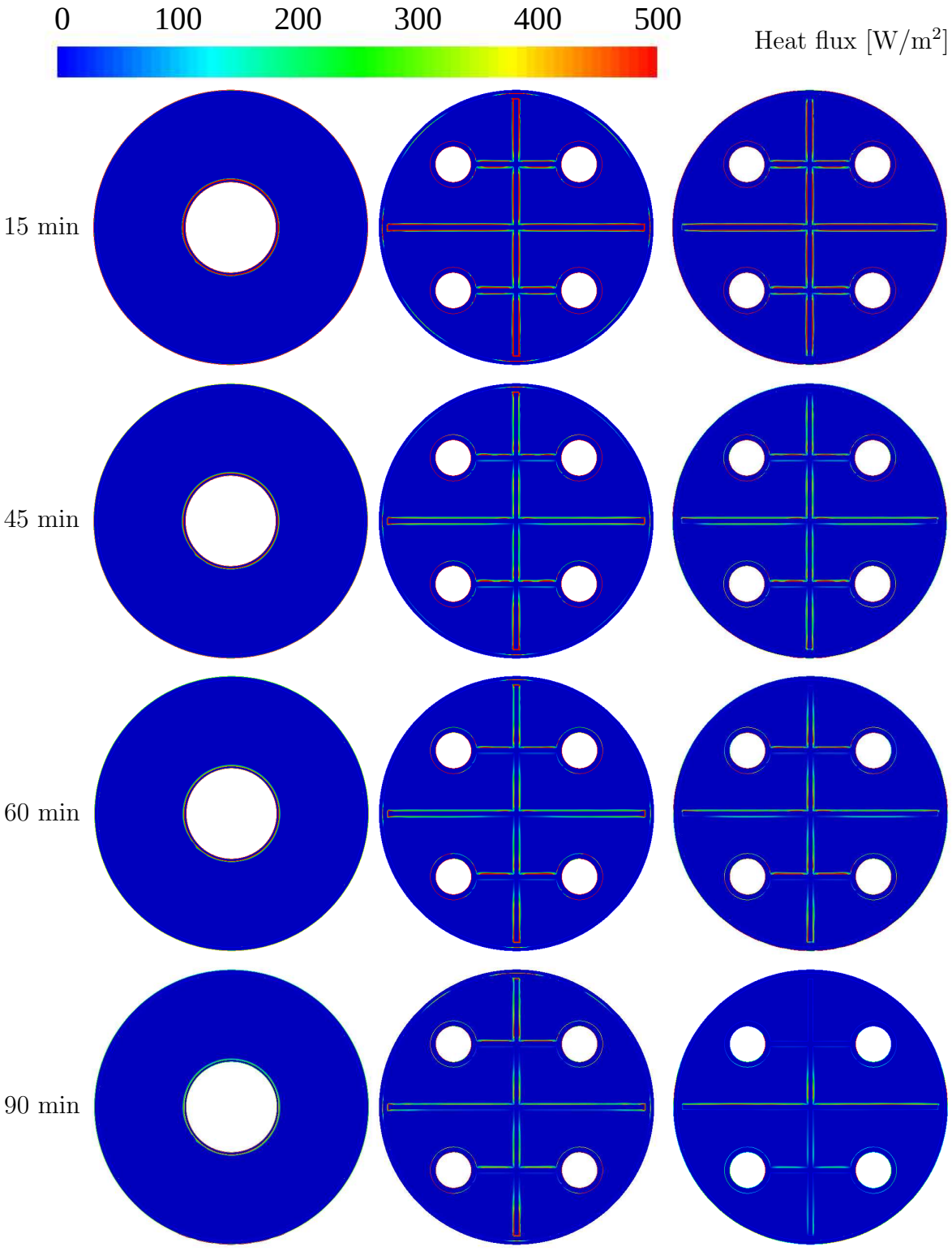

Figure 7.8: Surface heat flux contours at different times for melting process for various heat exchangers: first from left TTHX, second WTHX, and third MWTHX.

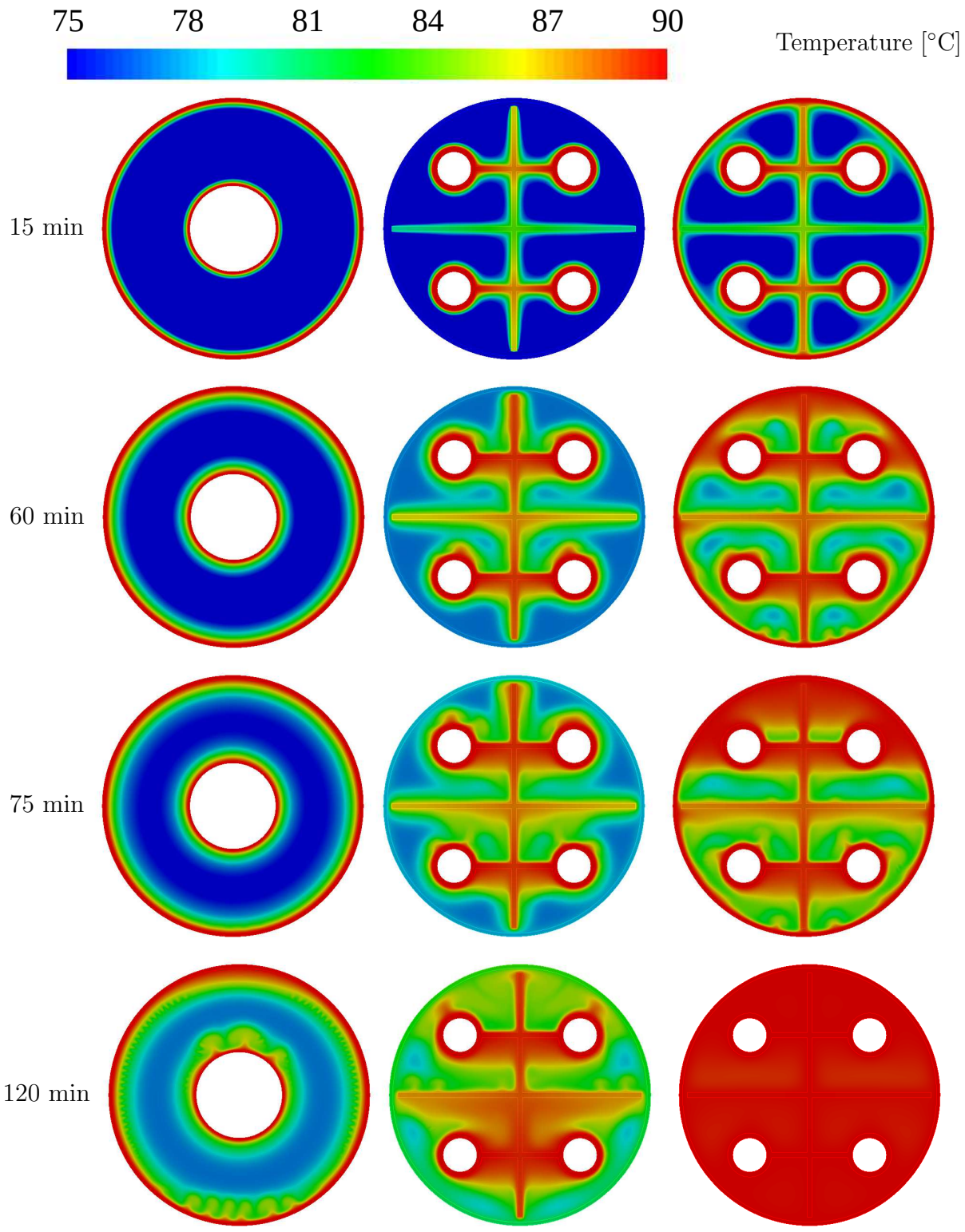

Figure 7.9: Contours of temperature at different times for melting process for various heat exchangers: first from left TTHX, second WTHX, and third MWTHX.

7.2.3 Solidification process

Fig. 7.10 shows the liquid fraction versus time for the various heat exchanger types. It is obvious from this figure, that by utilizing the MWTHX, the total PCM solidification time decreased significantly compared to the TTHX or the WTHX. The PCM completely solidified after 105 minutes when utilizing the MWTHX, while for the same time only around 73% and 88% of PCM solidified when utilizing the TTHX and the WTHX respectively. This acceleration in the solidification process, when using the MWTHX, occurred due to the increase of the heat transfer area. The heat transfer area increased due to the cooling by using the outer tube and utilizing the metal plates. The total PCM solidification time decreased by 36% when utilizing the MWTHX compared to the WTHX. The total solidification time and solidification time reductions for the various heat exchanger configurations are shown in Table 7.3.

The average PCM temperature versus time for various heat exchangers' configurations is shown in Fig. 7.11. As can be seen from this figure, the PCM average temperature, when employing the MWTHX, is lower at all time intervals compared to the WTHX and the TTHX. This proves the increase of heat transfer rate when utilizing the MWTHX compared to the WTHX and the TTHX.

Contours of liquid fraction for the various heat exchanger types at different times are shown in Fig. 7.12. The PCM solidification rate increased significantly by utilizing the MWTHX, compared to the other heat exchangers. This increase in solidification rate occurred due to the increase of heat transfer area when using the MWTHX. At the start of the solidification process the PCM is totally liquid and its temperature above the melting temperature while the HTF tubes walls temperature is lower than the melting temperature. The heat transfer rate is very high at the beginning since the liquid PCM is directly in contact with the HTF tubes walls. Since the thermal conductivity of metal plates utilized in the WTHX and the MWTHX more than that of the PCM, hence more heat transferred through the plates to the HTF tubes walls. As time passes, the solidification progress, the effect of natural convection decreases due to the decrease of liquid PCM and temperature gradient. Hence, the solidification font becomes symmetrical. Contours of surface heat flux

for the various heat exchangers at different times are presented in Fig. 7.13. Temperature contours for different heat exchanger configurations at different times are presented in Fig. 7.14. The MWTHX shows the higher heat transfer rate compared to the TTHX and the WTHX types, this reduces the total PCM solidification time.

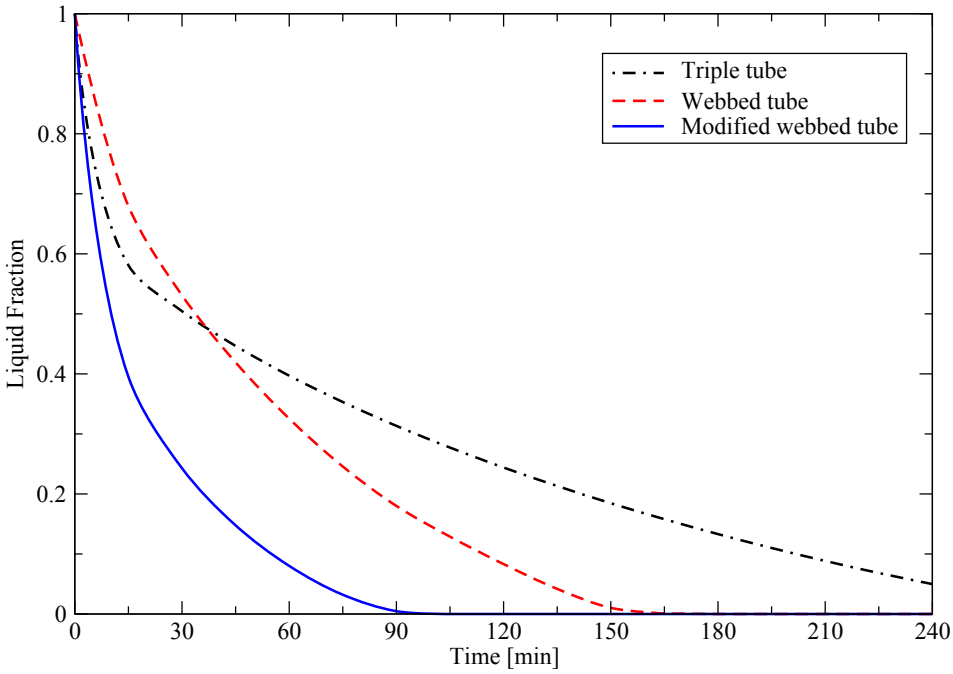

Figure 7.10: Liquid fraction comparison for solidification process for MWTHX, WTHX, and TTHX.

Table 7.3: Solidification time and solidification time reduction for various heat exchangers

Heat exchanger type	**Solidification time (min)**	**Reduction (%)**
TTHX (base case)	302	—
WTHX	165	45
MWTHX	105	65

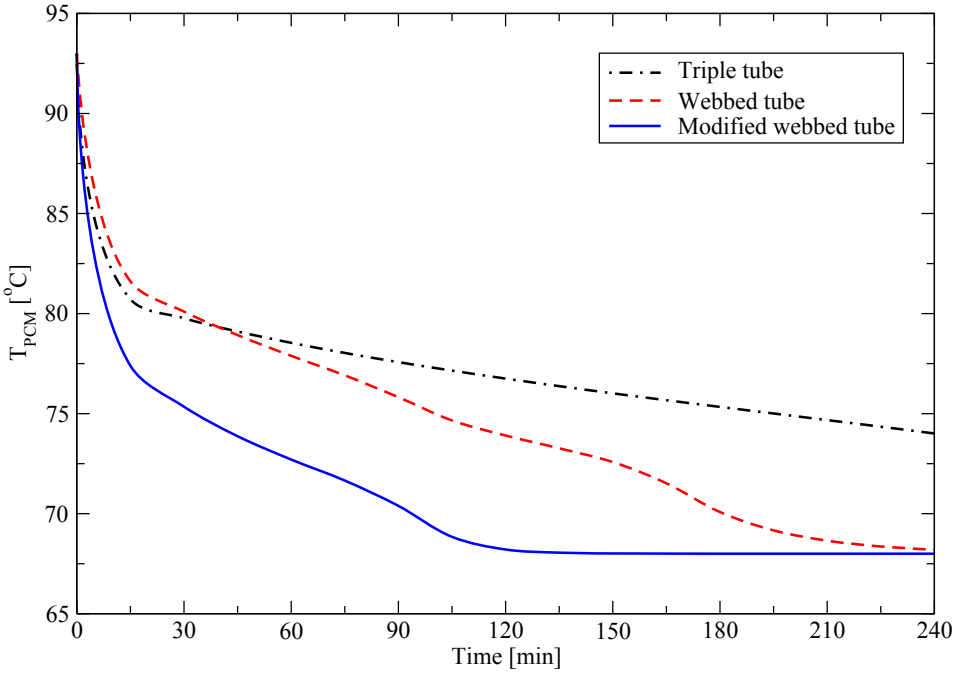

Figure 7.11: Average PCM temperature comparison for solidification process for MWTHX, WTHX, and TTHX.

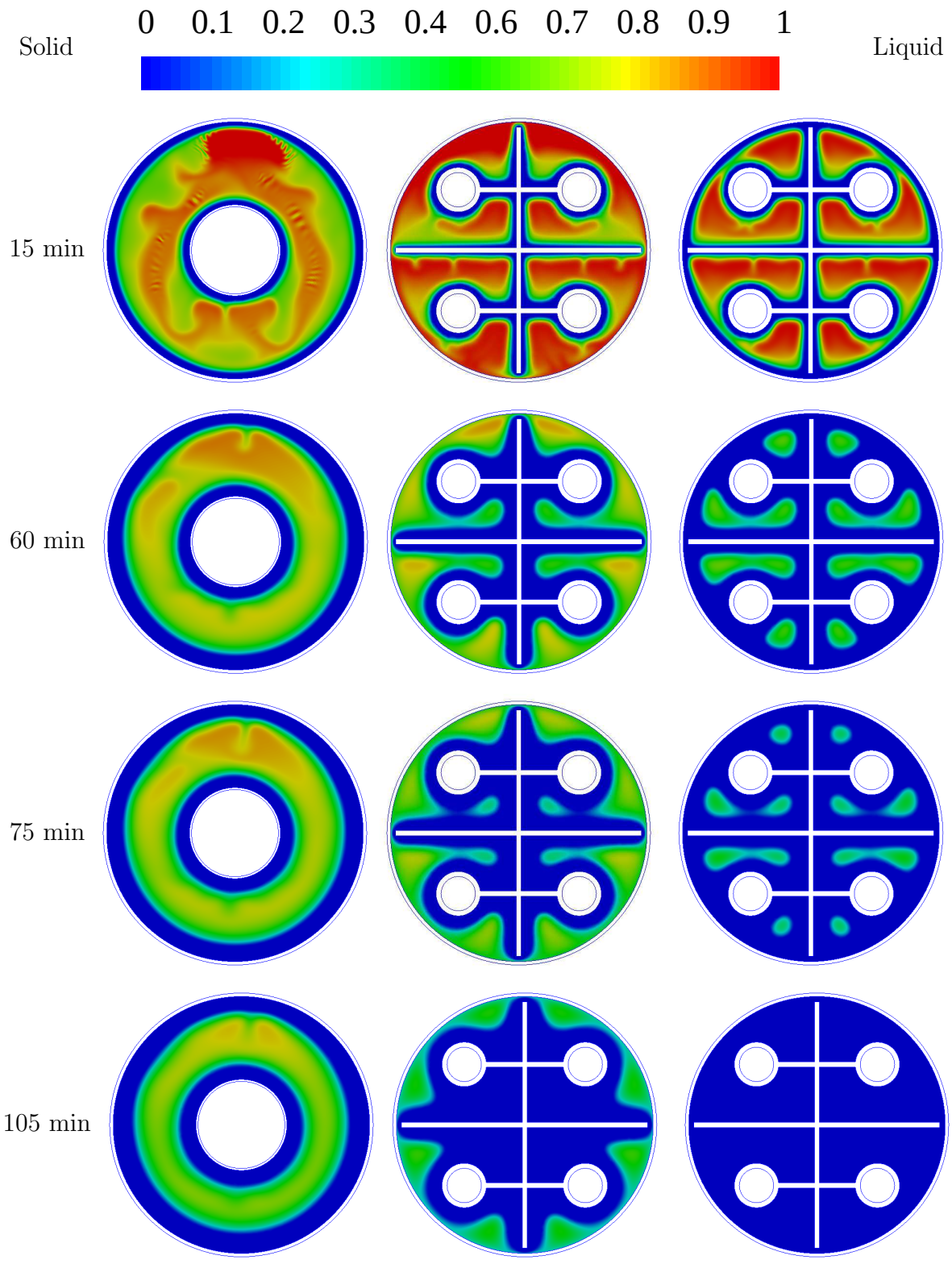

Figure 7.12: Liquid fraction contours at different times for solidification process for various heat exchangers: first from left TTHX, second WTHX, and third MWTHX.

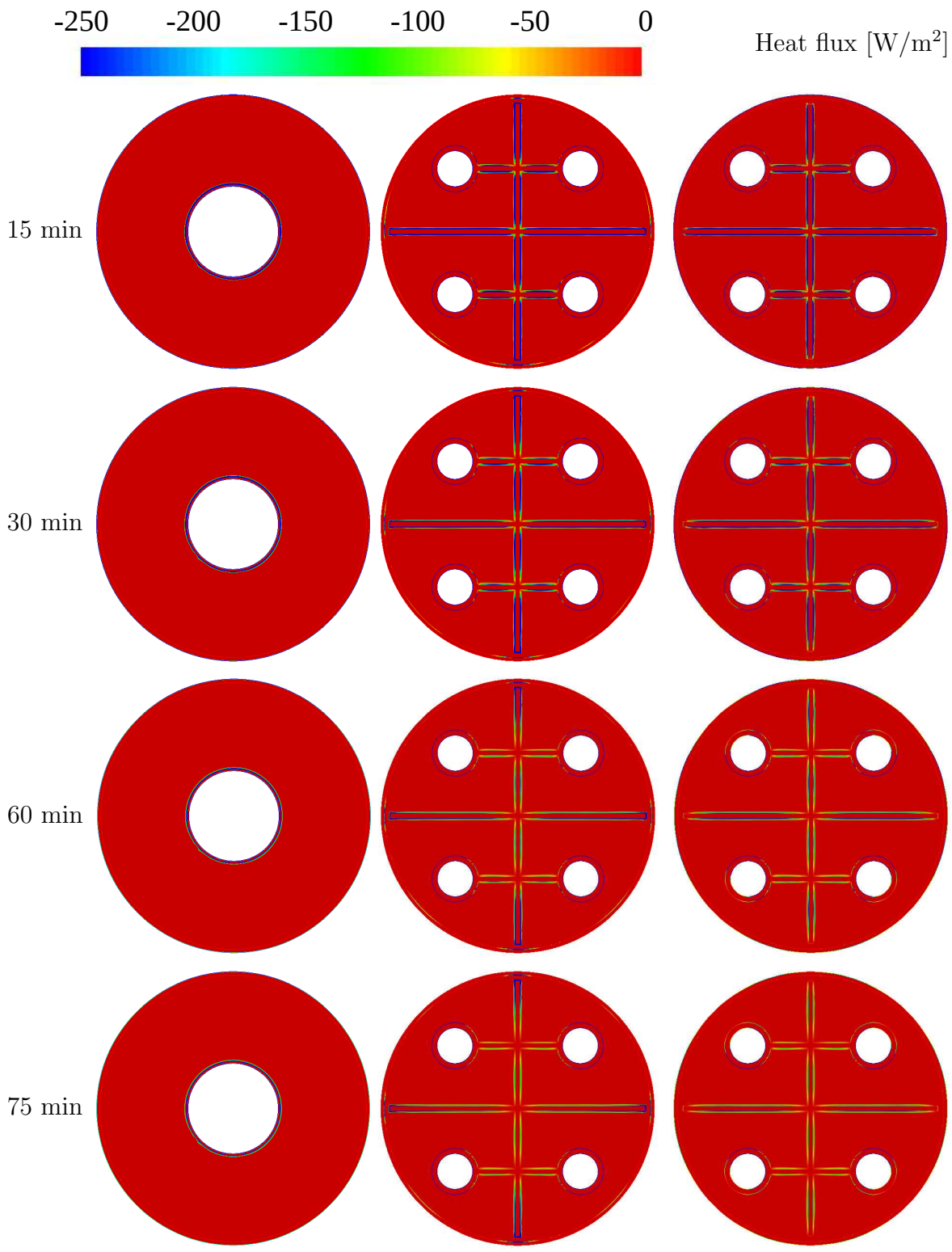

Figure 7.13: Surface heat flux contours at different times for solidification process for various heat exchangers: first from left TTHX, second WTHX, and third MWTHX.

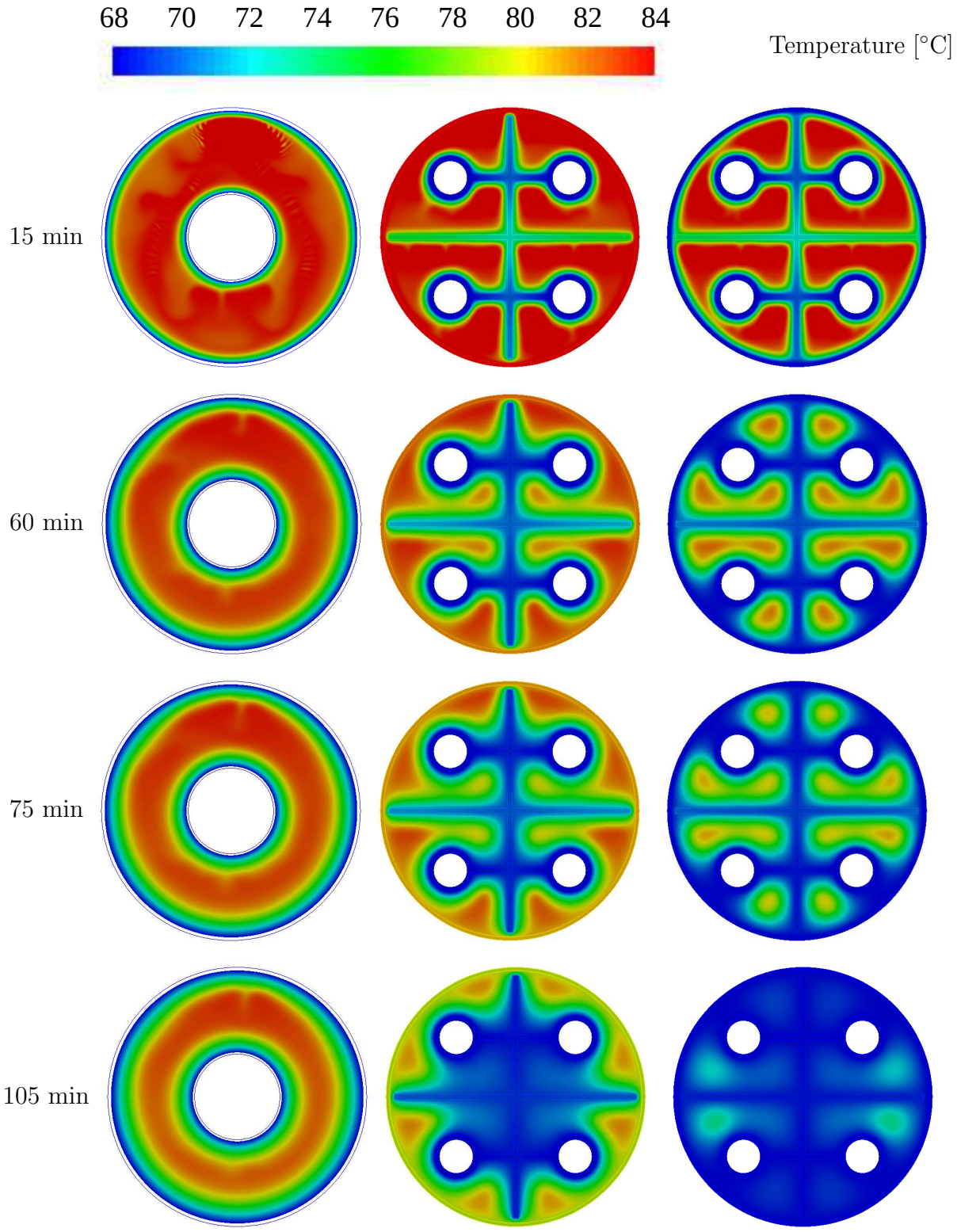

Figure 7.14: Contours of temperature at different times for solidification process for various heat exchangers: first from left TTHX, second WTHX, and third MWTHX.

7.3 Effect of changing the initial PCM temperature and the HTF temperature

For this test, the effect of changing the initial PCM temperature and the HTF temperature on the PCM melting process in the MWTHX was studied. Three HTF temperatures were tested which were: 87 °C, 90 °C and 93 °C. Furthermore, three initial PCM temperatures were tested which were: 27 °C, 30 °C and 33 °C. Fig. 7.15 shows the response surface of the total PCM melting time for different values of the initial PCM temperature and various values of the HTF temperature. It is clear from this figure, that changing the HTF temperature has a significant influence on the PCM melting process, while changing the initial PCM temperature has a weak influence. The total PCM melting time decreased by 45% by increasing the HTF temperature from 87 °C to 93 °C. The desirability for different values of HTF temperature and initial PCM temperature is illustrated in Fig. 7.16. It is obvious from this figure that the desirability increases by increasing the HTF temperature.

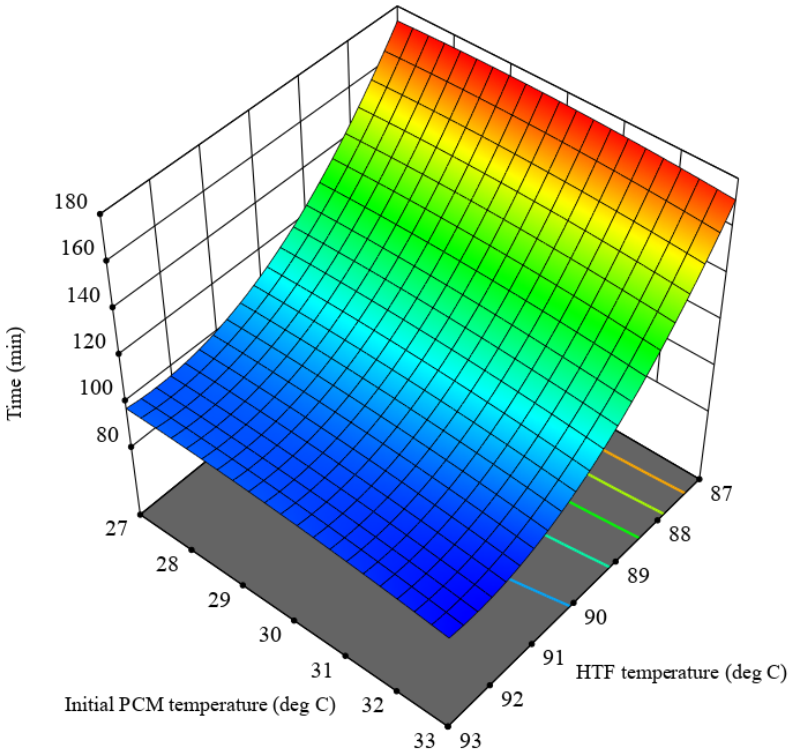

Figure 7.15: Response surface of the total melting time for different values of HTF temperature and initial PCM temperature for melting process.

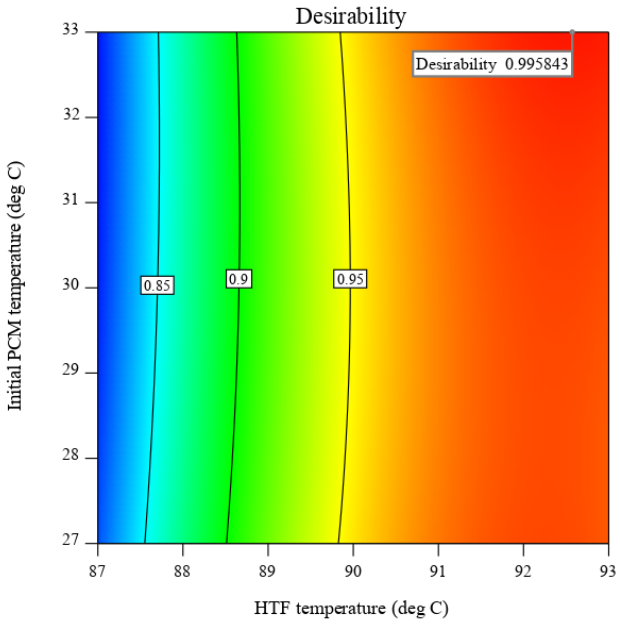

Figure 7.16: The desirability of the WTHX for different values of HTF temperature and initial PCM temperature for melting process.

Chapter 8

Conclusion and Suggestions for Further Work

8.1 Conclusion

Heat transfer enhancement for latent heat thermal energy storage (LHTES) systems, based on PCM by utilizing novel fins and innovative heat exchangers design, has been investigated in this thesis.

8.1.1 Triple tube heat exchanger with fins

Utilizing a triple tube heat exchanger (TTHX) to enhance the thermal performance of PCM in the LHTES systems is an effective strategy because of the heat transfer fluid flowing on both sides of the PCM, thereby increasing the heat transfer area. Using fins to improve the thermal performance of PCM is a simple and effective method because of their easy construction, low fabrication costs and being easy to optimize their design by utilizing computer simulation programs. The geometric design of fins has a strong effect on the thermal energy storage/release for the LHTES systems.

Many innovative fin designs were introduced to improve the poor thermal performance of PCM in the TTHX. The shapes of fins tested included:- plus-fin shape and tee-fin shape. To evaluate the thermal performance of these fins, a comparison was made with the traditional longitudinal fins. To compare the thermal performance of the various fins types, the same amounts of PCMs were used in all thermal energy storage systems. As such, the total cross-sectional area of all fin types was kept constant. To achieve this, the fins' dimensions were carefully chosen. The PCM melting time reduced by about 22% when utilizing the plus fins shape as compared to using the longitudinal fins. Moreover, the PCM solidification time reduced by 25% when utilizing the plus fins, compared to the longitudinal fins. The acceleration of the PCM melting and solidification process when utilizing the plus fins was due to the increase of the thermal penetration depth and the increase of the heat transfer area.

The number of plus fins has a strong influence on the PCM melting and solidification process. When the fins' number increased from four to six, the melting time reduced by 33%, and the solidification time reduced by 50%. The fins' positions in the bottom and top halves of the PCM container have a strong influence on heat distribution. Given this, appropriate fin arrangement could accelerate the PCM melting and solidification process. The fins' dimensions have a strong effect on the PCM melting and solidification process. When the plus-fins' length increased from 25 mm to 42 mm, the PCM melting time reduced by 33%, and the solidification time also decreased by 33%. If the plus-fins width is increased from 15 mm to 50 mm, the melting time is reduced by 30%, and the solidification time decreased by 40%. If the plus-fins' thickness is increased from 0.5 mm to 3 mm, the PCM melting time is reduced by 33%, and the solidification time decreased by 28%.

8.1.2 Shell and tube heat exchanger with fins

Many novel fins shapes were introduced to enhance the thermal performance of PCM in a shell and tube heat exchanger. These shapes included:- tee and tree fins. To evaluate the thermal performance of these fins, a comparison was made with the traditional longitudinal

fins. The total cross-sectional area was kept constant for all fin types to compare their thermal performance. To achieve this, fins' dimensions were carefully chosen. When utilizing the tee fins, the PCM melting time reduced by 33% and the solidification time decreased by 33% as compared to the case of using the longitudinal fins. This acceleration in melting and solidification process when employing the tee fins, was due to the increase of the heat transfer area and increase of the thermal penetration depth. The heat transfer fluid (HTF) temperature has a significant influence on the PCM melting and solidification process. The PCM melting time reduced by 58% if the HTF temperature increased from 87 °C to 96 °C. Moreover, if the HTF temperature reduced from 72 °C to 60 °C the PCM solidification time reduced by 50%.

8.1.3 Webbed tube heat exchanger

The heat exchanger geometry has a significant influence on the thermal energy storage system performance. An innovative webbed tube heat exchanger (WTHX) was introduced to enhance the thermal performance of the LHTES system, which is based on PCM. To evaluate the WTHX design, its thermal performance was compared with the traditional heat exchangers, which included: shell and tube heat exchanger (STHX), multitube heat exchanger (MTHX) and triple tube heat exchanger (TTHX). The total PCM solidification time reduced by 45% when utilizing the WTHX in comparison with the TTHX. Moreover, the total PCM solidification time decreased by 66% by using the WTHX as compared to the MTHX. The total PCM melting time reduced by 50% when utilizing the WTHX compared to the TTHX. Moreover, the total PCM melting time decreased by 72% when using the WTHX in comparison with the MTHX. This acceleration in melting and solidification process via the WTHX was because of the increase of the heat transfer area due to the use of the metal plates. The heat was uniformly distributed when using the WTHX compared to the other heat exchanger types.

The HTF temperature has a strong influence on the PCM melting and solidification process in the WTHX. The PCM melting time decreased by halve if the HTF temperature

increased from 87 °C to 96 °C. The PCM solidification time decreased by 40% if the HTF temperature decreased from 71 °C to 62 °C.

The metal plates' dimensions have a significant effect on the PCM melting and solidification process. If the horizontal plate length increased from 80 mm to 140 mm, the total PCM melting time decreased by 29%, and the total PCM solidification time reduced by 35%. If the vertical plate length increased from 80 mm to 140 mm, the total PCM melting time reduced by 33%, and the total PCM solidification time reduced by 33%. Increasing the length and width of the metal plates enhanced the thermal penetration depth and increased the heat transfer area.

8.1.4 Modified webbed tube heat exchanger

The webbed tube heat exchanger (WTHX) was employed, instead of the inner and middle tubes of the triple tube heat exchanger (TTHX), to produce the modified webbed tube heat exchanger (MWTHX). The MWTHX was proposed as a novel heat exchanger design to enhance the thermal performance of the LHTES systems, based on PCMs. In the MWTHX the HTF was passed through the inner tubes and outer tube, while the PCM was contained in the middle tube. In the MWTHX design, the heat transfer area was higher compared to the TTHX or the WTHX. Hence, the PCM thermal performance was enhanced, which led to accelerating the melting and solidification of PCM. To evaluate the thermal performance of the MWTHX, its thermal performance was compared with the TTHX and the WTHX. The PCM had completely melted after 106 minutes of utilizing the MWTHX, while for the same time period only around 39% and 70% of PCM had melted when utilizing the TTHX and the WTHX respectively. This acceleration in the melting process, when using the MWTHX, occurred because of the increase of the heat transfer area due to the heating from the outer tube. The total PCM melting time decreased by 41% by utilizing the MWTHX as compared to the WTHX. Moreover, by utilizing the MWTHX, the total PCM solidification time decreased significantly compared to the TTHX and the WTHX. The PCM completely solidified after 105 minutes when utilizing

the MWTHX, while for the same time period only around 73% and 88% of PCM had solidified when using the TTHX and the WTHX respectively. The total PCM solidification time decreased by 36% when utilizing the MWTHX as compared to the WTHX.

8.1.5 Comparison between all modifications of heat exchangers

The performance of various heat exchangers designs was compared. The dimensionless time for total melting and solidification time comparison for STHX with 6 tee fins, TTHX with 6 plus fins, WTHX, and MWTHX is shown in Fig. 8.1. It is clear from this figure that the MWTHX shows the lower melting and solidification time compared to the other heat exchangers' designs. While the STHX with 6 tee fins show the higher melting and solidification time compared to the other heat exchangers designs.

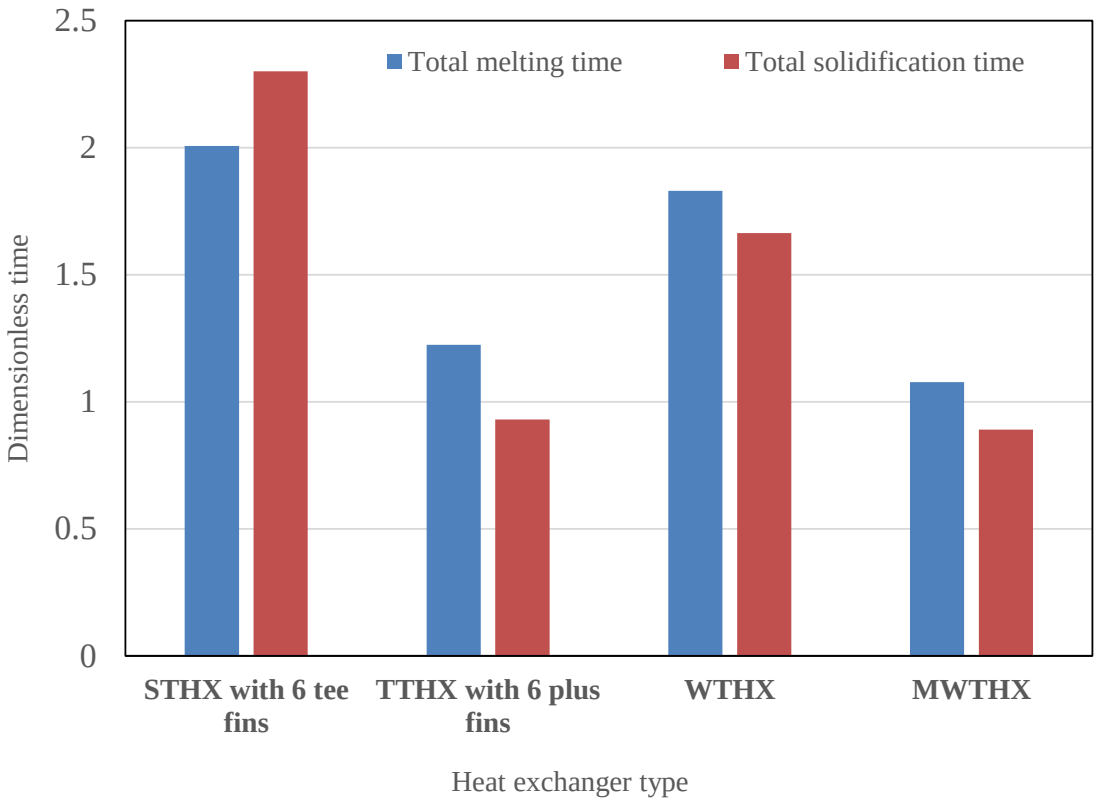

Figure 8.1: Dimensionless time comparison for melting and solidification process for STHX with 6 plus fins, TTHX with 6 plus fins, WTHX, and MWTHX.

8.2 Suggestions for further work

Utilizing nanoparticles

The effect of using innovative fins to enhance the poor thermal performance of PCM in the shell and tube heat exchanger and the triple tube heat exchanger has been studied in this thesis. Nanoparticles, which have high thermal conductivity, could be added to the PCM to improve its poor thermal performance. As such, a possible extension of the present work could be to examine utilizing nanoparticles in combination with the innovative fins introduced to enhance the thermal performance of PCM in the triple tube heat exchanger or the shell and tube heat exchanger. Moreover, the effect of adding the nanoparticles to the PCM in the webbed tube heat exchanger or the modified webbed tube heat exchanger could be studied to evaluate any enhancement in its thermal performance.

Further investigation of the webbed tube heat exchanger and the modified webbed tube heat exchanger

Relevant studies in this thesis lack a more detailed and parametric simulation of the webbed tube heat exchanger and the modified webbed tube heat exchanger. Further investigations could be conducted to consider the effects of more influencing parameters. These parameters could be the influence of changing the number of metal plates, the effect of changing plates' position and the effect of changing the heat transfer fluid flow rates.

Experimental work

The webbed tube heat exchanger and the modified webbed tube heat exchanger have shown excellent capability in improving the thermal performance of PCM in the LHTES systems. Before applying them in a real application, the present work in this thesis could be extended experimentally by manufacturing the webbed tube heat exchanger or the modified webbed tube heat exchanger to test its thermal performance.

Moreover, the effect of utilizing the plus fin shape or the tee fin shape in the triple tube heat exchanger or the shell and tube heat exchanger could be studied experimentally to test its thermal performance.

Bibliography

[1] IEA, *How solar energy could be the largest source of electricity by mid-century.* Available at `https://www.iea.org/newsroom/news/2014/september/`; 2014.

[2] A. M. Abdulateef, S. Mat, J. Abdulateef, K. Sopian, and A. A. Al-Abidi, "Geometric and design parameters of fins employed for enhancing thermal energy storage systems: a review," *Renewable and Sustainable Energy Reviews*, 2017.

[3] I. Dincer and M. Rosen, *Thermal energy storage: systems and applications.* John Wiley & Sons, 2002.

[4] X. Cheng, X. Zhai, and R. Wang, "Thermal performance analysis of a packed bed cold storage unit using composite PCM capsules for high temperature solar cooling application," *Applied Thermal Engineering*, vol. 100, pp. 247–255, 2016.

[5] B. M. Diaconu, S. Varga, and A. C. Oliveira, "Numerical simulation of a solar-assisted ejector air conditioning system with cold storage," *Energy*, vol. 36, no. 2, pp. 1280–1291, 2011.

[6] A. A. Al-Abidi, S. B. Mat, K. Sopian, M. Sulaiman, C. H. Lim, and A. Th, "Review of thermal energy storage for air conditioning systems," *Renewable and Sustainable Energy Reviews*, vol. 16, no. 8, pp. 5802–5819, 2012.

[7] D. Zhou, C.-Y. Zhao, and Y. Tian, "Review on thermal energy storage with phase change materials (PCMs) in building applications," *Applied Energy*, vol. 92, pp. 593–605, 2012.

[8] A. Mishra, A. Shukla, and A. Sharma, "Latent heat storage through phase change materials," *Resonance*, vol. 20, no. 6, pp. 532–541, 2015.

[9] Z. A. Qureshi, H. M. Ali, and S. Khushnood, "Recent advances on thermal conductivity enhancement of phase change materials for energy storage system: A review," *International Journal of Heat and Mass Transfer*, vol. 127, pp. 838–856, 2018.

[10] A. A. Al-Abidi, S. B. Mat, K. Sopian, M. Sulaiman, and A. T. Mohammed, "CFD applications for latent heat thermal energy storage: a review," *Renewable and Sustainable Energy Reviews*, vol. 20, pp. 353–363, 2013.

[11] H. Ibrahim, A. Ilinca, and J. Perron, "Energy storage systemscharacteristics and comparisons," *Renewable and Sustainable Energy Reviews*, vol. 12, no. 5, pp. 1221–1250, 2008.

[12] I. Sarbu and A. Dorca, "Review on heat transfer analysis in thermal energy storage using latent heat storage systems and phase change materials," *International Journal of Energy Research*, 2018.

[13] Y. Tian, *Heat transfer enhancement in phase change materials (PCMs) by metal foams and cascaded thermal energy storage*. PhD thesis, University of Warwick, 2012.

[14] A. Sharma, V. V. Tyagi, C. Chen, and D. Buddhi, "Review on thermal energy storage with phase change materials and applications," *Renewable and Sustainable Energy Reviews*, vol. 13, no. 2, pp. 318–345, 2009.

[15] J. M. Mahdi and E. C. Nsofor, "Solidification enhancement of PCM in a triplex-tube thermal energy storage system with nanoparticles and fins," *Applied Energy*, vol. 211, pp. 975–986, 2018.

[16] D. Fernandes, F. Pitié, G. Cáceres, and J. Baeyens, "Thermal energy storage:how previous findings determine current research priorities," *Energy*, vol. 39, no. 1, pp. 246–257, 2012.

[17] N. I. Ibrahim, F. A. Al-Sulaiman, S. Rahman, B. S. Yilbas, and A. Z. Sahin, "Heat transfer enhancement of phase change materials for thermal energy storage applications: A critical review," *Renewable and Sustainable Energy Reviews*, vol. 74, pp. 26–50, 2017.

[18] A. A. Al-Abidi, S. Mat, K. Sopian, M. Sulaiman, and A. T. Mohammad, "Numerical study of PCM solidification in a triplex tube heat exchanger with internal and external fins," *International Journal of Heat and Mass Transfer*, vol. 61, pp. 684–695, 2013.

[19] K. Y. Leong, M. R. A. Rahman, and B. A. Gurunathan, "Nano-enhanced phase change materials: A review of thermo-physical properties, applications and challenges," *Journal of Energy Storage*, vol. 21, pp. 18–31, 2019.

[20] S. J. Chang, S. Wi, S.-G. Jeong, and S. Kim, "Thermal performance evaluation of macro-packed phase change materials (PCMs) using heat transfer analysis device," *Energy and Buildings*, vol. 117, pp. 120–127, 2016.

[21] F. Agyenim, N. Hewitt, P. Eames, and M. Smyth, "A review of materials, heat transfer and phase change problem formulation for latent heat thermal energy storage systems (LHTESS)," *Renewable and Sustainable Energy Reviews*, vol. 14, no. 2, pp. 615–628, 2010.

[22] A. Abhat, "Low temperature latent heat thermal energy storage: heat storage materials," *Solar Energy*, vol. 30, no. 4, pp. 313–332, 1983.

[23] M. K. Rathod, "Phase change materials and their applications," IntechOpen, 2018.

[24] A. H. Al-Mudhafar, A. F. Nowakowski, and F. C. Nicolleau, "Thermal performance enhancement of energy storage systems via phase change materials utilising an innovative webbed tube heat exchanger," *Energy Procedia*, vol. 151, pp. 57–61, 2018.

[25] J. M. Mahdi, S. Lohrasbi, and E. C. Nsofor, "Hybrid heat transfer enhancement for latent-heat thermal energy storage systems: A review," *International Journal of Heat and Mass Transfer*, vol. 137, pp. 630–649, 2019.

[26] U. Stritih and V. Butala, "Experimental investigation of energy saving in buildings with PCM cold storage," *International Journal of Refrigeration*, vol. 33, no. 8, pp. 1676–1683, 2010.

[27] Y. Xiang and G. Zhou, "Thermal performance of a window-based cooling unit using phase change materials combined with night ventilation," *Energy and Buildings*, vol. 108, pp. 267–278, 2015.

[28] E. Osterman, V. Butala, and U. Stritih, "PCM thermal storage system for free heating and cooling of buildings," *Energy and Buildings*, vol. 106, pp. 125–133, 2015.

[29] A. Mosaffa, L. G. Farshi, C. I. Ferreira, and M. Rosen, "Energy and exergy evaluation of a multiple-PCM thermal storage unit for free cooling applications," *Renewable Energy*, vol. 68, pp. 452–458, 2014.

[30] V. A. A. Raj and R. Velraj, "Heat transfer and pressure drop studies on a PCM-heat exchanger module for free cooling applications," *International Journal of Thermal Sciences*, vol. 50, no. 8, pp. 1573–1582, 2011.

[31] L. Navarro, A. de Gracia, A. Castell, and L. F. Cabeza, "Experimental evaluation of a concrete core slab with phase change materials for cooling purposes," *Energy and Buildings*, vol. 116, pp. 411–419, 2016.

[32] A. Waqas and Z. U. Din, "Phase change material (PCM) storage for free cooling of buildings a review," *Renewable and Sustainable Energy Reviews*, vol. 18, pp. 607–625, 2013.

[33] A. de Gracia, L. Navarro, A. Castell, Á. Ruiz-Pardo, S. Álvarez, and L. F. Cabeza, "Thermal analysis of a ventilated facade with PCM for cooling applications," *Energy and Buildings*, vol. 65, pp. 508–515, 2013.

[34] P. Principi and R. Fioretti, "Thermal analysis of the application of PCM and low emissivity coating in hollow bricks," *Energy and Buildings*, vol. 51, pp. 131–142, 2012.

[35] R. Barzin, J. J. Chen, B. R. Young, and M. M. Farid, "Application of PCM energy storage in combination with night ventilation for space cooling," *Applied Energy*, vol. 158, pp. 412–421, 2015.

[36] M. Sayyar, R. R. Weerasiri, P. Soroushian, and J. Lu, "Experimental and numerical study of shape-stable phase-change nanocomposite toward energy-efficient building constructions," *Energy and Buildings*, vol. 75, pp. 249–255, 2014.

[37] J. Kośny, K. Biswas, W. Miller, and S. Kriner, "Field thermal performance of naturally ventilated solar roof with PCM heat sink," *Solar Energy*, vol. 86, no. 9, pp. 2504–2514, 2012.

[38] R. M. Novais, G. Ascensão, M. Seabra, and J. Labrincha, "Lightweight dense/porous PCM-ceramic tiles for indoor temperature control," *Energy and Buildings*, vol. 108, pp. 205–214, 2015.

[39] F. Bruno, N. Tay, and M. Belusko, "Minimising energy usage for domestic cooling with off-peak PCM storage," *Energy and Buildings*, vol. 76, pp. 347–353, 2014.

[40] P. Moreno, A. Castell, C. Solé, G. Zsembinszki, and L. F. Cabeza, "PCM thermal energy storage tanks in heat pump system for space cooling," *Energy and Buildings*, vol. 82, pp. 399–405, 2014.

[41] X. Zhai, X. Cheng, C. Wang, and R. Wang, "Experimental investigation and performance analysis of a fin tube phase change cold storage unit for high temperature cooling application," *Energy and Buildings*, vol. 89, pp. 9–17, 2015.

[42] C. Zamfirescu and A. Bejan, "Tree-shaped structures for cold storage," *International Journal of Refrigeration*, vol. 28, no. 2, pp. 231–241, 2005.

[43] N. Tay, M. Belusko, and F. Bruno, "An effectiveness-NTU technique for characterising tube-in-tank phase change thermal energy storage systems," *Applied Energy*, vol. 91, no. 1, pp. 309–319, 2012.

[44] E. Oro, L. Miró, M. M. Farid, and L. F. Cabeza, "Thermal analysis of a low temperature storage unit using phase change materials without refrigeration system," *International Journal of Refrigeration*, vol. 35, no. 6, pp. 1709–1714, 2012.

[45] M. Liu, F. Bruno, and W. Saman, "Thermal performance analysis of a flat slab phase change thermal storage unit with liquid-based heat transfer fluid for cooling applications," *Solar Energy*, vol. 85, no. 11, pp. 3017–3027, 2011.

[46] M. Liu, W. Saman, and F. Bruno, "Development of a novel refrigeration system for refrigerated trucks incorporating phase change material," *Applied Energy*, vol. 92, pp. 336–342, 2012.

[47] F. Agyenim, P. Eames, and M. Smyth, "Experimental study on the melting and solidification behaviour of a medium temperature phase change storage material (Erythritol) system augmented with fins to power a LiBr/H2O absorption cooling system," *Renewable Energy*, vol. 36, no. 1, pp. 108–117, 2011.

[48] F. Agyenim, "The use of enhanced heat transfer phase change materials (PCM) to improve the coefficient of performance (COP) of solar powered LiBr/H2O absorption cooling systems," *Renewable Energy*, vol. 87, pp. 229–239, 2016.

[49] Z. Fan, C. I. Ferreira, and A. Mosaffa, "Numerical modelling of high temperature latent heat thermal storage for solar application combining with double-effect H2O/LiBr absorption refrigeration system," *Solar Energy*, vol. 110, pp. 398–409, 2014.

[50] A. Gil, E. Oró, L. Miró, G. Peiró, Á. Ruiz, J. M. Salmerón, and L. F. Cabeza, "Experimental analysis of hydroquinone used as phase change material (PCM) to be applied in solar cooling refrigeration," *International Journal of Refrigeration*, vol. 39, pp. 95–103, 2014.

[51] A. A. Godarzi, M. Jalilian, J. Samimi, A. Jokar, and M. A. Vesaghi, "Design of a PCM storage system for a solar absorption chiller based on exergoeconomic analysis and genetic algorithm," *International Journal of Refrigeration*, vol. 36, no. 1, pp. 88–101, 2013.

[52] D. Qv, L. Ni, Y. Yao, and W. Hu, "Reliability verification of a solar–air source heat pump system with PCM energy storage in operating strategy transition," *Renewable Energy*, vol. 84, pp. 46–55, 2015.

[53] B.-w. Hu, Q. Wang, and Z.-H. Liu, "Fundamental research on the gravity assisted heat pipe thermal storage unit (GAHP-TSU) with porous phase change materials (PCMs) for medium temperature applications," *Energy Conversion and Management*, vol. 89, pp. 376–386, 2015.

[54] M. Fiorentini, P. Cooper, and Z. Ma, "Development and optimization of an innovative HVAC system with integrated PVT and PCM thermal storage for a net-zero energy retrofitted house," *Energy and Buildings*, vol. 94, pp. 21–32, 2015.

[55] G. R. Dheep and A. Sreekumar, "Influence of accelerated thermal charging and discharging cycles on thermo-physical properties of organic phase change materials for solar thermal energy storage applications," *Energy Conversion and Management*, vol. 105, pp. 13–19, 2015.

[56] M. Lacroix, "Study of the heat transfer behavior of a latent heat thermal energy storage unit with a finned tube," *International Journal of Heat and Mass Transfer*, vol. 36, no. 8, pp. 2083–2092, 1993.

[57] A. Sciacovelli, F. Gagliardi, and V. Verda, "Maximization of performance of a PCM latent heat storage system with innovative fins," *Applied Energy*, vol. 137, pp. 707–715, 2015.

[58] C. Ji, Z. Qin, Z. Low, S. Dubey, F. H. Choo, and F. Duan, "Non-uniform heat transfer suppression to enhance PCM melting by angled fins," *Applied Thermal Engineering*, vol. 129, pp. 269–279, 2018.

[59] A. Rozenfeld, Y. Kozak, T. Rozenfeld, and G. Ziskind, "Experimental demonstration, modeling and analysis of a novel latent-heat thermal energy storage unit with a helical fin," *International Journal of Heat and Mass Transfer*, vol. 110, pp. 692–709, 2017.

[60] Z. Khan, Z. Khan, and K. Tabeshf, "Parametric investigations to enhance thermal performance of paraffin through a novel geometrical configuration of shell and tube latent thermal storage system," *Energy Conversion and Management*, vol. 127, pp. 355–365, 2016.

[61] K. Ismail, C. Alves, and M. Modesto, "Numerical and experimental study on the solidification of PCM around a vertical axially finned isothermal cylinder," *Applied Thermal Engineering*, vol. 21, no. 1, pp. 53–77, 2001.

[62] M. K. Rathod and J. Banerjee, "Thermal performance enhancement of shell and tube latent heat storage unit using longitudinal fins," *Applied Thermal Engineering*, vol. 75, pp. 1084–1092, 2015.

[63] Y. Yuan, X. Cao, B. Xiang, and Y. Du, "Effect of installation angle of fins on melting characteristics of annular unit for latent heat thermal energy storage," *Solar Energy*, vol. 136, pp. 365–378, 2016.

[64] A. A. Al-Abidi, S. Mat, K. Sopian, M. Sulaiman, and A. T. Mohammad, "Internal and external fin heat transfer enhancement technique for latent heat thermal energy storage in triplex tube heat exchangers," *Applied Thermal Engineering*, vol. 53, no. 1, pp. 147–156, 2013.

[65] S. Mat, A. A. Al-Abidi, K. Sopian, M. Y. Sulaiman, and A. T. Mohammad, "Enhance heat transfer for PCM melting in triplex tube with internal–external fins," *Energy Conversion and Management*, vol. 74, pp. 223–236, 2013.

[66] A. A. Al-Abidi, S. Mat, K. Sopian, M. Sulaiman, and A. T. Mohammad, "Experimental study of melting and solidification of PCM in a triplex tube heat exchanger with fins," *Energy and Buildings*, vol. 68, pp. 33–41, 2014.

[67] L. Kalapala and J. K. Devanuri, "Influence of operational and design parameters on the performance of a PCM based heat exchanger for thermal energy storage–A review," *Journal of Energy Storage*, vol. 20, pp. 497–519, 2018.

[68] B. Cárdenas and N. León, "High temperature latent heat thermal energy storage: Phase change materials, design considerations and performance enhancement techniques," *Renewable and Sustainable Energy Reviews*, vol. 27, pp. 724–737, 2013.

[69] I. Sarbu and C. Sebarchievici, "A comprehensive review of thermal energy storage," *Sustainability*, vol. 10, no. 1, p. 191, 2018.

[70] R. Seeniraj and N. L. Narasimhan, "Performance enhancement of a solar dynamic LHTS module having both fins and multiple PCMs," *Solar Energy*, vol. 82, no. 6, pp. 535–542, 2008.

[71] A. M. Sefidan, A. Sojoudi, S. C. Saha, and M. Cholette, "Multi-layer PCM solidification in a finned triplex tube considering natural convection," *Applied Thermal Engineering*, 2017.

[72] A. M. Abdulateef, S. Mat, J. Abdulateef, K. Sopian, and A. A. Al-Abidi, "Thermal performance enhancement of triplex tube latent thermal storage using fins-nano-phase change material technique," *Heat Transfer Engineering*, pp. 1–14, 2017.

[73] M. Al-Maghalseh, *Compact solar thermal energy storage systems using phase change materials*. PhD thesis, Northumbria University, 2014.

[74] Y. Seki, Ş. İnce, M. A. Ezan, A. Turgut, and A. Erek, "Graphite nanoplates loading into eutectic mixture of adipic acid and sebacic acid as phase change material," *Solar Energy Materials and Solar Cells*, vol. 140, pp. 457–463, 2015.

[75] K. Hosseinzadeh, M. Alizadeh, and D. Ganji, "Solidification process of hybrid nano-enhanced phase change material in a LHTESS with tree-like branching fin in the presence of thermal radiation," *Journal of Molecular Liquids*, 2018.

[76] J. M. Mahdi, S. Lohrasbi, D. D. Ganji, and E. C. Nsofor, "Accelerated melting of PCM in energy storage systems via novel configuration of fins in the triplex-tube heat exchanger," *International Journal of Heat and Mass Transfer*, vol. 124, pp. 663–676, 2018.

[77] Z. Liu, Y. Yao, and H. Wu, "Numerical modeling for solid–liquid phase change phenomena in porous media: Shell-and-tube type latent heat thermal energy storage," *Applied Energy*, vol. 112, pp. 1222–1232, 2013.

[78] J. M. Mahdi and E. C. Nsofor, "Solidification enhancement in a triplex-tube latent heat energy storage system using nanoparticles-metal foam combination," *Energy*, vol. 126, pp. 501–512, 2017.

[79] Y. Tian and C.-Y. Zhao, "A numerical investigation of heat transfer in phase change materials (PCMs) embedded in porous metals," *Energy*, vol. 36, no. 9, pp. 5539–5546, 2011.

[80] J. M. Mahdi and E. C. Nsofor, "Multiple-segment metal foam application in the shell-and-tube PCM thermal energy storage system," *Journal of Energy Storage*, vol. 20, pp. 529–541, 2018.

[81] S. Wang, P. Qin, X. Fang, Z. Zhang, S. Wang, and X. Liu, "A novel sebacic acid/expanded graphite composite phase change material for solar thermal medium-temperature applications," *Solar Energy*, vol. 99, pp. 283–290, 2014.

[82] F. Agyenim, P. Eames, and M. Smyth, "Heat transfer enhancement in medium temperature thermal energy storage system using a multitube heat transfer array," *Renewable Energy*, vol. 35, no. 1, pp. 198–207, 2010.

[83] M. Esapour, M. Hosseini, A. Ranjbar, Y. Pahamli, and R. Bahrampoury, "Phase change in multi-tube heat exchangers," *Renewable Energy*, vol. 85, pp. 1017–1025, 2016.

[84] M. Esapour, M. Hosseini, A. Ranjbar, and R. Bahrampoury, "Numerical study on geometrical specifications and operational parameters of multi-tube heat storage systems," *Applied Thermal Engineering*, vol. 109, pp. 351–363, 2016.

[85] D. Dandotiya and N. Banker, "Numerical investigation of heat transfer enhancement in a multitube thermal energy storage heat exchanger using fins," *Numerical Heat Transfer, Part A: Applications*, vol. 72, no. 5, pp. 389–400, 2017.

[86] Y. Pahamli, M. Hosseini, A. Ranjbar, and R. Bahrampoury, "Inner pipe downward movement effect on melting of PCM in a double pipe heat exchanger," *Applied Mathematics and Computation*, vol. 316, pp. 30–42, 2018.

[87] M. Alizadeh, K. Hosseinzadeh, H. Mehrzadi, and D. Ganji, "Investigation of LHTESS filled by Hybrid nano-enhanced PCM with Koch snowflake fractal cross section in the presence of thermal radiation," *Journal of Molecular Liquids*, 2018.

[88] A. Pourakabar and A. A. R. Darzi, "Enhancement of phase change rate of pcm in cylindrical thermal energy storage," *Applied Thermal Engineering*, vol. 150, pp. 132–142, 2019.

[89] J. M. Mahdi, S. Lohrasbi, D. D. Ganji, and E. C. Nsofor, "Simultaneous energy storage and recovery in the triplex-tube heat exchanger with PCM, copper fins and Al2O3 nanoparticles," *Energy Conversion and Management*, vol. 180, pp. 949–961, 2019.

[90] C. Swaminathan and V. Voller, "On the enthalpy method," *International Journal of Numerical Methods for Heat & Fluid Flow*, vol. 3, no. 3, pp. 233–244, 1993.

[91] V. Voller, M. Cross, and N. Markatos, "An enthalpy method for convection/diffusion phase change," *International Journal for Numerical Methods in Engineering*, vol. 24, no. 1, pp. 271–284, 1987.

[92] "Fluent 6.1 users guide," *Fluent Inc., New Hampshire*, 2003.

[93] V. R. Voller and C. Prakash, "A fixed grid numerical modelling methodology for convection-diffusion mushy region phase-change problems," *International Journal of Heat and Mass Transfer*, vol. 30, no. 8, pp. 1709–1719, 1987.

[94] J. Lopez Sahuquillo *et al.*, "Master thesis: Implementation of a melting/solidification process with the enthalpy method," 2017.

[95] A. Demuren and H. Grotjans, "Buoyancy-driven flows beyond the boussinesq approximation," *Numerical Heat Transfer, Part B: Fundamentals*, vol. 56, no. 1, pp. 1–22, 2009.

[96] M. Costa, A. Oliva, C. F. Segarra, and R. Alba, "Numerical simulation of solid-liquid phase change phenomena," *Computer Methods in Applied Mechanics and Engineering*, vol. 91, no. 1-3, pp. 1123–1134, 1991.

[97] *Rubitherm Technologies GmbH.* Available at `www.rubitherm.eu/en/productCategories.html`; 2017.

[98] A. M. Abdulateef, J. Abdulateef, S. Mat, K. Sopian, B. Elhub, and M. A. Mussa, "Experimental and numerical study of solidifying phase-change material in a triplex-tube heat exchanger with longitudinal/triangular fins," *International Communications in Heat and Mass Transfer*, vol. 90, pp. 73–84, 2018.